Agenzia nazionale per le nuove tecnologie,
l'energia e lo sviluppo economico sostenibile

MINISTERO DELLO SVILUPPO ECONOMICO

Ricerca di Sistema elettrico

Dati Nucleari per la Sicurezza Reattore - PAR 2017: Attività di validazione librerie e code-package ANITA

M. Pescarini, R. Orsi, M. Frisoni

Report RdS/PAR2017/121

Dati Nucleari per la Sicurezza Reattore – PAR 2017: Attività di validazione librerie e code-package ANITA

M. Pescarin, R. Orsi, M. Frisoni (ENEA)

Settembre 2018

Report Ricerca di Sistema Elettrico

Accordo di Programma Ministero dello Sviluppo Economico - ENEA
Piano Annuale di Realizzazione 2017
Area: Generazione di energia elettrica con basse emissioni di carbonio
Progetto: Sviluppo competenze scientifiche nel campo della sicurezza nucleare e collaborazione ai programmi internazionali per il nucleare di IV generazione - Linea Progettuale 1
Obiettivo: Metodi e analisi per verifiche di sicurezza
Responsabile del Progetto: Federico Rocchi, ENEA

Questo rapporto contiene i due seguenti Rapporti Tecnici ENEA:

- M. Pescarini, R. Orsi, Validation of the BUGJEFF311.BOLIB, BUGENDF70.BOLIB, BUGLE-B7 and BUGLE-96 Cross Section Libraries on the Iron-88 (Fe) Neutron Shielding Benchmark Experiment, ADPFISS-LP1-106

- M. Frisoni, Production of the ANITA-NC system able to treat material activation due to neutral or charged particles, ADPFISS-LP1-107

ENEA Ricerca Sistema Elettrico	Sigla di identificazione	Distrib.	Pag.	di
	ADPFISS-LP1-106	L	1	121

Titolo

Validation of the BUGJEFF311.BOLIB, BUGENDF70.BOLIB, BUGLE-B7 and BUGLE-96 Cross Section Libraries on the Iron-88 Neutron Shielding Benchmark Experiment

Descrittori

Tipologia del documento: Rapporto tecnico

Collocazione contrattuale: Accordo di programma ENEA-MSE su sicurezza nucleare e reattori di IV generazione

Argomenti trattati: Fisica nucleare, dati nucleari, fisica dei reattori nucleari

Sommario

Three-dimensional (3D) fixed source transport calculations in Cartesian (X,Y,Z) geometry for the Iron-88 single-material (Fe) neutron shielding benchmark experiment were performed using the TORT-3.2 discrete ordinates (S_N) transport code. The ENEA-Bologna BUGJEFF311.BOLIB (JEFF-3.1.1 data) and BUGENDF70.BOLIB (ENDF/B-VII.0 data) broad-group coupled (47 n + 20 γ) working cross section libraries in FIDO-ANISN format together with the similar ORNL BUGLE-B7 (ENDF/B-VII.0 data) and BUGLE-96 (ENDF/B-VI.3 data) libraries, specifically conceived for LWR shielding and pressure vessel dosimetry applications, were alternatively used together with dosimeter cross sections, processed from the IAEA IRDF-2002 dosimetry file. The ENEA-Bologna programs ADEFTA-4.1 and BOT3P-5.3 were respectively employed for the calculation of the isotopic atomic densities and for the automatic generation of the spatial mesh grid of the geometrical model. The calculated dosimetric results were compared with the corresponding experimental data, obtained with Au-198(n,γ)Au-198 activation dosimeters and with Rh-103(n,n')Rh-103m, In-115(n,n')In-115m, S-32(n,p)P-32 and Al-27(n,α)Na-24 threshold activation dosimeters. Given the total experimental uncertainties at 1σ, then the computational results presented exhibit good statistical consistency with the corresponding measurements except for the Al-27(n,α)Na-24 strongly overestimated results.

Note

Authors: Massimo PESCARINI, Roberto ORSI

Copia n. **In carico a:**

REV.	DESCRIZIONE	DATA		REDAZIONE	CONVALIDA	APPROVAZIONE
2			NOME			
			FIRMA			
1			NOME			
			FIRMA			
0	EMISSIONE	14/11/2018	NOME	M. Pescarini	F. Padoani	F. Rocchi
			FIRMA	M. Pescarini	F. Padoani	Roberto Rocchi

INDEX

Validation of the BUGJEFF311.BOLIB, BUGENDF70.BOLIB, BUGLE-B7 and BUGLE-96 Cross Section Libraries on the Iron-88 Neutron Shielding Benchmark Experiment

Massimo PESCARINI, Roberto ORSI

November 2018

1 - INTRODUCTION

The ENEA-Bologna Nuclear Data Group generated two broad-group coupled neutron/photon (47 n + 20 γ) working cross section libraries in FIDO-ANISN /1/ format, named BUGJEFF311.BOLIB /2/ and BUGENDF70.BOLIB /3/ and respectively based on the OECD-NEADB JEFF-3.1.1 /4/ (see also /5/) and US ENDF/B-VII.0 /6/ evaluated nuclear data libraries. The same neutron and photon energy group structure of the ORNL BUGLE-B7 /7/ (US ENDF/B-VII.0 evaluated nuclear data) and BUGLE-96 /8/ (US ENDF/B-VI.3 /9/ evaluated nuclear data) working cross section libraries was adopted by the ENEA-Bologna libraries together with the same FIDO-ANISN data format and similar data processing methodology. All these ENEA-Bologna and ORNL libraries were specifically conceived for LWR shielding and pressure vessel dosimetry applications and contain problem-dependent parameterized sets of self-shielded neutron cross sections, specifically prepared for BWR and PWR applications.
It was considered a meaningful test to validate the two ENEA-Bologna libraries and the two ORNL libraries on the Iron-88 /10/ single-material (iron) neutron shielding benchmark experiment (Winfrith, 1988, UK), included in particular in the SINBAD REACTOR /11/ /12/ international database of neutron shielding benchmark experiments, dedicated to nuclear fission reactors. In fact the previously cited experiment permits to verify the neutron deep penetration (decades of neutron flux attenuation) through a mild steel layer with a thickness of about 67 cm. In particular it is underlined that the performance of the iron nuclear data are obviously essential for any fission reactor applications. In fact it is well known that, for example, the LWR pressure vessels and the so-called reactor internals are made of different types of steels. This implies that in any case the iron cross sections, and in particular those of Fe-56 with an isotopic abundance of about 92% in natural iron, play a crucial role in the accurate prediction of the EoL (End-of-Life) neutron fluence of the steel reactor components as, for example, the reactor pressure vessel.
The four cited working libraries were alternatively used in fixed source transport calculations, performed in Cartesian (X,Y,Z) geometry with the TORT-3.2 /13/ three-dimensional (3D) discrete ordinates (S_N) transport code, included in the ORNL DOORS /14/ system of deterministic transport codes. The ENEA-Bologna ADEFTA-4.1 /15/ and BOT3P-5.3 /16/ (see also /17/, /18/ and /19/) codes were respectively employed for the calculation of the isotopic atomic densities and for the automatic generation of the spatial mesh grid of the geometrical model.
The calculated dosimetric integral results were compared with the corresponding experimental data, obtained using neutron activation dosimeters The neutron activation dosimeter cross sections used in the calculations were processed (see /20/) from the IAEA

IRDF-2002 /21/ reactor dosimetry file. In particular the activation cross sections for the Au-198(n,γ)Au-198 dosimeters and the threshold activation cross sections for the Rh-103(n,n')Rh-103m, In-115(n,n')In-115m, S-32(n,p)P-32 and Al-27(n,α)Na-24 dosimeters were involved in the present analysis of the Iron-88 experiment.
Finally, it is underlined that the results obtained using the BUGLE-96 library permitted to obtain in particular a reliable reference comparison with the results of the other similar libraries employed in the present transport calculations, based on more recent evaluated nuclear data. In fact BUGLE-96 was widely and successfully used all over the world in the previously cited applications since 1996. In particular it is specifically recommended by the American National Standard /22/ of the American Nuclear Society "Neutron and Gamma-Ray Cross Sections for Nuclear Radiation Protection Calculations for Nuclear Power Plants" (ANSI/ANS-6.1.2-1999, R2009) for LWR shielding and radiation damage applications.
Parts of the present results were already published in the references /23/ and /24/.

2 - IRON-88 EXPERIMENT

The ASPIS shielding facility of the Winfrith NESTOR reactor, the Iron-88 benchmark experimental array, the activation dosimeter measurements and the fission plate neutron source are described, taking the relative information integrally from reference /10/ and from the document of the Iron-88 benchmark experiment section of SINBAD REACTOR /11/, entitled “General Description of the Experiment”.

2.1 - ASPIS Shielding Facility

The ASPIS shielding facility (see FIG. 2.1) was installed on the NESTOR reactor (presently dismantled) at Winfrith. NESTOR was a light water cooled, graphite and light water moderated reactor which operated at powers of up to 30 kW and was used as a source of neutrons for a wide range of applications. The core of the reactor, which comprised 26 MTR (Materials Test Reactor) type fuel elements, was contained within an annulus formed by two concentric aluminium vessels through which water circulated. The inner vessel was filled with graphite to form an inner reflector. The outer tank was surrounded by an external graphite reflector in the form of a block having dimensions 182 cm × 182 cm × 122 cm which contained the control plate slots adjacent to the vessel wall. Leading off each of the four faces of the external reflector was an experiment cave which could be isolated from the reactor by shutters composed of boral or combinations of neutron/gamma-ray shield materials. ASPIS was located in the NESTOR cave C. Shield components, which were in the main slabs or tanks, were mounted vertically in a mobile tank which had an internal cross-sectional area of 1.8 m × 1.9 m and a length of 3.7 m. A fission plate was located within the experimental shield array. The loaded tank was moved into the cave where thermal neutrons, leaking from the outer graphite reflector of NESTOR, were used to drive the fission plate to provide a well defined neutron source for penetration measurements. The neutron flux levels within an ASPIS shield contained contributions from sources in the fission plate and from the NESTOR core and it was essential that the NESTOR contribution was subtracted from all measured responses to arrive at the response resulting from the fission plate sources.

2.2 - Iron-88 Benchmark Experimental Array

The Iron-88 benchmark experimental array, irradiated in the ASPIS shielding facility, is shown schematically in side elevation in FIG. 2.2. The array comprised three regions; the source region containing moderator and the fission plate, the shield made from 13 mild steel plates, each of approximately 5.1 cm thickness, and a deep backing shield manufactured from mild and stainless steel. To allow dosimeter access within the shield, 6 mm spacers were placed between each slab component. In practice the depth of the air gaps varied owing to positional uncertainties of the plates and their flatness. The 6 mm gap was therefore nominal and an average gap of 7.4 mm was measured for the experiment. The axial dimensions of the experimental components are given in TAB. 2.1. The outer boundaries of the experimental region were formed by the walls and floor of the ASPIS trolley (see FIG. 2.1) and by the roof of the ASPIS cave. The floor and walls of the trolley were manufactured from 1.91 cm thick mild steel plate. The trolley base had a 25 cm high steel chassis in-filled with concrete. The structure of NESTOR surrounding the trolley comprised concrete bulk shielding blocks except on the NESTOR core side of the trolley front face where it was graphite. This graphite

extended away from the trolley to the external graphite reflector of the reactor. The compositions of the materials used in the Iron-88 experiment are given in TAB. 2.2.

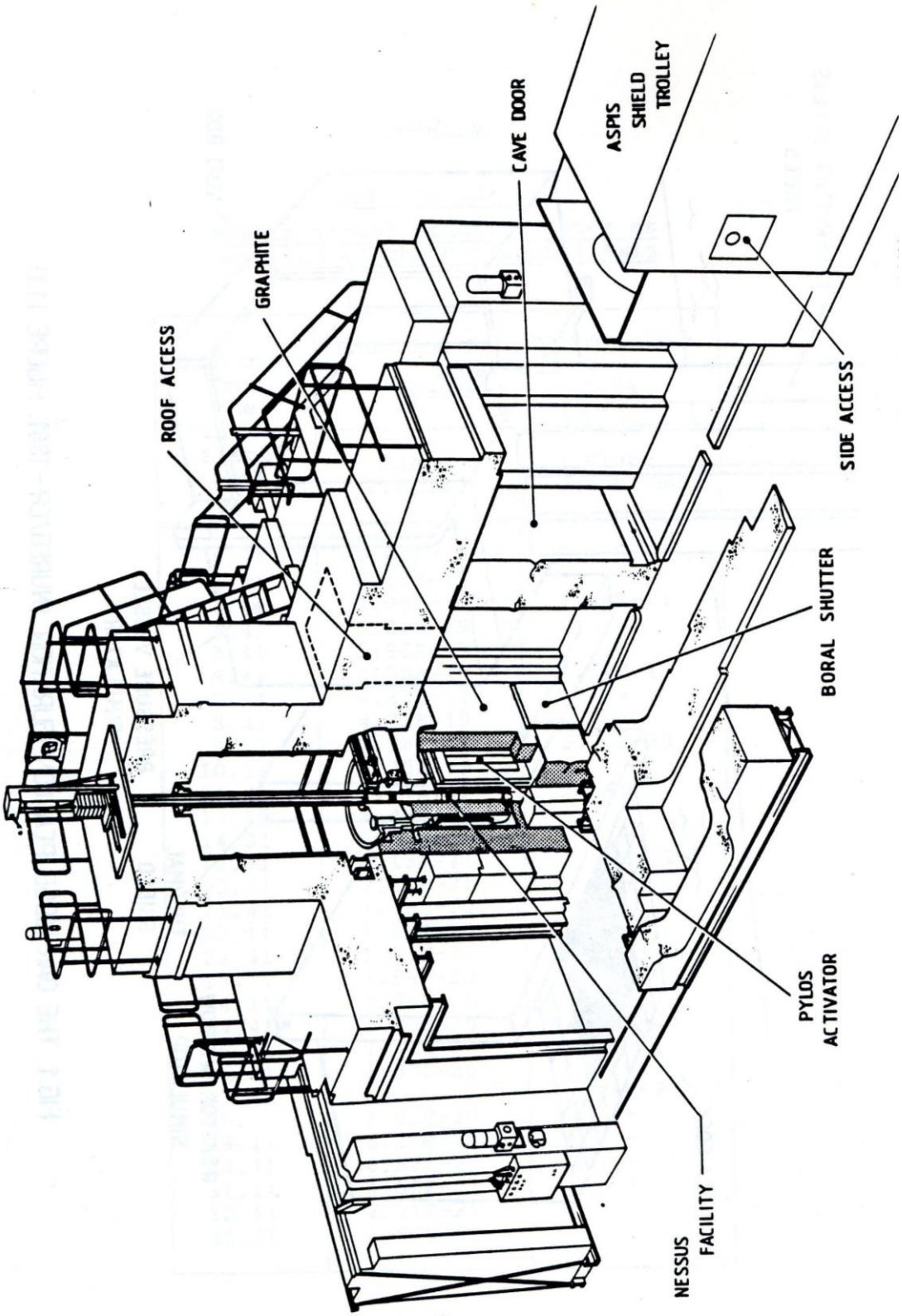

FIG. 2.1 The Shielding Facilities of the NESTOR Reactor.

FIG. 2.2

Iron-88 - Schematic Side Elevation of the Shield [a].

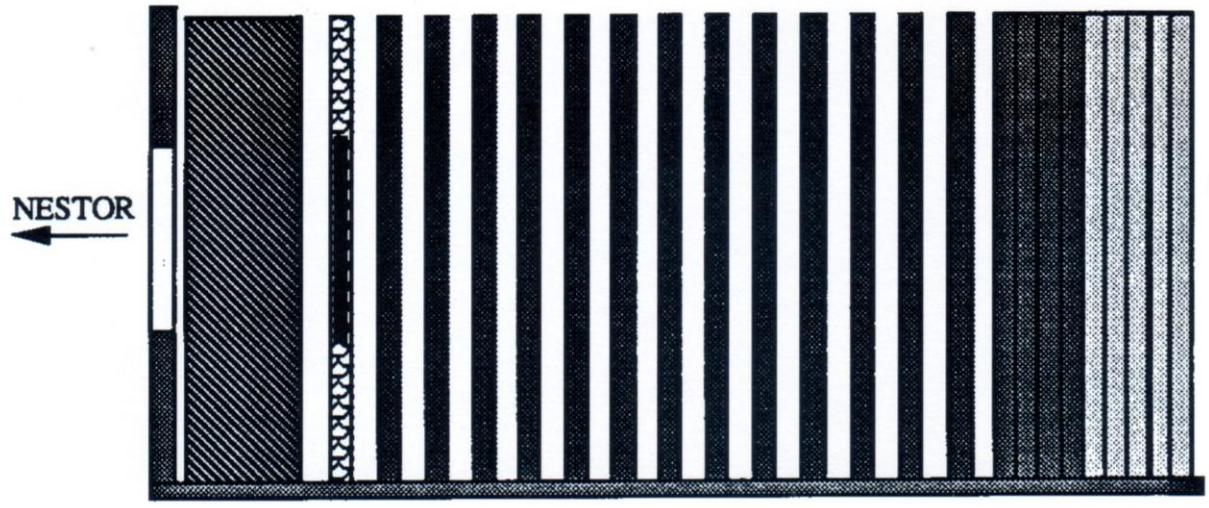

KEY

- Fuel
- Mild Steel
- Stainless Steel
- Fission Plate
- Graphite
- Aluminium

All components are 182.9cm wide by 191.0cm high

Not To Scale

([a]) Figure derived from Figure 1 of reference /10/.

TAB. 2.1

Iron-88 - Shield Dimensions.

Component	Material Thickness [cm]	Coordinate at End of Region [cm]	Material Reference Number
Trollev Face	3.18	-16.62	1 & 2
Void	0.52	-16.10	-
Graphite	15.00	-1.10	3
Void	1.10	0.00	-
Fission Plate	2.90	2.90	4 & 5
Void	0.74	3.64	-
Mild Steel	5.10	8.74	6
Void	0.74	9.48	-
Mild Steel	5.12	14.60	6
Void	0.74	15.34	-
Mild Steel	5.12	20.46	6
Void	0.74	21.20	-
Mild Steel	5.10	26.30	6
Void	0.74	27.04	-
Mild Steel	5.20	32.24	6
Void	0.74	32.98	-
Mild Steel	5.15	38.13	6
Void	0.74	38.87	-
Mild Steel	5.20	44.07	6
Void	0.74	44.81	-
Mild Steel	5.20	50.01	6
Void	0.74	50.75	-
Mild Steel	5.25	56.00	6
Void	0.74	56.74	-
Mild Steel	5.18	61.92	6
Void	0.74	62.66	-
Mild Steel	5.07	67.73	6
Void	0.74	68.47	-
Mild Steel	5.12	73.59	6
Void	0.74	74.33	-
Mild Steel	5.18	79.51	6
Void	0.74	80.25	-
Mild Steel	5.10	85.35	6
Mild Steel	5.25	90.60	6
Mild Steel	5.00	95.60	6
Mild Steel	4.67	100.27	6
Stainless Steel	22.41	122.68	7
Concrete	100.00	222.68	8

Notes

1. For material compositions see TAB. 2.2.
2. The trolley face is manufactured from mild steel with a central aluminium “window” of radius equal to 56.1 cm.
3. The construction of the fission plate is shown in FIG. 2.5.
4. All slab components are 182.9 cm wide by 191.0 cm high and fill the full width and height of the ASPIS trolley.

TAB. 2.2

Iron-88 - Material Composition.

Material	Material Reference No.	Density [g × cm^{-3}]	Element/ Isotope	Weight Fraction [%]
Mild Steel	1	7.835	Fe Mn C Si	0.9865 0.0109 0.0022 0.0004
Aluminium	2	2.700	Al	1.0000
Graphite	3	1.650	C	1.0000
Fuel	4	3.256	Al U-235 U-238	0.7998 0.1864 0.0138
Aluminium	5	2.666	Fe Si Al	0.0056 0.0015 0.9929
Mild Steel	6	7.850	Fe Mn C	0.9903 0.0074 0.0023
Stainless Steel	7	7.917	Fe Mn Cr Ni C Si P S Mo	0.6695 0.0157 0.1677 0.1166 0.0006 0.0050 0.0003 0.0002 0.0244
Concrete	8	2.242	Fe Si Al H O Ca K Na	0.0141 0.3369 0.0340 0.0100 0.5290 0.0379 0.0200 0.0161

2.3 - Iron-88 Benchmark Fission Plate

A schematic diagram of the fission plate is shown in FIG. 2.3. It comprises an aluminium frame which fills the height and width of the ASPIS trolley. Located within the frame are 13 separate fuel elements. A schematic view of an individual fuel element is shown in FIG. 2.4. Each element has two 12 mm thick aluminium cover plates which attach on either side of the top and bottom locating end pieces leaving a 5 mm separation in which U/Al alloy fuel strips are located. The fuel strips are 80% by weight aluminium and 20% by weight of uranium enriched to 93% having a density of 3.256 $g \times cm^{-3}$. Each strip is nominally 30.5 mm wide and 1 mm thick and is fixed to the rear cover plate by M5 screws.

Three columns of fuel strips laid side by side fill the width of the element. There is depth for 4 fuel strips within each element leaving a 1 mm clearance gap next to the front cover plate. In the current configuration only the central two strips in each column contain U/Al alloy, the outer two are both blanks manufactured from aluminium. To approximate to a disc fission neutron source the axial fuel loading within each element has been arranged to the specification shown in FIG. 2.5 by the substitution of aluminium blanks for fuel where necessary giving 4 mm of aluminium in the unfuelled regions.

The position of the fission plate is shown in FIG. 2.6. The centre of the fuel is at a height of 889 mm from the floor of the trolley and at 889 mm from the right hand wall of the trolley when looking towards the NESTOR core. The measurements were made on this Z horizontal nuclear axis passing through the centre of the fission plate.

The approach taken to obtain the absolute power distribution within the fission plate is summarised as follows:

1. Mn-55(n,γ)Mn-56 reaction rates are measured over the front surface of the fission plate to define a thermal flux profile in X and Y.

2. The distribution of the U-235 content within the fuel is assessed.

3. 1. and 2. are combined to provide a relative fission rate profile in X and Y.

4. The relative fission profile in the Z direction through the fuel is obtained from absolute measurements of fission rate in the plate as described below.

5. The fission rate profile is normalised to absolute measurements of the fission rate per NESTOR Watt in the plate which are made by counting fission product decay rates in samples taken from the central strip of the central element at the centre, bottom and halfway between the centre and bottom of the fuel.

6. The neutron source distribution is obtained from the absolute fission rate distribution.

The manganese reaction rate measurements on the front face of the plate were input to the CRISP code /25/ to define the manganese reaction rate surface covering the plate. From this surface the average manganese reaction rate within the elements of any source mesh overlaid onto the fission plate can be defined. The fission rate profile in X and Y is taken as the

manganese reaction rate profile on the front face of the fuel plate. This has been normalised to give a plate power of 1 Watt and the resulting neutron source distribution is shown in TAB. 2.3. Constants of 3.121E+10 fissions per Watt and 2.437 neutrons per fission have been used in this derivation.

The absolute fission rate in the fuel was found to be between 5% and 16% higher in the strip nearer to NESTOR. This difference is caused by the attenuation of thermal neutrons from NESTOR through the 1 mm fuel strips. However, the attenuation of the neutrons produced by fission is small over this distance so an assumption of no Z dependence in the source strength has been made.

The absolute power in the fission plate, expressed as plate Watts per NESTOR Watt, has been determined by combining measurements of the absolute fission rate at spot values, gained by fission product decay line counting, with the fission rate profile data derived in CRISP. The analysis is rather involved and the result was an absolute plate power of 5.68E-04 Watts per NESTOR Watt. The uncertainty on the plate power is 8% at the two standard deviations (2σ) level.

TAB. 2.3

Iron-88 - Source Distribution on the Fission Plate.

0	0	0	0	0	0	2.973	2.994	2.865	0	0	0	0	0	0
0	0	0	0	0	3.173	3.496	3.537	3.404	2.975	0	0	0	0	0
0	0	0	0	3.176	3.711	4.088	4.149	4.015	3.529	2.890	0	0	0	0
0	0	0	3.186	3.500	4.092	4.514	4.587	4.446	3.925	3.240	2.886	0	0	0
0	0	3.249	3.635	3.999	4.696	5.197	5.286	5.130	4.555	3.807	3.422	3.009	0	0
0	3.150	3.575	4.003	4.412	5.202	5.770	5.870	5.699	5.080	4.282	3.873	3.431	2.970	0
3.040	3.322	3.769	4.223	4.660	5.505	6.110	6.215	6.034	5.387	4.559	4.133	3.673	3.188	2.850
3.132	3.427	3.893	4.364	4.815	5.684	6.304	6.412	6.227	5.563	4.710	4.270	3.792	3.287	2.932
3.026	3.325	3.784	4.239	4.669	5.491	6.079	6.183	6.009	5.364	4.523	4.084	3.607	3.103	2.751
0	3.136	3.574	4.001	4.400	5.157	5.701	5.802	5.643	5.031	4.221	3.795	3.331	2.843	0
0	0	3.182	3.562	3.912	4.572	5.053	5.149	5.013	4.461	3.713	3.317	2.887	0	0
0	0	0	3.004	3.299	3.855	4.267	4.357	4.247	3.766	3.101	2.748	0	0	0
0	0	0	0	2.896	3.396	3.770	3.855	3.758	3.320	2.712	0	0	0	0
0	0	0	0	0	2.745	3.072	3.150	3.067	2.685	0	0	0	0	0
0	0	0	0	0	0	2.458	2.525	2.448	0	0	0	0	0	0

Units are neutrons × cm^{-3} × $second^{-1}$ × 1.0E+07.
The plate power for this distribution is 1 Watt.

Coordinate boundaries for source distribution.
Units are cm.

X	-52.25	-49.08	-45.92	-39.58	-36.42	-30.08	-14.25	-4.75
	4.75	14.25	30.08	36.42	39.58	45.92	49.08	52.25
Y	-51.44	-47.63	-40.64	-35.56	-31.75	-19.69	-15.88	-5.29
	5.29	15.88	19.69	31.75	35.56	40.64	47.63	51.44

FIG. 2.3

Iron-88 - Schematic Diagram of the Fission Plate [a].

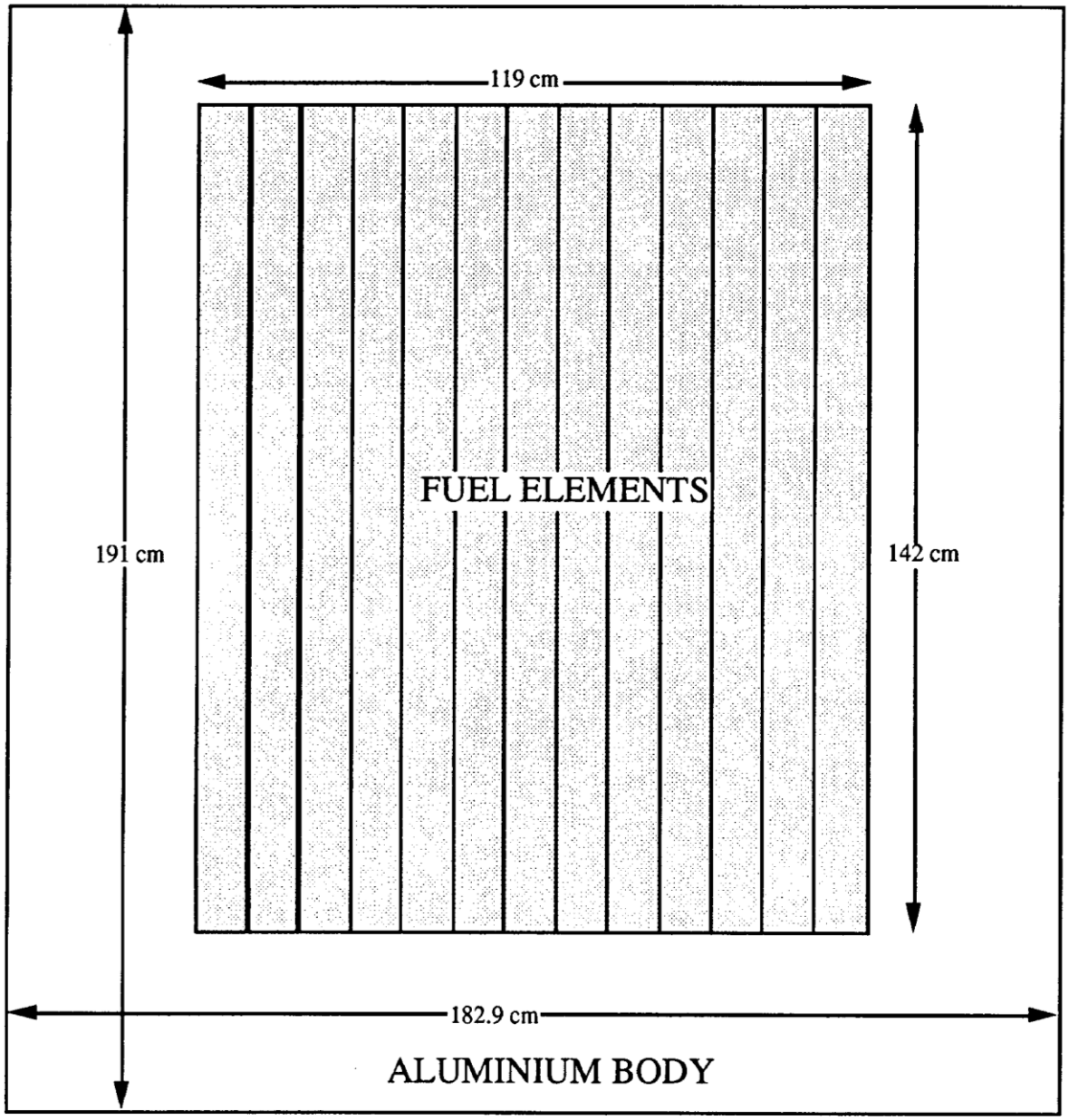

([a]) Figure derived from Figure 3 of reference /10/.

FIG. 2.4

Iron-88 - Schematic Diagram of the Fuel Element of the Fission Plate [a].

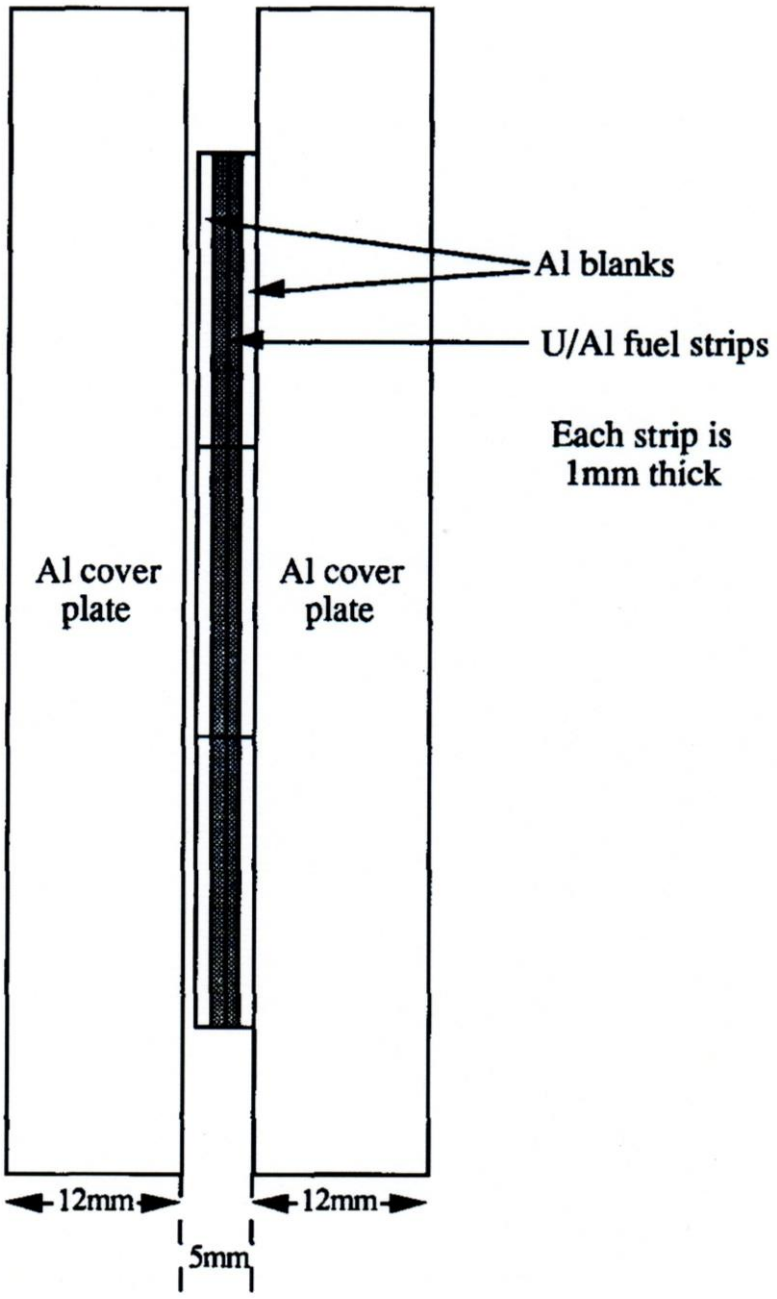

([a]) Figure derived from Figure 4 of reference /10/.

FIG. 2.5

Iron-88 - Disposition of the Fuel Elements in the Fission Plate [a].

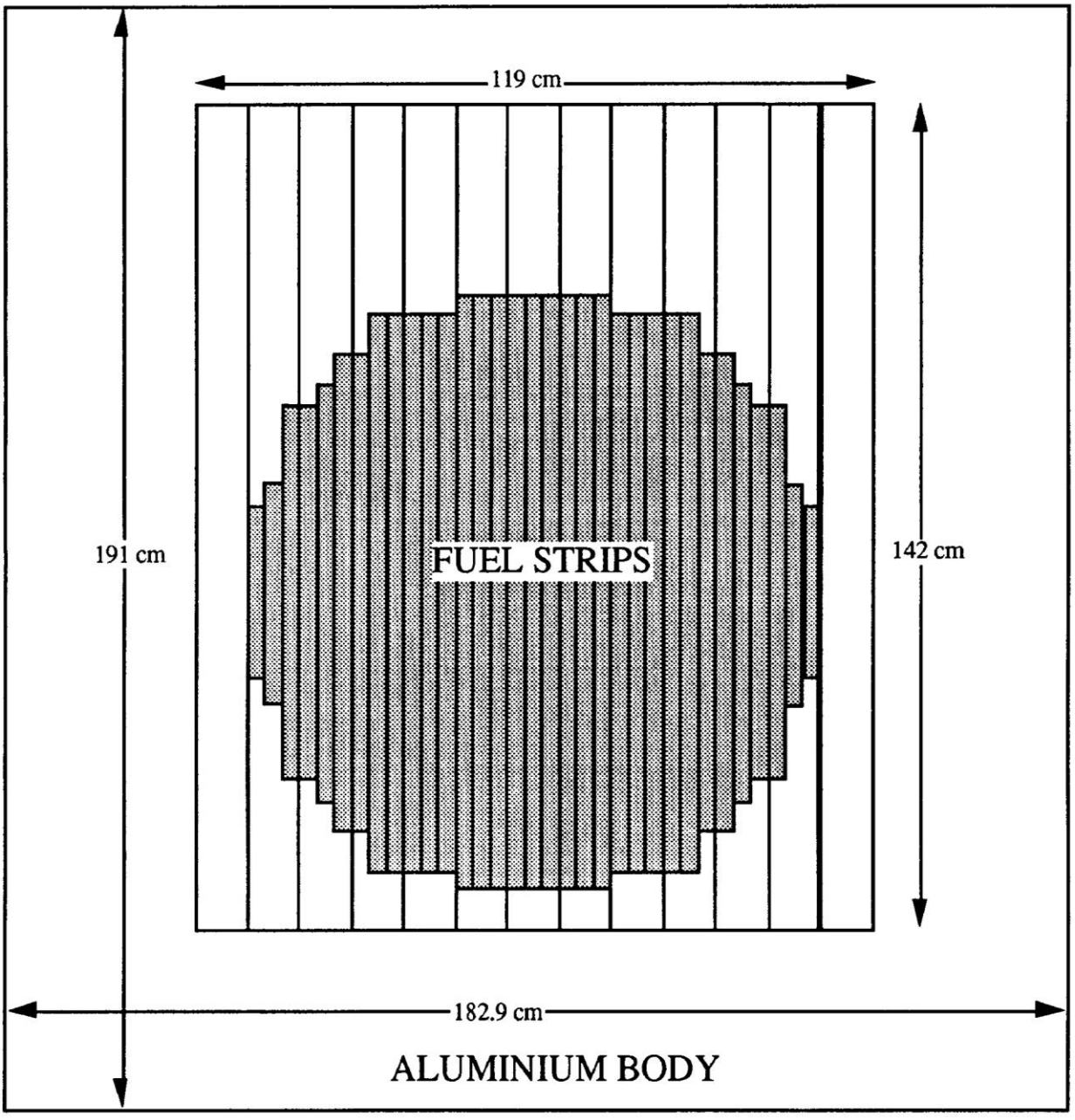

([a]) Figure derived from Figure 5 of reference /10/.

FIG. 2.6

Iron-88 - Details of the Fuel Loading Pattern in the Fission Plate
when Viewed Looking towards the NESTOR Reactor Core [a].

Section Normal to the Z Horizontal Axis at the Fission Plate Centre.

Position of the Fission Plate with Respect to the ASPIS Trolley.

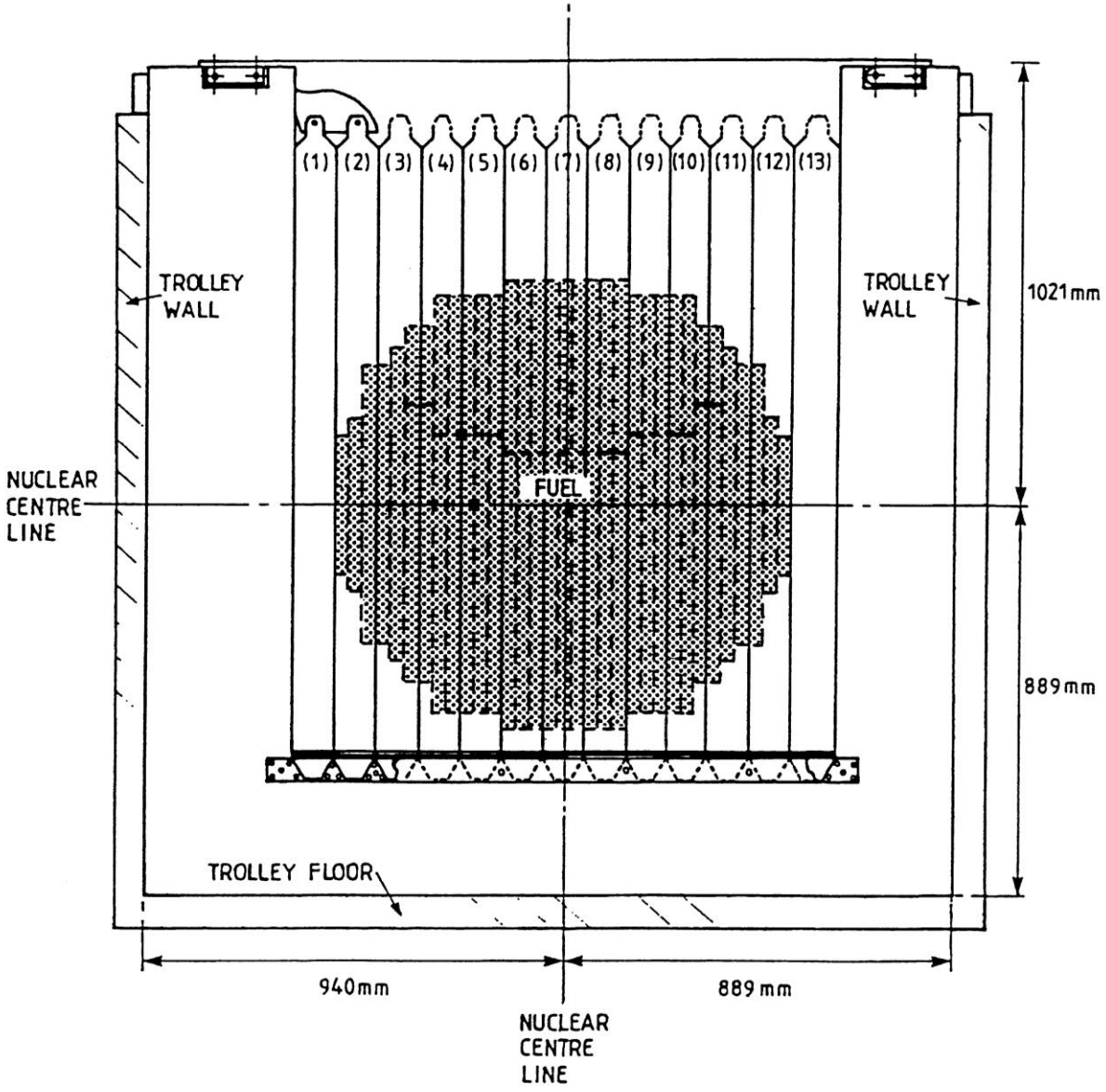

([a]) Figure derived from the Iron-88 benchmark experiment section of reference /11/.

2.4 - Activation Dosimeter Measurements in the Iron-88 Experiment

The neutron distribution through the experimental shield was mapped using activation foils attached to thin aluminium carriers (0.5 mm thick by 9 cm wide) located between the slab components. The dosimeter set comprised activation foils to measure the Au-197(n,γ)Au-198 epi-cadmium reaction rates and the Rh-103(n,n')Rh-103m, In-115(n,n')In-115m, S-32(n,p)P-32 and Al-27(n,α)Na-24 threshold reaction rates. In particular the epi-cadmium activation reaction rate measurements were performed using cylindrical gold foils with a diameter of 12.7 mm, a thickness of 0.05 mm, a typical mass of 0.12 g - 0.13 g and a cadmium cover thickness of 50/1000 inches, equivalent to 1.27 mm. Penetration measurements were made along the nuclear centre line, which was the horizontal axis of the system passing through the centre of the fission plate. Lateral distributions were also measured at various positions in the shields, the foils being located at intervals of 25 cm up and down from the nuclear centre line. The labelling convention for the measurement locations is given in FIG. 2.7.

A fraction of the neutrons present in the experimental array originated from leakage from the NESTOR core. To obtain a true comparison between measurement and a calculation using the fission plate source, the NESTOR core component must be subtracted from the measurement. There are two methods by which the background component can be estimated.

The best method is to repeat the measurement with the fissile content of the fission plate removed, i.e. an unfuelled measurement. This is a time consuming method as measurements have to be made twice at every point, once with the fuel and once without. The combination of low fluxes and low sensitivities of integral dosimeters can make foreground fuelled measurements difficult at deep penetration with the result that unfuelled measurements become impossible.

Background corrections of acceptable accuracy can be made for the high energy threshold reactions by a second method using the hydrogen filled proportional counters of the TNS system /26/ in integral mode. Here measurements of the neutron count-rates in the shield with the ASPIS shutter open and closed are required together with a measure of the shut-down ratio of the fission plate when the neutron shutter is closed. This technique was used for determining the background correction for the proportional counters; the correction was found to be around 2% throughout the shield and a value of 2% is recommended for the four threshold activation dosimeters at all positions in the shield.

The unfuelled technique for background correction was adopted for the gold measurements as there was a significant component of the low energy flux which did not arise from the fission plate, particularly near the fission plate itself where the fuelled to unfuelled ratio could be as low as 3.

The reaction effective threshold energies for the Rh-103(n,n'), In-115(n,n'), S-32(n,p) and Al-27(n,α) dosimeters, in a U-235 fission neutron spectrum similar to that of the Iron-88 experiment, are respectively 0.69 MeV, 1.30 MeV, 2.8 MeV and 7.30 MeV (see /27/). Nevertheless, since the effective threshold energy is not a completely satisfactory parameter for the characterization of the energy dependent cross section functions, the reported values give only a rough indication of the start of the response for the specific dosimeter.

If one wishes to characterize the dosimeter response energy range more accurately, the energy range corresponding to 90% of the response and the median energy of the response should be taken into account. The median energy is defined such that, in the specific spectrum, the responses below and above this energy numerical value are equal. Secondly, the definition of the energy range corresponding to 90% of the total response of a dosimeter implies that 5% of the response is below the lower boundary and 5% above the upper boundary of this energy range. A synthesis of these data for the four dosimeters used in the Iron-88 experiment was taken from reference /27/ and it is reported in TAB. 2.4 to give more specific detailed information, addressed to obtain a more precise analysis in the comparison of the experimental and calculated dosimetric results.
In practice the experimental results coming from Rh-103(n,n'), In-115(n,n') (see /28/), S-32(n,p) and Al-27(n,α) correspond respectively to neutron fluxes above about 0.1 MeV, 1.0 MeV, 3.0 MeV and 8.0 MeV.

TAB. 2.4

Iron-88 - Threshold Activation Dosimeter Parameters in a U-235 Fission Neutron Spectrum.

Dosimeter	Effective Threshold Energy [MeV]	90% Response Energy Range [MeV]	Median Energy [MeV]
Rh-103(n,n')	0.69	0.72 - 5.8	2.3
In-115(n,n')	1.30	1.1 - 5.9	2.6
S-32(n,p)	2.80	2.3 - 7.3	4.0
Al-27(n,α)	7.30	6.4 - 12.0	8.6

FIG. 2.7

Iron-88 - Measurement Locations [a].

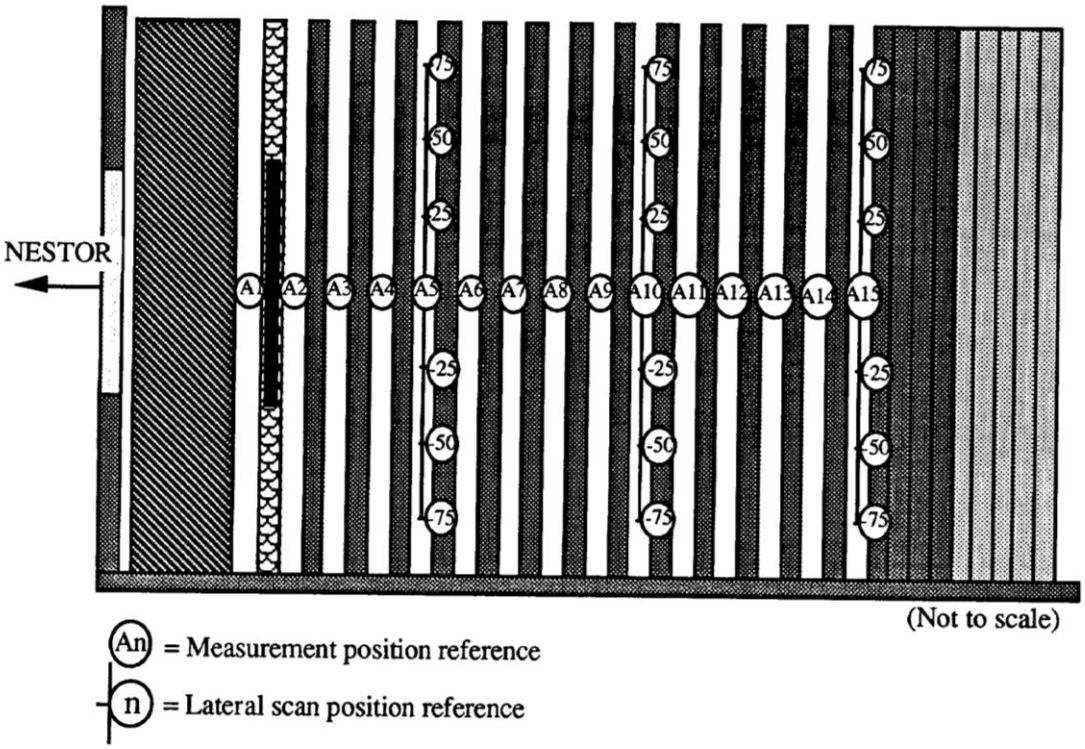

Penetration measurements are located on the nuclear centre line as defined below

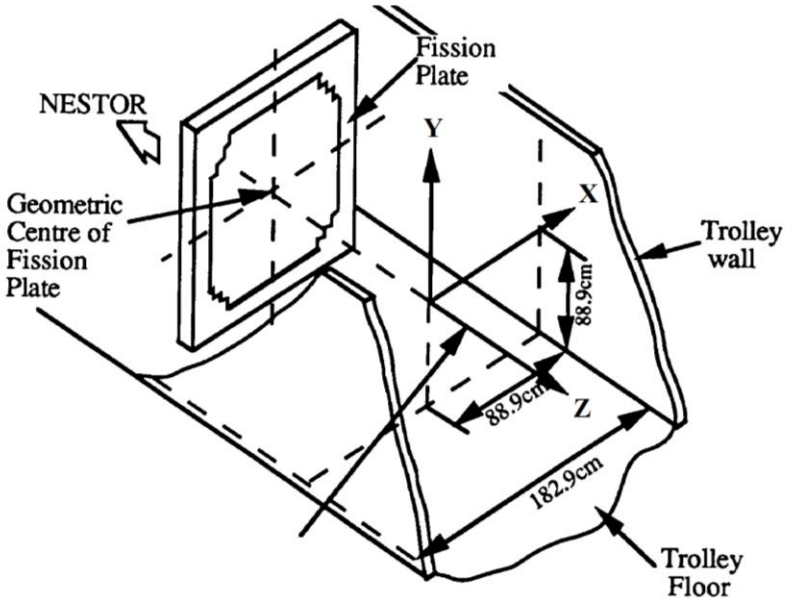

([a]) Figure derived from Figure 2 of reference /10/.

3 - CROSS SECTION LIBRARIES AND NUCLEAR DATA

The group working cross section libraries (BUGJEFF311.BOLIB /2/, BUGENDF70.BOLIB /3/, BUGLE-B7 /7/ and BUGLE-96 /8/) and the nuclear data (the reactor dosimetry cross sections /20/ derived from IRDF-2002 /21/ and the JEFF-3.1.1, ENDF/B-VII.0 and ENDF/B-VI.3 U-235 fission neutron spectra in the BUGLE-96 neutron group structure) used in the present deterministic transport analysis are briefly described in this chapter. It is underlined that the ENEA-Bologna BUGJEFF311.BOLIB and BUGENDF70.BOLIB libraries and the ORNL BUGLE-B7 library adopt the same neutron (see TAB. 3.1) and photon (see TAB. 3.2) group structure (47 neutron groups + 20 photon groups) of the ORNL BUGLE-96 library. The cited libraries are broad-group coupled neutron/photon working cross section libraries in FIDO-ANISN /1/ format with parameterized cross section sets of problem-dependent self-shielded neutron cross sections, dedicated to LWR radiation shielding and radiation damage applications and, in particular, to the reactor pressure vessel (RPV) dosimetry analyses. At present they are the only free-released BUGLE-type libraries at OECD-NEADB and ORNL-RSICC.

3.1 - BUGJEFF311.BOLIB Cross Section Library

BUGJEFF311.BOLIB /2/ is an ENEA-Bologna broad-group (47 neutron groups + 20 photon groups) coupled neutron and photon working cross section library in FIDO-ANISN format, generated in 2011 in the same energy group structure of the ORNL BUGLE-96 /8/ similar library. It is based on the OECD-NEADB JEFF-3.1.1 /4/ /5/ evaluated nuclear data library. The BUGJEFF311.BOLIB broad-group library was obtained through problem-dependent cross section collapsing and self-shielding from the ENEA-Bologna VITJEFF311.BOLIB /29/ fine-group coupled neutron and photon pseudo-problem-independent library in AMPX format for nuclear fission applications. VITJEFF311.BOLIB adopts the same fine-group energy structure (199 neutron groups + 42 photon groups) of the ORNL VITAMIN-B6 /8/ library (mother library of BUGLE-96) and it is based on the Bondarenko /30/ (f-factor) method for the treatment of neutron resonance self-shielding and temperature effects.
BUGJEFF311.BOLIB, dedicated to LWR shielding and pressure vessel dosimetry applications, was generated using the ENEA-Bologna 2007 Revision /31/ of the ORNL SCAMPI /32/ nuclear data processing system, able to treat double precision data and freely released at OECD-NEADB and ORNL-RSICC.
The BUGJEFF311.BOLIB library was firstly freely released to OECD-NEADB and then to ORNL-RSICC, assuming respectively the designations NEA-1866 ZZ BUGJEFF311.BOLIB and DLC-254 BUGJEFF311.BOLIB. It is underlined that BUGJEFF311.BOLIB was the first BUGLE-type multi-group working library, based on OECD-NEADB JEFF nuclear data.

3.2 - BUGENDF70.BOLIB Cross Section Library

BUGENDF70.BOLIB /3/ is an ENEA-Bologna broad-group (47 neutron groups + 20 photon groups) coupled neutron and photon working cross section library in FIDO-ANISN format, generated in 2013 in the same energy group structure of the ORNL BUGLE-96 /8/ similar library. It is based on the US ENDF/B-VII.0 /6/ evaluated nuclear data library. The BUGENDF70.BOLIB broad-group library was obtained through problem-dependent cross section collapsing and self-shielding from the ENEA-Bologna VITENDF70.BOLIB /33/ fine-group coupled neutron and photon pseudo-problem-independent library in AMPX format

for nuclear fission applications. VITENDF70.BOLIB adopts the same fine-group energy structure (199 neutron groups + 42 photon groups) of the ORNL VITAMIN-B6 /8/ library (mother library of BUGLE-96) and it is based on the Bondarenko /30/ (f-factor) method for the treatment of neutron resonance self-shielding and temperature effects.
BUGENDF70.BOLIB, dedicated to LWR shielding and pressure vessel dosimetry applications, was generated using the ENEA-Bologna 2007 Revision /31/ of the ORNL SCAMPI /32/ nuclear data processing system, able to treat double precision data and freely released at OECD-NEADB and ORNL-RSICC.
The BUGENDF70.BOLIB library was firstly freely released to OECD-NEADB and then to ORNL-RSICC, assuming respectively the designations NEA-1872 ZZ BUGENDF70.BOLIB and DLC-262 BUGENDF70.BOLIB.

3.3 - BUGLE-B7 Cross Section Library

BUGLE-B7 /7/ is an ORNL broad-group (47 neutron groups + 20 photon groups) coupled neutron and photon working cross section library in FIDO-ANISN format, generated in 2011 in the same energy group structure of the ORNL BUGLE-96 /8/ similar library. It is based on the US ENDF/B-VII.0 /6/ evaluated nuclear data library. The BUGLE-B7 broad-group library was obtained through problem-dependent cross section collapsing and self-shielding from the ORNL VITAMIN-B7 /7/ fine-group coupled neutron and photon pseudo-problem-independent library in AMPX format for nuclear fission applications. VITAMIN-B7 adopts the same fine-group energy structure (199 neutron groups + 42 photon groups) of the ORNL VITAMIN-B6 /8/ library (mother library of BUGLE-96) and it is based on the Bondarenko /30/ (f-factor) method for the treatment of neutron resonance self-shielding and temperature effects.
BUGLE-B7, dedicated to LWR shielding and pressure vessel dosimetry applications, was generated through the ORNL AMPX-6-1.0 /34/ nuclear data processing system (not freely released at the time of the library generation in 2011), used also to produce the VITAMIN-B7 fine-group mother library of BUGLE-B7.
The BUGLE-B7 library was firstly freely released to ORNL-RSICC and then to OECD-NEADB, assuming respectively the designations DLC-245 VITAMIN-B7/BUGLE-B7 and DLC-0245 ZZ-VITAMINB7/BUGLEB7.

3.4 - BUGLE-96 Cross Section Library

BUGLE-96 /8/ is an ORNL broad-group (47 neutron groups + 20 photon groups) coupled neutron and photon working cross section library in FIDO-ANISN format generated in 1996. It is based on the US ENDF/B-VI.3 /9/ evaluated nuclear data library. BUGLE-96 was obtained through problem-dependent cross section collapsing and self-shielding from the ORNL VITAMIN-B6 /8/ fine-group (199 neutron groups + 42 photon groups) coupled neutron and photon pseudo-problem-independent library in AMPX format. VITAMIN-B6 was generated through the NJOY-94.15 nuclear data processing system and it is based on the Bondarenko /30/ (f-factor) method for the treatment of neutron resonance self-shielding and temperature effects. BUGLE-96, dedicated to LWR shielding and pressure vessel dosimetry applications, was generated using the version of the ORNL SCAMPI /32/ nuclear data processing system available in 1996. This library was freely released to ORNL-RSICC and then to OECD-NEADB where respectively assumed the designations DLC-0185 BUGLE-96 and DLC-0185 ZZ-BUGLE-96. It is underlined that BUGLE-96 and the fine-group mother library VITAMIN-B6, became reference standards (see /22/, ANSI/ANS-6.1.2-1999 (R2009))

as multi-group libraries recommended for shielding applications and they were successfully used all over the world.

TAB. 3.1

Neutron Group Energy and Lethargy Boundaries for the BUGLE-Type Libraries.

Group	Upper Energy [MeV]	Upper Lethargy
1	1.7332E+07	-5.4997E-01
2	1.4191E+07	-3.5002E-01
3	1.2214E+07	-2.0000E-01
4	1.0000E+07	0.
5	8.6071E+06	1.5000E-01
6	7.4082E+06	3.0000E-01
7	6.0653E+06	5.0000E-01
8	4.9659E+06	7.0000E-01
9	3.6788E+06	1.0000E-00
10	3.0119E+06	1.2000E+00
11	2.7253E+06	1.3000E+00
12	2.4660E+06	1.4000E+00
13	2.3653E+06	1.4417E+00
14	2.3457E+06	1.4500E+00
15	2.2313E+06	1.5000E+00
16	1.9205E+06	1.6500E+00
17	1.6530E+06	1.8000E+00
18	1.3534E+06	2.0000E+00
19	1.0026E+06	2.3000E+00
20	8.2085E+05	2.5000E+00
21	7.4274E+05	2.6000E+00
22	6.0810E+05	2.8000E+00
23	4.9787E+05	3.0000E+00
24	3.6883E+05	3.3000E+00
25	2.9721E+05	3.5159E+00
26	1.8316E+05	4.0000E+00
27	1.1109E+05	4.5000E+00
28	6.7379E+04	5.0000E+00
29	4.0868E+04	5.5000E+00
30	3.1828E+04	5.7500E+00
31	2.6058E+04	5.9500E+00
32	2.4176E+04	6.0250E+00
33	2.1875E+04	6.1250E+00
34	1.5034E+04	6.5000E+00
35	7.1017E+03	7.2500E+00
36	3.3546E+03	8.0000E+00
37	1.5846E+03	8.7500E+00
38	4.5400E+02	1.0000E+01
39	2.1445E+02	1.0750E+01
40	1.0130E+02	1.1500E+01
41	3.7266E+01	1.2500E+01
42	1.0677E+01	1.3750E+01
43	5.0435E+00	1.4500E+01
44	1.8554E+00	1.5500E+01
45	8.7643E-01	1.6250E+01
46	4.1399E-01	1.7000E+01
47	1.0000E-01	1.8421E+01
	1.0000E-05	2.7631E+01

TAB. 3.2

Photon Group Energy Boundaries for the BUGLE-Type Libraries.

Group	Upper Energy [MeV]
1	1.4000E+07
2	1.0000E+07
3	8.0000E+06
4	7.0000E+06
5	6.0000E+06
6	5.0000E+06
7	4.0000E+06
8	3.0000E+06
9	2.0000E+06
10	1.5000E+06
11	1.0000E+06
12	8.0000E+05
13	7.0000E+05
14	6.0000E+05
15	4.0000E+05
16	2.0000E+05
17	1.0000E+05
18	6.0000E+04
19	3.0000E+04
20	2.0000E+04
	1.0000E+04

3.5 - IRDF-2002 Dosimeter Cross Sections

The activation dosimeter cross sections for the Au-197(n,γ)Au-198 nuclear reactions (see FIGs. 3.1÷3.7 and TABs. 3.3÷3.4) and the threshold activation dosimeter cross sections for the Rh-103(n,n')Rh-103m (see FIGs. 3.8÷3.9 and TABs. 3.5÷3.9), In-115(n,n')In-115m (see FIGs. 3.10÷3.11 and TABs. 3.5÷3.9), S-32(n,p)P-32 (see FIGs. 3.12÷3.13 and TABs. 3.5÷3.9) and Al-27(n,α)Na-24 (see FIGs. 3.14÷3.17 and TABs. 3.5÷3.9) nuclear reactions, used in the present Iron-88 transport analysis, were derived (see for example /2/, /3/ and /20/) from the IAEA IRDF-2002 /21/ International Reactor Dosimetry File.

The nuclear reaction cross sections for the Au-197(n,γ)Au-198, Rh-103(n,n')Rh-103m, In-115(n,n')In-115m, S-32(n,p)P-32 and Al-27(n,α)Na-24 activation dosimeters were obtained in the 47-group neutron energy structure (see TAB. 3.1), typical of the BUGJEFF311.BOLIB /2/, BUGENDF70.BOLIB /3/, BUGLE-B7 /7/ and BUGLE-96 /8/ libraries.

The dosimeter cross sections for the calculations using the BUGJEFF311.BOLIB, BUGENDF70.BOLIB, BUGLE-B7 and BUGLE-96 libraries were obtained from IRDF-2002, through the GROUPIE module of the PREPRO /35/ nuclear data processing system. Two types of neutron weighting spectrum in the 199-group neutron energy structure, typical of the VITJEFF311.BOLIB /29/, VITENDF70.BOLIB /33/, VITAMIN-B7 /7/ and VITAMIN-B6 /8/ corresponding mother libraries, were used in GROUPIE to generate the 47-group dosimeter cross sections. In particular the same flat weighting spectrum was used to generate the corresponding 47-group activation dosimeter cross section set to be used with all the four BUGLE-type libraries whilst four 1/4 T PV weighting spectra, separately generated through the use (see for example /2/and /3/) of each VITAMIN-type mother library, were employed to produce the corresponding four 47-group activation dosimeter cross section sets to be singularly used with each corresponding BUGLE-type library.

In particular, as flat neutron weighting spectrum, the constant numerical value of unity was attributed to all the neutron groups of the 199-group flat neutron spectrum used in GROUPIE to generate five flat weighting dosimeter cross section sets (one for each of the total five types of dosimeters employed in Iron-88), obviously used by all the four BUGLE-type libraries.
On the contrary, the four 1/4 T PV neutron weighting spectra, used to generate the four dosimeter cross section sets separately employed in the calculations with the BUGJEFF311.BOLIB, BUGENDF70.BOLIB, BUGLE-B7 and BUGLE-96 libraries, were obtained (see for example /2/, /3/ and /20/) through four fixed source one-dimensional transport calculations. These 1D transport analyses, using respectively the VITJEFF311.BOLIB, VITENDF70.BOLIB, VITAMIN-B7 and VITAMIN-B6 corresponding fine-group mother libraries, were conceived to describe the in-vessel and ex-vessel radial geometry of a PWR. In particular the four previously cited 1/4 T PV neutron weighting spectra were calculated in a steel zone, the reactor pressure vessel (PV) of a PWR, at a spatial position corresponding to one quarter of the thickness (T) of the reactor pressure vessel (1/4 T PV).
Concerning the two 1/4 T PV weighting dosimeter cross section sets, separately employed in the transport calculations using BUGLE-B7 and BUGLE-96, they were obtained in ENEA-Bologna, for the present transport analysis, with the same PREPRO calculation procedure previously cited. In this case, the two original 199-group 1/4 T PV neutron weighting spectra, calculated at ORNL in the same PV spatial position through the

VITAMIN-B7 and VITAMIN-B6 fine-group mother libraries of BUGLE-B7 and BUGLE-96 respectively, were alternatively used in GROUPIE.

The 47-group dosimeter cross sections, obtained with both the flat weighting and the 1/4 T PV weighting neutron spectra, were in general employed in all the calculations but, for the transport analysis dedicated to the Iron-88 single-material (iron) neutron shielding benchmark experiment, the dosimeter cross sections obtained with the four 1/4 T PV weighting spectra were considered more proper. In fact these neutron weighting spectra, obtained within a reactor PV steel region, are obviously more similar to the neutron spectrum present in the Iron-88 experimental region made of steel.

It is underlined that a unique flat weighting cross section set in the 47-group neutron energy structure for each specific dosimeter nuclear reaction was employed in the transport calculations using the BUGJEFF311.BOLIB, BUGENDF70.BOLIB, BUGLE-B7 and BUGLE-96 libraries, as already previously reported.
On the contrary, for each specific dosimeter nuclear reaction, the corresponding group numerical values of the four 1/4 T PV weighting cross section sets, respectively used to obtain the dosimetric results in the BUGJEFF311.BOLIB, BUGENDF70.BOLIB, BUGLE-B7 and BUGLE-96 calculations, are slightly different. In fact the four 1/4 T PV weighting dosimeter cross section sets, respectively used in the calculations with BUGJEFF311.BOLIB, BUGENDF70.BOLIB, BUGLE-B7 and BUGLE-96, were obtained through GROUPIE, using separately four slightly different 199-group 1/4 T PV neutron weighting spectra. The last cited neutron spectra, previously calculated using the VITJEFF311.BOLIB, VITENDF70.BOLIB, VITAMIN-B7 and VITAMIN-B6 corresponding mother libraries, based respectively on JEFF-3.1.1 /4/, ENDF/B-VII.0 /6/, ENDF/B-VII.0 and ENDF/B-VI.3 /9/ nuclear data, are in particular slightly different since they were obtained from calculations using libraries based on different nuclear data or libraries processed with different nuclear data processing systems. For example, for the two fine-group mother libraries VITENDF70.BOLIB and VITAMIN-B7 based on ENDF/B-VII.0, the LANL NJOY-99.259 /36/ and the ORNL AMPX-6.1 /34/ data processing systems were respectively used for their generation and so slightly different 199-group 1/4 T PV neutron weighting spectra were calculated.

It is then underlined that, differently from the four threshold activation dosimeters used in the Iron-88 experiment, the Au-197(n,γ)Au-198 cross sections must be self-shielded for the neutron resonance absorption through a methodology described hereinafter.

For the Au-197(n,γ)Au-198 and Al-27(n,α)Na-24 dosimeter cross sections, characterized by the highest differences between the flat weighting and the 1/4 T PV weighting cross sections, the ratios of the 1/4 T PV weighting cross sections divided by the corresponding flat weighting cross sections used in the calculations with the BUGJEFF311.BOLIB and the BUGLE-96 libraries are reported. In particular the self-shielded cross section ratios for Au-197(n,γ)Au-198 are reported in the FIGs. 3.6 and 3.7, respectively for BUGJEFF311.BOLIB and BUGLE-96, whilst the corresponding cross section ratios for Al-27(n,α)Na-24 are respectively shown in the FIGs. 3.16 and 3.17. In particular, the self-shielded cross section ratios reproduced in the FIGs. 3.6 and 3.7 for Au-197(n,γ)Au-198 are derived respectively from the corresponding cross section data shown in the FIGs. 3.4 and 3.5 and tabulated in the TABs. 3.3 and 3.4. The cross section ratios presented in the FIGs. 3.16 and 3.17 for Al-27(n,α)Na-24 are instead derived respectively from the

corresponding cross section data represented in the FIGs. 3.14 and 3.15 and tabulated in the TABs. 3.5, 3.6 and 3.9.

The flat weighting Au-197(n,γ)Au-198 activation cross sections with proper self-shielding were compared in FIG. 3.1 with the corresponding cross sections without self-shielding.
Comparisons of the 1/4 T PV weighting Au-197(n,γ)Au-198 cross sections with and without self-shielding are shown in FIG. 3.2 and FIG. 3.3, exclusively for the BUGJEFF311.BOLIB library and the BUGLE-96 reference library respectively. Comparisons of flat weighting vs. 1/4 T PV weighting Au-197(n,γ)Au-198 neutron self-shielded cross sections are represented in FIG. 3.4 and FIG. 3.5, respectively for the cross sections used in the calculations with the BUGJEFF311.BOLIB and the BUGLE-96 Libraries. With respect to the self-shielded cross sections shown in FIG. 3.4 and FIG. 3.5, the ratios of the Au-197(n,γ)Au-198 1/4 T PV weighting cross sections divided by the corresponding flat weighting cross sections are reported in FIG. 3.6 and FIG. 3.7, respectively for the self-shielded cross sections used in the calculations with the BUGJEFF311.BOLIB and the BUGLE-96 libraries.

Finally it is reported herewith in detail the methodology used to self-shield the Au-197(n,γ)Au-198 cross sections and to identify the proper numerical value of the cadmium cutoff energy for the Au-197(n,γ)Au-198 epi-cadmium reaction rate measurements, taking into account the thickness of the cadmium cover employed together with the gold dosimeters, in the Iron-88 benchmark experiment specific conditions. The generation of the Au-197(n,γ)Au-198 cross sections was performed through the GROUPIE module of the PREPRO nuclear data processing system using a background cross section σ_0 equal to 1695.0 barns to take into account, in particular, the neutron self-shielding in the resolved resonance energy region. The reported numerical value of the background cross section σ_0 was obtained assuming that the total background cross section for a lump with finite dimensions is given by (see /37/, pages 9-41 and 9-42) the sum of a first component, given by the background cross section depending on the dilution rate of a specific nuclide in the isotopic material mixture of the lump, plus a second component, given by an escape cross section from the lump. For the gold foils, composed by a monoisotopic material, the first component is a negligible quantity equal to 0.0 or 1.0E-06 barns, as commonly assumed in the data processing calculation procedures. The second component is calculated herewith and can be considered equivalent to the total background cross section, used to self-shield properly the gold cross sections, since the first component is negligible.
For a lump of resonance material (gold foil) embedded in a large moderating region, escapes from the lump also increase the background cross section and the Wigner rational approximation is used to obtain an effective escape cross section “sigmaescape”. This additional escape cross section is given by:

$$sigmaescape = 1/(N \times \langle \ell \rangle),$$

where the mean chord length of the lump is given by $\langle \ell \rangle = 4V/S$ where:

S = Total area of the surface of the cylindrical gold foil (lump);
V = Total volume of the cylindrical gold foil (lump);
N = Atomic density of gold.

Therefore $4V/S = 4 \times \pi r^2 h / 2\pi r^2 = 2h$, where h (0.005 cm) is the thickness (or height) of the cylindrical gold foils used in the Iron-88 experiment, expressed in cm.

So we have $4V/S = 2 \times 0.005 = 0.01$ cm = mean chord length of the cylindrical lump (<ℓ> gold foil), considering negligible the area of the lateral cylindrical surface of the gold foils.

Then we have:

sigmaescape = $S/4V \times 1/N = 1/2h \times 1/N$.
Taking into account that N(Au-197) = gold density × Avogadro constant / gold gram atomic weight, we have:

N(Au-197) = $19.3 \times 0.602214129 / 196.967 = 5.9E\text{-}02$ atoms × $barns^{-1} \times cm^{-1}$

where:

gold density = 19.3 g × cm^{-3};
Avogadro constant = 0.60221414129 × 1.0E+24 atoms × mol^{-1};
gold gram atomic weight = 196.967 gram-atom.

Finally we have:

sigmaescape = $1/0.01 \times 1/5.9E\text{-}02 = 100 \times 169.949 = 1695.0$ barns

The epi-cadmium measurements with gold dosimeters were performed using gold foils inserted in cadmium covers able to absorb the thermal neutrons below a cutoff energy, depending on the cadmium cover thickness.
Taking into account that the cadmium cover thickness for the gold dosimeters employed in Iron-88 was equal to 50/1000 inches (1.27 mm), the cadmium cutoff energy for a thin 1/v neutron absorber, as a gold dosimeter, is about 0.73 eV, as can be deduced from reference /38/ (specifically from Figure 12.2.5 at page 276). The identification of an energy value for the effective experimental cadmium cutoff energy is necessary to decide how many neutron groups of the 47-group BUGLE-type neutron energy structure must be excluded to calculate correctly the total gold epi-cadmium reaction rates for the Iron-88 benchmark experiment.

Eliminating in particular, in the calculations with the BUGLE-type libraries, the two last neutron groups No. 46 and No. 47 of the BUGLE-type neutron energy structure (see TAB. 3.1), the effective cadmium cutoff energy is implicitly assumed at the classical 0.414 eV upper thermal threshold energy. Eliminating an additional neutron group, i.e. the neutron group No. 45, the effective cadmium cutoff energy is implicitly assumed at 0.876 eV, the upper energy limit of the neutron group No. 45.
Probably the most correct choice, adopted in the present work, is to eliminate from the calculations the gold reaction rate contributions of the three previously cited last neutron groups. In fact the energy value nearer to 0.73 eV, i.e. the effective cadmium cutoff energy corresponding to a cadmium cover thickness of 1.27 mm, is 0.876 eV, the upper energy limit of the neutron group No. 45 in a BUGLE-type neutron energy group structure.

FIG. 3.1

Comparison of the Flat Weighting Au-197(n,γ)Au-198 Neutron Cross Sections with and without Self-Shielding Used in the Calculations with the BUGJEFF311.BOLIB, BUGENDF70.BOLIB, BUGLE-B7 and BUGLE-96 Libraries.

47-Group Neutron Energy Structure Typical of the BUGLE-Type Libraries.

Self-Shielding Calculated Assuming a Background Cross Section σ_0 = 1695.0 barns.

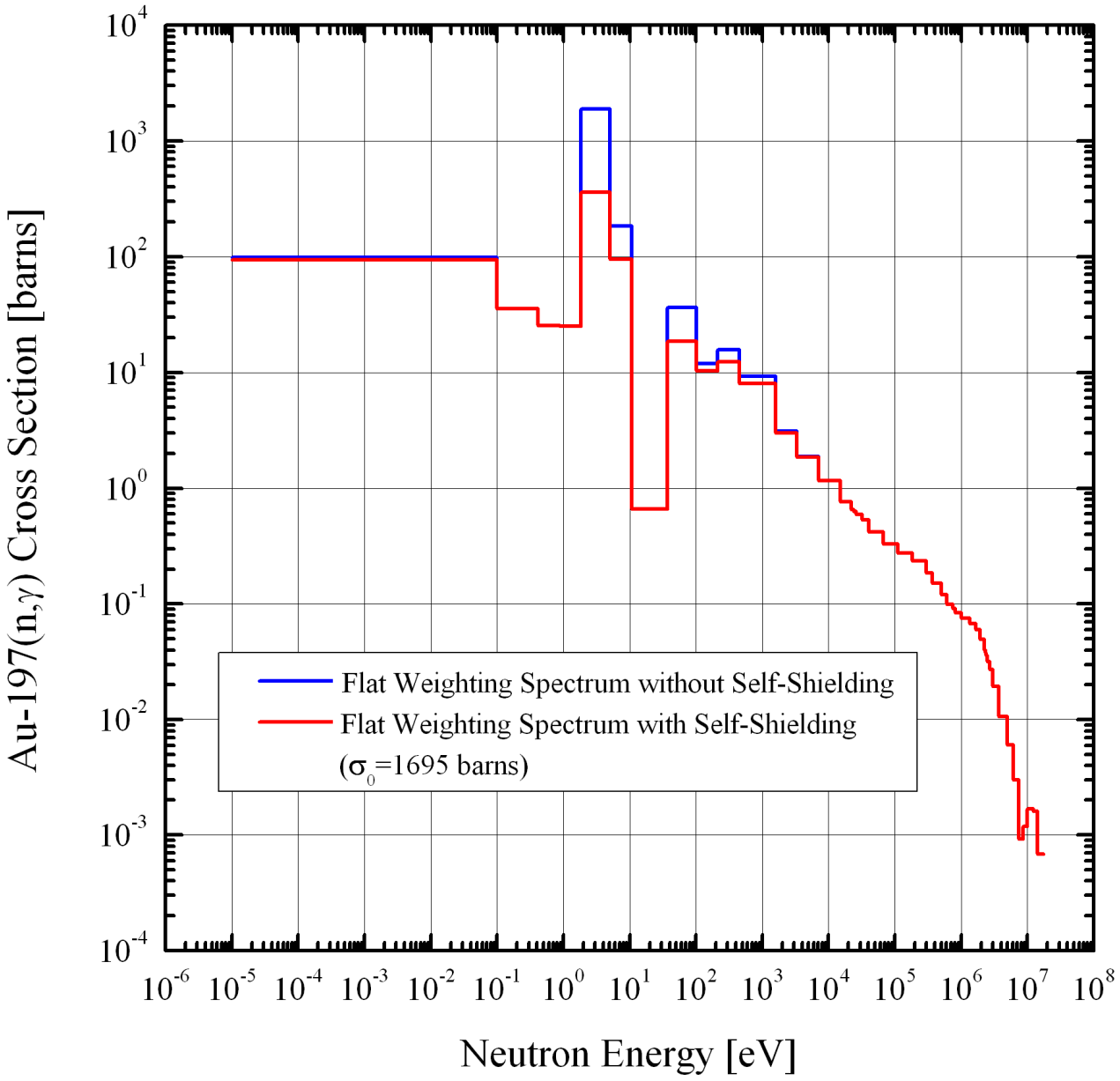

FIG. 3.2

Comparison of the 1/4 T PV Weighting Au-197(n,γ)Au-198 Neutron Cross Sections
with and without Self-Shielding Used in the Calculations
with the BUGJEFF311.BOLIB Library.

47-Group Neutron Energy Structure Typical of the BUGLE-Type Libraries.

Self-Shielding Calculated Assuming a Background Cross Section σ_0 = 1695.0 barns.

1/4 T PV Weighting Au-197(n,γ)Au-198 Neutron Cross Sections
Obtained through Data Processing Using the 199-Group Neutron Spectrum
Calculated in the 1/4 T PV Position with the VITJEFF311.BOLIB Library.

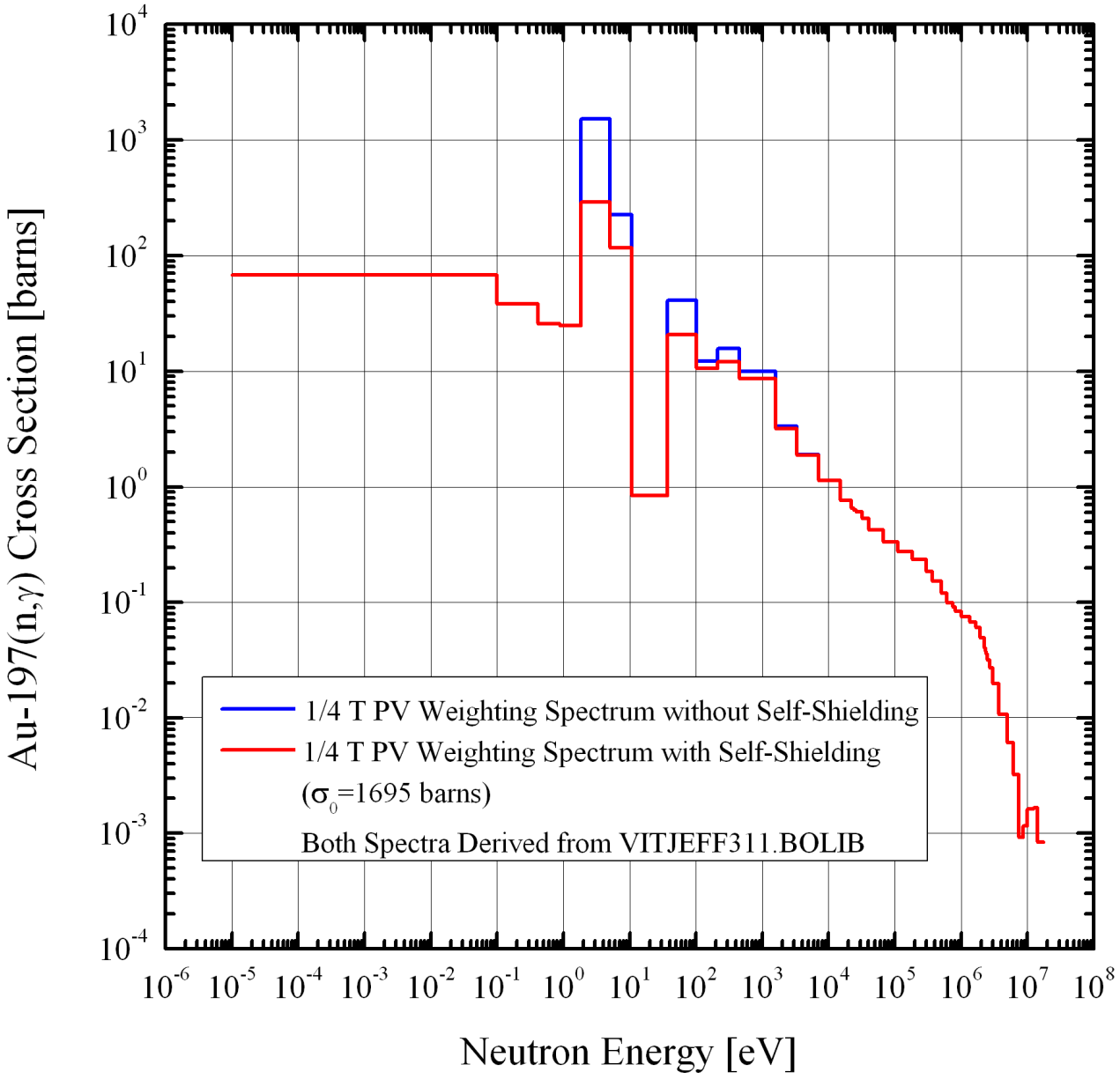

FIG. 3.3

Comparison of the 1/4 T PV Weighting Au-197(n,γ)Au-198 Neutron Neutron Cross Sections
with and without Self-Shielding Used in the Calculations
with the BUGLE-96 Library.

47-Group Neutron Energy Structure Typical of the BUGLE-Type Libraries.

Self-Shielding Calculated Assuming a Background Cross Section σ_0 = 1695.0 barns.

1/4 T PV Weighting Au-197(n,γ)Au-198 Neutron Cross Sections
Obtained through Data Processing Using the 199-Group Neutron Spectrum
Calculated in the 1/4 T PV Position with the VITAMIN-B6 Library.

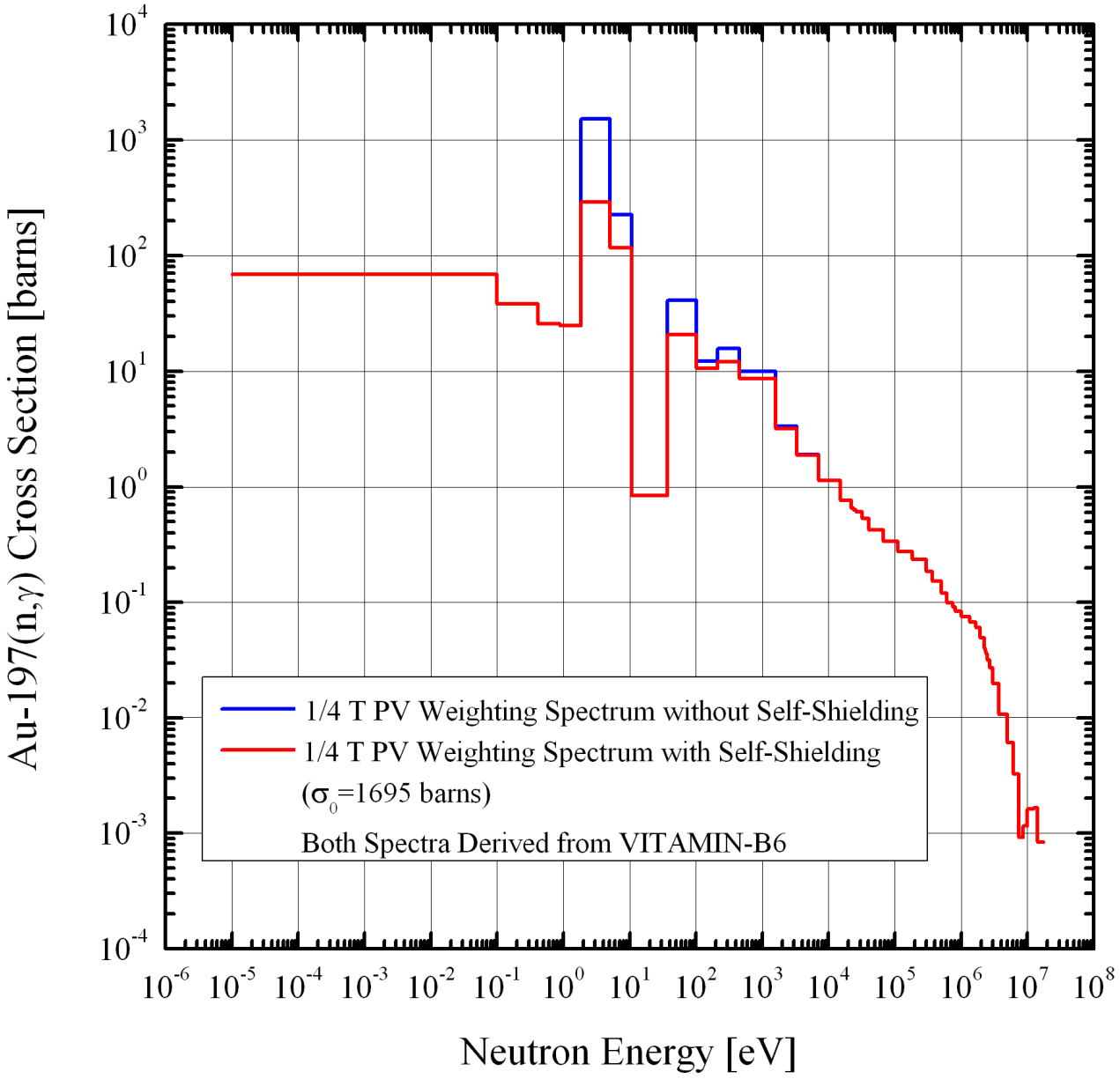

FIG. 3.4

Comparison of Flat Weighting vs. 1/4 T PV Weighting Au-197(n,γ)Au-198
Neutron Cross Sections with Self-Shielding Used in the Calculations
with the BUGJEFF311.BOLIB Library.

47-Group Neutron Energy Structure Typical of the BUGLE-Type Libraries.

Self-Shielding Calculated Assuming a Background Cross Section σ_0 = 1695.0 barns.

1/4 T PV Weighting Au-197(n,γ)Au-198 Neutron Self-Shielded Cross Sections
Obtained through Data Processing Using the 199-Group Neutron Spectrum
Calculated in the 1/4 T PV Position with the VITJEFF311.BOLIB Library.

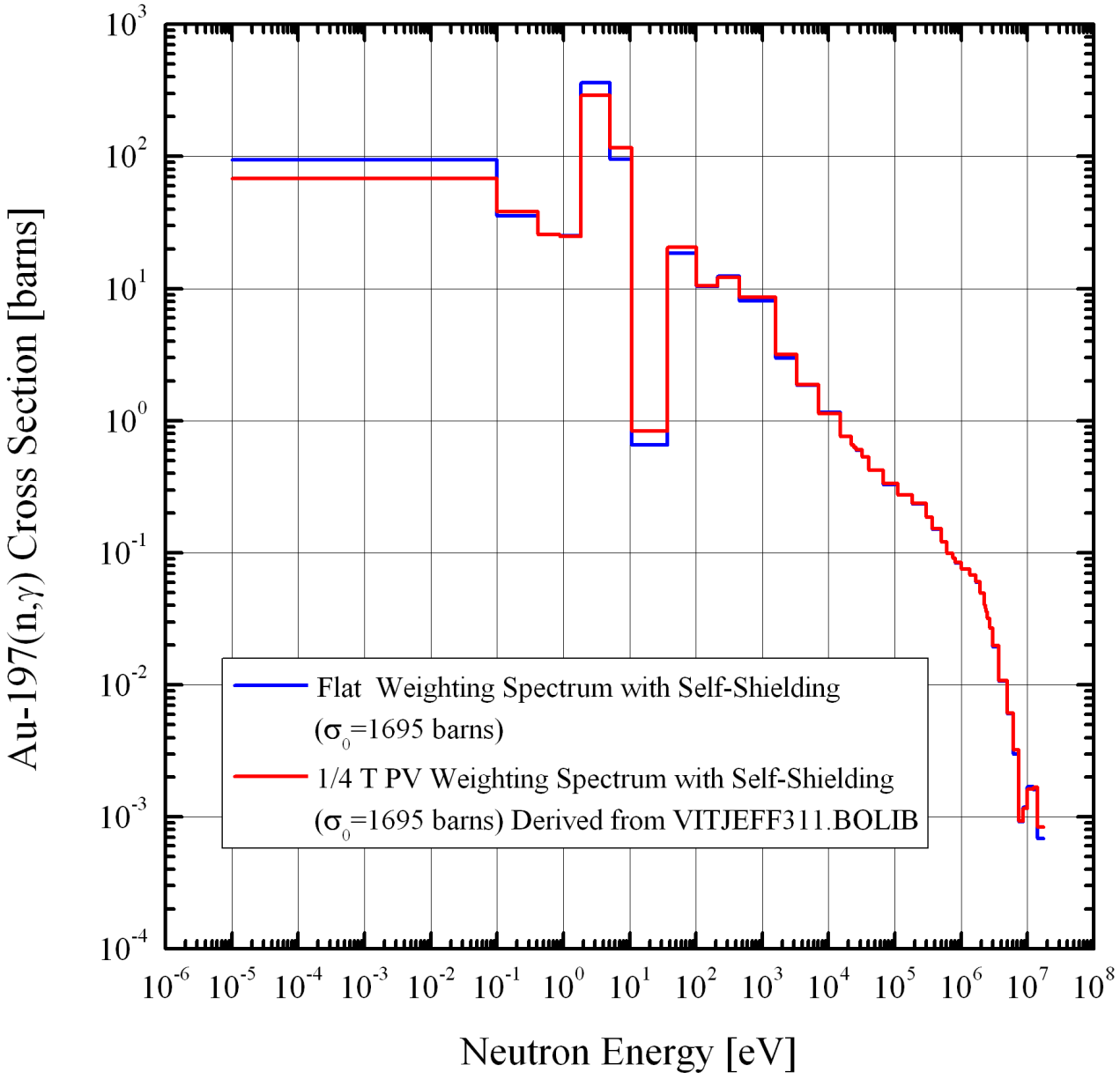

FIG. 3.5

Comparison of Flat Weighting vs. 1/4 T PV Weighting Au-197(n,γ)Au-198
Neutron Cross Sections with Self-Shielding Used in the Calculations
with the BUGLE-96 Library.

47-Group Neutron Energy Structure Typical of the BUGLE-Type Libraries.

Self-Shielding Calculated Assuming a Background Cross Section σ_0 = 1695.0 barns.

1/4 T PV Weighting Au-197(n,γ)Au-198 Neutron Self-Shielded Cross Sections
Obtained through Data Processing Using the 199-Group Neutron Spectrum
Calculated in the 1/4 T PV Position with the VITAMIN-B6 Library.

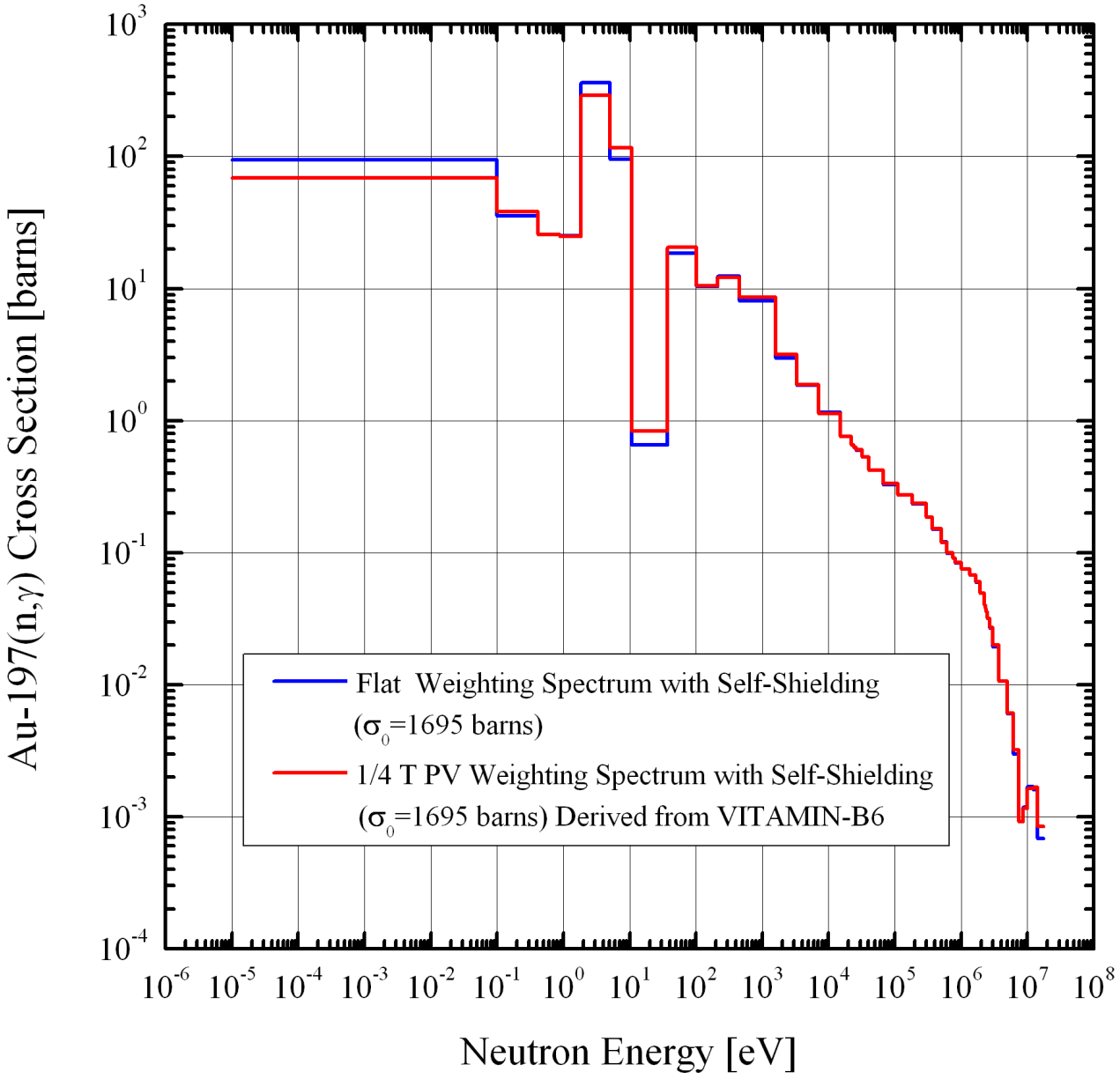

FIG. 3.6

Ratio (1/4 T PV Weighting / Flat Weighting) of the Au-197(n,γ)Au-198
Neutron Cross Sections with Self-Shielding Used in the Calculations
with the BUGJEFF311.BOLIB Library.

47-Group Neutron Energy Structure Typical of the BUGLE-Type Libraries.

1/4 T PV Weighting Au-197(n,γ)Au-198 Neutron Cross Sections
Obtained through Data Processing Using the 199-Group Neutron Spectrum
Calculated in the 1/4 T PV Position with the VITJEFF311.BOLIB Library.

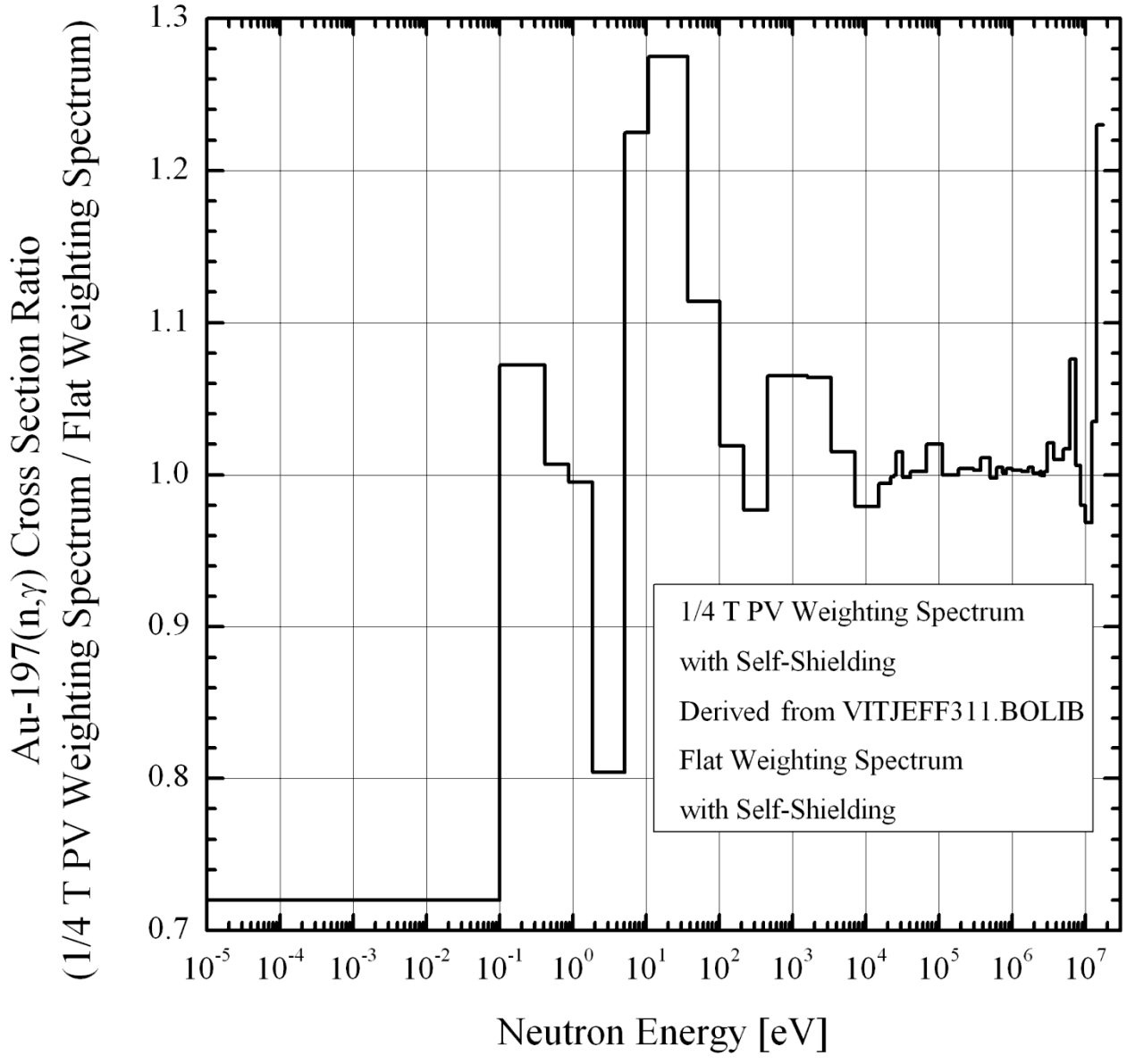

FIG. 3.7

Ratio (1/4 T PV Weighting / Flat Weighting) of the Au-197(n,γ)Au-198
Neutron Cross Sections with Self-Shielding Used in the Calculations
with the BUGLE-96 Library.

47-Group Neutron Energy Structure Typical of the BUGLE-Type Cross Section Libraries.

1/4 T PV Weighting Au-197(n,γ)Au-198 Neutron Self-Shielded Cross Sections
Obtained through Data Processing Using the 199-Group Neutron Spectrum
Calculated in the 1/4 T PV Position with the VITAMIN-B6 Library.

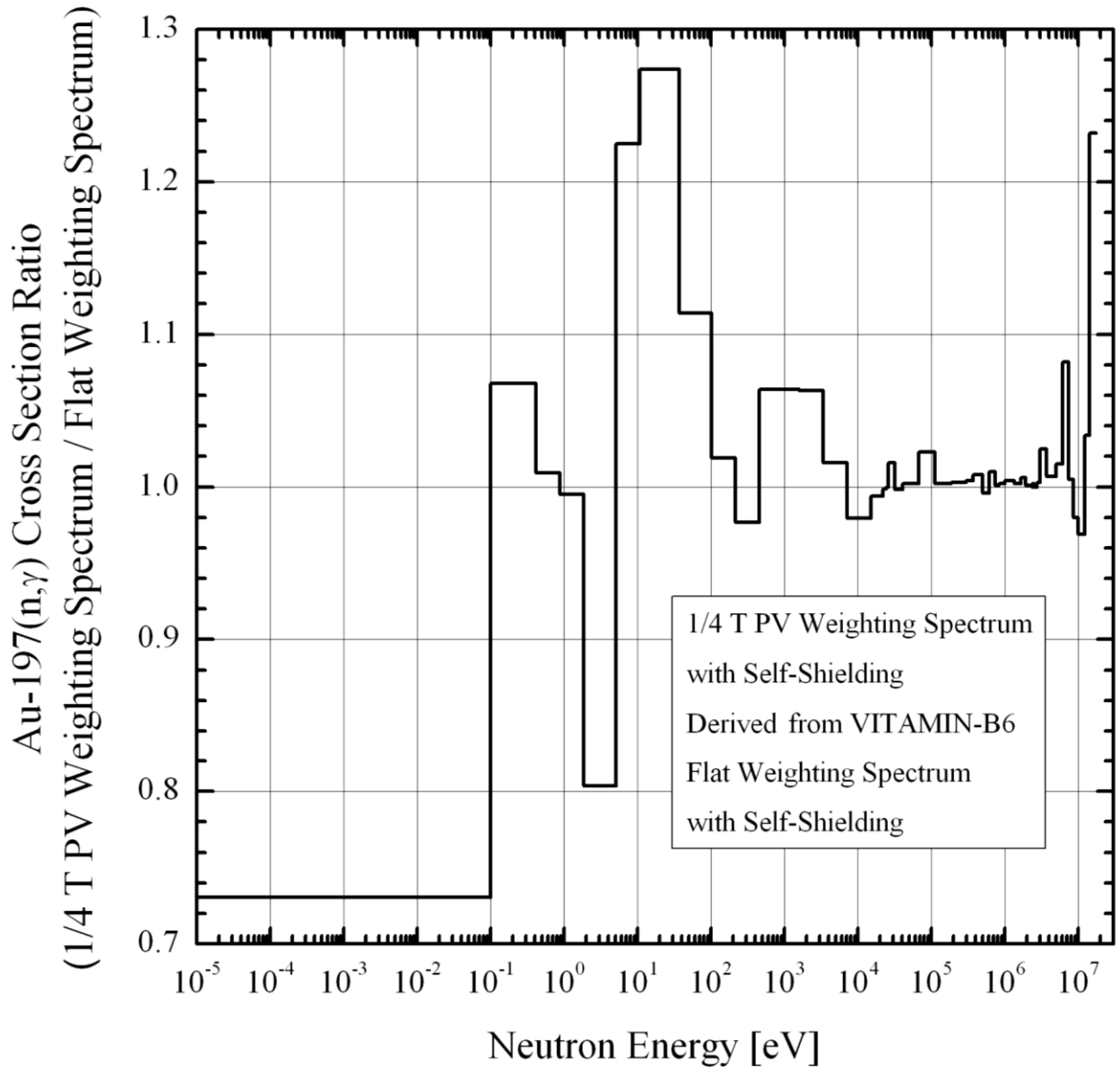

FIG. 3.8

Comparison of the IRDF-2002 Flat Weighting vs. 1/4 T PV Weighting
Rh-103(n,n')Rh-103m Dosimeter Cross Sections
Used with the BUGJEFF311.BOLIB Library.

47-Group Neutron Energy Structure Typical of the BUGLE-Type Libraries.

1/4 T PV Weighting Rh-103(n,n')Rh-103m Neutron Cross Sections
Obtained through Data Processing Using the 199-Group Neutron Spectrum
Calculated in the 1/4 T PV Position with the VITJEFF311.BOLIB Library.

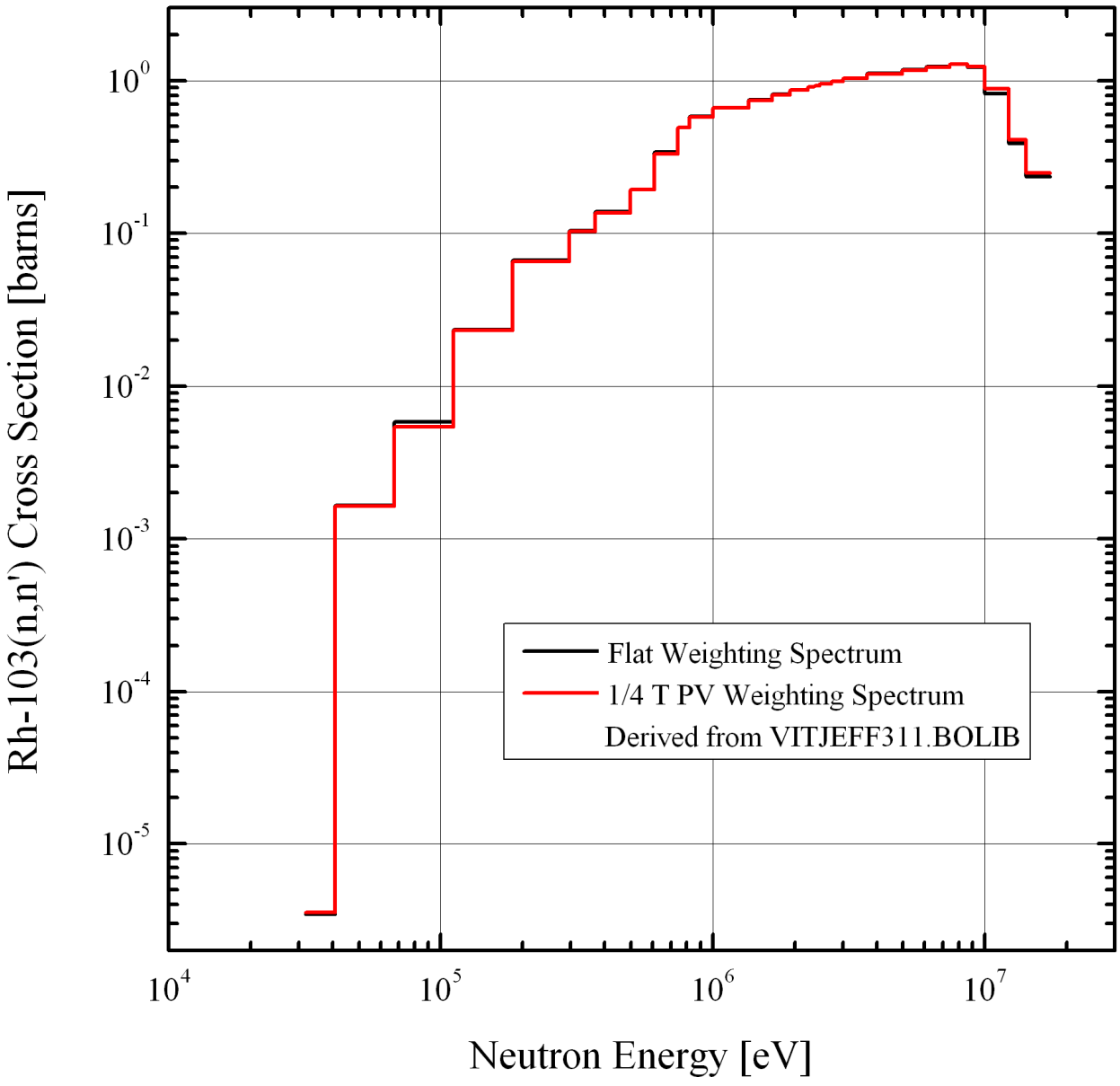

FIG. 3.9

Comparison of the IRDF-2002 Flat Weighting vs. 1/4 T PV Weighting
Rh-103(n,n')Rh-103m Dosimeter Cross Sections
Used with the BUGLE-96 library

47-Group Neutron Energy Structure Typical of the BUGLE-Type Libraries.

1/4 T PV Weighting Rh-103(n,n')Rh-103m Neutron Cross Sections
Obtained through Data Processing Using the 199-Group Neutron Spectrum
Calculated in the 1/4 T PV Position with the VITAMIN-B6 Library.

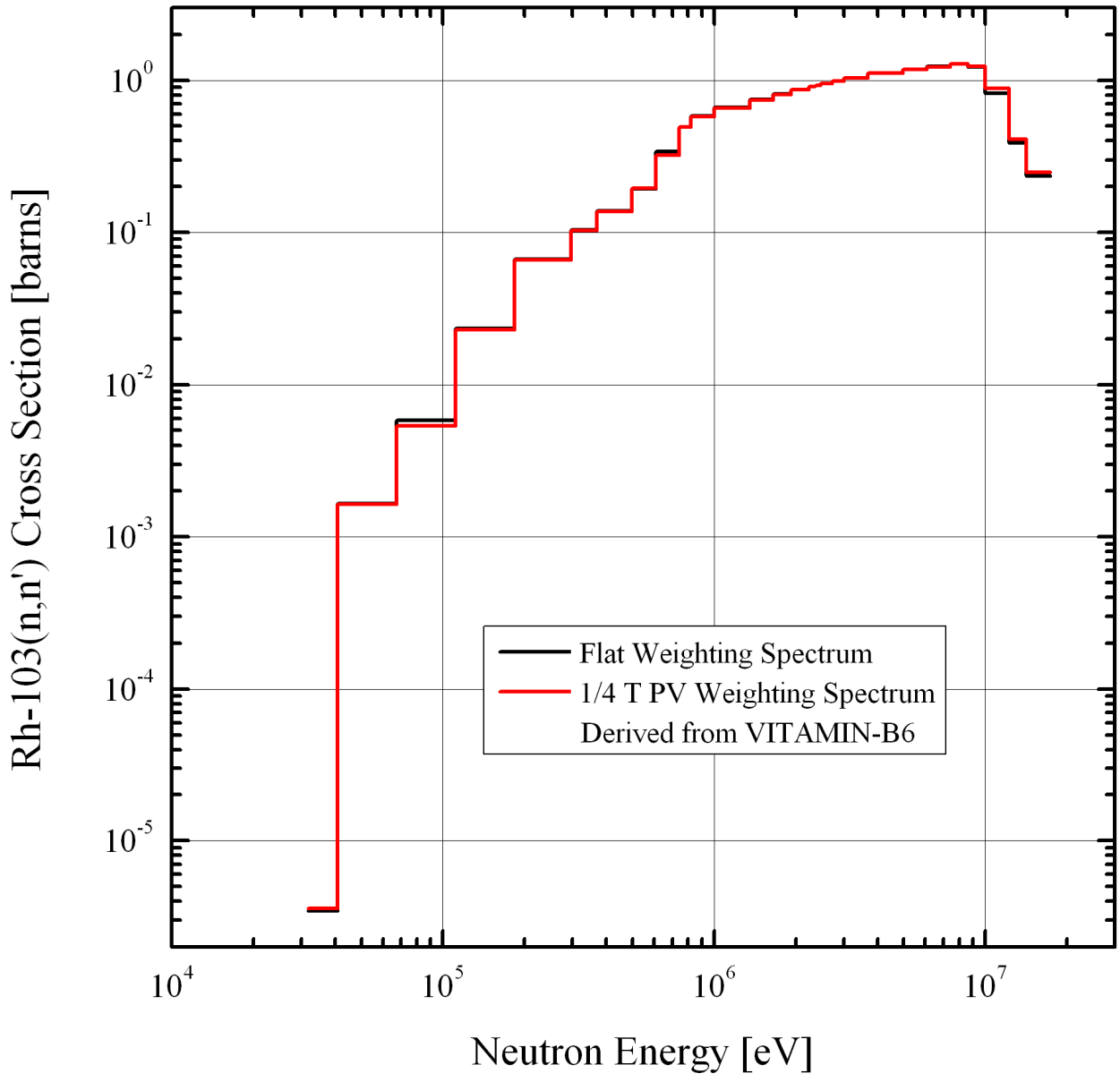

FIG. 3.10

Comparison of the IRDF-2002 Flat Weighting vs. 1/4 T PV Weighting
In-115(n,n')In-115m Dosimeter Cross Sections
Used with the BUGJEFF311.BOLIB Library.

47-Group Neutron Energy Structure Typical of the BUGLE-Type Libraries.

1/4 T PV Weighting In-115(n,n')In-115m Neutron Cross Sections
Obtained through Data Processing Using the 199-Group Neutron Spectrum
Calculated in the 1/4 T PV Position with the VITJEFF311.BOLIB Library.

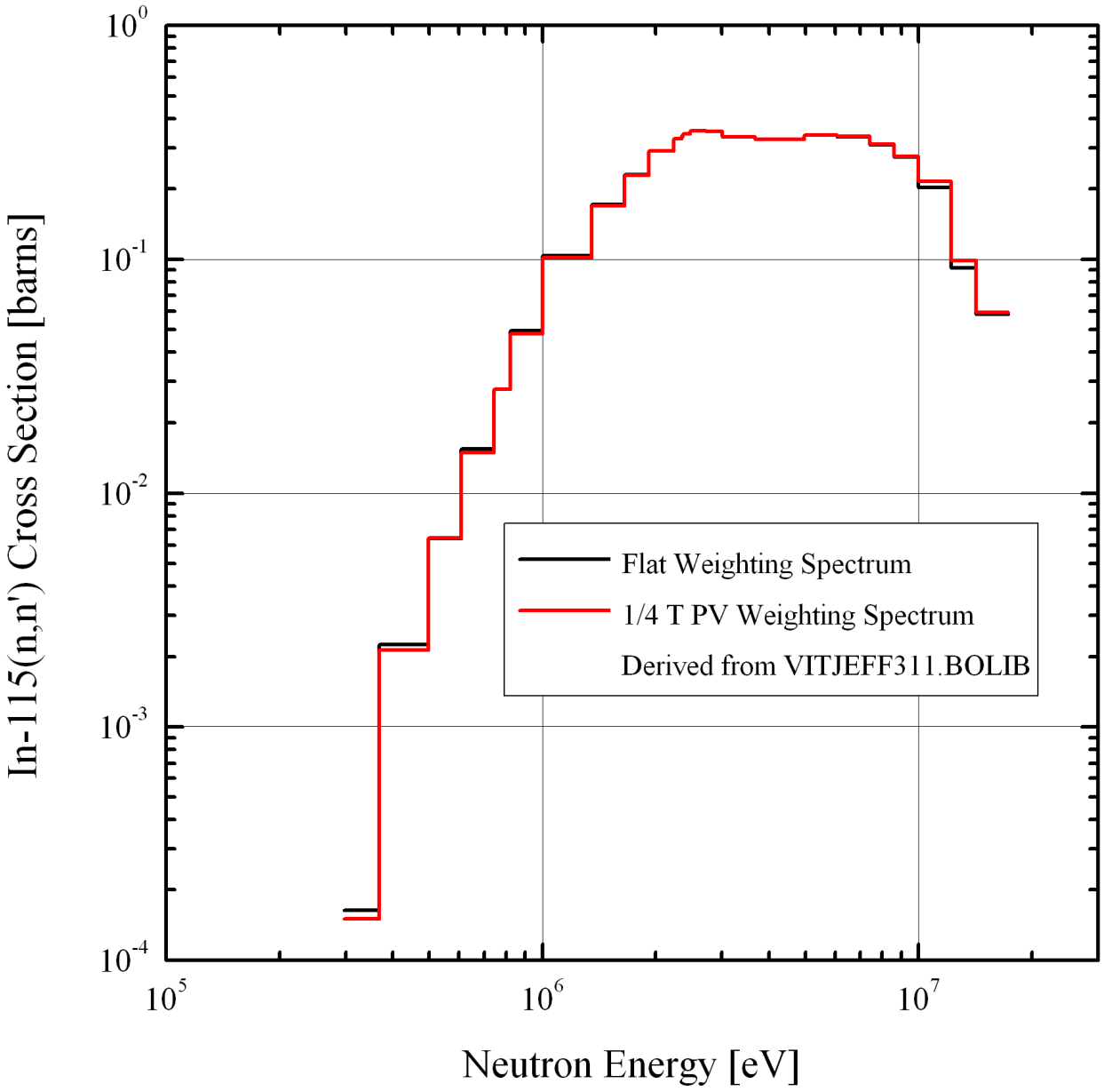

FIG. 3.11

Comparison of the IRDF-2002 Flat Weighting vs. 1/4 T PV Weighting
In-115(n,n')In-115m Dosimeter Cross Sections
Used with the BUGLE-96 Library.

47-Group Neutron Energy Structure Typical of the BUGLE-Type Libraries.

1/4 T PV Weighting In-115(n,n')In-115m Neutron Cross Sections
Obtained through Data Processing Using the 199-Group Neutron Spectrum
Calculated in the 1/4 T PV Position with the VITAMIN-B6 Library.

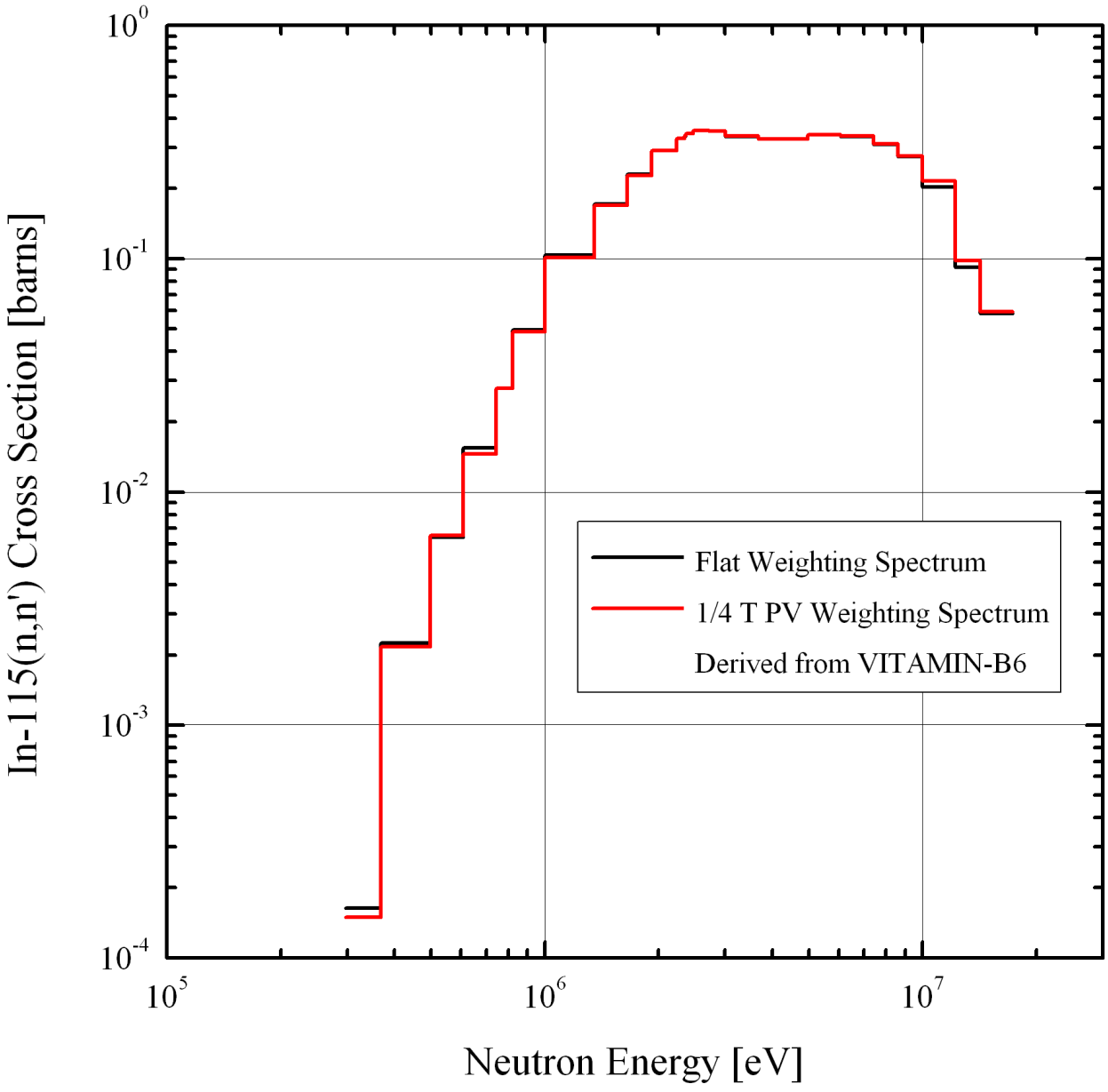

FIG. 3.12

Comparison of the IRDF-2002 Flat Weighting vs. 1/4 T PV Weighting
S-32(n,p)P-32 Dosimeter Cross Sections
Used with the BUGJEFF311.BOLIB Library.

47-Group Neutron Energy Structure Typical of the BUGLE-Type Libraries.

1/4 T PV Weighting S-32(n,p)P-32 Neutron Cross Sections
Obtained through Data Processing Using the 199-Group Neutron Spectrum
Calculated in the 1/4 T PV Position with the VITJEFF311.BOLIB Library.

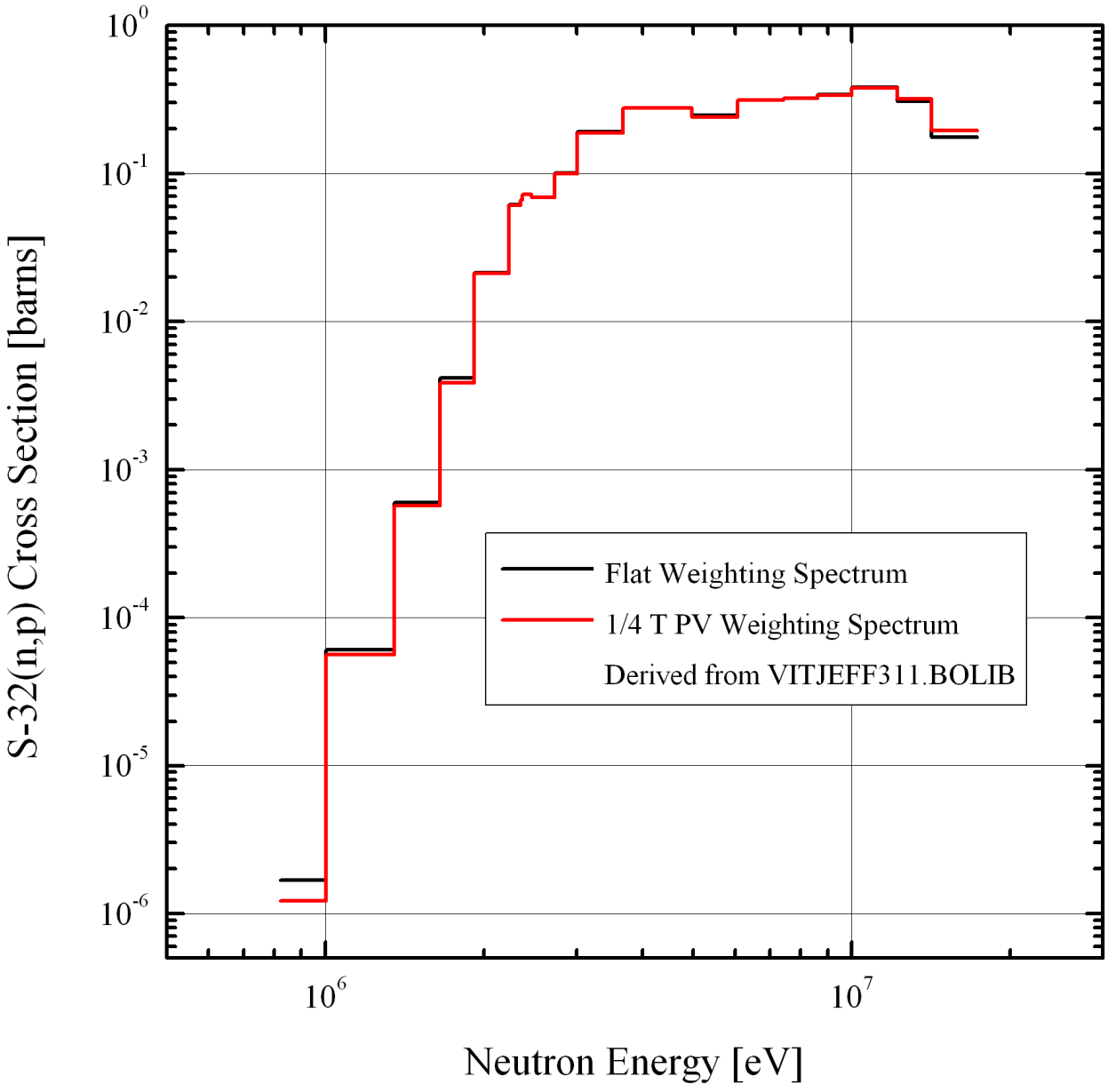

FIG. 3.13

Comparison of the IRDF-2002 Flat Weighting vs. 1/4 T PV Weighting
S-32(n,p)P-32 Dosimeter Cross Sections
Used with the BUGLE-96 Library.

47-Group Neutron Energy Structure Typical of the BUGLE-Type Libraries.

1/4 T PV Weighting S-32(n,p)P-32 Neutron Cross Sections
Obtained through Data Processing Using the 199-Group Neutron Spectrum
Calculated in the 1/4 T PV Position with the VITAMIN-B6 Library.

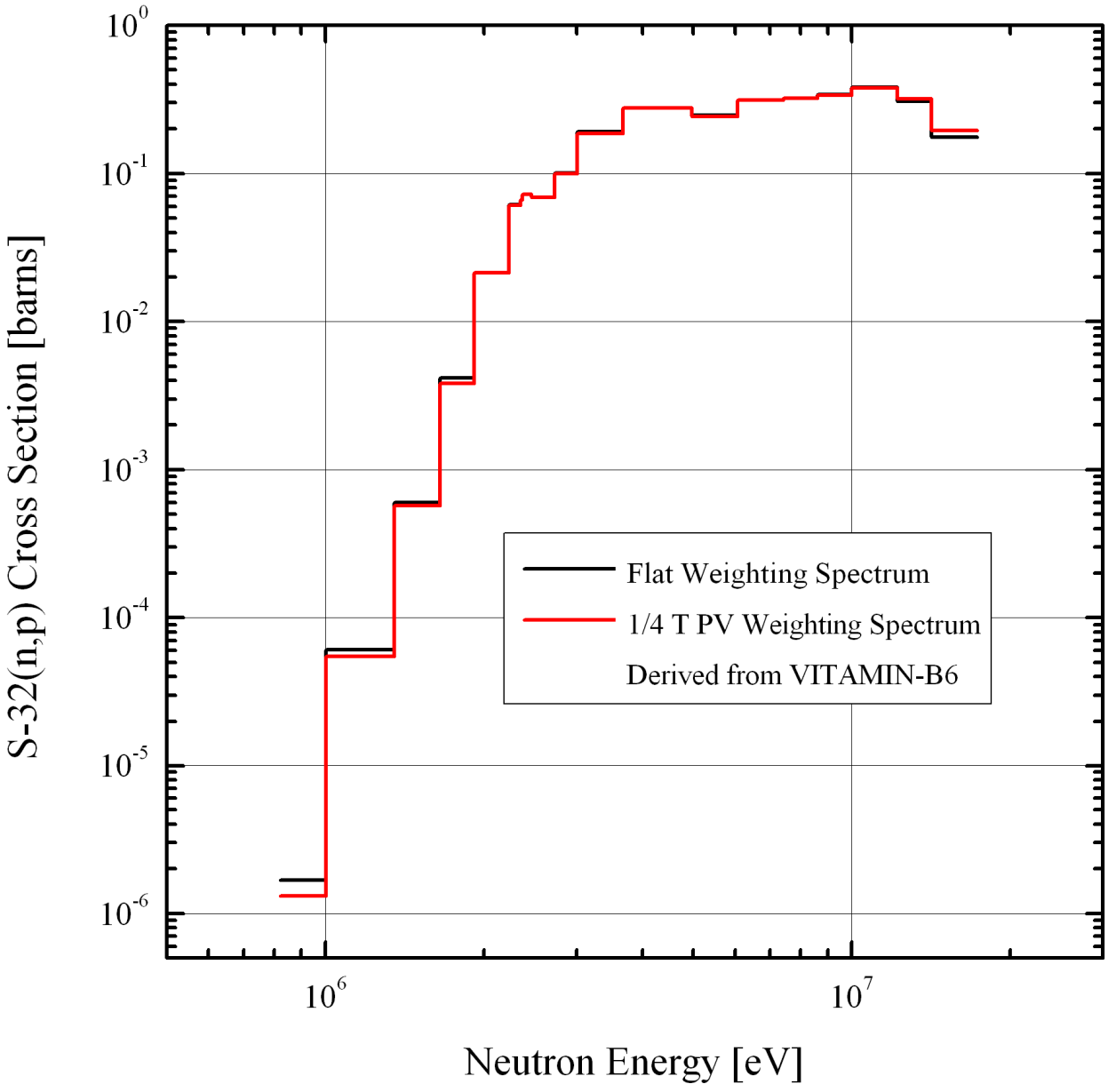

FIG. 3.14

Comparison of the IRDF-2002 Flat Weighting vs. 1/4 T PV Weighting
Al-27(n,α)Na-24 Dosimeter Cross Sections
Used with the BUGJEFF311.BOLIB Library.

47-Group Neutron Energy Structure Typical of the BUGLE-Type Libraries.

1/4 T PV Weighting Al-27(n,α)Na-24 Neutron Cross Sections
Obtained through Data Processing Using the 199-Group Neutron Spectrum
Calculated in the 1/4 T PV Position with the VITJEFF311.BOLIB Library.

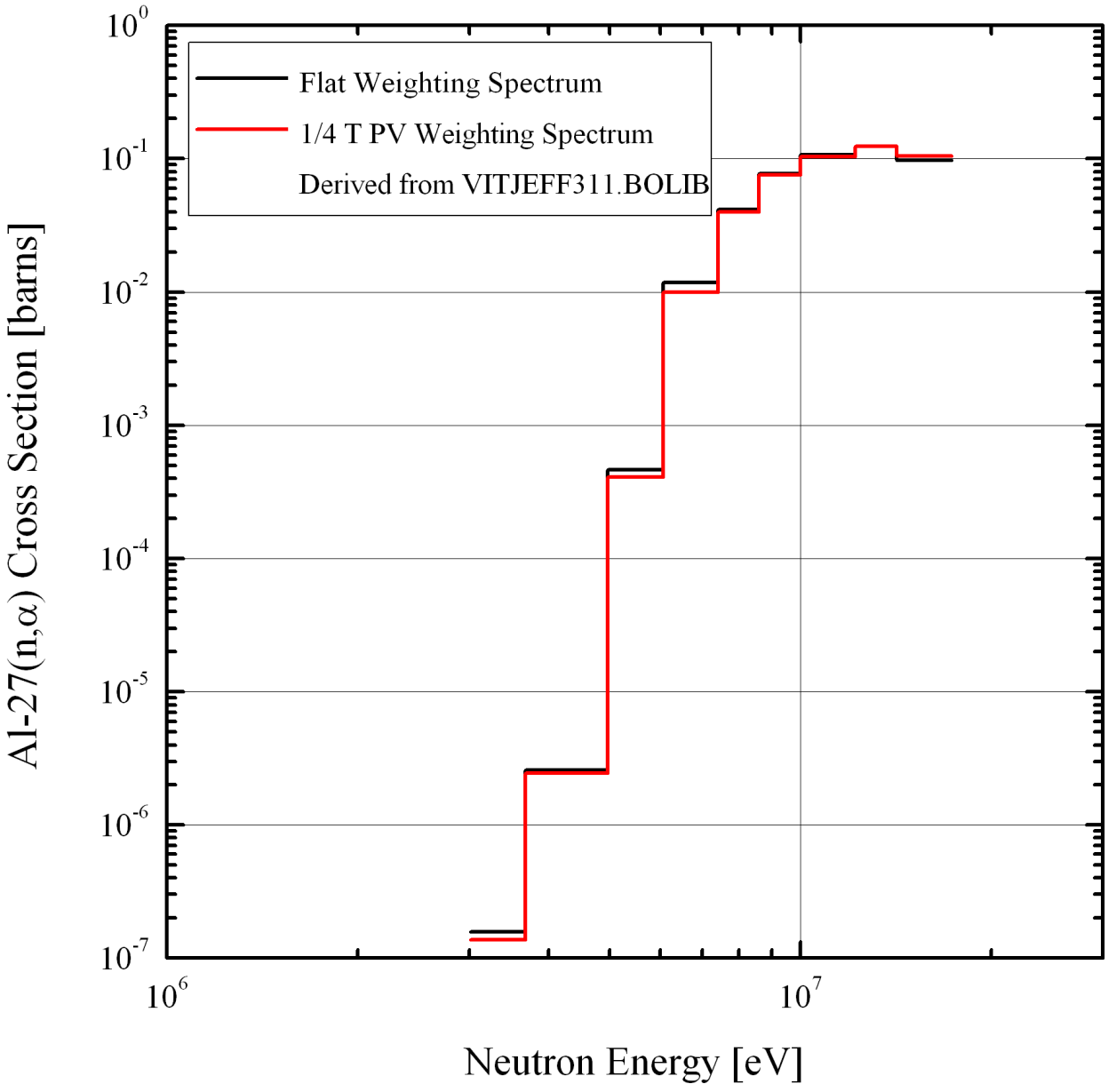

FIG. 3.15

Comparison of the IRDF-2002 Flat Weighting vs. 1/4 T PV Weighting
Al-27(n,α)Na-24 Dosimeter Cross Sections
Used with the BUGLE-96 Library.

47-Group Neutron Energy Structure Typical of the BUGLE-Type Libraries.

1/4 T PV Weighting Al-27(n,α)Na-24 Neutron Cross Sections
Obtained through Data Processing Using the 199-Group Neutron Spectrum
Calculated in the 1/4 T PV Position with the VITAMIN-B6 Library.

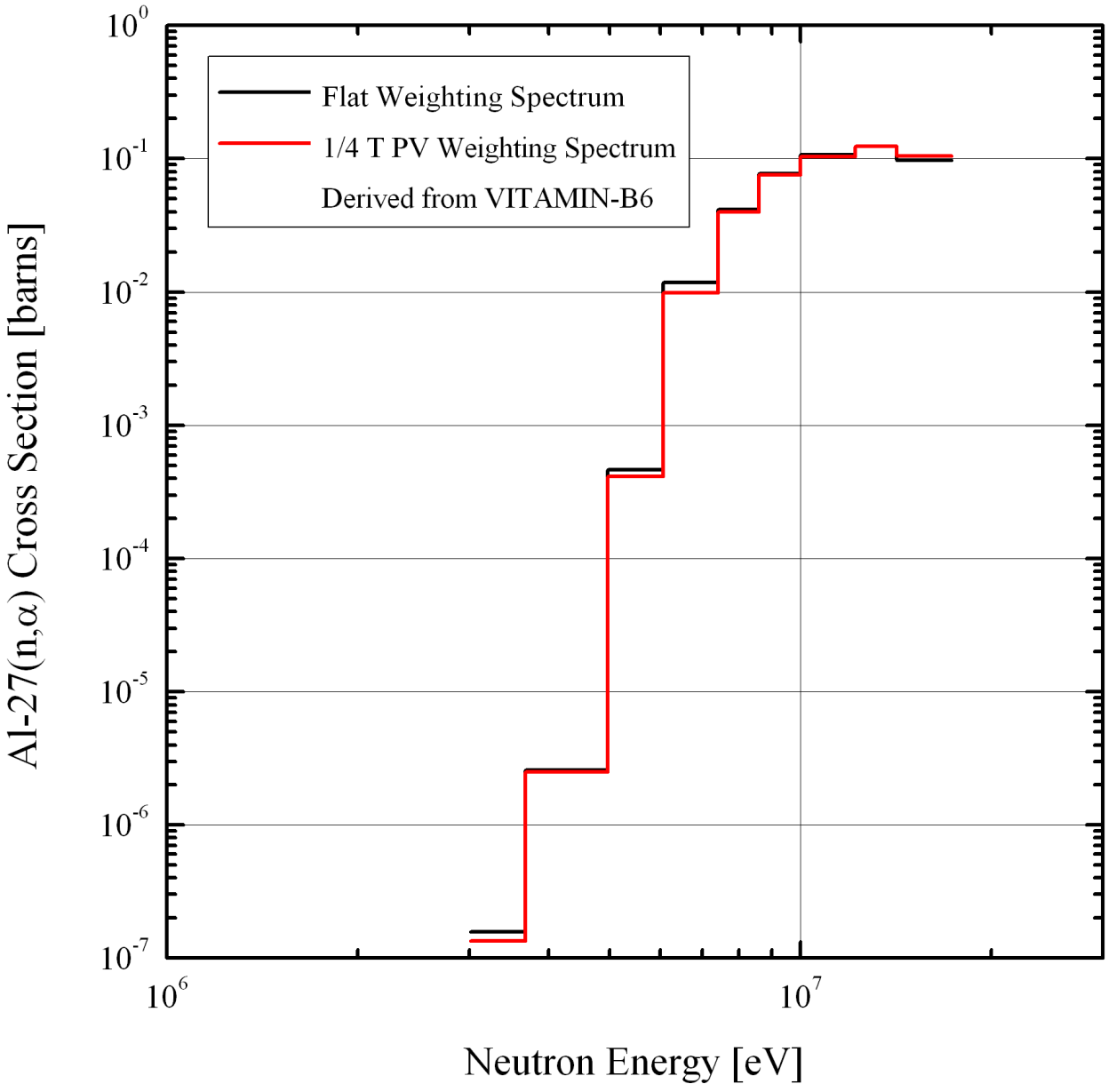

FIG. 3.16

Ratio (1/4 T PV Weighting / Flat Weighting)
of the Al-27(n,α)Na-24 Neutron Cross Sections
Used with the BUGJEFF311.BOLIB Library.

47-Group Neutron Energy Structure Typical of the BUGLE-Type Libraries.

1/4 T PV Weighting Al-27(n,α)Na-24 Neutron Cross Sections
Obtained through Data Processing Using the 199-Group Neutron Spectrum
Calculated in the 1/4 T PV Position with the VITJEFF311.BOLIB Library.

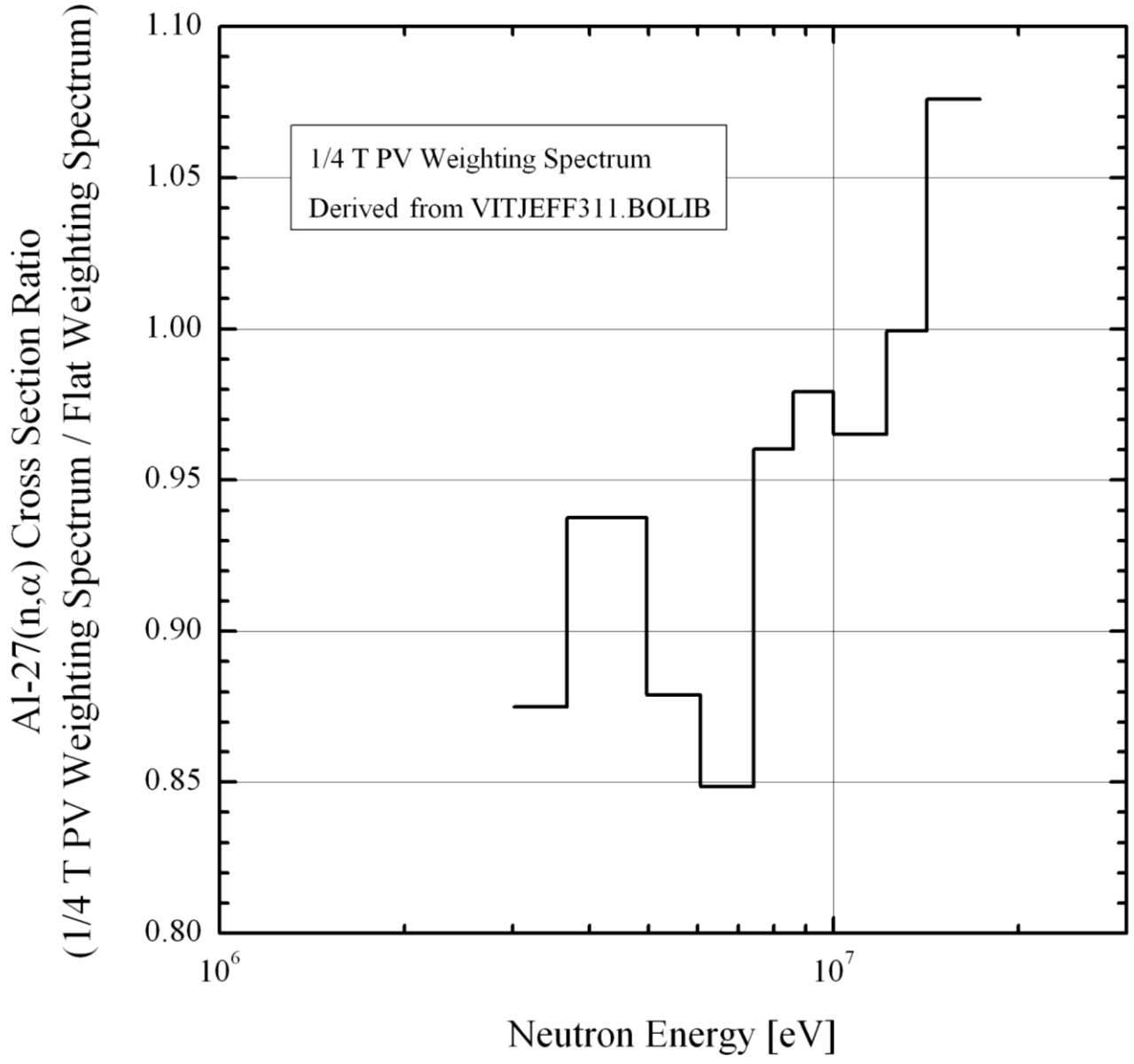

FIG. 3.17

Ratio (1/4 T PV Weighting / Flat Weighting)
of the Al-27(n,α)Na-24 Neutron Cross Sections
Used with the BUGLE-96 Library.

47-Group Neutron Energy Structure Typical of the BUGLE-Type Libraries.

1/4 T PV Weighting Al-27(n,α)Na-24 Neutron Cross Sections
Obtained through Data Processing Using the 199-Group Neutron Spectrum
Calculated in the 1/4 T PV Position with the VITAMIN-B6 Library.

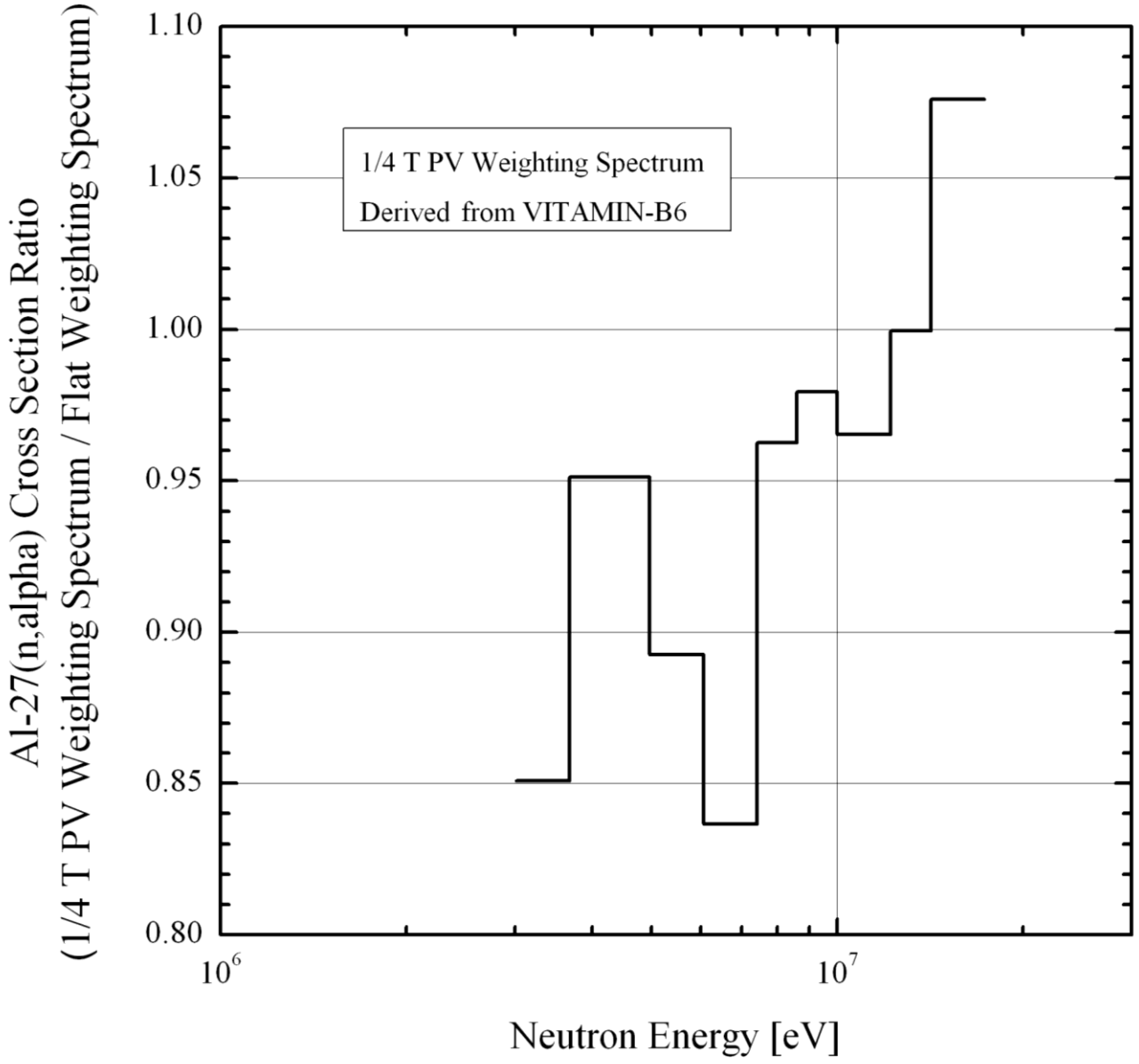

TAB. 3.3

IRDF-2002 Au-197(n,γ)Au-198 Flat Weighting Neutron Dosimeter Cross Sections [barns] Used in the TORT-3.2 Calculations with the BUGJEFF311.BOLIB, BUGENDF70.BOLIB, BUGLE-B7 and BUGLE-96 Libraries.

The Cross Sections Were Self-Shielded Assuming a Background Cross Section σ_0 = 1695.0 barns.

Group	Upper Energy [MeV]	Au-197 (n,γ)
1	1.7332E+01	6.8138E-04
2	1.4191E+01	1.6063E-03
3	1.2214E+01	1.6769E-03
4	1.0000E+01	1.1792E-03
5	8.6071E+00	9.1672E-04
6	7.4082E+00	2.9908E-03
7	6.0653E+00	6.0619E-03
8	4.9659E+00	1.0673E-02
9	3.6788E+00	1.9494E-02
10	3.0119E+00	2.7032E-02
11	2.7253E+00	3.1752E-02
12	2.4660E+00	3.5656E-02
13	2.3653E+00	3.7624E-02
14	2.3457E+00	4.0070E-02
15	2.2313E+00	4.9391E-02
16	1.9205E+00	6.0152E-02
17	1.6530E+00	6.7842E-02
18	1.3534E+00	7.5077E-02
19	1.0026E+00	8.4031E-02
20	8.2085E-01	9.0899E-02
21	7.4274E-01	9.8907E-02
22	6.0810E-01	1.2061E-01
23	4.9787E-01	1.5148E-01
24	3.6883E-01	1.8519E-01
25	2.9721E-01	2.3553E-01
26	1.8316E-01	2.7527E-01
27	1.1109E-01	3.2852E-01
28	6.7379E-02	4.2145E-01
29	4.0868E-02	5.3159E-01
30	3.1828E-02	5.9625E-01
31	2.6058E-02	6.3013E-01
32	2.4176E-02	6.5349E-01
33	2.1875E-02	7.6339E-01
34	1.5034E-02	1.1561E+00
35	7.1017E-03	1.8461E+00
36	3.3546E-03	2.9907E+00
37	1.5846E-03	8.0657E+00
38	4.5400E-04	1.2390E+01
39	2.1445E-04	1.0332E+01
40	1.0130E-04	1.8528E+01
41	3.7266E-05	6.5715E-01
42	1.0677E-05	9.5267E+01
43	5.0435E-06	3.6192E+02
44	1.8554E-06	2.5048E+01
45	8.7643E-07	2.5505E+01
46	4.1399E-07	3.5582E+01
47	1.0000E-07	9.4230E+01
	1.0000E-11	

TAB. 3.4

IRDF-2002 Au-197(n,γ)Au-198 1/4 T PV Weighting Neutron Dosimeter Cross Sections [barns] Used in the TORT-3.2 Calculations with the BUGJEFF311.BOLIB, BUGENDF70.BOLIB, BUGLE-B7 and BUGLE-96 Libraries.

The Cross Sections Were Self-Shielded Assuming a Background Cross Section σ_0 = 1695.0 barns.

Group	Upper Energy [MeV]	Au-197(n,γ) BUGJEFF311.BOLIB	Au-197(n,γ) BUGENDF70.BOLIB	Au-197(n,γ) BUGLE-B7	Au-197(n,γ) BUGLE-96
1	1.7332E+01	8.3799E-04	8.3465E-04	8.3467E-04	8.3919E-04
2	1.4191E+01	1.6630E-03	1.6633E-03	1.6632E-03	1.6616E-03
3	1.2214E+01	1.6244E-03	1.6248E-03	1.6248E-03	1.6250E-03
4	1.0000E+01	1.1555E-03	1.1551E-03	1.1551E-03	1.1556E-03
5	8.6071E+00	9.2183E-04	9.2211E-04	9.2202E-04	9.2147E-04
6	7.4082E+00	3.2177E-03	3.2299E-03	3.2297E-03	3.2356E-03
7	6.0653E+00	6.1638E-03	6.1612E-03	6.1632E-03	6.1508E-03
8	4.9659E+00	1.0778E-02	1.0768E-02	1.0773E-02	1.0751E-02
9	3.6788E+00	1.9894E-02	1.9964E-02	1.9964E-02	1.9986E-02
10	3.0119E+00	2.7081E-02	2.7109E-02	2.7108E-02	2.7108E-02
11	2.7253E+00	3.1738E-02	3.1753E-02	3.1751E-02	3.1751E-02
12	2.4660E+00	3.5740E-02	3.5716E-02	3.5718E-02	3.5716E-02
13	2.3653E+00	3.7624E-02	3.7624E-02	3.7624E-02	3.7624E-02
14	2.3457E+00	4.0129E-02	4.0110E-02	4.0112E-02	4.0106E-02
15	2.2313E+00	4.9455E-02	4.9426E-02	4.9418E-02	4.9422E-02
16	1.9205E+00	6.0480E-02	6.0528E-02	6.0528E-02	6.0532E-02
17	1.6530E+00	6.7970E-02	6.7956E-02	6.7951E-02	6.7955E-02
18	1.3534E+00	7.5320E-02	7.5386E-02	7.5396E-02	7.5395E-02
19	1.0026E+00	8.4390E-02	8.4235E-02	8.4230E-02	8.4227E-02
20	8.2085E-01	9.0962E-02	9.0947E-02	9.0943E-02	9.0945E-02
21	7.4274E-01	9.9387E-02	9.9769E-02	9.9846E-02	9.9849E-02
22	6.0810E-01	1.2037E-01	1.2016E-01	1.2009E-01	1.2010E-01
23	4.9787E-01	1.5320E-01	1.5300E-01	1.5274E-01	1.5274E-01
24	3.6883E-01	1.8579E-01	1.8581E-01	1.8589E-01	1.8589E-01
25	2.9721E-01	2.3642E-01	2.3623E-01	2.3622E-01	2.3630E-01
26	1.8316E-01	2.7531E-01	2.7556E-01	2.7570E-01	2.7571E-01
27	1.1109E-01	3.3518E-01	3.3608E-01	3.3595E-01	3.3596E-01
28	6.7379E-02	4.2224E-01	4.2233E-01	4.2222E-01	4.2224E-01
29	4.0868E-02	5.3069E-01	5.3060E-01	5.3060E-01	5.3060E-01
30	3.1828E-02	6.0536E-01	6.0556E-01	6.0555E-01	6.0555E-01
31	2.6058E-02	6.3008E-01	6.3011E-01	6.3015E-01	6.3015E-01
32	2.4176E-02	6.5264E-01	6.5271E-01	6.5269E-01	6.5269E-01
33	2.1875E-02	7.5910E-01	7.5889E-01	7.5886E-01	7.5881E-01
34	1.5034E-02	1.1317E+00	1.1324E+00	1.1326E+00	1.1323E+00
35	7.1017E-03	1.8736E+00	1.8761E+00	1.8761E+00	1.8760E+00
36	3.3546E-03	3.1830E+00	3.1791E+00	3.1787E+00	3.1792E+00
37	1.5846E-03	8.5877E+00	8.5846E+00	8.5835E+00	8.5832E+00
38	4.5400E-04	1.2102E+01	1.2102E+01	1.2102E+01	1.2102E+01
39	2.1445E-04	1.0530E+01	1.0530E+01	1.0532E+01	1.0530E+01
40	1.0130E-04	2.0634E+01	2.0632E+01	2.0635E+01	2.0632E+01
41	3.7266E-05	8.3767E-01	8.3750E-01	8.3772E-01	8.3730E-01
42	1.0677E-05	1.1673E+02	1.1670E+02	1.1664E+02	1.1666E+02
43	5.0435E-06	2.9092E+02	2.9102E+02	2.9157E+02	2.9075E+02
44	1.8554E-06	2.4922E+01	2.4922E+01	2.4930E+01	2.4925E+01
45	8.7643E-07	2.5685E+01	2.5684E+01	2.5694E+01	2.5727E+01
46	4.1399E-07	3.8156E+01	3.8169E+01	3.8151E+01	3.8000E+01
47	1.0000E-07	6.7837E+01	6.7849E+01	6.7693E+01	6.8829E+01
	1.0000E-11				

TAB. 3.5

IRDF-2002 Rh-103(n,n')Rh-103m, In-115(n,n')In-115m, S-32(n,p)P-32 and Al-27(n,α)Na-24 Flat Weighting Neutron Dosimeter Cross Sections [barns] Used in the TORT-3.2 Calculations with the BUGJEFF311.BOLIB, BUGENDF70.BOLIB, BUGLE-B7 and BUGLE-96 Libraries.

Group	Upper Energy [MeV]	Rh-103 (n,n')	In-115 (n,n')	S-32 (n,p)	Al-27 (n,α)
1	1.7332E+01	2.3466E-01	5.8133E-02	1.7639E-01	9.7222E-02
2	1.4191E+01	3.8742E-01	9.1680E-02	3.0787E-01	1.2398E-01
3	1.2214E+01	8.1816E-01	2.0239E-01	3.8051E-01	1.0678E-01
4	1.0000E+01	1.2190E+00	2.7381E-01	3.3979E-01	7.7279E-02
5	8.6071E+00	1.2753E+00	3.0859E-01	3.2202E-01	4.1475E-02
6	7.4082E+00	1.2305E+00	3.3417E-01	3.1380E-01	1.1792E-02
7	6.0653E+00	1.1732E+00	3.3897E-01	2.4629E-01	4.6528E-04
8	4.9659E+00	1.1091E+00	3.2538E-01	2.7592E-01	2.6020E-06
9	3.6788E+00	1.0370E+00	3.3341E-01	1.9108E-01	1.5730E-07
10	3.0119E+00	9.8735E-01	3.5259E-01	1.0053E-01	0.
11	2.7253E+00	9.5185E-01	3.5385E-01	6.8686E-02	0.
12	2.4660E+00	9.2536E-01	3.4311E-01	7.2417E-02	0.
13	2.3653E+00	9.1570E-01	3.3654E-01	6.6472E-02	0.
14	2.3457E+00	9.0494E-01	3.2759E-01	6.1245E-02	0.
15	2.2313E+00	8.6764E-01	2.9012E-01	2.1377E-02	0.
16	1.9205E+00	8.0955E-01	2.3022E-01	4.1502E-03	0.
17	1.6530E+00	7.4452E-01	1.7096E-01	5.9998E-04	0.
18	1.3534E+00	6.6193E-01	1.0336E-01	6.0917E-05	0.
19	1.0026E+00	5.8044E-01	4.9401E-02	1.6785E-06	0.
20	8.2085E-01	4.9269E-01	2.7891E-02	0.	0.
21	7.4274E-01	3.3867E-01	1.5489E-02	0.	0.
22	6.0810E-01	1.9319E-01	6.3893E-03	0.	0.
23	4.9787E-01	1.3801E-01	2.2558E-03	0.	0.
24	3.6883E-01	1.0374E-01	1.6310E-04	0.	0.
25	2.9721E-01	6.6383E-02	0.	0.	0.
26	1.8316E-01	2.3291E-02	0.	0.	0.
27	1.1109E-01	5.8219E-03	0.	0.	0.
28	6.7379E-02	1.6581E-03	0.	0.	0.
29	4.0868E-02	3.4572E-06	0.	0.	0.
30	3.1828E-02	0.	0.	0.	0.
31	2.6058E-02	0.	0.	0.	0.
32	2.4176E-02	0.	0.	0.	0.
33	2.1875E-02	0.	0.	0.	0.
34	1.5034E-02	0.	0.	0.	0.
35	7.1017E-03	0.	0.	0.	0.
36	3.3546E-03	0.	0.	0.	0.
37	1.5846E-03	0.	0.	0.	0.
38	4.5400E-04	0.	0.	0.	0.
39	2.1445E-04	0.	0.	0.	0.
40	1.0130E-04	0.	0.	0.	0.
41	3.7266E-05	0.	0.	0.	0.
42	1.0677E-05	0.	0.	0.	0.
43	5.0435E-06	0.	0.	0.	0.
44	1.8554E-06	0.	0.	0.	0.
45	8.7643E-07	0.	0.	0.	0.
46	4.1399E-07	0.	0.	0.	0.
47	1.0000E-07	0.	0.	0.	0.
	1.0000E-11				

TAB. 3.6

IRDF-2002 Rh-103(n,n')Rh-103m, In-115(n,n')In-115m, S-32(n,p)P-32 and Al-27(n,α)Na-24
1/4 T PV Weighting Neutron Dosimeter Cross Sections [barns]
Used in the TORT-3.2 Calculations with the BUGJEFF311.BOLIB Library.

Group	Upper Energy [MeV]	Rh-103 (n,n')	In-115 (n,n')	S-32 (n,p)	Al-27 (n,α)
1	1.7332E+01	2.4762E-01	5.9192E-02	1.9546E-01	1.0459E-01
2	1.4191E+01	4.0937E-01	9.8480E-02	3.1934E-01	1.2390E-01
3	1.2214E+01	8.8683E-01	2.1539E-01	3.7876E-01	1.0305E-01
4	1.0000E+01	1.2278E+00	2.7598E-01	3.3761E-01	7.5681E-02
5	8.6071E+00	1.2744E+00	3.1011E-01	3.2276E-01	3.9827E-02
6	7.4082E+00	1.2262E+00	3.3546E-01	3.1147E-01	1.0004E-02
7	6.0653E+00	1.1713E+00	3.3869E-01	2.4085E-01	4.0899E-04
8	4.9659E+00	1.1079E+00	3.2516E-01	2.7606E-01	2.4394E-06
9	3.6788E+00	1.0344E+00	3.3444E-01	1.8725E-01	1.3764E-07
10	3.0119E+00	9.8700E-01	3.5268E-01	1.0010E-01	0.
11	2.7253E+00	9.5196E-01	3.5387E-01	6.8656E-02	0.
12	2.4660E+00	9.2492E-01	3.4283E-01	7.2333E-02	0.
13	2.3653E+00	9.1570E-01	3.3654E-01	6.6472E-02	0.
14	2.3457E+00	9.0468E-01	3.2736E-01	6.1061E-02	0.
15	2.2313E+00	8.6739E-01	2.8986E-01	2.1176E-02	0.
16	1.9205E+00	8.0741E-01	2.2810E-01	3.8470E-03	0.
17	1.6530E+00	7.4261E-01	1.6934E-01	5.7068E-04	0.
18	1.3534E+00	6.5961E-01	1.0148E-01	5.6340E-05	0.
19	1.0026E+00	5.7702E-01	4.7963E-02	1.2101E-06	0.
20	8.2085E-01	4.9153E-01	2.7746E-02	0.	0.
21	7.4274E-01	3.2977E-01	1.4938E-02	0.	0.
22	6.0810E-01	1.9398E-01	6.4499E-03	0.	0.
23	4.9787E-01	1.3615E-01	2.1316E-03	0.	0.
24	3.6883E-01	1.0322E-01	1.5017E-04	0.	0.
25	2.9721E-01	6.5599E-02	0.	0.	0.
26	1.8316E-01	2.3237E-02	0.	0.	0.
27	1.1109E-01	5.3946E-03	0.	0.	0.
28	6.7379E-02	1.6350E-03	0.	0.	0.
29	4.0868E-02	3.5663E-06	0.	0.	0.
30	3.1828E-02	0.	0.	0.	0.
31	2.6058E-02	0.	0.	0.	0.
32	2.4176E-02	0.	0.	0.	0.
33	2.1875E-02	0.	0.	0.	0.
34	1.5034E-02	0.	0.	0.	0.
35	7.1017E-03	0.	0.	0.	0.
36	3.3546E-03	0.	0.	0.	0.
37	1.5846E-03	0.	0.	0.	0.
38	4.5400E-04	0.	0.	0.	0.
39	2.1445E-04	0.	0.	0.	0.
40	1.0130E-04	0.	0.	0.	0.
41	3.7266E-05	0.	0.	0.	0.
42	1.0677E-05	0.	0.	0.	0.
43	5.0435E-06	0.	0.	0.	0.
44	1.8554E-06	0.	0.	0.	0.
45	8.7643E-07	0.	0.	0.	0.
46	4.1399E-07	0.	0.	0.	0.
47	1.0000E-07	0.	0.	0.	0.
	1.0000E-11				

TAB. 3.7

IRDF-2002 Rh-103(n,n')Rh-103m, In-115(n,n')In-115m, S-32(n,p)P-32 and Al-27(n,α)Na-24
1/4 T PV Weighting Neutron Dosimeter Cross Sections [barns]
Used in the TORT-3.2 Calculations with the BUGENDF70.BOLIB Library.

Group	Upper Energy [MeV]	Rh-103 (n,n')	In-115 (n,n')	S-32 (n,p)	Al-27 (n,α)
1	1.7332E+01	2.4736E-01	5.9174E-02	1.9504E-01	1.0443E-01
2	1.4191E+01	4.0943E-01	9.8495E-02	3.1939E-01	1.2391E-01
3	1.2214E+01	8.8628E-01	2.1529E-01	3.7877E-01	1.0308E-01
4	1.0000E+01	1.2280E+00	2.7602E-01	3.3756E-01	7.5654E-02
5	8.6071E+00	1.2743E+00	3.1014E-01	3.2279E-01	3.9795E-02
6	7.4082E+00	1.2259E+00	3.3553E-01	3.1134E-01	9.9044E-03
7	6.0653E+00	1.1713E+00	3.3870E-01	2.4087E-01	4.0980E-04
8	4.9659E+00	1.1080E+00	3.2519E-01	2.7597E-01	2.4639E-06
9	3.6788E+00	1.0340E+00	3.3463E-01	1.8679E-01	1.3485E-07
10	3.0119E+00	9.8681E-01	3.5274E-01	9.9856E-02	0.
11	2.7253E+00	9.5184E-01	3.5384E-01	6.8690E-02	0.
12	2.4660E+00	9.2505E-01	3.4291E-01	7.2357E-02	0.
13	2.3653E+00	9.1570E-01	3.3654E-01	6.6472E-02	0.
14	2.3457E+00	9.0476E-01	3.2744E-01	6.1120E-02	0.
15	2.2313E+00	8.6750E-01	2.8997E-01	2.1288E-02	0.
16	1.9205E+00	8.0709E-01	2.2780E-01	3.8128E-03	0.
17	1.6530E+00	7.4285E-01	1.6955E-01	5.7288E-04	0.
18	1.3534E+00	6.5898E-01	1.0098E-01	5.5136E-05	0.
19	1.0026E+00	5.7853E-01	4.8555E-02	1.3091E-06	0.
20	8.2085E-01	4.9180E-01	2.7780E-02	0.	0.
21	7.4274E-01	3.2413E-01	1.4595E-02	0.	0.
22	6.0810E-01	1.9458E-01	6.4916E-03	0.	0.
23	4.9787E-01	1.3637E-01	2.1464E-03	0.	0.
24	3.6883E-01	1.0321E-01	1.5024E-04	0.	0.
25	2.9721E-01	6.5947E-02	0.	0.	0.
26	1.8316E-01	2.3120E-02	0.	0.	0.
27	1.1109E-01	5.3290E-03	0.	0.	0.
28	6.7379E-02	1.6314E-03	0.	0.	0.
29	4.0868E-02	3.5772E-06	0.	0.	0.
30	3.1828E-02	0.	0.	0.	0.
31	2.6058E-02	0.	0.	0.	0.
32	2.4176E-02	0.	0.	0.	0.
33	2.1875E-02	0.	0.	0.	0.
34	1.5034E-02	0.	0.	0.	0.
35	7.1017E-03	0.	0.	0.	0.
36	3.3546E-03	0.	0.	0.	0.
37	1.5846E-03	0.	0.	0.	0.
38	4.5400E-04	0.	0.	0.	0.
39	2.1445E-04	0.	0.	0.	0.
40	1.0130E-04	0.	0.	0.	0.
41	3.7266E-05	0.	0.	0.	0.
42	1.0677E-05	0.	0.	0.	0.
43	5.0435E-06	0.	0.	0.	0.
44	1.8554E-06	0.	0.	0.	0.
45	8.7643E-07	0.	0.	0.	0.
46	4.1399E-07	0.	0.	0.	0.
47	1.0000E-07	0.	0.	0.	0.
	1.0000E-11				

TAB. 3.8

IRDF-2002 Rh-103(n,n')Rh-103m, In-115(n,n')In-115m, S-32(n,p)P-32 and Al-27(n,α)Na-24
1/4 T PV Weighting Neutron Dosimeter Cross Sections [barns]
Used in the TORT-3.2 Calculations with the BUGLE-B7 Library.

Group	Upper Energy [MeV]	Rh-103 (n,n')	In-115 (n,n')	S-32 (n,p)	Al-27 (n,α)
1	1.7332E+01	2.4736E-01	5.9174E-02	1.9505E-01	1.0443E-01
2	1.4191E+01	4.0941E-01	9.8489E-02	3.1938E-01	1.2391E-01
3	1.2214E+01	8.8634E-01	2.1530E-01	3.7877E-01	1.0308E-01
4	1.0000E+01	1.2280E+00	2.7603E-01	3.3756E-01	7.5651E-02
5	8.6071E+00	1.2743E+00	3.1013E-01	3.2278E-01	3.9809E-02
6	7.4082E+00	1.2260E+00	3.3553E-01	3.1134E-01	9.9059E-03
7	6.0653E+00	1.1713E+00	3.3869E-01	2.4087E-01	4.0921E-04
8	4.9659E+00	1.1079E+00	3.2518E-01	2.7593E-01	2.4602E-06
9	3.6788E+00	1.0340E+00	3.3463E-01	1.8679E-01	1.3486E-07
10	3.0119E+00	9.8681E-01	3.5274E-01	9.9856E-02	0.
11	2.7253E+00	9.5186E-01	3.5385E-01	6.8685E-02	0.
12	2.4660E+00	9.2504E-01	3.4290E-01	7.2355E-02	0.
13	2.3653E+00	9.1570E-01	3.3654E-01	6.6472E-02	0.
14	2.3457E+00	9.0475E-01	3.2743E-01	6.1113E-02	0.
15	2.2313E+00	8.6753E-01	2.9001E-01	2.1310E-02	0.
16	1.9205E+00	8.0709E-01	2.2779E-01	3.8115E-03	0.
17	1.6530E+00	7.4292E-01	1.6961E-01	5.7404E-04	0.
18	1.3534E+00	6.5889E-01	1.0091E-01	5.5072E-05	0.
19	1.0026E+00	5.7858E-01	4.8572E-02	1.3126E-06	0.
20	8.2085E-01	4.9188E-01	2.7790E-02	0.	0.
21	7.4274E-01	3.2311E-01	1.4534E-02	0.	0.
22	6.0810E-01	1.9478E-01	6.5064E-03	0.	0.
23	4.9787E-01	1.3666E-01	2.1655E-03	0.	0.
24	3.6883E-01	1.0314E-01	1.4951E-04	0.	0.
25	2.9721E-01	6.5980E-02	0.	0.	0.
26	1.8316E-01	2.3024E-02	0.	0.	0.
27	1.1109E-01	5.3402E-03	0.	0.	0.
28	6.7379E-02	1.6344E-03	0.	0.	0.
29	4.0868E-02	3.5772E-06	0.	0.	0.
30	3.1828E-02	0.	0.	0.	0.
31	2.6058E-02	0.	0.	0.	0.
32	2.4176E-02	0.	0.	0.	0.
33	2.1875E-02	0.	0.	0.	0.
34	1.5034E-02	0.	0.	0.	0.
35	7.1017E-03	0.	0.	0.	0.
36	3.3546E-03	0.	0.	0.	0.
37	1.5846E-03	0.	0.	0.	0.
38	4.5400E-04	0.	0.	0.	0.
39	2.1445E-04	0.	0.	0.	0.
40	1.0130E-04	0.	0.	0.	0.
41	3.7266E-05	0.	0.	0.	0.
42	1.0677E-05	0.	0.	0.	0.
43	5.0435E-06	0.	0.	0.	0.
44	1.8554E-06	0.	0.	0.	0.
45	8.7643E-07	0.	0.	0.	0.
46	4.1399E-07	0.	0.	0.	0.
47	1.0000E-07	0.	0.	0.	0.
	1.0000E-11				

TAB. 3.9

IRDF-2002 Rh-103(n,n')Rh-103m, In-115(n,n')In-115m, S-32(n,p)P-32 and Al-27(n,α)Na-24
1/4 T PV Weighting Neutron Dosimeter Cross Sections [barns]
Used in the TORT-3.2 Calculations with the BUGLE-96 Library.

Group	Upper Energy [MeV]	Rh-103 (n,n')	In-115 (n,n')	S-32 (n,p)	Al-27 (n,α)
1	1.7332E+01	2.4772E-01	5.9202E-02	1.9559E-01	1.0463E-01
2	1.4191E+01	4.0865E-01	9.8250E-02	3.1902E-01	1.2392E-01
3	1.2214E+01	8.8555E-01	2.1510E-01	3.7870E-01	1.0309E-01
4	1.0000E+01	1.2278E+00	2.7598E-01	3.3761E-01	7.5687E-02
5	8.6071E+00	1.2744E+00	3.1003E-01	3.2271E-01	3.9922E-02
6	7.4082E+00	1.2258E+00	3.3556E-01	3.1129E-01	9.8648E-03
7	6.0653E+00	1.1715E+00	3.3873E-01	2.4137E-01	4.1534E-04
8	4.9659E+00	1.1082E+00	3.2521E-01	2.7623E-01	2.4751E-06
9	3.6788E+00	1.0339E+00	3.3469E-01	1.8660E-01	1.3384E-07
10	3.0119E+00	9.8682E-01	3.5273E-01	9.9863E-02	0.
11	2.7253E+00	9.5186E-01	3.5385E-01	6.8684E-02	0.
12	2.4660E+00	9.2505E-01	3.4291E-01	7.2357E-02	0.
13	2.3653E+00	9.1570E-01	3.3654E-01	6.6472E-02	0.
14	2.3457E+00	9.0478E-01	3.2745E-01	6.1132E-02	0.
15	2.2313E+00	8.6752E-01	2.8999E-01	2.1297E-02	0.
16	1.9205E+00	8.0707E-01	2.2777E-01	3.8088E-03	0.
17	1.6530E+00	7.4286E-01	1.6956E-01	5.7312E-04	0.
18	1.3534E+00	6.5890E-01	1.0091E-01	5.5073E-05	0.
19	1.0026E+00	5.7861E-01	4.8582E-02	1.3126E-06	0.
20	8.2085E-01	4.9185E-01	2.7786E-02	0.	0.
21	7.4274E-01	3.2307E-01	1.4531E-02	0.	0.
22	6.0810E-01	1.9477E-01	6.5054E-03	0.	0.
23	4.9787E-01	1.3666E-01	2.1654E-03	0.	0.
24	3.6883E-01	1.0314E-01	1.4947E-04	0.	0.
25	2.9721E-01	6.5891E-02	0.	0.	0.
26	1.8316E-01	2.3016E-02	0.	0.	0.
27	1.1109E-01	5.3395E-03	0.	0.	0.
28	6.7379E-02	1.6339E-03	0.	0.	0.
29	4.0868E-02	3.5776E-06	0.	0.	0.
30	3.1828E-02	0.	0.	0.	0.
31	2.6058E-02	0.	0.	0.	0.
32	2.4176E-02	0.	0.	0.	0.
33	2.1875E-02	0.	0.	0.	0.
34	1.5034E-02	0.	0.	0.	0.
35	7.1017E-03	0.	0.	0.	0.
36	3.3546E-03	0.	0.	0.	0.
37	1.5846E-03	0.	0.	0.	0.
38	4.5400E-04	0.	0.	0.	0.
39	2.1445E-04	0.	0.	0.	0.
40	1.0130E-04	0.	0.	0.	0.
41	3.7266E-05	0.	0.	0.	0.
42	1.0677E-05	0.	0.	0.	0.
43	5.0435E-06	0.	0.	0.	0.
44	1.8554E-06	0.	0.	0.	0.
45	8.7643E-07	0.	0.	0.	0.
46	4.1399E-07	0.	0.	0.	0.
47	1.0000E-07	0.	0.	0.	0.
	1.0000E-11				

3.6 - U-235 Fission Neutron Spectra

The U-235 fission neutron spectra (χ) used to obtain the Iron-88 neutron source in the fixed source transport calculations (see Chapter 4) are reported in TAB. 3.10.
It is underlined that, whereas the U-235 fission spectrum data included in the packages of the ORNL BUGLE-B7 /7/ and BUGLE-96 /8/ libraries refer only to prompt neutrons. The U-235 fission spectrum data, contained respectively in the packages of the ENEA-Bologna BUGJEFF311.BOLIB /2/ and BUGENDF70.BOLIB /3/ similar libraries, are instead total fission spectra, i.e. they include the contributions of both prompt and delayed neutrons. This option was made available through the use of the ENEA-Bologna 2007 Revision /31/ of the ORNL SCAMPI /32/ nuclear data processing system, freely released at OECD-NEADB and ORNL-RSICC.
Graphical representations of the U-235 total fission neutron spectra (χ) for the BUGJEFF311.BOLIB, BUGENDF70.BOLIB, BUGLE-B7 and BUGLE-96 libraries are reported in FIG. 3.18. An enlargement of the cited fission spectra, in the 1.0E+00 eV - 1.0E+04 eV energy range where the differences in the χ group numerical values are higher, is represented in FIG. 3.19.

TAB. 3.10

Total or Prompt U-235 Fission Neutron Spectra (χ) Used in the TORT-3.2 Calculations with the BUGJEFF311.BOLIB, BUGENDF70.BOLIB, BUGLE-B7 and BUGLE-96 Libraries.

Group	Upper Energy [MeV]	Total χ(U-235) BUGJEFF311.BOLIB	Total χ(U-235) BUGENDF70.BOLIB	Prompt χ(U-235) BUGLE-B7	Prompt χ(U-235) BUGLE-96
1	1.7332E+01	4.9847E-05	4.9839E-05	4.8822E-05	5.0179E-05
2	1.4191E+01	2.0032E-04	2.0031E-04	2.0162E-04	2.0166E-04
3	1.2214E+01	1.1384E-03	1.1384E-03	1.1459E-03	1.1460E-03
4	1.0000E+01	2.5055E-03	2.5055E-03	2.5220E-03	2.5222E-03
5	8.6071E+00	5.6193E-03	5.6195E-03	5.6564E-03	5.6568E-03
6	7.4082E+00	1.6040E-02	1.6041E-02	1.6146E-02	1.6147E-02
7	6.0653E+00	3.0508E-02	3.0511E-02	3.0711E-02	3.0712E-02
8	4.9659E+00	7.9978E-02	7.9986E-02	8.0511E-02	8.0512E-02
9	3.6788E+00	7.6252E-02	7.6258E-02	7.6758E-02	7.6758E-02
10	3.0119E+00	4.3722E-02	4.3728E-02	4.4010E-02	4.4010E-02
11	2.7253E+00	4.6381E-02	4.6388E-02	4.6685E-02	4.6685E-02
12	2.4660E+00	1.9899E-02	1.9903E-02	2.0029E-02	2.0028E-02
13	2.3653E+00	4.0004E-03	4.0013E-03	4.0263E-03	4.0262E-03
14	2.3457E+00	2.4188E-02	2.4193E-02	2.4344E-02	2.4344E-02
15	2.2313E+00	7.3086E-02	7.3105E-02	7.3548E-02	7.3547E-02
16	1.9205E+00	7.1516E-02	7.1538E-02	7.1947E-02	7.1946E-02
17	1.6530E+00	8.9032E-02	8.9083E-02	8.9497E-02	8.9495E-02
18	1.3534E+00	1.1467E-01	1.1474E-01	1.1503E-01	1.1503E-01
19	1.0026E+00	6.2706E-02	6.2734E-02	6.2687E-02	6.2685E-02
20	8.2085E-01	2.7337E-02	2.7329E-02	2.7240E-02	2.7239E-02
21	7.4274E-01	4.7125E-02	4.7130E-02	4.6852E-02	4.6851E-02
22	6.0810E-01	3.8049E-02	3.8038E-02	3.7617E-02	3.7615E-02
23	4.9787E-01	4.2477E-02	4.2436E-02	4.1772E-02	4.1771E-02
24	3.6883E-01	2.1827E-02	2.1807E-02	2.1390E-02	2.1390E-02
25	2.9721E-01	3.0837E-02	3.0779E-02	3.0048E-02	3.0048E-02
26	1.8316E-01	1.5950E-02	1.5922E-02	1.5408E-02	1.5408E-02
27	1.1109E-01	7.7421E-03	7.7147E-03	7.4253E-03	7.4251E-03
28	6.7379E-02	3.7043E-03	3.6943E-03	3.5462E-03	3.5461E-03
29	4.0868E-02	1.0482E-03	1.0459E-03	9.9809E-04	9.9806E-04
30	3.1828E-02	6.0737E-04	6.0374E-04	5.6978E-04	5.6977E-04
31	2.6058E-02	1.8654E-04	1.8501E-04	1.7337E-04	1.7337E-04
32	2.4176E-02	2.1922E-04	2.1735E-04	2.0306E-04	2.0305E-04
33	2.1875E-02	5.9716E-04	5.8781E-04	5.4039E-04	5.4037E-04
34	1.5034E-02	5.3875E-04	5.3054E-04	4.8421E-04	4.8419E-04
35	7.1017E-03	1.7068E-04	1.7033E-04	1.5747E-04	1.5746E-04
36	3.3546E-03	5.7556E-05	5.7386E-05	5.1157E-05	5.1156E-05
37	1.5846E-03	2.4994E-05	2.4884E-05	1.4763E-05	2.0827E-05
38	4.5400E-04	3.4437E-06	3.4200E-06	0.	2.5484E-06
39	2.1445E-04	1.2527E-06	1.2414E-06	0.	8.2729E-07
40	1.0130E-04	5.5078E-07	5.4440E-07	0.	3.0900E-07
41	3.7266E-05	1.7589E-07	1.7323E-07	0.	5.9997E-08
42	1.0677E-05	2.2718E-08	2.9006E-08	0.	5.4050E-12
43	5.0435E-06	1.2140E-08	1.3842E-08	0.	0.
44	1.8554E-06	3.7279E-09	3.8754E-09	0.	0.
45	8.7643E-07	1.7610E-09	1.7694E-09	0.	0.
46	4.1399E-07	1.1957E-09	1.1790E-09	0.	0.
47	1.0000E-07	3.8080E-10	3.7167E-10	0.	0.
	1.0000E-11				

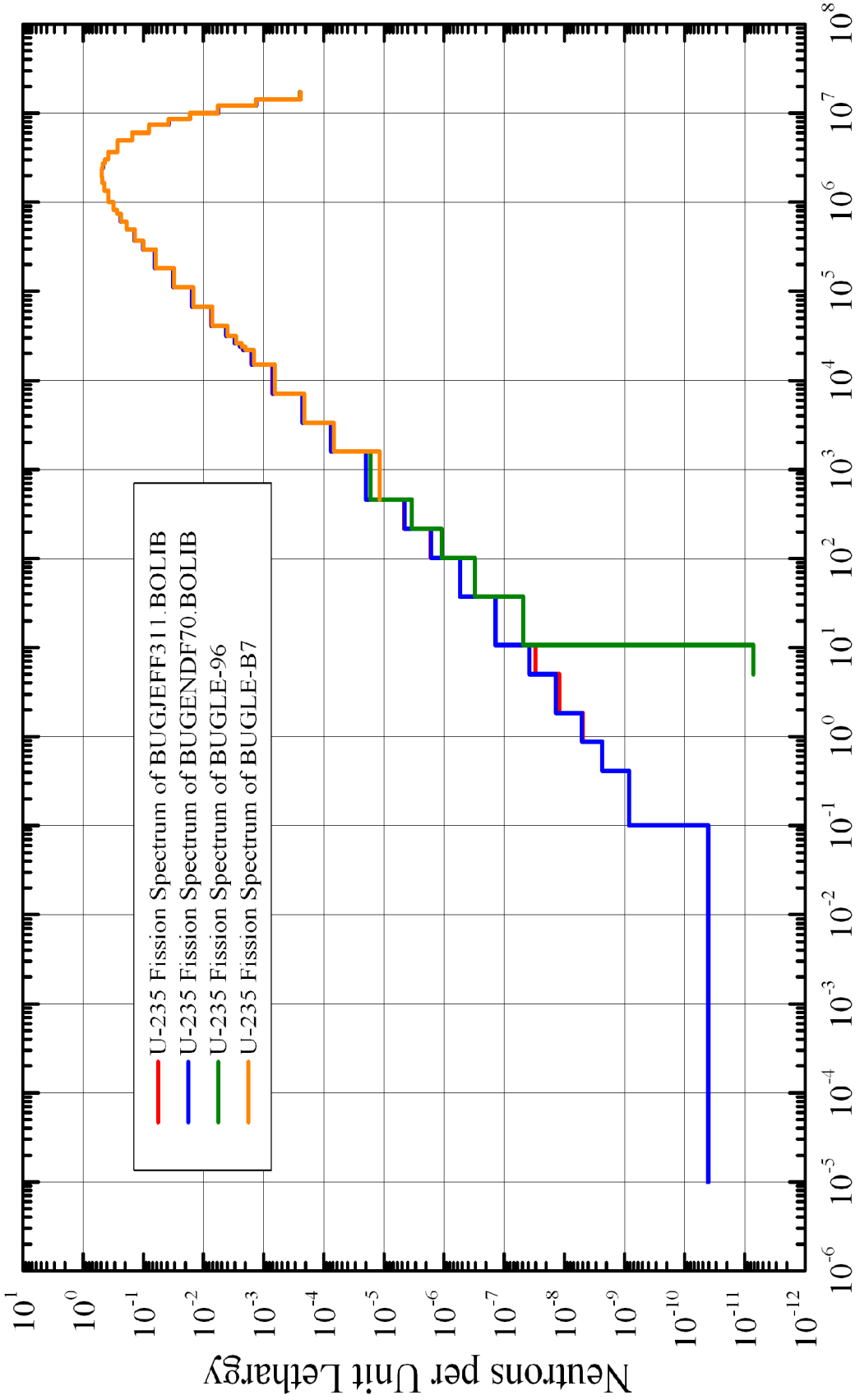

FIG. 3.18 BUGLE-Type 47-Group Neutron Structure Representation of the U-235 Total (Prompt + Delayed) Fission Neutron Spectra of the BUGJEFF311.BOLIB and BUGENDF70.BOLIB Libraries in Comparison with the U-235 Prompt Fission Neutron Spectra of the BUGLE-96 and BUGLE-B7 Libraries. Spectra Averaged on Incident Neutron Energies and Normalized to 1 Neutron per Fission.

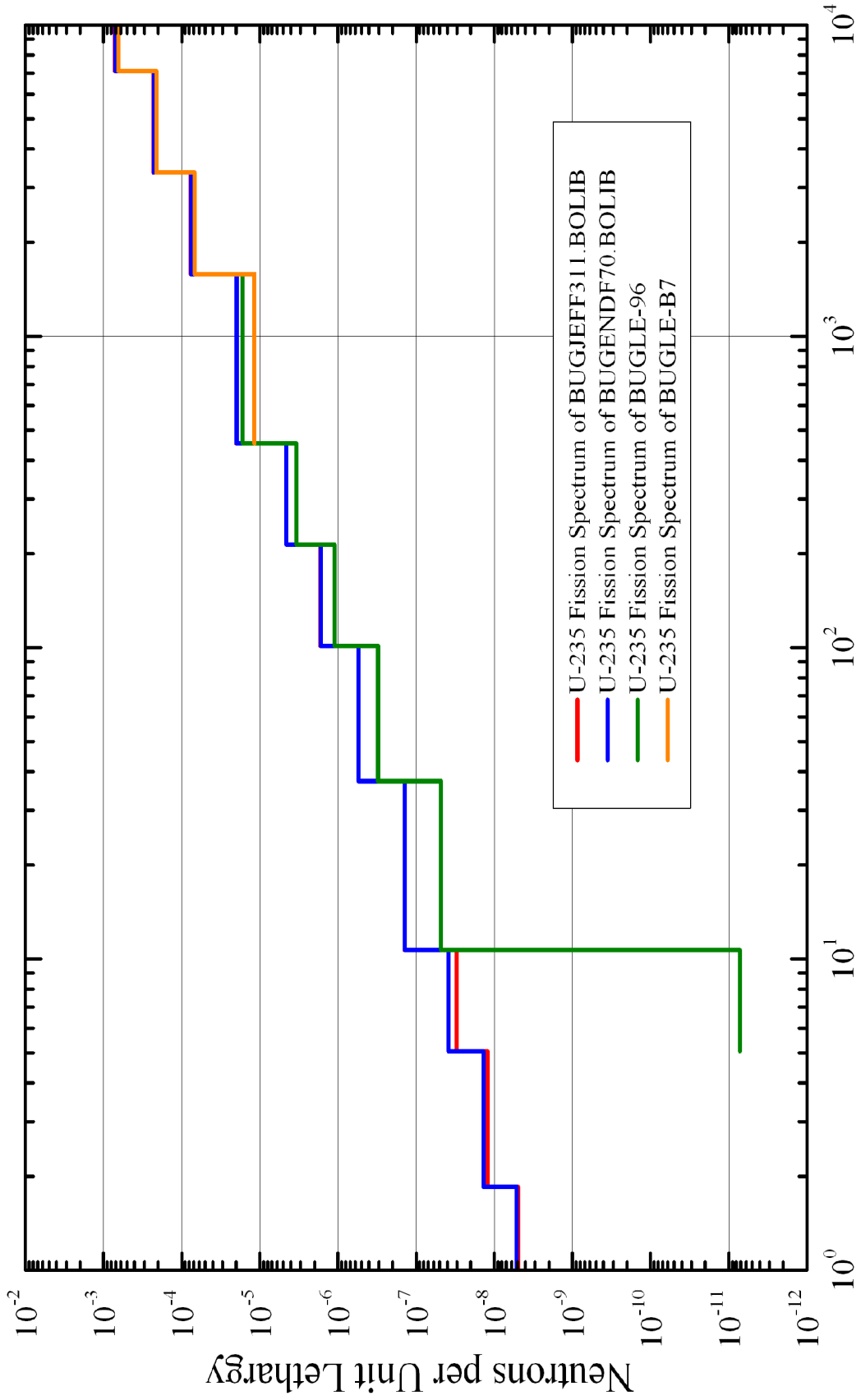

FIG. 3.19 Partial Detail of the BUGLE-Type 47-Group Neutron Structure Representation of the U-235 Total (Prompt + Delayed) Fission Neutron Spectra of the BUGJEFF311.BOLIB and BUGENDF70.BOLIB Libraries in Comparison with the U-235 Prompt Fission Neutron Spectra of the BUGLE-96 and BUGLE-B7 Libraries. Spectra Averaged on Incident Nutron Energies and Normalized to 1 Neutron per Fission.

4.0 - TRANSPORT CALCULATIONS

4.1 - Transport Calculation General Features

Fixed source transport calculations in Cartesian geometry were performed for the Iron-88 neutron shielding benchmark experiment using the ORNL TORT-3.2 /13/ three-dimensional discrete ordinates (S_N) code included in the ORNL DOORS-3.2 /14/ system of deterministic transport codes. The whole Iron-88 experimental array (see 2.2 and /10/) was reproduced with the TORT-3.2 code using the realistic inhomogeneous fission neutron source (see 2.3, TAB. 2.3 and FIG. 4.1) emitted by the fission plate.

The TORT-3.2 code was used on a personal computer (CPU: INTEL PENTIUM D 3.40 GHz, 3.10 GB of RAM) under Linux openSUSE 10.2 (i586) operating system with FORTRAN-77 compiler g77, version 3.3.5-38.

The automatic generation of the spatial mesh grid and the graphical verification of the Iron-88 benchmark experiment geometrical model for TORT-3.2 were performed through the ENEA-Bologna BOT3P-5.3 /16/ (see also /17/, /18/ and /19/) pre/post-processor system.

The reference system adopted in the present calculations has its origin on the Z horizontal axis passing through the centre of the fission plate (see FIGs. 2.6 and 2.7) and normal to it. It is underlined that the centre of the fission plate is not aligned with the centre of the trolley face. In fact the centre of the trolley face is shifted by -2.55 cm in the X horizontal axis direction and by +6.6 cm in the Y vertical axis direction.

The whole Iron-88 three-dimensional experimental array was reproduced in the (X,Y,Z) Cartesian geometry and adopted in all the calculations in order to assure a proper detailed description (see FIG. 4.1) of the spatial inhomogeneity of the neutron source (see TAB. 2.3) emitted by the fission plate. In particular it was described a parallelepiped geometry with a 69X×86Y×278Z fine spatial mesh grid, being Z the horizontal nuclear axis (see FIG. 2.7) where the dosimetric measurement positions were located. Volumetric meshes with sides always inferior to 1.0 cm were described along the Z axis, in correspondence of the measurement region, to obtain the best calculated result accuracy. Volumetric meshes with sides always inferior to 0.25 cm were used in the measurement positions along the Z axis, i.e. in the 0.74 cm air gaps between each mild steel slab component.

The horizontal section (at the vertical axis position Y = 0.0 cm) of the Iron-88 compositional and geometrical model, reproduced in all the TORT-3.2 (X,Y,Z) calculations, is reported in FIG. 4.2 together with the dosimeter locations (×). A detail of the FIG. 4.2 is reproduced in the FIG. 4.3, representing an enlargement of the compositional and geometrical model in the measurement region, where it is possible to see better the 0.74 cm thick air gaps between the various mild steel slab components and the related dosimeter measurement locations.

The mild steel floor, the roof and the trolley lateral walls with 1.91 cm thickness (see 2.2) were simulated in the TORT calculations since they were originally represented in the input data of the Monte Carlo MCBEND /39/ code calculation example, reported in the Iron-88 benchmark experiment section of reference /11/.

The adopted calculation model includes a 1.0 m long graphite region (see FIG. 4.2) to represent the region of the NESTOR reactor behind the trolley face and the fission plate (i.e. towards the NESTOR reactor from the fission plate), not contained in TAB. 2.1, where only the regions behind the fission plate up to the end of the trolley are indicated. As confirmed in the original Iron-88 report (see /10/, page 4), the realistic presence of the graphite zone will permit to obtain more accurate Au-197(n,γ)Au-198/Cd calculated reaction rate results, particularly in the first five measurement positions (see FIG. 2.7). Concerning this, it was decided to introduce the previously cited additional graphite region in all the calculations (producing in particular more accurate gold reaction rate results) to compare all the reaction rate results in a consistent way.

The ENEA-Bologna ADEFTA-4.1 /15/ program was employed in the calculation of the atomic densities of the isotopes involved in the compositional model, on the basis of the atomic abundances reported in the BNL-NNDC database /40/, included in ADEFTA. The Iron-88 atomic densities were calculated using the material densities and the element/isotope weight fractions reported in the Table 2 of reference /10/ (see TAB. 2.2).

The BUGJEFF311.BOLIB /2/, BUGENDF70.BOLIB /3/, BUGLE-B7 /7/ and BUGLE-96 /8/ working libraries were alternatively used in the transport calculations with TORT-3.2, considering BUGLE-96 as a well tested reference library.

The calculations of the epi-cadmium Au-197(n,γ)Au-198 activation dosimeter reaction rates were performed (see more detail in 3.5) using the first 44 neutron groups (see TAB. 3.1) of the BUGLE-type libraries. This implicitly assumes 0.876 eV as the nearer energy value, in the BUGLE-type neutron energy structure, to the 0.73 eV epi-cadmium cutoff thermal neutron energy, corresponding to the cadmium cover thickness of 1.27 mm (see 2.4 and /10/), used in the reaction rate measurements with gold dosimeters in the Iron-88 benchmark experiment.

All the calculated reaction rates for the Rh-103(n,n')Rh-103m, In-115(n,n')In-115m, S-32(n,p)P-32 and Al-27(n,α)Na-24 threshold activation dosimeters were obtained taking into account only the first 29 neutron groups (see TAB. 3.1) of the four BUGLE-type libraries employed, above 3.1828E+04 eV, since all the neutron threshold energies of the four cited dosimeters are above this neutron energy value.

It is underlined that it was not possible to use the same set of atomic densities in all the calculations with the four BUGLE-type previously cited libraries. In fact the BUGJEFF311.BOLIB and BUGENDF70.BOLIB libraries include all the needed processed cross sections for all the isotopes of each natural element involved in the Iron-88 compositional model whereas, on the contrary, this possibility is not always assured for the BUGLE-B7 and BUGLE-96 libraries. Several processed cross sections needed in the description of the Iron-88 compositional model are in fact available in BUGLE-B7 and BUGLE-96 only as natural element cross section files. In particular the common set of atomic densities used in the calculations with the BUGJEFF311.BOLIB and BUGENDF70.BOLIB libraries is reported in TAB. 4.1 whilst different sets of atomic densities, shown in the TAB. 4.2 and TAB. 4.3, were respectively used in the calculations with the BUGLE-B7 and BUGLE-96 libraries. The two last sets of atomic densities are different because some elements (Ca, K and Si) of the mixture of nuclides of the material “concrete” are specifically available in BUGLE-B7 (see TAB. 4.2) as cross section data files of their component isotopes

whilst the cited elements in BUGLE-96 are available (see TAB. 4.3) only as natural element cross section data files.

Both infinite dilution and self-shielded neutron cross sections were selected. Proper self-shielded neutron cross sections from the four BUGLE-type library packages were used when available. In particular it is underlined that the mild steel and stainless steel regions of Iron-88 are characterized by atomic densities quite similar to those used to calculate the background cross sections, employed in the self-shielding of the neutron cross sections of the four cited BUGLE-type libraries. Group-organized files of macroscopic cross sections, requested by TORT-3.2 and derived from the four cited BUGLE-type working libraries in FIDO-ANISN format, were prepared through the ORNL GIP (see /14/) program, specifically dedicated to the discrete ordinates transport codes (ANISN-ORNL, DORT, TORT) of the DOORS system. The ENEA-Bologna ADEFTA-4.1 program was used not only to calculate the atomic densities for the Iron-88 compositional model but also to handle them properly in order to automatically prepare the macroscopic cross section sets for the material mixtures of elements/isotopes in the format required by GIP.

Fixed source transport calculations with one source (outer) iteration and 60 inner iterations were performed using fully symmetrical discrete ordinates directional quadrature sets for the flux solution. The P_3-S_8 approximation was adopted as a standard in all the calculations using alternatively the four cited BUGLE-type libraries. P_N corresponds to the order of the expansion in Legendre polynomials of the scattering cross section matrix and S_N represents the order of the flux angular discretization. It is underlined that the P_3-S_8 approximation is the most widely used option in the fixed source calculations dedicated to LWR safety analyses.

The theta-weighted difference approximation was selected for the flux extrapolation model.
In all the calculations the same numerical value (1.0E-03) for the point-wise flux convergence criterion was employed.

The vacuum boundary condition was selected at the left, right, inside, outside, bottom and top geometrical boundaries.

The calculated reaction rates were obtained in all the experimental dosimeter positions in the 0.74 cm air gaps (see FIGs. 2.7, 4.2 and 4.3) between each mild steel slab component.

FIG. 4.1

Iron-88 - Vertical Section of the Fission Plate Neutron Source Distribution
Described in the TORT-3.2 (X,Y,X) Calculations.

Vertical Section at Z = 1.5 cm.
69X×86Y×278Z Spatial Meshes.

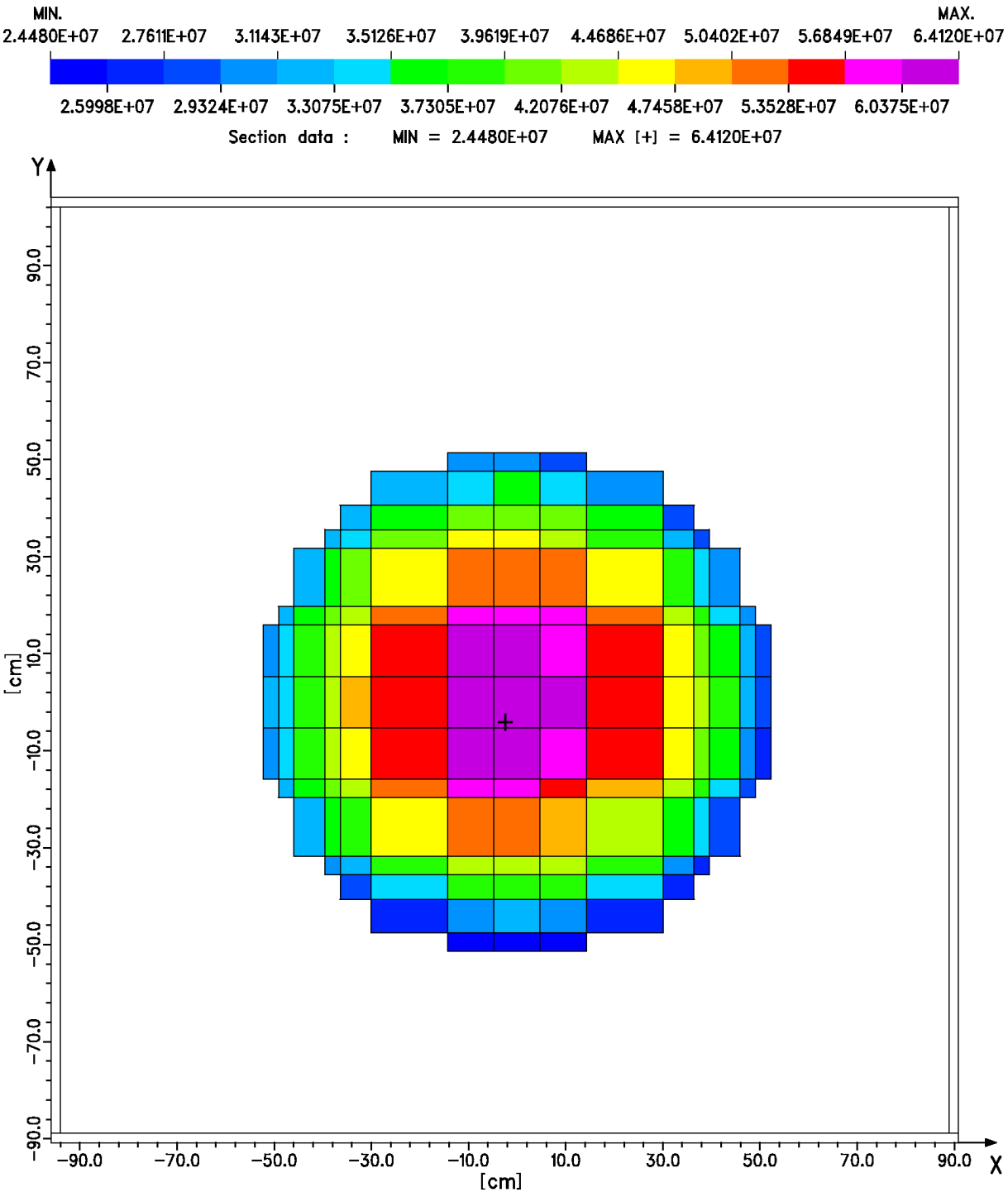

FIG. 4.2

Iron-88 - Compositional and Geometrical Model in the TORT-3.2 (X,Y,Z) Calculations.

Horizontal Section at Y = 0.0 cm.
Dosimeter Locations "×", 69X×86Y×278Z Spatial Meshes.

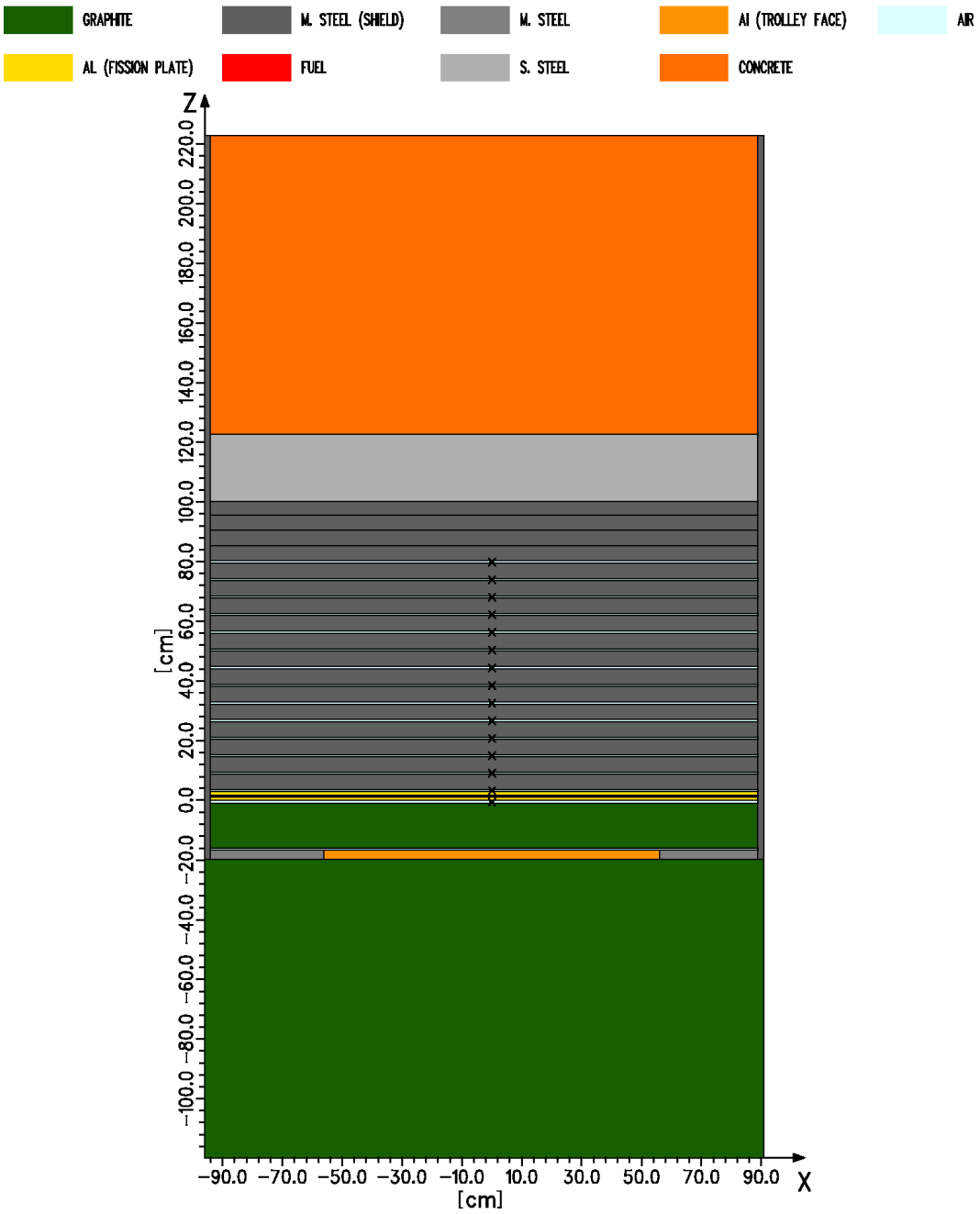

FIG. 4.3

Iron-88 - Compositional and Geometrical Model in the TORT-3.2 (X,Y,Z) Calculations.

Enlargement of the Measurement Region, Horizontal Section at Y = 0.0 cm.
Dosimeter Locations "×", 69X×86Y×278Z Spatial Meshes.

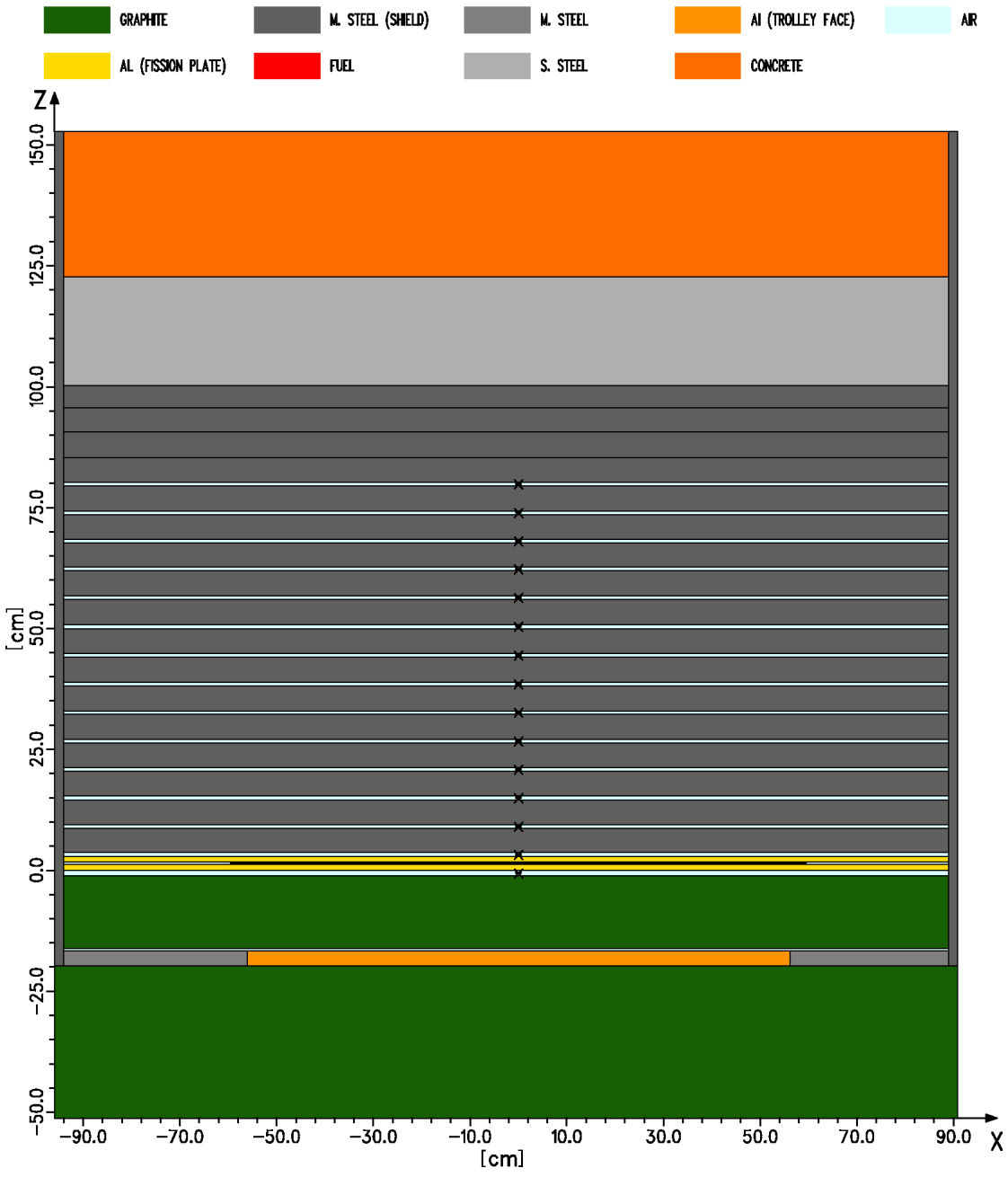

TAB. 4.1

Iron-88 - Atomic Densities Used in the TORT-3.2 Calculations
with the BUGJEFF311.BOLIB and BUGENDF70.BOLIB Libraries.

Material	Material Density [g × cm^{-3}]	Element/ Isotope	Isotopic Abundance [%]	Atomic Density [atoms × barn^{-1} × cm^{-1}]
Mild Steel in Trolley Face	7.835	C-nat[a]	1.	8.64238E-04
		Si-28	0.92230	6.19784E-05
		Si-29	0.04683	3.14697E-06
		Si-30	0.03087	2.07446E-06
		Mn-55	1.	9.36145E-04
		Fe-54	0.05845	4.87178E-03
		Fe-56	0.91754	7.64765E-02
		Fe-57	0.02119	1.76618E-03
		Fe-58	0.00282	2.35046E-04
Aluminium in Trolley Face	2.700	Al-27	1.	6.02626E-02
Graphite	1.650	C-nat	1.	8.27286E-02
Fuel[b]	3.256	Al-27	1.	5.81233E-02
		U-235	0.93	1.55501E-03
		U-238	0.07	1.13670E-04
Aluminium in Fission Plate	2.666	Al-27	1	5.90813E-02
		Si-28	0.92230	7.90847E-05
		Si-29	0.04683	4.01555E-06
		Si-30	0.03087	2.64702E-06
		Fe-54	0.05845	9.41022E-06
		Fe-56	0.91754	1.47720E-04
		Fe-57	0.02119	3.41151E-06
		Fe-58	0.00282	4.54009E-07
Mild Steel in Shield	7.850	C-nat	1.	9.05252E-04
		Mn-55	1.	6.36765E-04
		Fe-54	0.05845	4.89990E-03
		Fe-56	0.91754	7.69180E-02
		Fe-57	0.02119	1.77637E-03
		Fe-58	0.00282	2.36403E-04
Air	1.205E-03[c]	N-14	0.99634	3.95960E-05
		N-15	0.00366	1.45454E-07
		O-16	1.	1.05642E-05

([a]) Extension "-nat" refers to natural elements.
([b]) Uranium enriched to 93 w% in U-235.
([c]) Air density at the temperature of 20.0 °C taken from "Air Properties" in www.engineeringtoolbox.com.

4.1 Continued

Iron-88 - Atomic Densities Used in the TORT-3.2 Calculations
with the BUGJEFF311.BOLIB and BUGENDF70.BOLIB Libraries.

Material	Material Density [g × cm^{-3}]	Element/ Isotope	Isotopic Abundance [%]	Atomic Density [atoms × barn^{-1} × cm^{-1}]
Stainless Steel	7.917	C-nat	1.	2.38168E-04
		Si-28	0.92230	7.82837E-04
		Si-29	0.04683	3.97487E-05
		Si-30	0.03087	2.62021E-05
		P-31	1.	4.61784E-05
		S-32	0.95020	2.82570E-05
		S-33	0.00750	2.23034E-07
		S-34	0.04210	1.25197E-06
		S-36	0.00020	5.94758E-09
		Cr-50	0.04345	6.68135E-04
		Cr-52	0.83789	1.28843E-02
		Cr-53	0.09501	1.46098E-03
		Cr-54	0.02365	3.63668E-04
		Mn-55	1.	1.36250E-03
		Fe-54	0.05845	3.34089E-03
		Fe-56	0.91754	5.24448E-02
		Fe-57	0.02119	1.21118E-03
		Fe-58	0.00282	1.61186E-04
		Ni-58	0.68077	6.44795E-03
		Ni-60	0.26223	2.48372E-03
		Ni-61	0.01140	1.07976E-04
		Ni-62	0.03634	3.44196E-04
		Ni-64	0.00926	8.77066E-05
		Mo-92	0.14840	1.79944E-04
		Mo-94	0.09250	1.12162E-04
		Mo-95	0.15920	1.93040E-04
		Mo-96	0.16680	2.02255E-04
		Mo-97	0.09550	1.15799E-04
		Mo-98	0.24130	2.92591E-04
		Mo-100	0.09630	1.16770E-04
Concrete	2.242	H-1	1.	1.34221E-02
		O-16	1.	4.47309E-02
		Na-23	1.	9.47430E-04
		Al-27	1.	1.70478E-03
		Si-28	0.92230	1.49675E-02
		Si-29	0.04683	7.59976E-04
		Si-30	0.03087	5.00971E-04
		K-39	0.932581	6.45379E-04
		K-40	0.000117	8.09681E-08
		K-41	0.067302	4.65753E-05
		Ca-40	0.96941	1.24021E-03
		Ca-42	0.00647	8.27739E-06
		Ca-43	0.00135	1.72712E-06
		Ca-44	0.02086	2.66872E-05
		Ca-46	0.00004	5.11740E-08
		Ca-48	0.00187	2.39238E-06
		Fe-54	0.05845	1.99653E-05
		Fe-56	0.91754	3.13412E-04
		Fe-57	0.02119	7.23806E-06
		Fe-58	0.00282	9.63253E-07

TAB. 4.2

Iron-88 - Atomic Densities Used in the TORT-3.2 Calculations
with the BUGLE-B7 Library.

Material	Material Density [g × cm^{-3}]	Element/ Isotope	Isotopic Abundance [%]	Atomic Density [atoms × barn^{-1} × cm^{-1}]
Mild Steel in Trolley Face	7.835	C-nat[a]	1.	8.64238E-04
		Si-nat	1.	6.71998E-05
		Mn-55	1.	9.36145E-04
		Fe-54	0.05845	4.87178E-03
		Fe-56	0.91754	7.64765E-02
		Fe-57	0.02119	1.76618E-03
		Fe-58	0.00282	2.35046E-04
Aluminium in Trolley Face	2.700	Al-27	1.	6.02626E-02
Graphite	1.650	C-nat	1.	8.27286E-02
Fuel[b]	3.256	Al-27	1.	5.81233E-02
		U-235	0.93	1.55501E-03
		U-238	0.07	1.13670E-04
Aluminium in Fission Plate	2.666	Al-27	1.	5.90813E-02
		Si-nat	1.	8.57473E-05
		Fe-54	0.05845	9.41022E-06
		Fe-56	0.91754	1.47720E-04
		Fe-57	0.02119	3.41151E-06
		Fe-58	0.00282	4.54009E-07
Mild Steel in Shield	7.850	C-nat	1.	9.05252E-04
		Mn-55	1.	6.36765E-04
		Fe-54	0.05845	4.89990E-03
		Fe-56	0.91754	7.69180E-02
		Fe-57	0.02119	1.77637E-03
		Fe-58	0.00282	2.36403E-04
Air	1.205E-03[c]	N-14	0.99634	3.95960E-05
		N-15	0.00366	1.45454E-07
		O-16	1.	1.05642E-05

([a]) Extension "-nat" refers to natural elements.
([b]) Uranium enriched to 93 w% in U-235.
([c]) Air density at the temperature of 20.0 °C taken from "Air Properties" in www.engineeringtoolbox.com.

TAB. 4.2 Continued

Iron-88 - Atomic Densities Used in the TORT-3.2 Calculations
with the BUGLE-B7 Library.

Material	Material Density [g × cm^{-3}]	Element/ Isotope	Isotopic Abundance [%]	Atomic Density [atoms × barn^{-1} × cm^{-1}]
Stainless Steel	7.917	C-nat	1.	2.38168E-04
		Si-nat	1.	8.48788E-04
		P-31	1.	4.61784E-05
		S-nat	1.	2.97379E-05
		Cr-50	0.04345	6.68135E-04
		Cr-52	0.83789	1.28843E-02
		Cr-53	0.09501	1.46098E-03
		Cr-54	0.02365	3.63668E-04
		Mn-55	1.	1.36250E-03
		Fe-54	0.05845	3.34089E-03
		Fe-56	0.91754	5.24448E-02
		Fe-57	0.02119	1.21118E-03
		Fe-58	0.00282	1.61186E-04
		Ni-58	0.68077	6.44795E-03
		Ni-60	0.26223	2.48372E-03
		Ni-61	0.01140	1.07976E-04
		Ni-62	0.03634	3.44196E-04
		Ni-64	0.00926	8.77066E-05
		Mo-nat	1.	1.21256E-03
Concrete	2.242	H-1	1.	1.34221E-02
		O-16	1.	4.47309E-02
		Na-23	1.	9.47430E-04
		Al-27	1.	1.70478E-03
		Si-28	0.92230	1.49675E-02
		Si-29	0.04683	7.59976E-04
		Si-30	0.03087	5.00971E-04
		K-39	0.932581	6.45379E-04
		K-40	0.000117	8.09681E-08
		K-41	0.067302	4.65753E-05
		Ca-40	0.96941	1.24021E-03
		Ca-42	0.00647	8.27739E-06
		Ca-43	0.00135	1.72712E-06
		Ca-44	0.02086	2.66872E-05
		Ca-46	0.00004	5.11740E-08
		Ca-48	0.00187	2.39238E-06
		Fe-54	0.05845	1.99653E-05
		Fe-56	0.91754	3.13412E-04
		Fe-57	0.02119	7.23806E-06
		Fe-58	0.00282	9.63253E-07

TAB. 4.3

Iron-88 - Atomic Densities Used in the TORT-3.2 Calculations
with the BUGLE-96 Library.

Material	Material Density [g × cm^{-3}]	Element/ Isotope	Isotopic Abundance [%]	Atomic Density [atoms × barn^{-1} × cm^{-1}]
Mild Steel in Trolley Face	7.835	C-nat[a]	1.	8.64238E-04
		Si-nat	1.	6.71998E-05
		Mn-55	1.	9.36145E-04
		Fe-54	0.05845	4.87178E-03
		Fe-56	0.91754	7.64765E-02
		Fe-57	0.02119	1.76618E-03
		Fe-58	0.00282	2.35046E-04
Aluminium in Trolley Face	2.700	Al-27	1.	6.02626E-02
Graphite	1.650	C-nat	1.	8.27286E-02
Fuel[b]	3.256	Al-27	1.	5.81233E-02
		U-235	0.93	1.55501E-03
		U-238	0.07	1.13670E-04
Aluminium in Fission Plate	2.666	Al-27	1.	5.90813E-02
		Si-nat	1.	8.57473E-05
		Fe-54	0.05845	9.41022E-06
		Fe-56	0.91754	1.47720E-04
		Fe-57	0.02119	3.41151E-06
		Fe-58	0.00282	4.54009E-07
Mild Steel in Shield	7.850	C-nat	1.	9.05252E-04
		Mn-55	1.	6.36765E-04
		Fe-54	0.05845	4.89990E-03
		Fe-56	0.91754	7.69180E-02
		Fe-57	0.02119	1.77637E-03
		Fe-58	0.00282	2.36403E-04
Air	1.205E-03[c]	N-14	0.99634	3.95960E-05
		N-15	0.00366	1.45454E-07
		O-16	1.	1.05642E-05

([a]) Extension “-nat” refers to natural elements.
([b]) Uranium enriched to 93 w% in U-235.
([c]) Air density at the temperature of 20.0 °C taken from “Air Properties” in www.engineeringtoolbox.com.

TAB. 4.3 Continued

Iron-88 - Atomic Densities Used in the TORT-3.2 Calculations
with the BUGLE-96 Library.

Material	Material Density [g × cm^{-3}]	Element/ Isotope	Isotopic Abundance [%]	Atomic Density [atoms × barn^{-1} × cm^{-1}]
Stainless Steel	7.917	C-nat	1.	2.38168E-04
		Si-nat	1.	8.48788E-04
		P-31	1.	4.61784E-05
		S-nat	1.	2.97379E-05
		Cr-50	0.04345	6.68135E-04
		Cr-52	0.83789	1.28843E-02
		Cr-53	0.09501	1.46098E-03
		Cr-54	0.02365	3.63668E-04
		Mn-55	1.	1.36250E-03
		Fe-54	0.05845	3.34089E-03
		Fe-56	0.91754	5.24448E-02
		Fe-57	0.02119	1.21118E-03
		Fe-58	0.00282	1.61186E-04
		Ni-58	0.68077	6.44795E-03
		Ni-60	0.26223	2.48372E-03
		Ni-61	0.01140	1.07976E-04
		Ni-62	0.03634	3.44196E-04
		Ni-64	0.00926	8.77066E-05
		Mo-nat	1.	1.21256E-03
Concrete	2.242	H-1	1.	1.34221E-02
		O-16	1.	4.47309E-02
		Na-23	1.	9.47430E-04
		Al-27	1.	1.70478E-03
		Si-nat	1.	1.62284E-02
		K-nat	1.	6.92035E-04
		Ca-nat	1.	1.27935E-03
		Fe-54	0.05845	1.99653E-05
		Fe-56	0.91754	3.13412E-04
		Fe-57	0.02119	7.23806E-06
		Fe-58	0.00282	9.63253E-07

4.2 - Neutron Source Normalization

The following approach was adopted with respect to the fission neutron source normalization. Taking into account that the fission plate neutron source is given in units of neutrons × cm^{-3} × $second^{-1}$ × 1.0E+07 (see TAB. 2.3), corresponding to 1 Watt of fission plate power, the "xnf" normalization factor in TORT-3.2 is given by:

$$xnf = 5.68E\text{-}04 \times 3.0E+04 \times 1.0E\text{-}24 = 1.704E\text{-}25$$

where

5.68E-04 (see /10/) are the fission plate Watts per NESTOR reactor Watt,

3.0E+04 Watts (see /10/) is the NESTOR reactor power and

1.0E-24 is a conversion factor taking into account that the atomic densities introduced in TORT-3.2 were expressed in atoms × $barn^{-1}$ × cm^{-1}.

5 - DISCUSSION OF THE RESULTS

The Iron-88 reaction rates for the Au-197(n,γ)Au-198/Cd activation dosimeters and for the Rh-103(n,n')Rh-103m, In-115(n,n')In-115m, S-32(n,p)P-32 and Al-27(n,α)Na-24 threshold activation dosimeters (see 2.4), calculated using the BUGJEFF311.BOLIB /2/, BUGENDF70.BOLIB /3/, BUGLE-B7 /7/ and BUGLE-96 /8/ libraries, were compared with the corresponding experimental results.

The experimental dosimetric results were obtained in Iron-88 using the five types of previously cited activation dosimeters located (see 2.4, FIG. 2.7, and TABs. 5.1÷5.6) in fourteen measurement positions. In particular the Au-197(n,γ)Au-198 and S-32(n,p)P-32 dosimeters were positioned in all the fourteen measurement positions located in the air gaps between the mild steel slab components, the Rh-103(n,n')Rh-103m dosimeters in thirteen positions, the In-115(n,n')In-115m dosimeters in ten positions and, finally, the Al-27(n,α)Na-24 dosimeters only in four positions.

The calculated reaction rate results obtained with flat weighting and 1/4 T PV weighting dosimeter cross sections are respectively reported in TABs. 5.1 and 5.2 for Au-197(n,γ)Au-198/Cd, in TAB. 5.3 for Rh-103(n,n')Rh-103m, in TAB. 5.4 for In-115(n,n')In-115m, in TAB. 5.5 for S-32(n,p)P-32 and in TAB. 5.6 for Al-27(n,α)Na-24. In the previously cited tables the calculated (C) reaction rate results are compared with the corresponding experimental (E) reaction rate results through the C/E reaction rate ratios.
The total experimental uncertainties for the five types of activation dosimeters, at the specific measurement positions and at the confidence level of one standard deviation (1σ), were taken from the "General Description of the Experiment" document, included in the Iron-88 benchmark experiment section of the SINBAD REACTOR /11/ database and were correspondingly reported on the previously cited TABs. 5.1÷5.6

The experimental reaction rates for all the five activation dosimeters were respectively taken from the Table 8 of reference /10/ for the sulphur dosimeters, from the Table 9 for the indium dosimeters, from the Table 10 for the rhodium dosimeters, from the Table 11 for the gold dosimeters and from the Table 12 for the aluminium dosimeters. It is underlined that the experimental results for the gold dosimeters, presented in the Table 11 of reference /10/, take into account a correction for the NESTOR core neutron leakage background whilst, on the contrary, the "as measured" experimental reaction rates for the other four threshold activation dosimeters, reported in the previously cited tables of reference /10/, contain a contribution from the NESTOR core neutron leakage background (see 2.3). Consequently, since the calculated (C) reaction rates refer only to the neutrons produced in the fission plate, the "as measured" experimental (E) reaction rate values in the C/E ratios, reported in the TABs. 5.3÷5.6 of the present work, were reduced by 2% to eliminate the NESTOR reactor background component from the experimental reaction rates of the four threshold activation dosimeters in all the measurement positions, as recommended at page 2 of reference /10/.

The TAB. 5.1 shows the differences in the gold calculated reaction rates obtained through transport calculations using alternatively the first 44 or the first 45 neutron groups of the BUGLE-type neutron energy structure (see TAB. 3.1) of the BUGJEFF311.BOLIB library. It was intended in this way to verify the impact of two different cadmium cutoff energies

(0.876 eV with the 44-group calculation and 0.414 eV with the 45-group calculation), for the upper thermal threshold energy (see 3.5), on the corresponding calculated reaction rates.
Taking into account the experimental cadmium cutoff energy of 0.73 eV, corresponding to the cadmium cover thickness of 1.27 mm, used for the gold dosimeters employed in the Iron-88 benchmark experiment, it was decided to assume the 44-group calculation (corresponding to a cadmium cutoff energy of 0.876 eV) with the BUGJEFF311.BOLIB library as the most proper reference choice also in the calculations (see TAB. 5.2) with the other three (BUGENDF70.BOLIB, BUGLE-B7 and BUGLE-96) BUGLE-type libraries used. In this way it was obtained, in particular, better agreement with the gold experimental reaction rates. On the other hand it was verified and it is underlined that, summing up alternatively the contributions of the first 44 or 45 neutron energy groups (see TAB. 3.1), in the Iron-88 calculations using the BUGJEFF311.BOLIB library, the total gold reaction rate difference in each dosimeter position between the two calculations is limited to few percents (see TAB. 5.1).

All the calculated results shown in the TABs. 5.1÷5.6 were obtained using the BUGJEFF311.BOLIB, BUGENDF70.BOLIB, BUGLE-B7 and BUGLE-96 libraries together with the TORT-3.2 code in P_3-S_8 approximation.

Each of the FIGs. 5.1÷5.10 shows the intercomparisons of the C/E reaction rate ratio results obtained through the calculations with the BUGJEFF311.BOLIB, BUGENDF70.BOLIB, BUGLE-B7 and BUGLE-96 libraries, using alternatively flat weighting or 1/4 T PV weighting dosimeter cross sections. In particular the FIGs. 5.1 and 5.2 for the gold dosimeters, respectively reporting C/E results obtained through flat weighting and 1/4 T PV weighting dosimeter cross sections, correspond to TAB. 5.2. In a similar way, the FIGs. 5.3 and 5.4 for the rhodium dosimeters refer to TAB. 5.3, the FIGs. 5.5 and 5.6 for the indium dosimeters to TAB. 5.4, the FIGs. 5.7 and 5.8 for the sulphur dosimeters to TAB. 5.5 and, finally, the FIGs. 5.9 and 5.10 for the aluminium dosimeters to TAB. 5.6.

Comparisons of the C/E reaction rate ratio results obtained using alternatively the flat weighting and the 1/4 T PV weighting dosimeter cross sections are reported in the FIGs. 5.11÷5.30 for each of the four corresponding BUGLE-type libraries (BUGJEFF311.BOLIB, BUGENDF70.BOLIB, BUGLE-B7 and BUGLE-96) and for each of the five types of activation dosimeters (Au-197(n,γ)Au-198/Cd, Rh-103(n,n')Rh-103m, In-115(n,n')In-115m, S-32(n,p)P-32 and Al-27(n,α)Na-24) used in the Iron-88 benchmark experiment. In particular the FIGs. 5.11÷5.14 refer to Au-197(n,γ)Au-198/Cd C/E reaction rate ratios, and similarly, the FIGs. 5.15÷5.18 to Rh-103(n,n')Rh-103m, the FIGs. 5.19÷5.22 to In-115(n,n')In-115m, the FIGs. 5.23÷5.26 to S-32(n,p)P-32 and, finally, the FIGs. 5.27÷5.30 to Al-27(n,α)Na-24.

Gold Dosimeter Results

The Au-197(n,γ)Au-198 C/E (calculated/experimental) epi-cadmium reaction rate ratios obtained using the four BUGLE-type libraries are completely represented in TAB. 5.2 whilst the C/E ratios obtained from calculated reaction rates using 1/4 T PV weighting and flat weighting dosimeter cross sections are respectively shown in FIG. 5.1 and FIG. 5.2.
The Au-197(n,γ)Au-198/Cd calculated reaction rates using 1/4 T PV weighting dosimeter cross sections, corresponding to the Iron-88 epi-cadmium measurements with gold

dosimeters, present deviations (see TAB. 5.2 and FIG. 5.1) from the corresponding experimental results contained within ±15% and a systematic trend to overestimate the experimental results. When flat weighting dosimeter cross sections are employed, the deviations (see TAB. 5.2 and FIG. 5.2) of the calculated epi-cadmium reaction rates are within an increased ±25%. Meaningful differences between the C/E results obtained with flat weighting dosimeter cross sections and those calculated with 1/4 T PV weighting dosimeter cross sections are found. In fact, with flat weighting dosimeter cross sections, the deviations from the corresponding experimental results are systematically overestimated, between about 6% and 10%, with respect to the corresponding results obtained with 1/4 T PV weighting dosimeter cross sections which permit to have calculated results significantly more in agreement with the corresponding experimental results. The FIGs. 3.6 and 3.7, referring to the Au-197(n,γ)Au-198 neutron cross sections, respectively used in the calculations with the BUGJEFF311.BOLIB and BUGLE-96 libraries, show, for example, group cross section ratios which permit in particular to appreciate the differences between flat weighting and 1/4 T PV weighting self-shielded cross sections.
As previously mentioned (see in particular 3.5), the neutron cross sections for the Au-197(n,γ)Au-198 dosimeters were properly self-shielded through the GROUPIE module of the PREPRO /35/ nuclear data processing system, using a background cross section equal to 1695.0 barns. The cadmium cutoff energy was assumed to be about 0.73 eV, taking into account the thickness of 0.127 cm of the cadmium cover of the gold dosimeters. The calculated gold reaction rates obtained with the first 44 neutron energy groups (i.e. assuming implicitly a cadmium cutoff energy of 0.876 eV, the nearest energy value in the Bugle-type neutron energy group structure to the 0.73 eV value previously cited) of the four BUGLE-type libraries gave reduced results by about 1%÷2% with respect to the corresponding results obtained with the first 45 groups (i.e. assuming implicitly a cadmium cutoff energy of 0.414 eV, at the thermal neutron energy upper threshold).

Rhodium Dosimeter Results

The Rh-103(n,n')Rh-103m C/E (calculated/experimental) reaction rate ratios using the four BUGLE-type libraries are completely represented in TAB. 5.3 whilst the C/E ratios obtained from calculated reaction rates using 1/4 T PV weighting and flat weighting dosimeter cross sections are respectively shown in FIG. 5.3 and FIG. 5.4.
The Rh-103(n,n')Rh-103m calculated reaction rates present deviations (see TAB. 5.3 and FIGs. 5.3 and 5.4) from the corresponding experimental results contained within ±20% and are characterized by a trend to overestimation, independently of the use of flat weighting or 1/4 T PV weighting dosimeter cross sections. Increasing the neutron penetration depth, the calculated results coming from the ENEA-Bologna libraries (BUGJEFF311.BOLIB and BUGENDF70.BOLIB) tend to overestimate those obtained from the ORNL libraries (BUGLE-B7 and BUGLE-96). It is noted in particular that, in the C/E results obtained with BUGENDF70.BOLIB, the deviations from the corresponding BUGLE-B7 values reach about 15% of overestimation at about 60.0 cm of neutron penetration depth in the Iron-88 steel shield. This was found despite the fact that both libraries are based on the same ENDF/B-VII.0 evaluated data but, it is on the other hand underlined that they were not generated through the same nuclear data processing system. In particular the LANL NJOY-99.259 /36/ and the ENEA-Bologna 2007 Revision /31/ of ORNL SCAMPI /32/ systems were used to generate BUGENDF70.BOLIB whilst the ORNL AMPX-6.1 /34/ system was employed to produce BUGLE-B7.

Indium Dosimeter Results

The In-115(n,n')In-115m C/E (calculated/experimental) reaction rate ratios using the four BUGLE-type libraries are completely represented in TAB. 5.4 whilst the C/E ratios obtained from calculated reaction rates using 1/4 T PV weighting and flat weighting dosimeter cross sections are respectively shown in FIG. 5.5 and FIG. 5.6.
The In-115(n,n')In-115m calculated reaction rates show deviations (see TAB. 5.4 and FIGs. 5.5 and 5.6) from the corresponding experimental results contained within ±15%-20% and present a trend to underestimation with increasing neutron penetration depth, independently of the use of flat weighting or 1/4 T PV weighting dosimeter cross sections. Also in this case, as in the case of the Rhodium results, the calculated results coming from the ENEA-Bologna libraries (BUGJEFF311.BOLIB and BUGENDF70.BOLIB) tend to overestimate those obtained from the ORNL libraries (BUGLE-B7 and BUGLE-96), increasing the neutron penetration depth. It is noted in particular that, in the C/E results obtained with BUGENDF70.BOLIB, the deviations from the corresponding BUGLE-B7 values reach about 5%-10% of overestimation at about 45.0 cm of neutron penetration depth in the Iron-88 steel shield.

Sulphur Dosimeter Results

The In-115(n,n')In-115m C/E (calculated/experimental) reaction rate ratios using the four BUGLE-type libraries are completely represented in TAB. 5.5 whilst the C/E ratios obtained from calculated reaction rates using 1/4 T PV weighting and flat weighting dosimeter cross sections are respectively shown in FIG. 5.7 and FIG. 5.8.
Concerning the S-32(n,p)P-32 calculated reaction rates, the results obtained with flat weighting and 1/4 T PV weighting dosimeter cross sections give deviations (see TAB. 5.5 and FIGs. 5.7 and 5.8) from the corresponding experimental results within ±15%-20% and show a systematic trend to underestimation. It is noted that the BUGJEFF311.BOLIB library gives results apparently less underestimated (of about 5%-10%) with respect to the corresponding results of the other three BUGLE-type libraries used.

Aluminium Dosimeter Results

Finally the Al-27(n,α)Na-24 C/E (calculated/experimental) reaction rate ratios using the four BUGLE-type libraries are completely represented in TAB. 5.6 whilst the C/E ratios obtained from calculated reaction rates using 1/4 T PV weighting and flat weighting dosimeter cross sections are respectively shown in FIG. 5.9 and FIG. 5.10.
The Al-27(n,α)Na-24 calculated reaction rates obtained with 1/4 T PV weighting dosimeter cross sections, overestimate systematically (see TAB. 5.6 and FIG. 5.9) the corresponding experimental results up to +30%. It is underlined that only for these threshold activation dosimeters, with the highest effective threshold energy of 7.30 MeV, there are meaningful differences between the results obtained with flat weighting dosimeter cross sections and those calculated with 1/4 T PV weighting dosimeter cross sections.
In fact with flat weighting dosimeter cross sections, the deviations from the corresponding experimental results are systematically overestimated (see TAB. 5.6 and FIG. 5.10) by about 8%, with respect to the corresponding results obtained with 1/4 T PV weighting dosimeter cross sections. The FIGs. 3.16 and 3.17, referring to the Al-27(n,α)Na-24 neutron cross sections, respectively used in the calculations with the BUGJEFF311.BOLIB and BUGLE-96

libraries, show for example group cross section ratios which permit in particular to appreciate the differences between the flat weighting and the 1/4 T PV weighting dosimeter cross sections.

The absolute values of the experimental and calculated reaction rates for the Au-197(n,γ)Au-198/Cd, Rh-103(n,n')Rh-103m, In-115(n,n')In-115m, S-32(n,p)P-32 and Al-27(n,α)Na-24 activation dosimeters are respectively shown in the FIGs. 5.31÷5.35 where subjective trend lines for the experimental reaction rates are represented. These trend lines connect in particular all the experimental reaction rates for the cited dosimeters and the experimental reaction rates are compared with the corresponding calculated reaction rates obtained using the BUGJEFF311.BOLIB library.

The spatial distributions of the neutron fluxes, the spatial distributions of the dosimeter reaction rates and the calculated neutron spectra in different measurement positions, obtained using the BUGJEFF311.BOLIB library and the TORT-3.2 code in P_3-S_8 approximation, are respectively reported in the FIGs. 5.36÷5.40 for the neutron fluxes, in the FIGs. 5.41÷5.45 for the dosimeter reaction rates and in the FIGs. 5.46÷5.47 for the calculated neutron spectra.
The spatial distributions of the neutron fluxes for neutron energies above 0.414 eV, 0.1 MeV, 1.0 MeV, 3.0 MeV and 8.0 MeV are respectively presented in the FIGs. 5.36÷5.40, in the Iron-88 horizontal section at Y = 0.0 cm (see FIG. 4.2).
The spatial distributions of the reaction rates for the Au-197(n,γ)Au-198/Cd, Rh-103(n,n')Rh-103m, In-115(n,n')In-115m, S-32(n,p)P-32 and Al-27(n,α)Na-24 activation dosimeters are shown respectively in the FIGs. 5.41÷5.45, in the Iron-88 horizontal section at Y = 0.0 cm (see FIG. 4.2).
It is underlined that, in practice, the reaction rate results coming from Au-197(n,γ)Au-198/Cd correspond to neutron fluxes above about 0.414 eV (see 3.5), the results coming from Rh-103(n,n')Rh-103m correspond to neutron fluxes above about 0.1 MeV, the results coming from In-115(n,n')In-115m to neutron fluxes above about 1.0 MeV, the results coming from S-32(n,p)P-32 to neutron fluxes above about 3.0 MeV and, finally, the results coming from Al-27(n,α)Na-24 to neutron fluxes above about 8.0 MeV (see also 3.5, TAB. 2.4 and TABs. 3.5÷3.9).

A comparison of the calculated neutron spectra above 0.414 eV, at various Iron-88 measurement positions (A2, A4, A8, A12 and A15), is shown in FIG. 5.46. An enlargement of the previous figure is reported in FIG. 5.47 for neutron energies above 0.1 MeV. The different black and red colours for the histograms reproduced in the previously cited figures are here alternatively used only to distinguish better the different spectral trends.

Finally, the following conclusive statements can be formulated on the Iron-88 calculated results, obtained in the present analysis.

1. The 1/4 T PV weighting dosimeter cross section files, obtained using neutron weighting spectra calculated in the steel of a PWR pressure vessel, permit to obtain reaction rate results, with the four BUGLE-type libraries, in general more adherent to the corresponding experimental results than those obtained through the use of the flat weighting dosimeter cross section files.

2. The impact of the 1/4 T PV weighting dosimeter cross section files in the present transport calculations is in particular meaningful for the Au-197(n,γ)Au-198/Cd and Al-27(n,α)Na-24) calculated reaction rate results, obtained through the four BUGLE-type libraries.

3. The 1/4 T PV weighting dosimeter cross section files used together with the four BUGLE-type libraries give calculated reaction rate results for the Al-27(n,α)Na-24 dosimeters, always excessively overestimated with respect to the corresponding experimental results, increasing the neutron penetration depth.

4. The calculated reaction rate results for the gold, rhodium, indium and sulphur dosimeters, obtained using the 1/4 T PV weighting dosimeter cross section files together with the four BUGLE-type libraries, are contained within a confidence level of the total experimental uncertainty equal to ±3σ (99.7% probability that the measurement result is between ±3 standard deviations). This corresponds to deviations of ±15%-20% from the experimental reaction rates. On the contrary, the calculated results of the aluminium dosimeters with the highest effective threshold energy (7.30 MeV) and a minor part of the results of the Rh-103(n,n')Rh-103m and In-115(n,n')In-115m dosimeters with the lowest effective threshold energies (0.69 MeV and 1.30 MeV respectively) are not contained within the same previously cited confidence level.

5. The neutron cross sections for the Au-197(n,γ)Au-198/Cd dosimeters were properly self-shielded using a background cross section equal to 1695.0 barns. The cadmium cutoff energy was assumed to be about 0.73 eV, taking into account the thickness of 0.127 cm of the cadmium cover of the gold dosimeters.

6. The BUGENDF70.BOLIB and BUGLE-B7 libraries are based on the same ENDF/B-VII.0 evaluated nuclear data. Despite this fact, the cited libraries give meaningful discrepancies in the calculated reaction rate results, above about 20.0 cm of neutron penetration depth in the Iron-88 steel slab. This fact is evident for the Au-197(n,γ)Au-198/Cd dosimeters and, in particular, for the Rh-103(n,n')Rh-103m and In-115(n,n')In-115m threshold dosimeters with the lowest effective threshold energies (0.69 MeV and 1.30 MeV respectively). The C/E results obtained using BUGENDF70.BOLIB overestimate those obtained from BUGLE-B7, increasing the neutron penetration depth. It would be important to establish if these different calculated results, approximately obtained in the neutron energy range 1.0 MeV - 6.0 MeV, (corresponding approximately to the 90% response energy ranges typical of the cited rhodium and indium threshold dosimeters) are due to possible different nuclear data processing approaches in the code systems used to generate the cited libraries. In particular the LANL NJOY-99.259 /36/ and the ENEA-Bologna 2007 Revision /31/ of ORNL SCAMPI /32/ were the data processing systems used to generate BUGENDF70.BOLIB whilst the ORNL AMPX-6.1 /34/ system was employed to produce BUGLE-B7.

TAB. 5.1

Iron-88 - Comparison of the Au-197(n,γ)Au-198 epi-Cadmium Reaction Rate Ratios (Calculated/Experimental) in 44-Group and 45-Group Calculations.

P_3-S_8 Calculations Using the BUGJEFF311.BOLIB Library with Flat Weighting and 1/4 T PV Weighting Dosimeter Cross Sections.

Au-197(n,γ) Flat Weighting

Position	Shield Thickness [cm]	Experiment RR[a,b] (E)	Total Error (1σ) [%]	44-Group Calculation RR[a] (C)	C/E	45-Group Calculation RR[a] (C)	C/E
A2	0.00	1.05E-14	4.2	1.31370E-14	1.25	1.34822E-14	1.28
A3	5.10	6.24E-15	4.2	7.55178E-15	1.21	7.65235E-15	1.23
A4	10.22	4.19E-15	4.2	4.89977E-15	1.17	4.94665E-15	1.18
A5	15.34	2.97E-15	4.2	3.40712E-15	1.15	3.43609E-15	1.16
A6	20.44	2.19E-15	4.2	2.51225E-15	1.15	2.53259E-15	1.16
A7	25.64	1.70E-15	4.2	1.93419E-15	1.14	1.94938E-15	1.15
A8	30.79	1.35E-15	4.2	1.54726E-15	1.15	1.55917E-15	1.15
A9	35.99	1.11E-15	4.2	1.26321E-15	1.14	1.27282E-15	1.15
A10	41.19	9.10E-16	4.2	1.04319E-15	1.15	1.05108E-15	1.16
A11	46.44	7.67E-16	4.2	8.63161E-16	1.13	8.69683E-16	1.13
A12	51.62	6.55E-16	4.2	7.15482E-16	1.09	7.20898E-16	1.10
A13	56.69	5.44E-16	4.2	5.94104E-16	1.09	5.98616E-16	1.10
A14	61.81	4.62E-16	4.2	4.91605E-16	1.06	4.95355E-16	1.07
A15	66.99	3.99E-16	4.2	4.06232E-16	1.02	4.09343E-16	1.03

[a] RR = Reaction Rates in units of reactions per second per atom at the NESTOR reactor maximum power (30 kW).
[b] The reported RR were already corrected for the NESTOR reactor background component. These data were used to obtain the C/E ratios.

Au-197(n,γ) 1/4 T PV Weighting

Position	Shield Thickness [cm]	Experiment RR[a,b] (E)	Total Error (1σ) [%]	44-Group Calculation RR[a] (C)	C/E	45-Group Calculation RR[a] (C)	C/E
A2	0.00	1.05E-14	4.2	1.19920E-14	1.14	1.23396E-14	1.18
A3	5.10	6.24E-15	4.2	7.01968E-15	1.12	7.12096E-15	1.14
A4	10.22	4.19E-15	4.2	4.58651E-15	1.09	4.63372E-15	1.11
A5	15.34	2.97E-15	4.2	3.19971E-15	1.08	3.22889E-15	1.09
A6	20.44	2.19E-15	4.2	2.36461E-15	1.08	2.38509E-15	1.09
A7	25.64	1.70E-15	4.2	1.82371E-15	1.07	1.83901E-15	1.08
A8	30.79	1.35E-15	4.2	1.46064E-15	1.08	1.47263E-15	1.09
A9	35.99	1.11E-15	4.2	1.19334E-15	1.08	1.20302E-15	1.08
A10	41.19	9.10E-16	4.2	9.85801E-16	1.08	9.93749E-16	1.09
A11	46.44	7.67E-16	4.2	8.15704E-16	1.06	8.22273E-16	1.07
A12	51.62	6.55E-16	4.2	6.76052E-16	1.03	6.81506E-16	1.04
A13	56.69	5.44E-16	4.2	5.61227E-16	1.03	5.65771E-16	1.04
A14	61.81	4.62E-16	4.2	4.64256E-16	1.00	4.68032E-16	1.01
A15	66.99	3.99E-16	4.2	3.83510E-16	0.96	3.86643E-16	0.97

[a] RR = Reaction Rates in units of reactions per second per atom at the NESTOR reactor maximum power (30 kW).
[b] The reported RR were already corrected for the NESTOR reactor background component. These data were used to obtain the C/E ratios.

TAB. 5.2

Iron-88 - Summary of Experimental (E) and Calculated (C)
Au-197(n,γ)Au-198/Cd Reaction Rates along the Horizontal Z Axis.

Au-197(n,γ) Flat Weighting

Position	Shield Thickness	Exp.RR as Measured	Total Error (1σ) [%]	BUGJEFF311 Calculated RR (C)	C/E	BUGENDF70 Calculated RR (C)	C/E	BUGLE-B7 Calculated RR (C)	C/E	BUGLE-96 Calculated RR (C)	C/E
A2	0.00	1.05e-14	4.2	1.31370E-14	1.25	1.31579E-14	1.25	1.30290E-14	1.24	1.28366E-14	1.22
A3	5.10	6.24e-15	4.2	7.55178E-15	1.21	7.56852E-15	1.21	7.30149E-15	1.17	7.24905E-15	1.16
A4	10.22	4.19e-15	4.2	4.89977E-15	1.17	4.92160E-15	1.17	4.75543E-15	1.13	4.72741E-15	1.13
A5	15.34	2.97e-15	4.2	3.40712E-15	1.15	3.43472E-15	1.16	3.33956E-15	1.12	3.31582E-15	1.12
A6	20.44	2.19e-15	4.2	2.51225E-15	1.15	2.54202E-15	1.16	2.48494E-15	1.13	2.46337E-15	1.12
A7	25.64	1.70e-15	4.2	1.93419E-15	1.14	1.96135E-15	1.15	1.92411E-15	1.13	1.90554E-15	1.12
A8	30.79	1.35e-15	4.2	1.54726E-15	1.15	1.56846E-15	1.16	1.54111E-15	1.14	1.52590E-15	1.13
A9	35.99	1.11e-15	4.2	1.26321E-15	1.14	1.27717E-15	1.15	1.25476E-15	1.13	1.24277E-15	1.12
A10	41.19	9.10e-16	4.2	1.04319E-15	1.15	1.05032E-15	1.15	1.03028E-15	1.13	1.02108E-15	1.12
A11	46.44	7.67e-16	4.2	8.63161E-16	1.13	8.64650E-16	1.13	8.45773E-16	1.10	8.38866E-16	1.09
A12	51.62	6.55e-16	4.2	7.15482E-16	1.09	7.12850E-16	1.09	6.94630E-16	1.06	6.89519E-16	1.05
A13	56.69	5.44e-16	4.2	5.94104E-16	1.09	5.88693E-16	1.08	5.70999E-16	1.05	5.67253E-16	1.04
A14	61.81	4.62e-16	4.2	4.91605E-16	1.06	4.84388E-16	1.05	4.67257E-16	1.01	4.64550E-16	1.01
A15	66.99	3.99e-16	4.2	4.06232E-16	1.02	3.97932E-16	1.00	3.81426E-16	0.96	3.79452E-16	0.95

Au-197(n,γ) 1/4 T PV Weighting

A2	0.00	1.05e-14	4.2	1.19920E-14	1.14	1.20122E-14	1.14	1.19244E-14	1.14	1.17502E-14	1.12
A3	5.10	6.24e-15	4.2	7.01968E-15	1.12	7.03660E-15	1.13	6.82979E-15	1.09	6.77962E-15	1.09
A4	10.22	4.19e-15	4.2	4.58651E-15	1.09	4.60824E-15	1.10	4.48302E-15	1.07	4.45462E-15	1.06
A5	15.34	2.97e-15	4.2	3.19971E-15	1.08	3.22688E-15	1.09	3.15877E-15	1.06	3.13459E-15	1.06
A6	20.44	2.19e-15	4.2	2.36461E-15	1.08	2.39368E-15	1.09	2.35545E-15	1.08	2.33373E-15	1.07
A7	25.64	1.70e-15	4.2	1.82371E-15	1.07	1.85008E-15	1.09	1.82674E-15	1.07	1.80817E-15	1.06
A8	30.79	1.35e-15	4.2	1.46064E-15	1.08	1.48115E-15	1.10	1.46462E-15	1.08	1.44946E-15	1.07
A9	35.99	1.11e-15	4.2	1.19334E-15	1.08	1.20684E-15	1.09	1.19316E-15	1.07	1.18122E-15	1.06
A10	41.19	9.10e-16	4.2	9.85801E-16	1.08	9.92752E-16	1.09	9.79927E-16	1.08	9.70733E-16	1.07
A11	46.44	7.67e-16	4.2	8.15704E-16	1.06	8.17271E-16	1.07	8.04426E-16	1.05	7.97499E-16	1.04
A12	51.62	6.55e-16	4.2	6.76052E-16	1.03	6.73694E-16	1.03	6.60566E-16	1.01	6.55411E-16	1.00
A13	56.69	5.44e-16	4.2	5.61227E-16	1.03	5.56225E-16	1.02	5.42864E-16	1.00	5.39060E-16	0.99
A14	61.81	4.62e-16	4.2	4.64256E-16	1.00	4.57534E-16	0.99	4.44097E-16	0.96	4.41326E-16	0.96
A15	66.99	3.99e-16	4.2	3.83510E-16	0.96	3.75754E-16	0.94	3.62408E-16	0.91	3.60374E-16	0.90

[a] RR = Reaction Rates in units of reactions per second per atom at at the NESTOR reactor maximum power (30 kW).

TAB. 5.3

Iron-88 - Summary of Experimental (E) and Calculated (C)
Rh-103(n,n')Rh-103m Reaction Rates along the Horizontal Z Axis.

Rh-103(n,n') Flat Weighting

Position	Shield Thickness	Exp.RR[a] as Measured	Total Error (1σ) [%]	Exp.RR[b] without Background (E)	BUGJEFF311 Calculated RR[a] (C)	C/E	BUGENDF70 Calculated RR[a] (C)	C/E	BUGLE-B7 Calculated RR[a] (C)	C/E	BUGLE-96 Calculated RR[a] (C)	C/E
A2	0.00	3.35e-16	5.1	3.28e-16	3.41199E-16	1.04	3.40121E-16	1.04	3.42534E-16	1.04	3.42557E-16	1.04
A3	5.10	1.42e-16	5.2	1.39e-16	1.51048E-16	1.09	1.50022E-16	1.08	1.50299E-16	1.08	1.50418E-16	1.08
A4	10.22	7.78e-17	5.1	7.62e-17	8.67446E-17	1.14	8.60041E-17	1.13	8.56448E-17	1.12	8.57925E-17	1.13
A5	15.34	4.70e-17	5.1	4.61e-17	5.27454E-17	1.15	5.23286E-17	1.14	5.16871E-17	1.12	5.18274E-17	1.13
A6	20.44	2.86e-17	5.2	2.80e-17	3.32293E-17	1.19	3.30412E-17	1.18	3.23181E-17	1.15	3.24350E-17	1.16
A7	25.64	1.82e-17	5.1	1.78e-17	2.12624E-17	1.19	2.12203E-17	1.19	2.05195E-17	1.15	2.06105E-17	1.16
A8	30.79	1.20e-17	5.1	1.18e-17	1.39110E-17	1.18	1.39499E-17	1.19	1.33213E-17	1.13	1.33898E-17	1.14
A9	35.99	7.97e-18	5.2	7.81e-18	9.19199E-18	1.18	9.27230E-18	1.19	8.73366E-18	1.12	8.78436E-18	1.12
A10	41.19	5.48e-18	5.2	5.37e-18	6.13836E-18	1.14	6.23477E-18	1.16	5.78692E-18	1.08	5.82415E-18	1.08
A11	46.44	3.84e-18	5.2	3.76e-18	4.11695E-18	1.09	4.21457E-18	1.12	3.85083E-18	1.02	3.87805E-18	1.03
A12	51.62	2.68e-18	5.1	2.63e-18	2.79268E-18	1.06	2.88333E-18	1.10	2.59190E-18	0.99	2.61189E-18	0.99
A13	56.69	1.89e-18	5.2	1.85e-18	1.91887E-18	1.04	1.99902E-18	1.08	1.76728E-18	0.95	1.78207E-18	0.96
A14	61.81	1.34e-18	5.1	1.31e-18	1.31927E-18	1.00	1.38764E-18	1.06	1.20547E-18	0.92	1.21640E-18	0.93
A15	66.99	-	-	-	-	-	-	-	-	-	-	-

Rh-103(n,n') 1/4 T PV Weighting

A2	0.00	3.35e-16	5.1	3.28e-16	3.39769E-16	1.03	3.38420E-16	1.03	3.40789E-16	1.04	3.40801E-16	1.04
A3	5.10	1.42e-16	5.2	1.39e-16	1.50094E-16	1.08	1.48832E-16	1.07	1.49080E-16	1.07	1.49189E-16	1.07
A4	10.22	7.78e-17	5.1	7.62e-17	8.60847E-17	1.13	8.51696E-17	1.12	8.47952E-17	1.11	8.49348E-17	1.11
A5	15.34	4.70e-17	5.1	4.61e-17	5.22917E-17	1.14	5.17516E-17	1.12	5.11048E-17	1.11	5.12387E-17	1.11
A6	20.44	2.86e-17	5.2	2.80e-17	3.29190E-17	1.17	3.26458E-17	1.16	3.19235E-17	1.14	3.20352E-17	1.14
A7	25.64	1.82e-17	5.1	1.78e-17	2.10526E-17	1.18	2.09532E-17	1.17	2.02561E-17	1.14	2.03431E-17	1.14
A8	30.79	1.20e-17	5.1	1.18e-17	1.37688E-17	1.17	1.37695E-17	1.17	1.31456E-17	1.12	1.32111E-17	1.12
A9	35.99	7.97e-18	5.2	7.81e-18	9.09603E-18	1.16	9.15107E-18	1.17	8.61715E-18	1.10	8.66558E-18	1.11
A10	41.19	5.48e-18	5.2	5.37e-18	6.07355E-18	1.13	6.15330E-18	1.15	5.70966E-18	1.06	5.74520E-18	1.07
A11	46.44	3.84e-18	5.2	3.76e-18	4.07328E-18	1.08	4.15995E-18	1.11	3.79972E-18	1.01	3.82570E-18	1.02
A12	51.62	2.68e-18	5.1	2.63e-18	2.76304E-18	1.05	2.84644E-18	1.08	2.55785E-18	0.97	2.57692E-18	0.98
A13	56.69	1.89e-18	5.2	1.85e-18	1.89855E-18	1.03	1.97383E-18	1.07	1.74432E-18	0.94	1.75843E-18	0.95
A14	61.81	1.34e-18	5.1	1.31e-18	1.30534E-18	0.99	1.37043E-18	1.04	1.19000E-18	0.91	1.20043E-18	0.91
A15	66.99	-	-	-	-	-	-	-	-	-	-	-

[a] RR = Reaction Rates in units of reactions per second per atom at at the NESTOR reactor maximum power (30 kW).
[b] RR Background are the experimental reaction rates reduced by 2% to eliminate the NESTOR reactor background component. These data are used to obtain the C/E ratios.

TAB. 5.4

Iron-88 - Summary of Experimental (E) and Calculated (C)
In-115(n,n')In-115m Reaction Rates along the Horizontal Z Axis.

In-115(n,n') Flat Weighting

Position	Shield Thickness	Exp.RR[a] as Measured	Total Error (1σ) [%]	Exp.RR[b] without Background (E)	BUGJEFF311 Calculated RR[a] (C)	C/E	BUGENDF70 Calculated RR[a] (C)	C/E	BUGLE-B7 Calculated RR[a] (C)	C/E	BUGLE-96 Calculated RR[a] (C)	C/E
A2	0.00	7.02e-17	4.5	6.88e-17	7.14086E-17	1.04	7.11809E-17	1.03	7.17280E-17	1.04	7.16735E-17	1.04
A3	5.10	2.40e-17	4.5	2.35e-17	2.29334E-17	0.98	2.27177E-17	0.97	2.27744E-17	0.97	2.27955E-17	0.97
A4	10.22	1.06e-17	4.5	1.04e-17	1.02797E-17	0.99	1.01557E-17	0.98	1.01212E-17	0.97	1.01480E-17	0.98
A5	15.34	5.14e-18	4.5	5.04e-18	4.89867E-18	0.97	4.84374E-18	0.96	4.78923E-18	0.95	4.81096E-18	0.96
A6	20.44	2.53e-18	4.5	2.48e-18	2.43093E-18	0.98	2.41141E-18	0.97	2.36091E-18	0.95	2.37602E-18	0.96
A7	25.64	1.32e-18	4.5	1.29e-18	1.22860E-18	0.95	1.22493E-18	0.95	1.18483E-18	0.92	1.19449E-18	0.92
A8	30.79	7.21e-19	4.5	7.07e-19	6.43030E-19	0.91	6.45063E-19	0.91	6.15302E-19	0.87	6.21232E-19	0.88
A9	35.99	3.93e-19	4.6	3.85e-19	3.43868E-19	0.89	3.47412E-19	0.90	3.26133E-19	0.85	3.29666E-19	0.86
A10	41.19	2.21e-19	4.6	2.17e-19	1.88646E-19	0.87	1.92081E-19	0.89	1.77159E-19	0.82	1.79232E-19	0.83
A11	46.44	1.28e-19	4.7	1.25e-19	1.05389E-19	0.84	1.08237E-19	0.86	9.79179E-20	0.78	9.91212E-20	0.79
A12	51.62	-	-	-	-	-	-	-	-	-	-	-
A13	56.69	-	-	-	-	-	-	-	-	-	-	-
A14	61.81	-	-	-	-	-	-	-	-	-	-	-
A15	66.99	-	-	-	-	-	-	-	-	-	-	-

In-115(n,n') 1/4 T PV Weighting

A2	0.00	7.02e-17	4.5	6.88e-17	7.10287E-17	1.03	7.07819E-17	1.03	7.13233E-17	1.04	7.12678E-17	1.04
A3	5.10	2.40e-17	4.5	2.35e-17	2.27344E-17	0.97	2.25031E-17	0.96	2.25579E-17	0.96	2.25781E-17	0.96
A4	10.22	1.06e-17	4.5	1.04e-17	1.01674E-17	0.98	1.00329E-17	0.97	9.99830E-18	0.96	1.00244E-17	0.96
A5	15.34	5.14e-18	4.5	5.04e-18	4.83468E-18	0.96	4.77272E-18	0.95	4.71885E-18	0.94	4.74014E-18	0.94
A6	20.44	2.53e-18	4.5	2.48e-18	2.39414E-18	0.97	2.36994E-18	0.96	2.32034E-18	0.94	2.33515E-18	0.94
A7	25.64	1.32e-18	4.5	1.29e-18	1.20749E-18	0.93	1.20074E-18	0.93	1.16152E-18	0.90	1.17099E-18	0.91
A8	30.79	7.21e-19	4.5	7.07e-19	6.30750E-19	0.89	6.30740E-19	0.89	6.01738E-19	0.85	6.07546E-19	0.86
A9	35.99	3.93e-19	4.6	3.85e-19	3.36688E-19	0.87	3.38886E-19	0.88	3.18212E-19	0.83	3.21668E-19	0.84
A10	41.19	2.21e-19	4.6	2.17e-19	1.84406E-19	0.85	1.86953E-19	0.86	1.72493E-19	0.80	1.74518E-19	0.81
A11	46.44	1.28e-19	4.7	1.25e-19	1.02874E-19	0.82	1.05137E-19	0.84	9.51592E-20	0.76	9.63328E-20	0.77
A12	51.62	-	-	-	-	-	-	-	-	-	-	-
A13	56.69	-	-	-	-	-	-	-	-	-	-	-
A14	61.81	-	-	-	-	-	-	-	-	-	-	-
A15	66.99	-	-	-	-	-	-	-	-	-	-	-

[a] RR = Reaction Rates in units of reactions per second per atom at at the NESTOR reactor maximum power (30 kW).
[b] RR Background are the experimental reaction rates reduced by 2% to eliminate the NESTOR reactor background component. These data are used to obtain the C/E ratios.

TAB. 5.5

Iron-88 - Summary of Experimental (E) and Calculated (C)
S-32(n,p)P-32 Reaction Rates along the Horizontal Z Axis.

S-32(n,p) Flat Weighting

Position	Shield Thickness	Exp.RR[a] as Measured	Total Error (1σ) [%]	Exp.RR[b] without Background (E)	BUGJEFF311 Calculated RR[a] (C)	C/E	BUGENDF70 Calculated RR[a] (C)	C/E	BUGLE-B7 Calculated RR[a] (C)	C/E	BUGLE-96 Calculated RR[a] (C)	C/E
A2	0.00	2.02e-17	6.5	1.98e-17	1.83350E-17	0.93	1.82973E-17	0.92	1.84237E-17	0.93	1.84186E-17	0.93
A3	5.10	4.29e-18	6.5	4.20e-18	3.76077E-18	0.89	3.67727E-18	0.87	3.69631E-18	0.88	3.69912E-18	0.88
A4	10.22	1.40e-18	6.5	1.37e-18	1.27846E-18	0.93	1.23186E-18	0.90	1.23614E-18	0.90	1.23850E-18	0.90
A5	15.34	5.12e-19	6.5	5.02e-19	4.65139E-19	0.93	4.42910E-19	0.88	4.43594E-19	0.88	4.45024E-19	0.89
A6	20.44	1.91e-19	6.5	1.87e-19	1.75044E-19	0.94	1.65044E-19	0.88	1.64948E-19	0.88	1.65719E-19	0.89
A7	25.64	7.13e-20	6.5	6.99e-20	6.55015E-20	0.94	6.12290E-20	0.88	6.10476E-20	0.87	6.14303E-20	0.88
A8	30.79	2.70e-20	6.6	2.65e-20	2.48524E-20	0.94	2.30572E-20	0.87	2.29310E-20	0.87	2.31127E-20	0.87
A9	35.99	1.03e-20	6.5	1.01e-20	9.37129E-21	0.93	8.63734E-21	0.86	8.56661E-21	0.85	8.64947E-21	0.86
A10	41.19	3.93e-21	6.5	3.85e-21	3.53114E-21	0.92	3.23569E-21	0.84	3.19991E-21	0.83	3.23661E-21	0.84
A11	46.44	1.49e-21	6.5	1.46e-21	1.32094E-21	0.90	1.20458E-21	0.82	1.18752E-21	0.81	1.20337E-21	0.82
A12	51.62	5.73e-22	6.5	5.62e-22	5.01227E-22	0.89	4.55356E-22	0.81	4.47406E-22	0.80	4.54241E-22	0.81
A13	56.69	2.27e-22	6.9	2.22e-22	1.94253E-22	0.87	1.76006E-22	0.79	1.72320E-22	0.77	1.75289E-22	0.79
A14	61.81	8.53e-23	8.6	8.36e-23	7.47202E-23	0.89	6.75995E-23	0.81	6.59252E-23	0.79	6.71957E-23	0.80
A15	66.99	3.50e-23	21.	3.43e-23	2.84783E-23	0.83	2.57586E-23	0.75	2.50109E-23	0.73	2.55468E-23	0.74

S-32(n,p) 1/4 T PV Weighting

Position	Shield Thickness	Exp.RR[a] as Measured	Total Error (1σ) [%]	Exp.RR[b] without Background (E)	BUGJEFF311 Calculated RR[a] (C)	C/E	BUGENDF70 Calculated RR[a] (C)	C/E	BUGLE-B7 Calculated RR[a] (C)	C/E	BUGLE-96 Calculated RR[a] (C)	C/E
A2	0.00	2.02e-17	6.5	1.98e-17	1.81803E-17	0.92	1.81319E-17	0.92	1.82568E-17	0.92	1.82577E-17	0.92
A3	5.10	4.29e-18	6.5	4.20e-18	3.72754E-18	0.89	3.64344E-18	0.87	3.66230E-18	0.87	3.66602E-18	0.87
A4	10.22	1.40e-18	6.5	1.37e-18	1.26678E-18	0.92	1.22033E-18	0.89	1.22458E-18	0.89	1.22720E-18	0.89
A5	15.34	5.12e-19	6.5	5.02e-19	4.60752E-19	0.92	4.38679E-19	0.87	4.39369E-19	0.88	4.40875E-19	0.88
A6	20.44	1.91e-19	6.5	1.87e-19	1.73340E-19	0.93	1.63430E-19	0.87	1.63342E-19	0.87	1.64136E-19	0.88
A7	25.64	7.13e-20	6.5	6.99e-20	6.48429E-20	0.93	6.06133E-20	0.87	6.04378E-20	0.86	6.08268E-20	0.87
A8	30.79	2.70e-20	6.6	2.65e-20	2.45938E-20	0.93	2.28179E-20	0.86	2.26951E-20	0.86	2.28783E-20	0.86
A9	35.99	1.03e-20	6.5	1.01e-20	9.27021E-21	0.92	8.54436E-21	0.85	8.47551E-21	0.84	8.55853E-21	0.85
A10	41.19	3.93e-21	6.5	3.85e-21	3.49153E-21	0.91	3.19937E-21	0.83	3.16457E-21	0.82	3.20116E-21	0.83
A11	46.44	1.49e-21	6.5	1.46e-21	1.30549E-21	0.89	1.19040E-21	0.82	1.17382E-21	0.80	1.18957E-21	0.81
A12	51.62	5.73e-22	6.5	5.62e-22	4.95091E-22	0.88	4.49706E-22	0.80	4.41993E-22	0.79	4.48761E-22	0.80
A13	56.69	2.27e-22	6.9	2.22e-22	1.91757E-22	0.86	1.73692E-22	0.78	1.70124E-22	0.76	1.73054E-22	0.78
A14	61.81	8.53e-23	8.6	8.36e-23	7.37082E-23	0.88	6.66514E-23	0.80	6.50345E-23	0.78	6.62849E-23	0.79
A15	66.99	3.50e-23	21.	3.43e-23	2.80691E-23	0.82	2.53701E-23	0.74	2.46502E-23	0.72	2.51759E-23	0.73

[a] RR = Reaction Rates in units of reactions per second per atom at at the NESTOR reactor maximum power (30 kW).
[b] RR Background are the experimental reaction rates reduced by 2% to eliminate the NESTOR reactor background component. These data are used to obtain the C/E ratios.

TAB. 5.6

Iron-88 - Summary of Experimental (E) and Calculated (C)
Al-27(n,α)Na-24 Reaction Rates along the Horizontal Z Axis.

Al-27(n,α) Flat Weighting

Position	Shield Thickness	Exp.RR[a] as Measured	Total Error (1σ) [%]	Exp.RR[b] without Background (E)	BUGJEFF311 Calculated RR[a] (C)	C/E	BUGENDF70 Calculated RR[a] (C)	C/E	BUGLE-B7 Calculated RR[a] (C)	C/E	BUGLE-96 Calculated RR[a] (C)	C/E
A2	0.00	-	-	-	-	-	-	-	-	-	-	-
A3	5.10	2.23e-20	4.7	2.19e-20	2.88764E-20	1.32	2.90774E-20	1.33	2.92646E-20	1.34	2.92791E-20	1.34
A4	10.22	-	-	-	-	-	-	-	-	-	-	-
A5	15.34	2.55e-21	4.7	2.50e-21	3.27462E-21	1.31	3.33560E-21	1.33	3.35805E-21	1.34	3.35944E-21	1.34
A6	20.44	9.56e-22	4.7	9.37e-22	1.24020E-21	1.32	1.26953E-21	1.36	1.27832E-21	1.36	1.27875E-21	1.36
A7	25.64	3.56e-22	4.7	3.49e-22	4.75763E-22	1.36	4.88797E-22	1.40	4.92297E-22	1.41	4.92409E-22	1.41
A8	30.79	-	-	-	-	-	-	-	-	-	-	-
A9	35.99	-	-	-	-	-	-	-	-	-	-	-
A10	41.19	-	-	-	-	-	-	-	-	-	-	-
A11	46.44	-	-	-	-	-	-	-	-	-	-	-
A12	51.62	-	-	-	-	-	-	-	-	-	-	-
A13	56.69	-	-	-	-	-	-	-	-	-	-	-
A14	61.81	-	-	-	-	-	-	-	-	-	-	-
A15	66.99	-	-	-	-	-	-	-	-	-	-	-

Al-27(n,α) 1/4 T PV Weighting

A2	0.00	-	-	-	-	-	-	-	-	-	-	-
A3	5.10	2.23e-20	4.7	2.19e-20	2.71286E-20	1.24	2.72480E-20	1.25	2.74256E-20	1.25	2.74531E-20	1.26
A4	10.22	-	-	-	-	-	-	-	-	-	-	-
A5	15.34	2.55e-21	4.7	2.50e-21	3.08380E-21	1.23	3.13304E-21	1.25	3.15439E-21	1.26	3.15751E-21	1.26
A6	20.44	9.56e-22	4.7	9.37e-22	1.16965E-21	1.25	1.19420E-21	1.27	1.20257E-21	1.28	1.20371E-21	1.28
A7	25.64	3.56e-22	4.7	3.49e-22	4.49460E-22	1.29	4.60584E-22	1.32	4.63919E-22	1.33	4.64320E-22	1.33
A8	30.79	-	-	-	-	-	-	-	-	-	-	-
A9	35.99	-	-	-	-	-	-	-	-	-	-	-
A10	41.19	-	-	-	-	-	-	-	-	-	-	-
A11	46.44	-	-	-	-	-	-	-	-	-	-	-
A12	51.62	-	-	-	-	-	-	-	-	-	-	-
A13	56.69	-	-	-	-	-	-	-	-	-	-	-
A14	61.81	-	-	-	-	-	-	-	-	-	-	-
A15	66.99	-	-	-	-	-	-	-	-	-	-	-

[a] RR = Reaction Rates in units of reactions per second per atom at the NESTOR reactor maximum power (30 kW).
[b] RR Background are the experimental reaction rates reduced by 2% to eliminate the NESTOR reactor background component. These data are used to obtain the C/E ratios.

FIG. 5.1

Iron-88 - Au-197(n,γ)Au-198 epi-Cadmium Reaction Rate Ratios (Calculated/Experimental)
Calculated Using the BUGJEFF311.BOLIB, BUGENDF70.BOLIB, BUGLE-B7
and BUGLE-96 Libraries with 1/4 T PV Weighting Dosimeter Cross Sections.

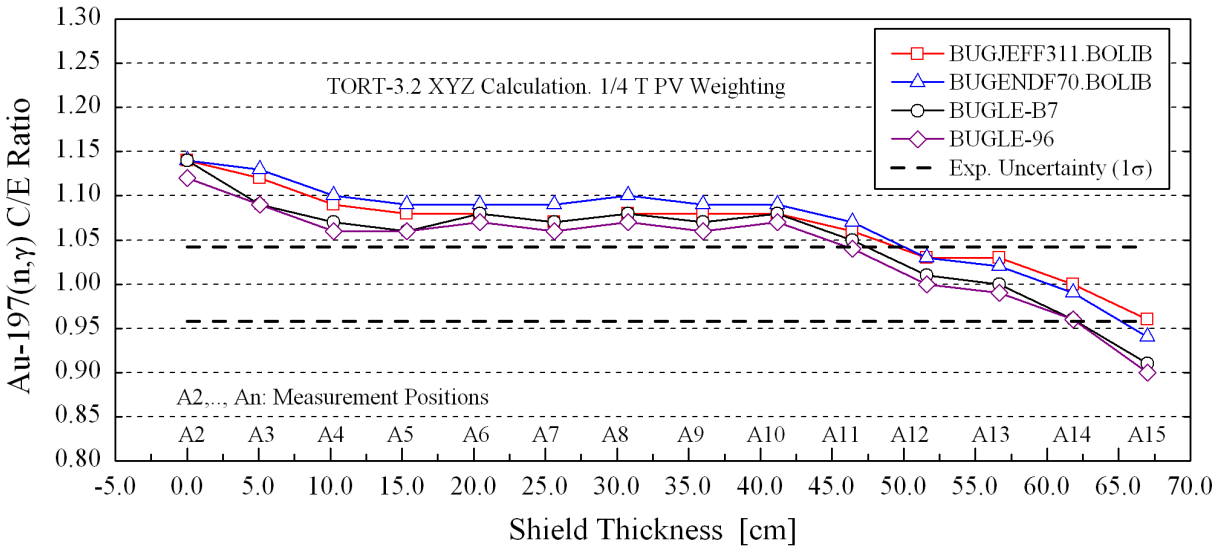

FIG. 5.2

Iron-88 - Au-197(n,γ)Au-198 epi-Cadmium Reaction Rate Ratios (Calculated/Experimental)
Calculated Using the BUGJEFF311.BOLIB, BUGENDF70.BOLIB, BUGLE-B7
and BUGLE-96 Libraries with Flat Weighting Dosimeter Cross Sections.

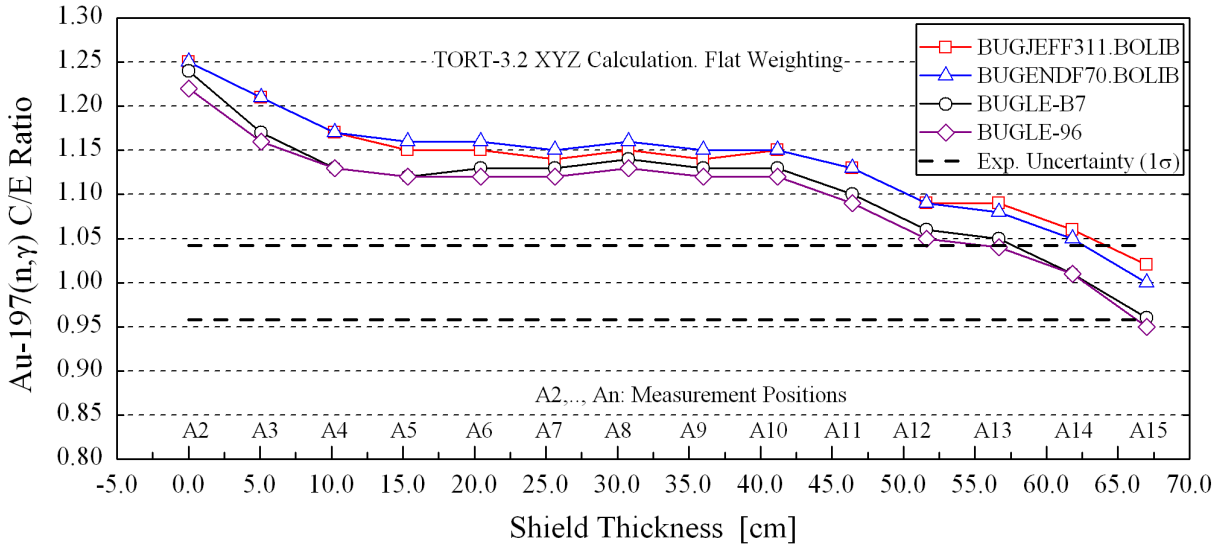

FIG. 5.3

Iron-88 - Rh-103(n,n')Rh-103m Reaction Rate Ratios (Calculated/Experimental) Calculated Using the BUGJEFF311.BOLIB, BUGENDF70.BOLIB, BUGLE-B7 and BUGLE-96 Libraries with 1/4 T PV Weighting Dosimeter Cross Sections.

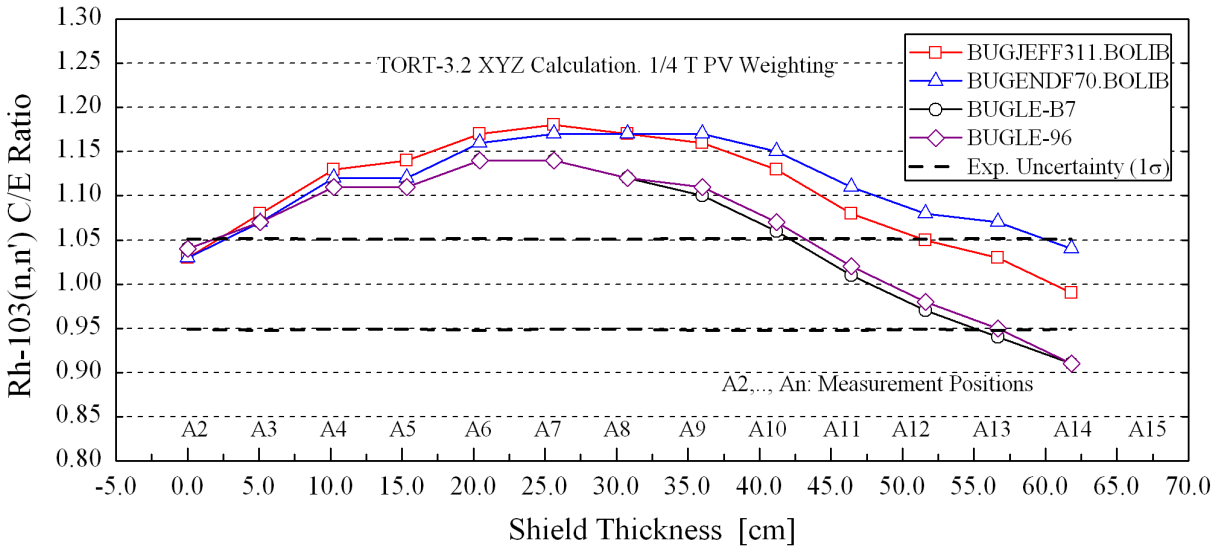

FIG. 5.4

Iron-88 - Rh-103(n,n')Rh-103m Reaction Rate Ratios (Calculated/Experimental) Calculated Using the BUGJEFF311.BOLIB, BUGENDF70.BOLIB, BUGLE-B7 and BUGLE-96 Libraries with Flat Weighting Dosimeter Cross Sections.

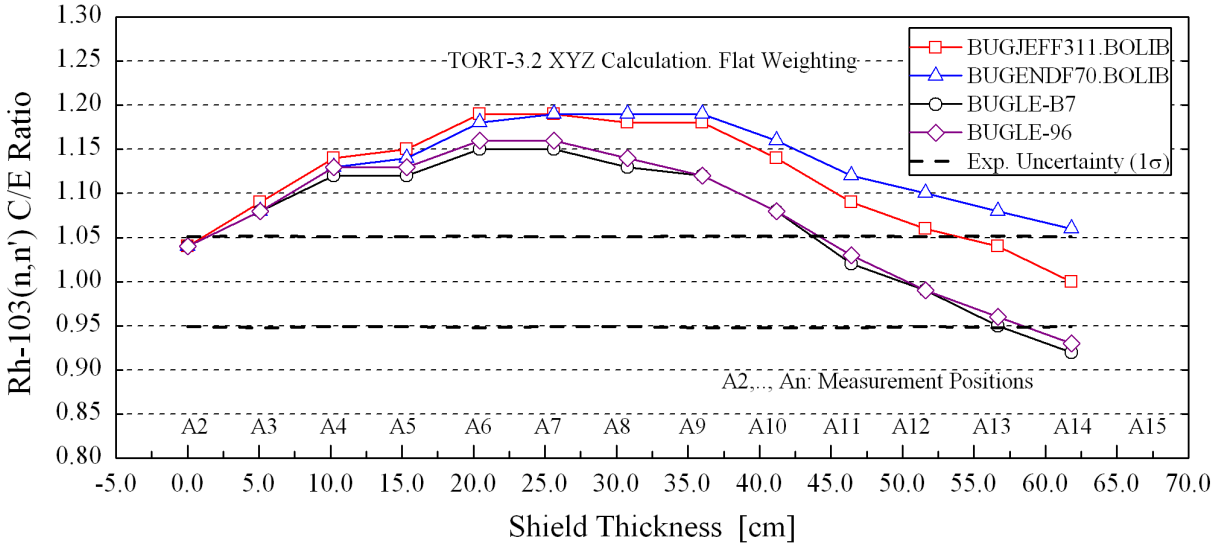

FIG. 5.5

Iron-88 - In-115(n,n')In-115m Reaction Rate Ratios (Calculated/Experimental) Calculated Using the BUGJEFF311.BOLIB, BUGENDF70.BOLIB, BUGLE-B7 and BUGLE-96 Libraries with 1/4 T PV Weighting Dosimeter Cross Sections.

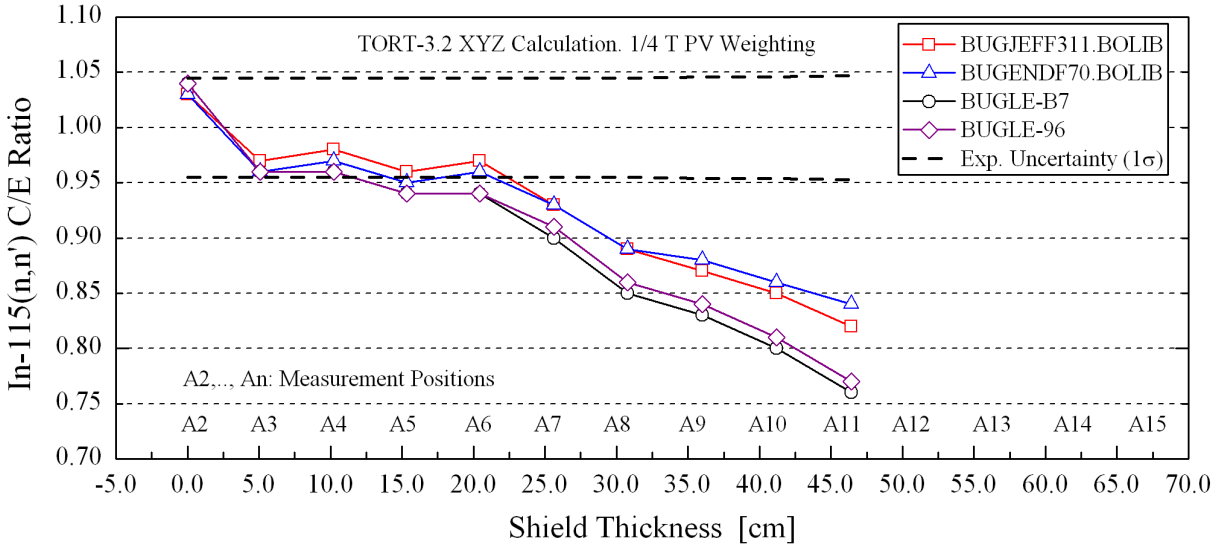

FIG. 5.6

Iron-88 - In-115(n,n')In-115m Reaction Rate Ratios (Calculated/Experimental) Calculated Using the BUGJEFF311.BOLIB, BUGENDF70.BOLIB, BUGLE-B7 and BUGLE-96 Libraries with Flat Weighting Dosimeter Cross Sections.

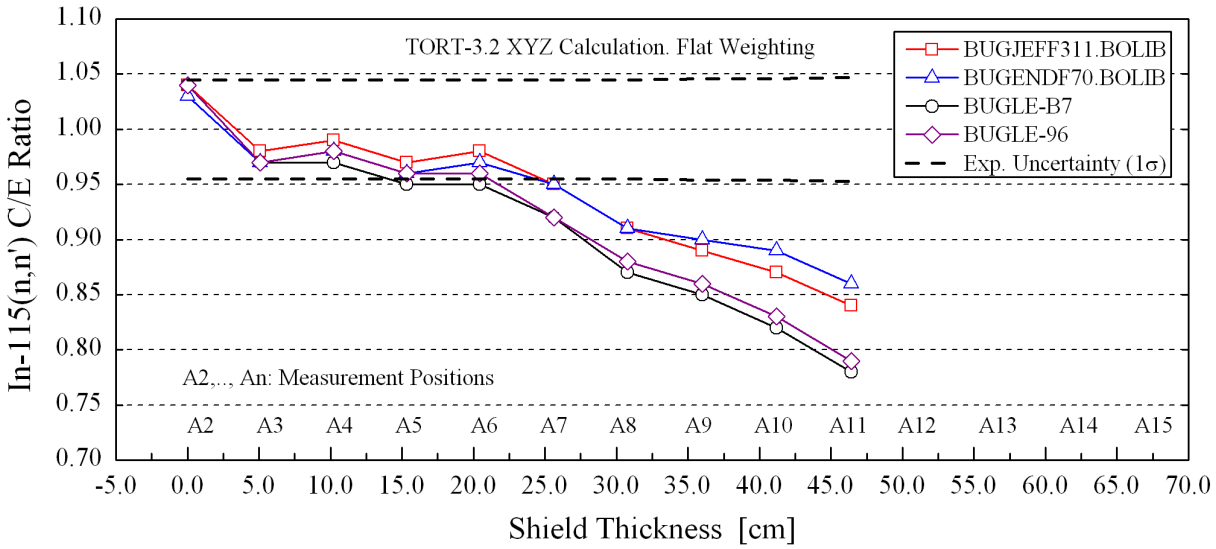

FIG. 5.7

Iron-88 - S-32(n,p)P-32 Reaction Rate Ratios (Calculated/Experimental)
Calculated Using the BUGJEFF311.BOLIB, BUGENDF70.BOLIB, BUGLE-B7
and BUGLE-96 Libraries with 1/4 T PV Weighting Dosimeter Cross Sections.

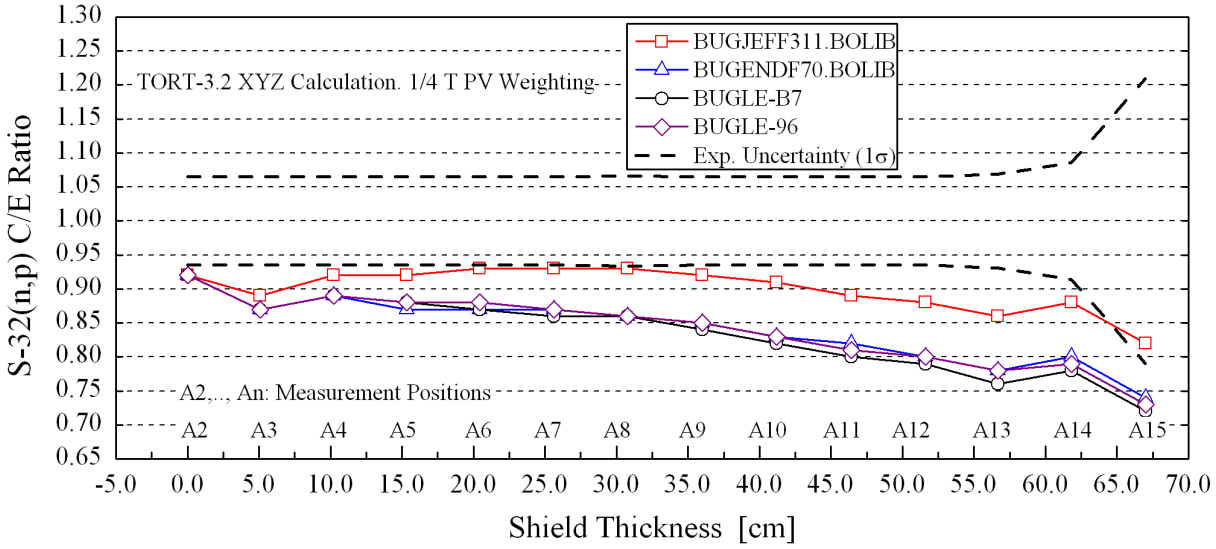

FIG. 5.8

Iron-88 - S-32(n,p)P-32 Reaction Rate Ratios (Calculated/Experimental)
Calculated Using the BUGJEFF311.BOLIB, BUGENDF70.BOLIB, BUGLE-B7
and BUGLE-96 Libraries with Flat Weighting Dosimeter Cross Sections.

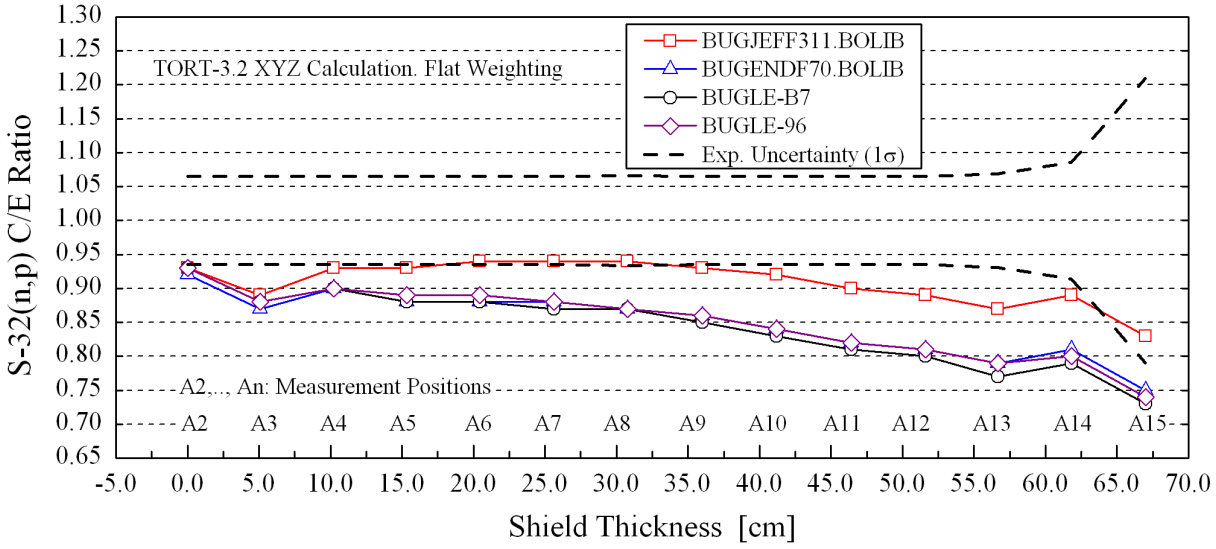

FIG. 5.9

Iron-88 - Al-27(n,α)Na-24 Reaction Rate Ratios (Calculated/Experimental)
Calculated Using the BUGJEFF311.BOLIB, BUGENDF70.BOLIB, BUGLE-B7
and BUGLE-96 Libraries with 1/4 T PV Weighting Dosimeter Cross Sections.

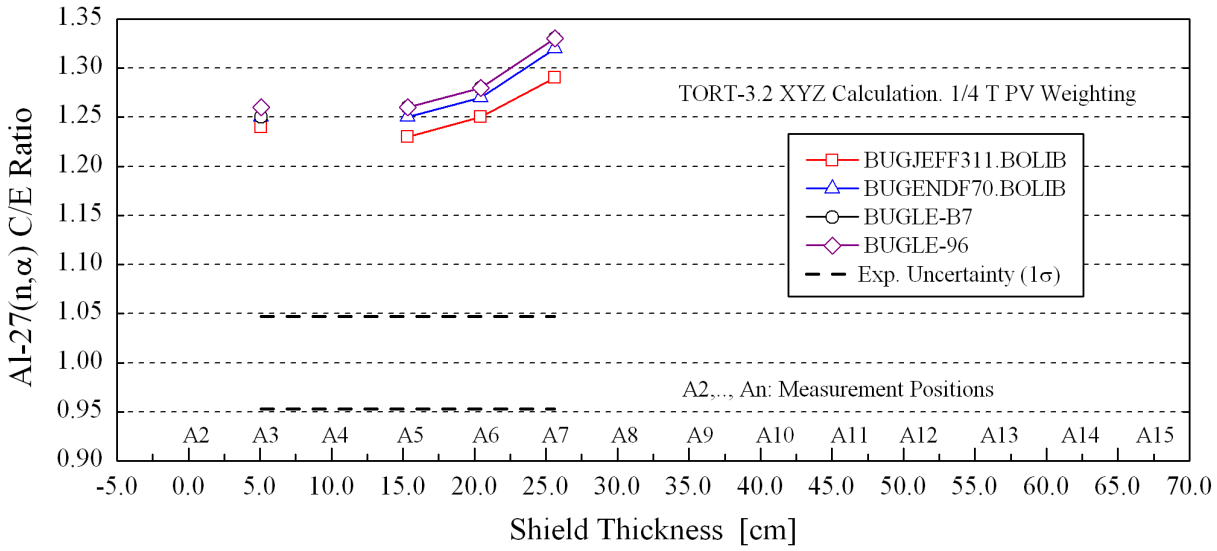

FIG. 5.10

Iron-88 - Al-27(n,α)Na-24 Reaction Rate Ratios (Calculated/Experimental)
Calculated Using the BUGJEFF311.BOLIB, BUGENDF70.BOLIB, BUGLE-B7
and BUGLE-96 Libraries with Flat Weighting Dosimeter Cross Sections.

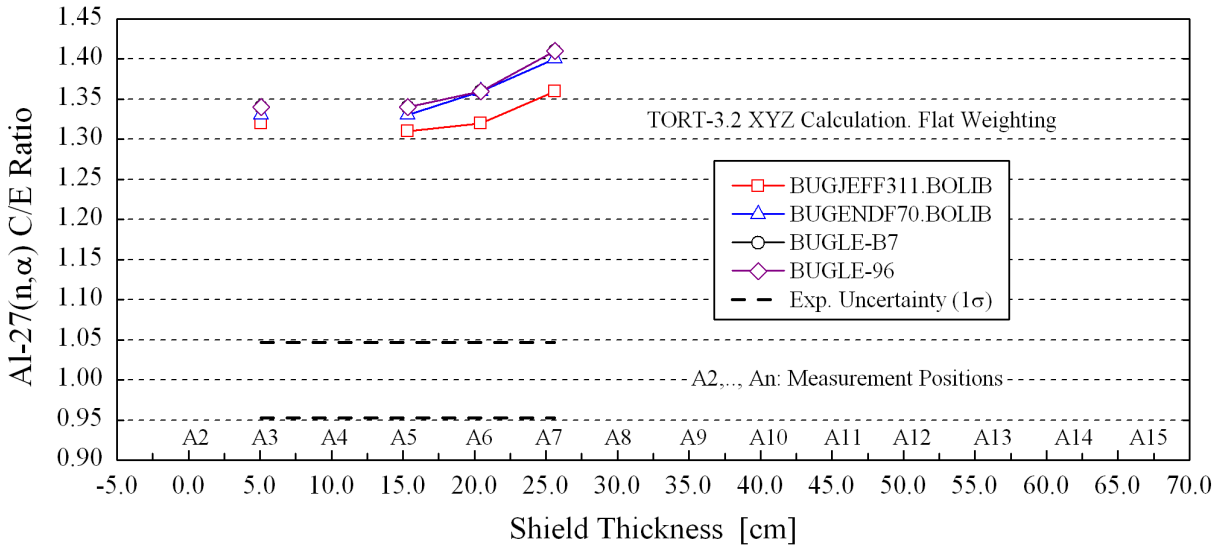

FIG. 5.11

Iron-88 - Au-197(n,γ)Au-198 epi-Cadmium Reaction Rate Ratios (Calculated/Experimental)
Calculated Using the BUGJEFF311.BOLIB Library and Dosimeter Cross Sections
with Flat Weighting and 1/4 T PV Weighting.

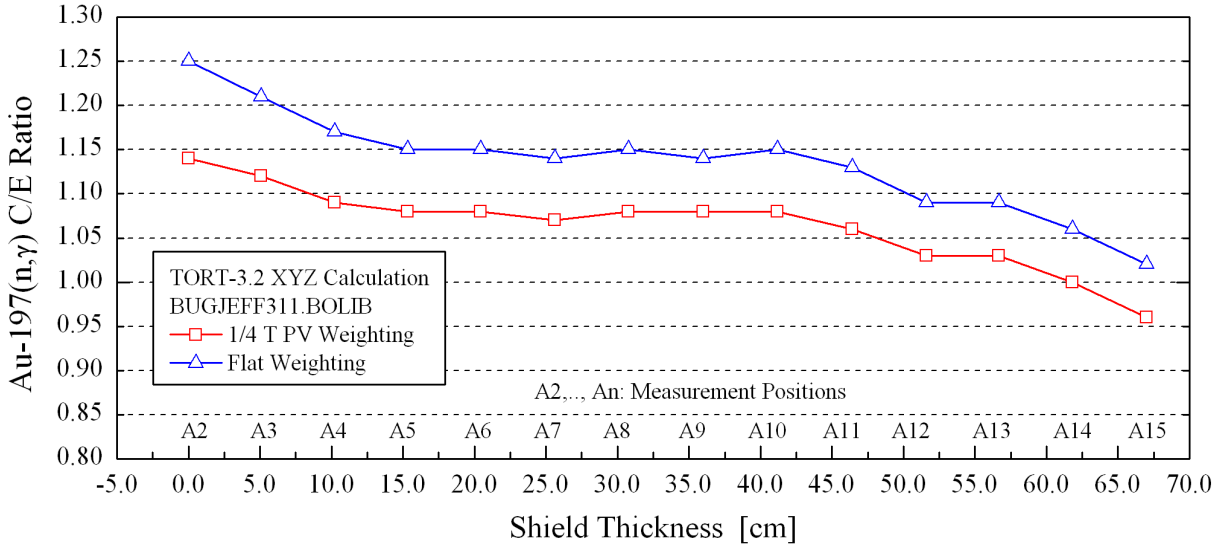

FIG. 5.12

Iron-88 - Au-197(n,γ)Au-198 epi-Cadmium Reaction Rate Ratios (Calculated/Experimental)
Calculated Using the BUGENDF70.BOLIB Library and Dosimeter Cross Sections
with Flat Weighting and 1/4 T PV Weighting.

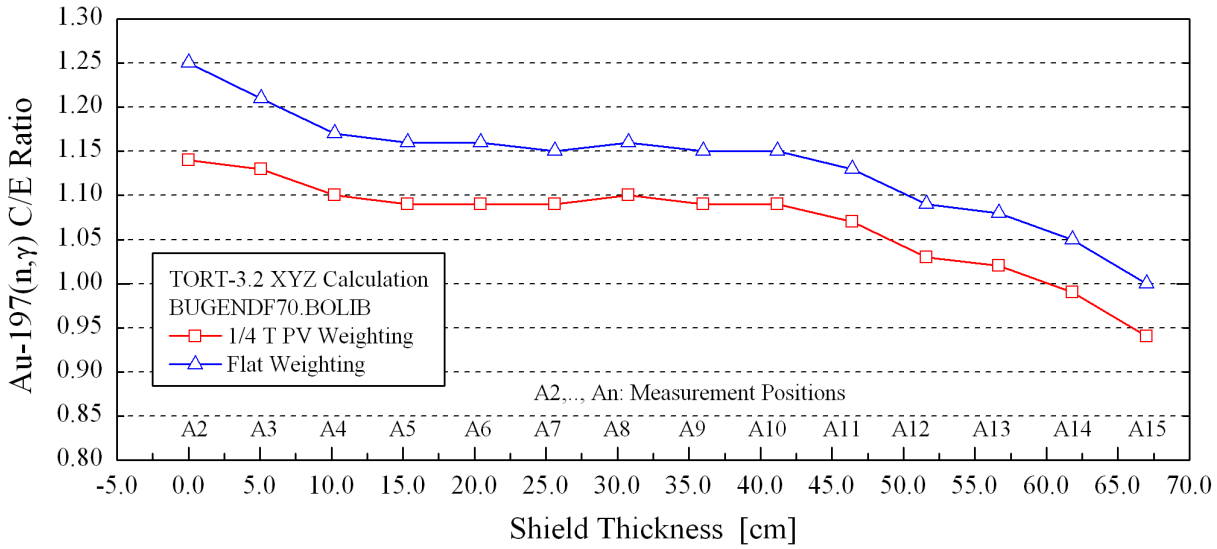

FIG. 5.13

Iron-88 - Au-197(n,γ)Au-198 epi-Cadmium Reaction Rate Ratios (Calculated/Experimental)
Calculated Using the BUGLE-B7 Library and Dosimeter Cross Sections
with Flat Weighting and 1/4 T PV Weighting.

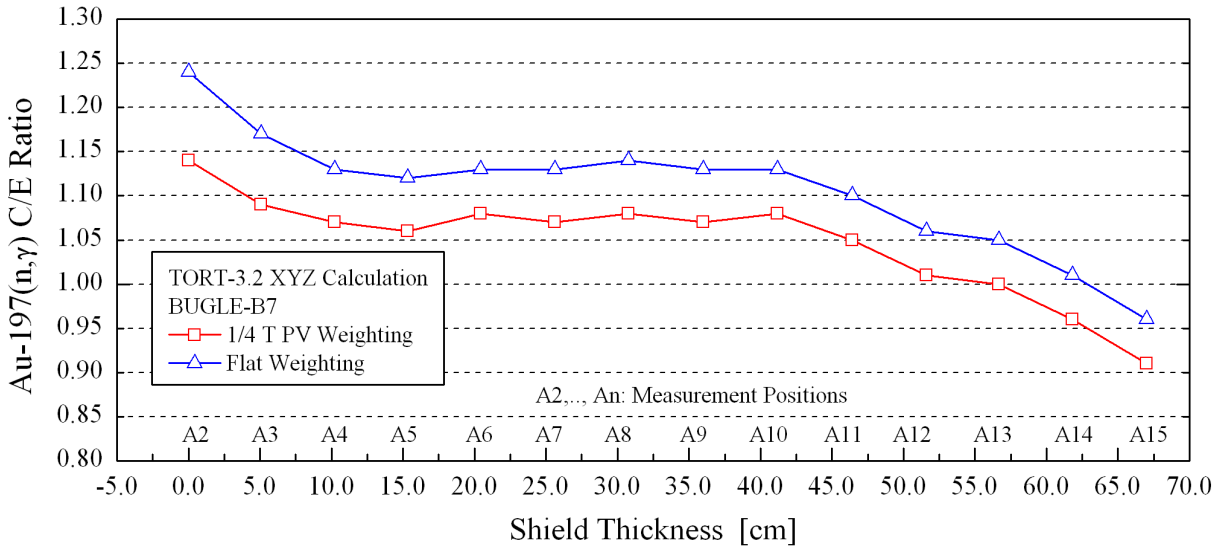

FIG. 5.14

Iron-88 - Au-197(n,γ)Au-198 epi-Cadmium Reaction Rate Ratios (Calculated/Experimental)
Calculated Using the BUGLE-96 Library and Dosimeter Cross Sections
with Flat Weighting and 1/4 T PV Weighting.

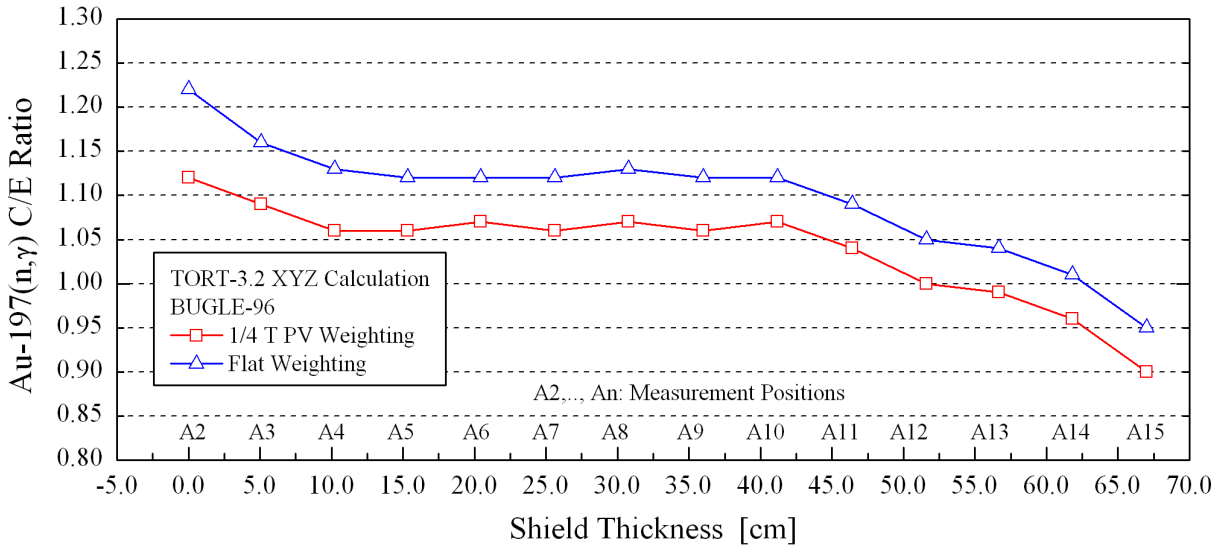

FIG. 5.15

Iron-88 - Rh-103(n,n')Rh-103m Reaction Rate Ratios (Calculated/Experimental)
Calculated Using the BUGJEFF311.BOLIB Library and Dosimeter Cross Sections
with Flat Weighting and 1/4 T PV Weighting.

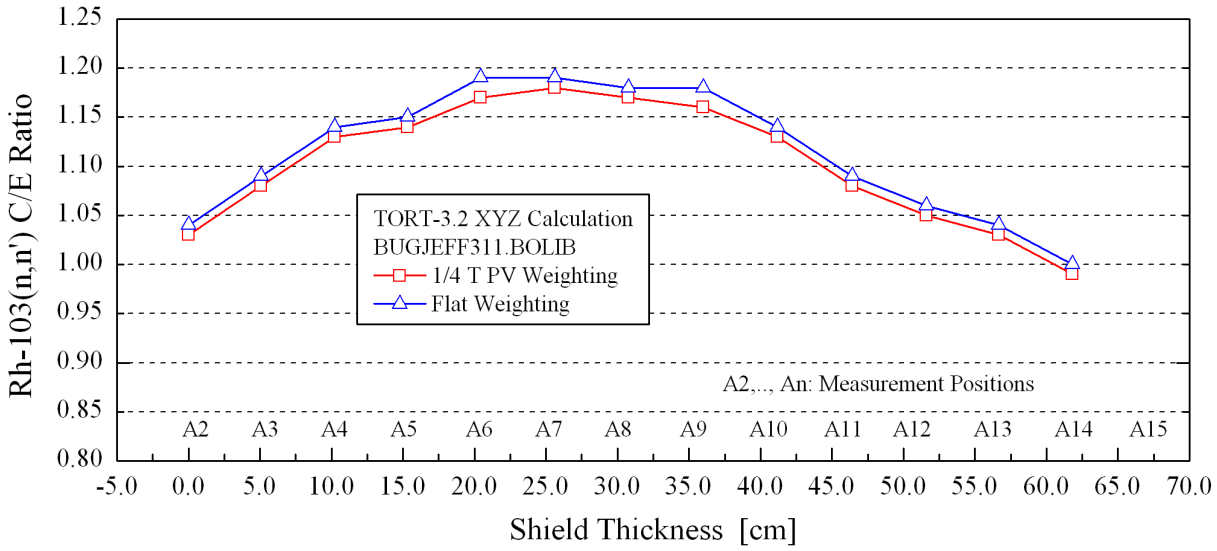

FIG. 5.16

Iron-88 - Rh-103(n,n')Rh-103m Reaction Rate Ratios (Calculated/Experimental)
Calculated Using the BUGENDF70.BOLIB Library and Dosimeter Cross Sections
with Flat Weighting and 1/4 T PV Weighting.

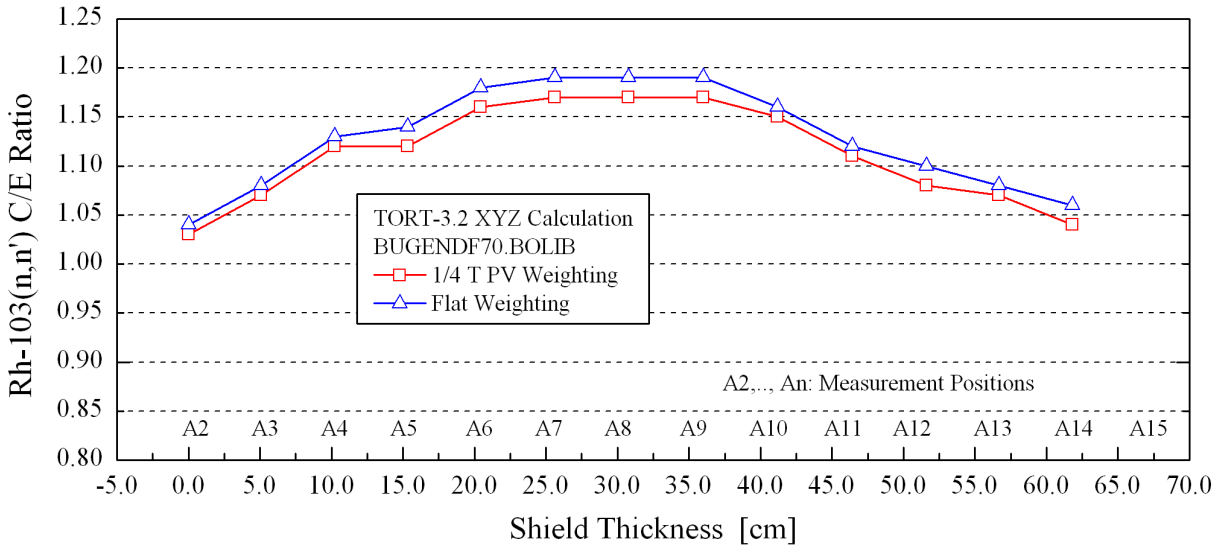

FIG. 5.17

Iron-88 - Rh-103(n,n')Rh-103m Reaction Rate Ratios (Calculated/Experimental)
Calculated Using the BUGLE-B7 Library and Dosimeter Cross Sections
with Flat Weighting and 1/4 T PV Weighting.

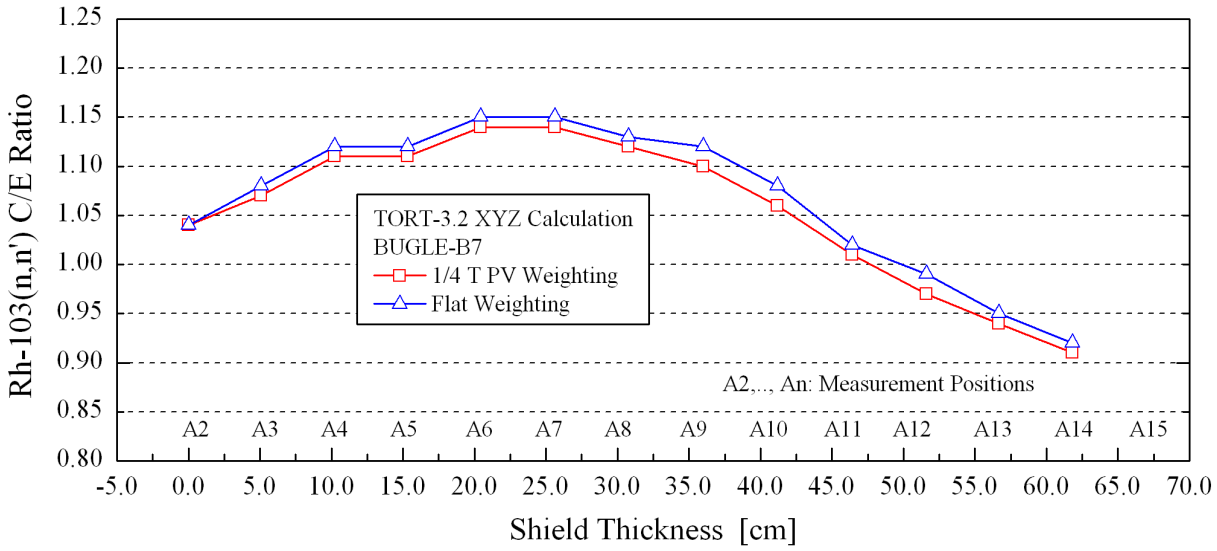

FIG. 5.18

Iron-88 - Rh-103(n,n')Rh-103m Reaction Rate Ratios (Calculated/Experimental)
Calculated Using the BUGLE-96 Library and Dosimeter Cross Sections
with Flat Weighting and 1/4 T PV Weighting.

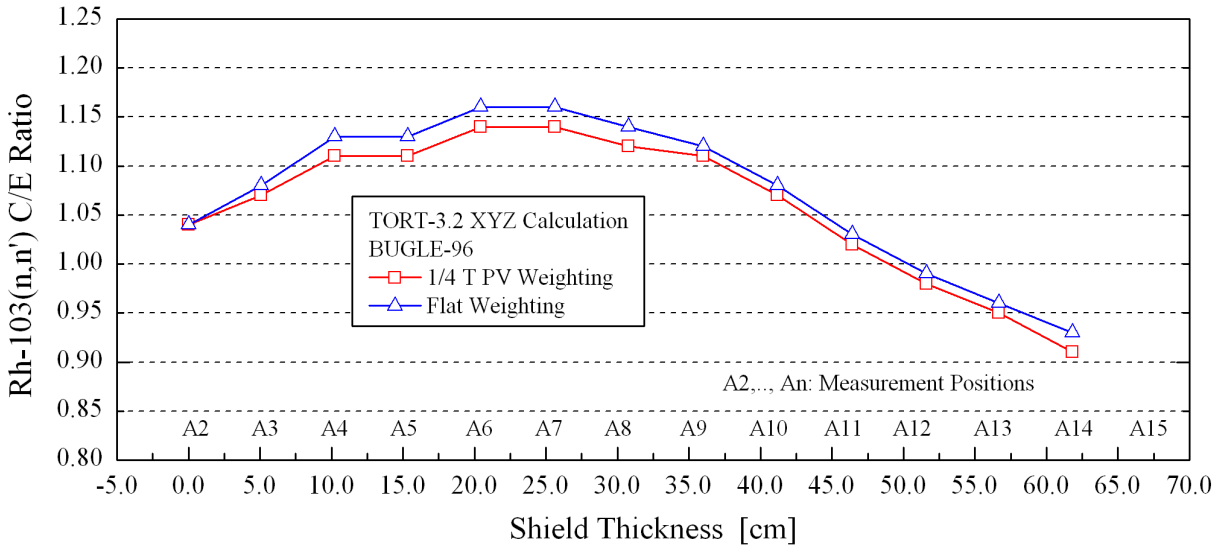

FIG. 5.19

Iron-88 - In-115(n,n')In-115m Reaction Rate Ratios (Calculated/Experimental)
Calculated Using the BUGJEFF311.BOLIB Library and Dosimeter Cross Sections
with Flat Weighting and 1/4 T PV Weighting.

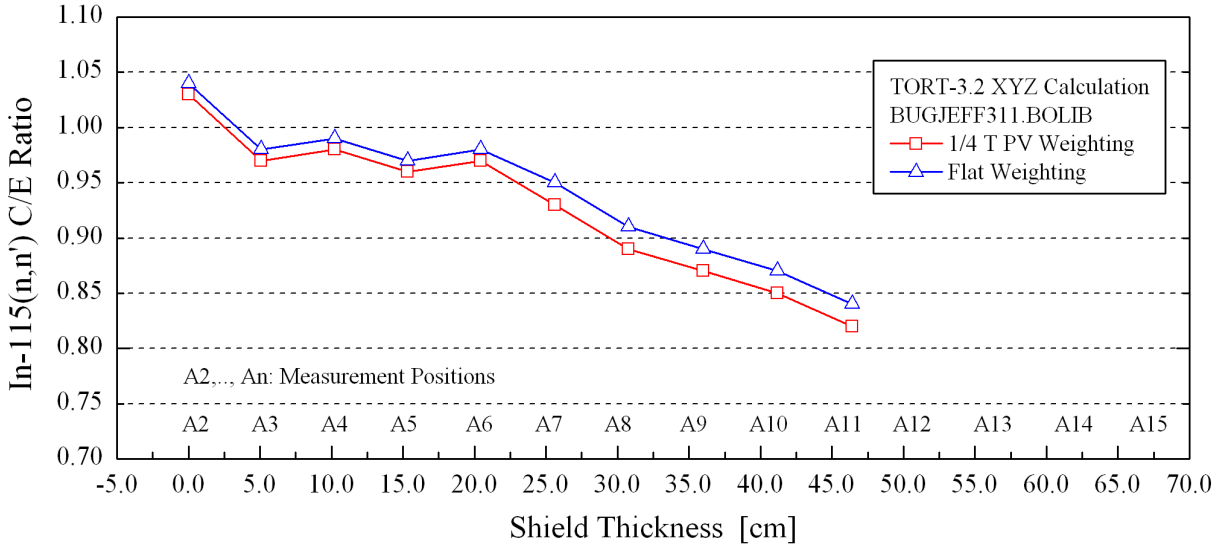

FIG.5.20

Iron-88 - In-115(n,n')In-115m Reaction Rate Ratios (Calculated/Experimental)
Calculated Using the BUGENDF70.BOLIB Library and Dosimeter Cross Sections
with Flat Weighting and 1/4 T PV Weighting.

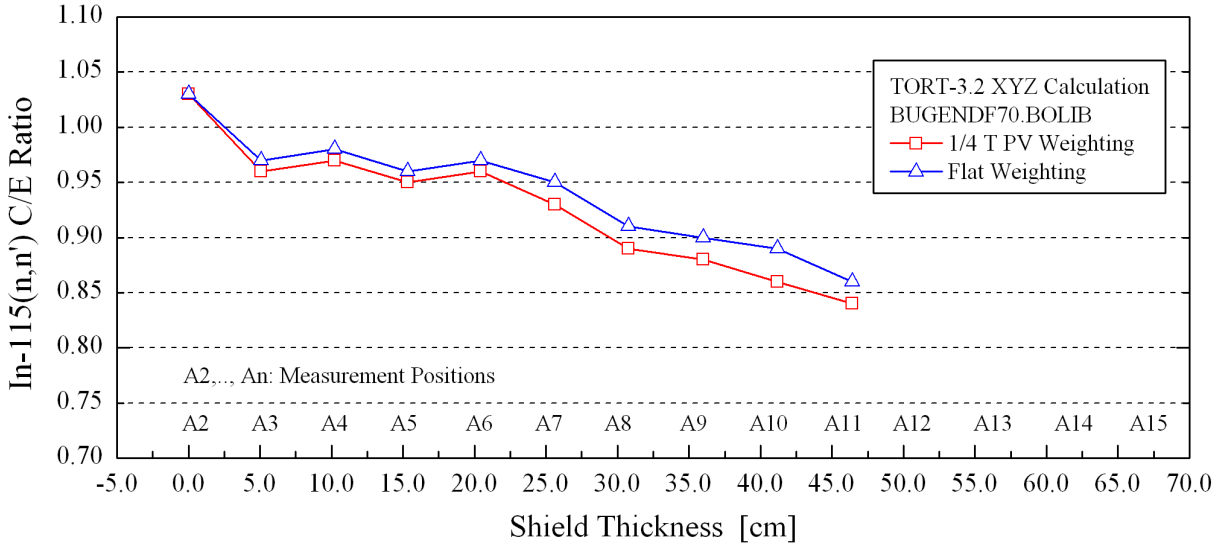

FIG. 5.21

Iron-88 - In-115(n,n')In-115m Reaction Rate Ratios (Calculated/Experimental)
Calculated Using the BUGLE-B7 Library and Dosimeter Cross Sections
with Flat Weighting and 1/4 T PV Weighting.

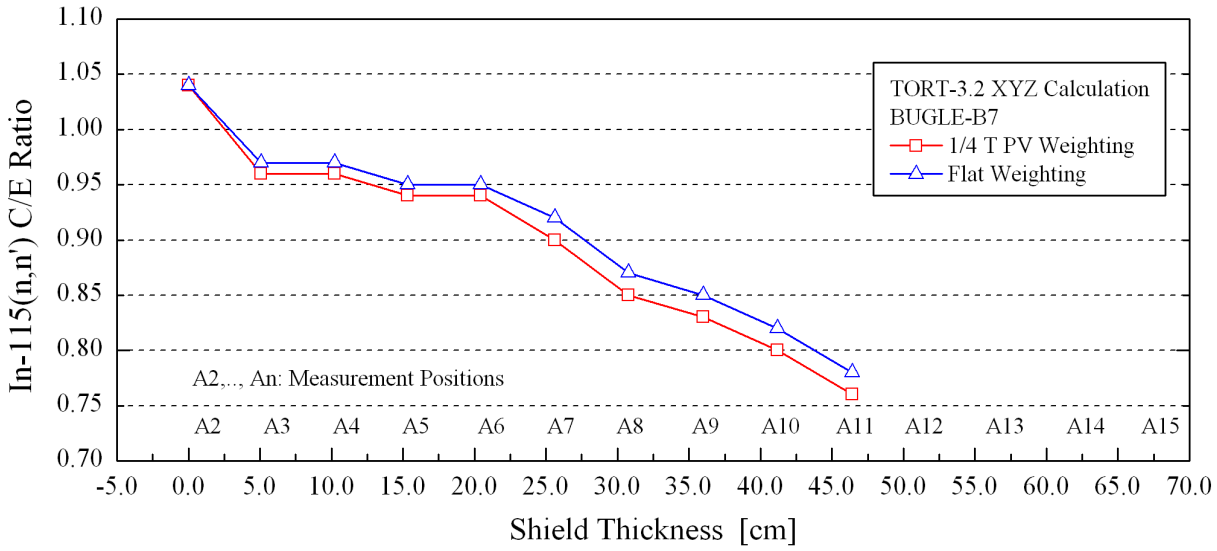

FIG. 5.22

Iron-88 - In-115(n,n')In-115m Reaction Rate Ratios (Calculated/Experimental)
Calculated Using the BUGLE-96 Library and Dosimeter Cross Sections
with Flat Weighting and 1/4 T PV Weighting.

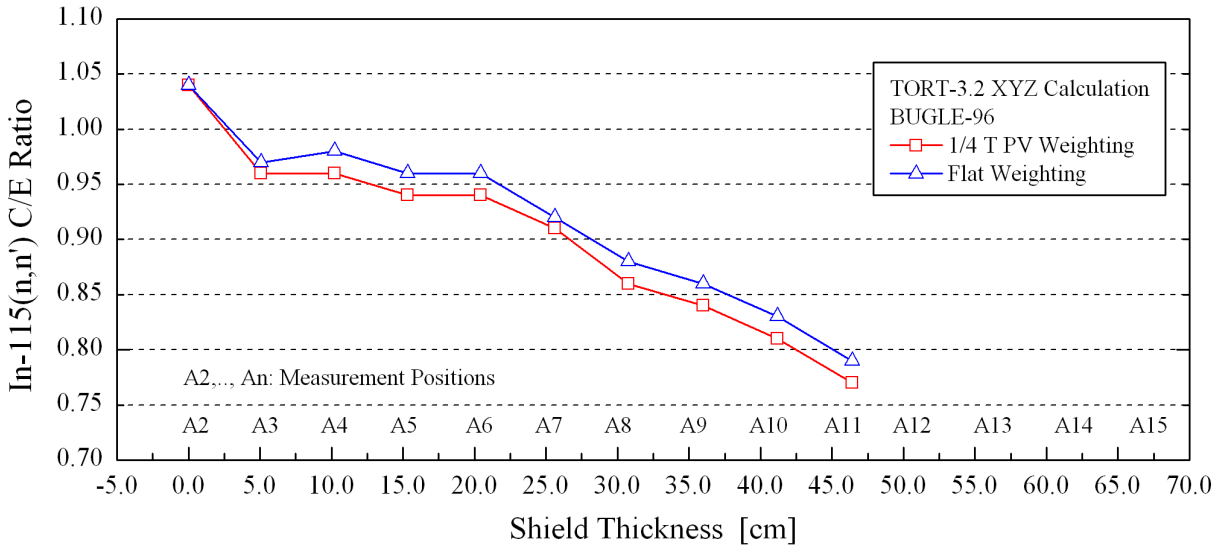

FIG. 5.23

Iron-88 - S-32(n,p)P-32 Reaction Rate Ratios (Calculated/Experimental)
Calculated Using the BUGJEFF311.BOLIB Library and Dosimeter Cross Sections
with Flat Weighting and 1/4 T PV Weighting.

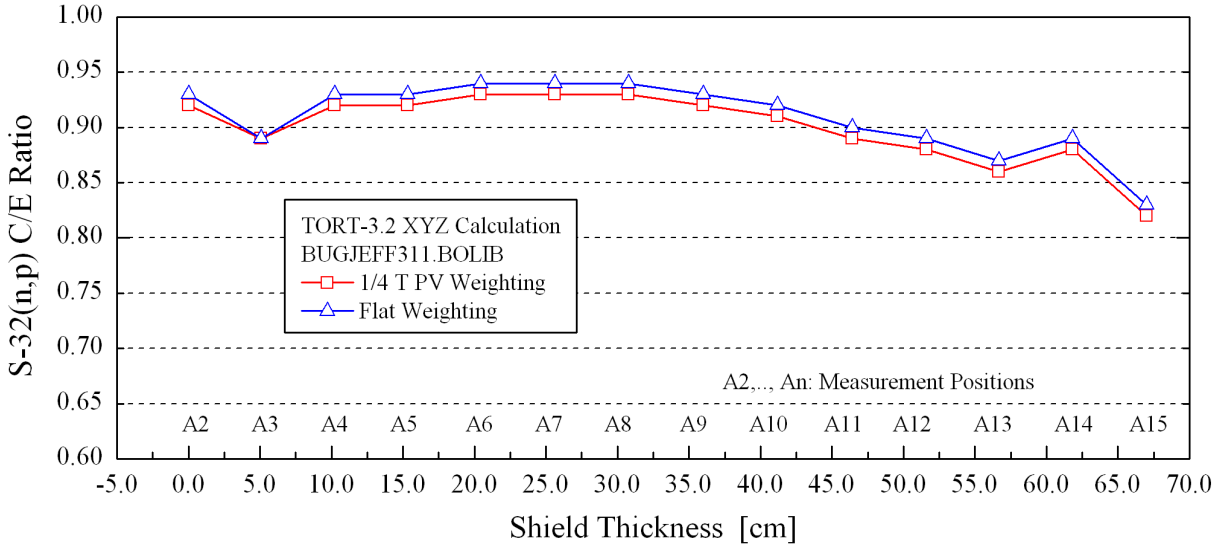

FIG. 5.24

Iron-88 - S-32(n,p)P-32 Reaction Rate Ratios (Calculated/Experimental)
Calculated Using the BUGENDF70.BOLIB Library and Dosimeter Cross Sections
with Flat Weighting and 1/4 T PV Weighting.

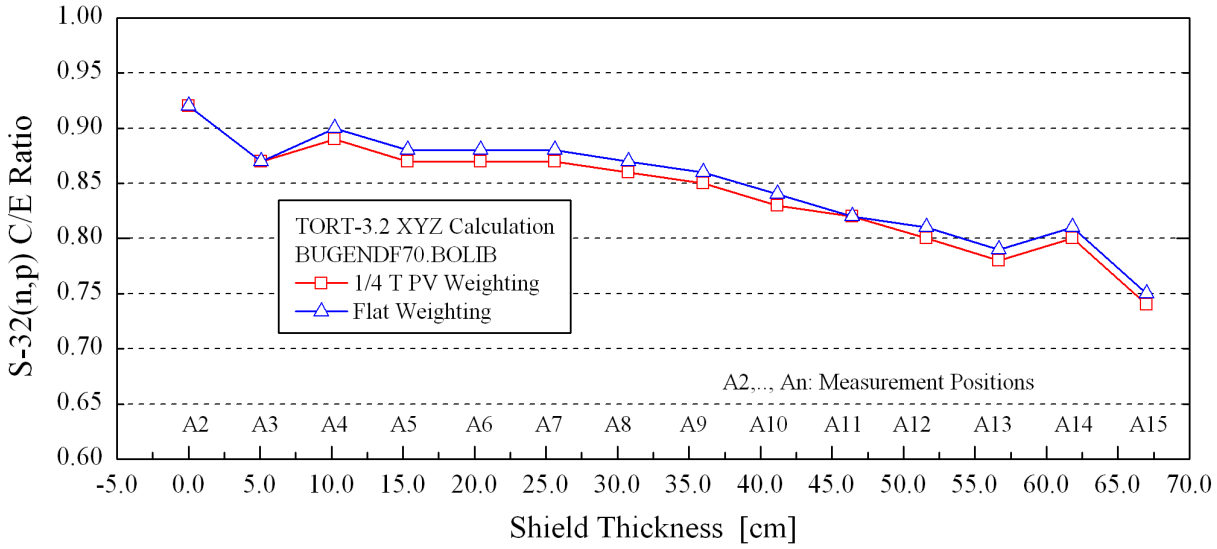

FIG. 5.25

Iron-88 - S-32(n,p)P-32 Reaction Rate Ratios (Calculated/Experimental)
Calculated Using the BUGLE-B7 Library and Dosimeter Cross Sections
with Flat Weighting and 1/4 T PV Weighting.

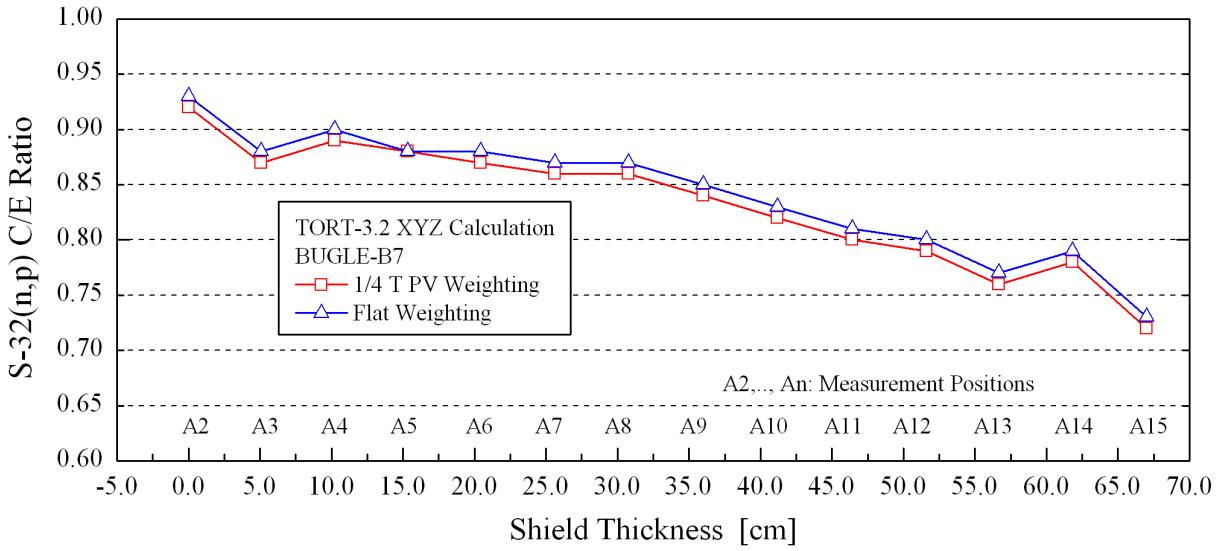

FIG. 5.26

Iron-88 - S-32(n,p)P-32 Reaction Rate Ratios (Calculated/Experimental)
Calculated Using the BUGLE-96 Library and Dosimeter Cross Sections
with Flat Weighting and 1/4 T PV Weighting.

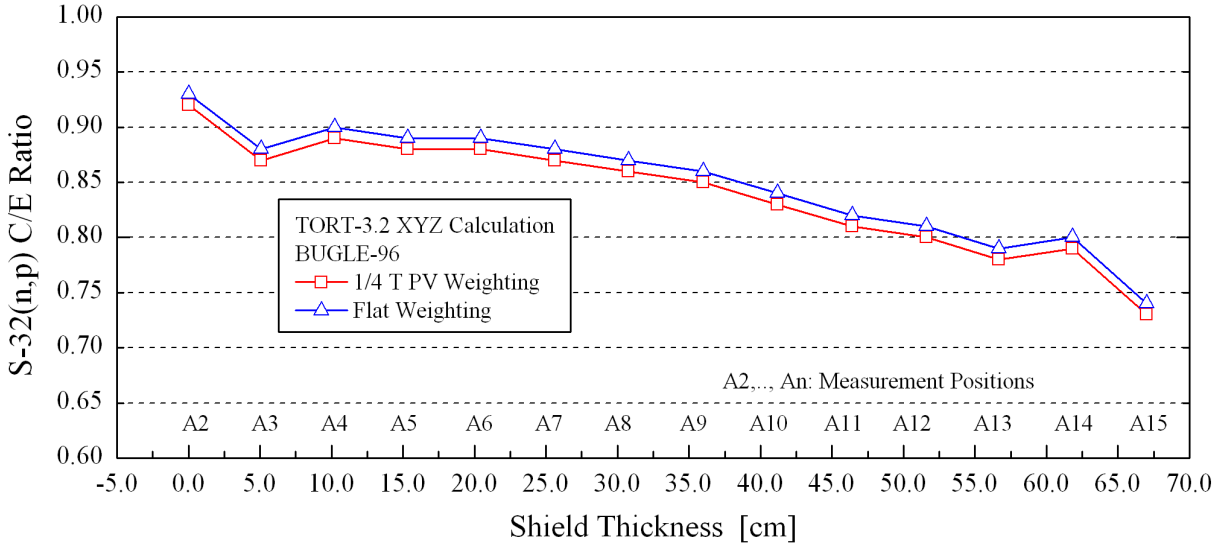

FIG. 5.27

Iron-88 - Al-27(n,α)Na-24 Reaction Rate Ratios (Calculated/Experimental)
Calculated Using the BUGJEFF311.BOLIB Library and Dosimeter Cross Sections
with Flat Weighting and 1/4 T PV Weighting.

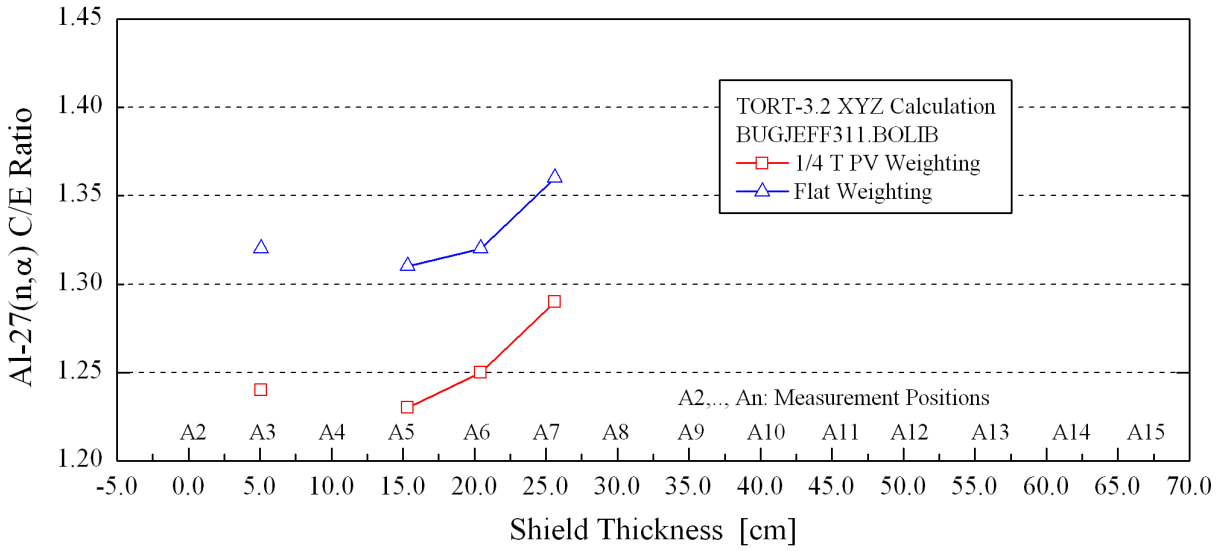

FIG. 5.28

Iron-88 - Al-27(n,α)Na-24 Reaction Rate Ratios (Calculated/Experimental)
Calculated Using the BUGENDF70.BOLIB Library and Dosimeter Cross Sections
with Flat Weighting and 1/4 T PV Weighting.

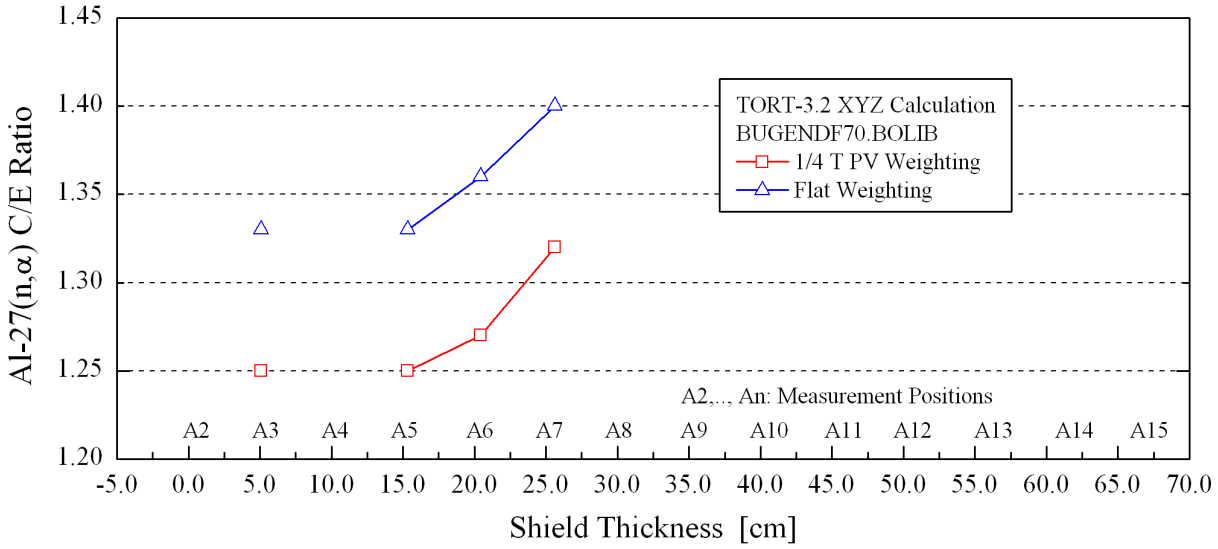

FIG. 5.29

Iron-88 - Al-27(n,α)Na-24 Reaction Rate Ratios (Calculated/Experimental)
Calculated Using the BUGLE-B7 Library and Dosimeter Cross Sections
with Flat Weighting and 1/4 T PV Weighting.

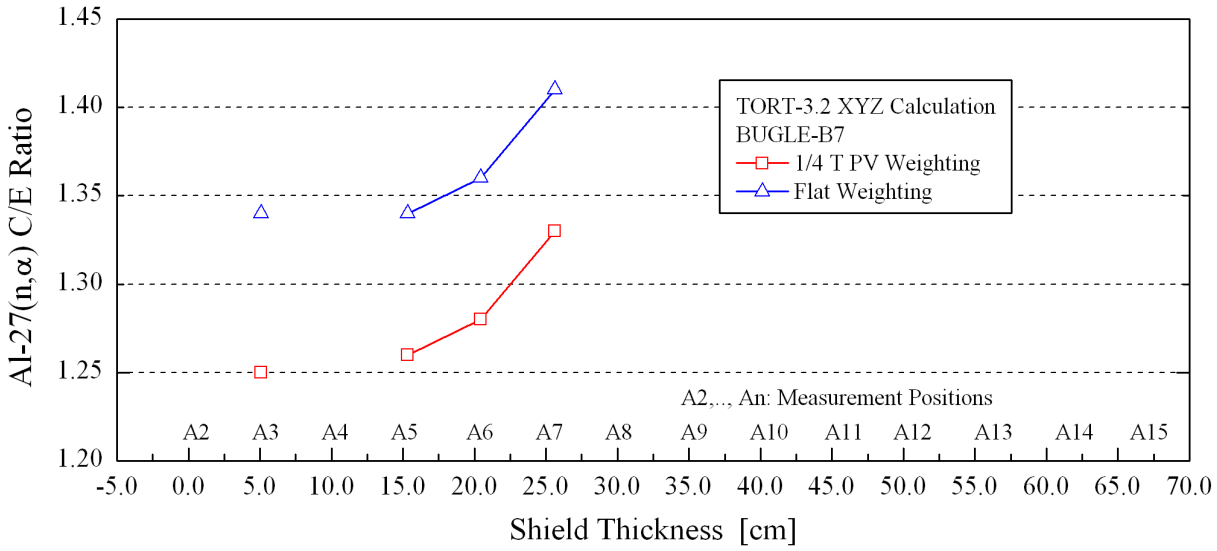

FIG. 5.30

Iron-88 - Al-27(n,α)Na-24 Reaction Rate Ratios (Calculated/Experimental)
Calculated Using the BUGLE-96 Library and Dosimeter Cross Sections
with Flat Weighting and 1/4 T PV Weighting.

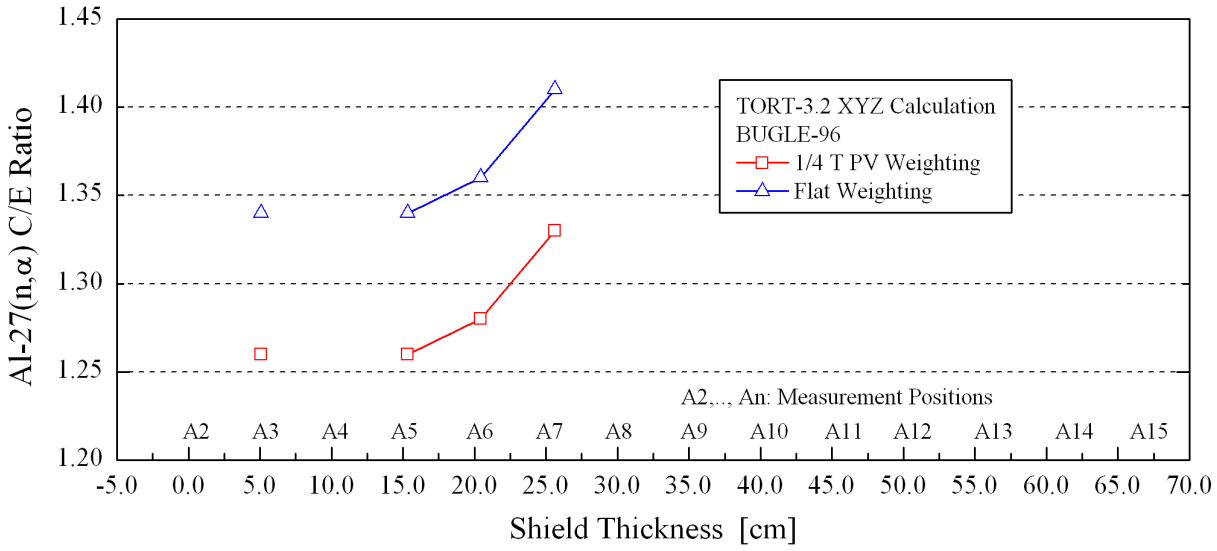

FIG. 5.31

Iron-88 - Au-197(n,γ)Au-198 epi-Cadmium Reaction Rates
at the NESTOR Reactor Maximum Power (30 kW)
on the Z Horizontal Axis.
[reactions × s^{-1} × $atom^{-1}$]

Comparison of Experimental and Calculated Reaction Rates.

P_3-S_8 Calculation Using the BUGJEFF311.BOLIB Library
and 1/4 T PV Weighting Dosimeter Cross Sections.

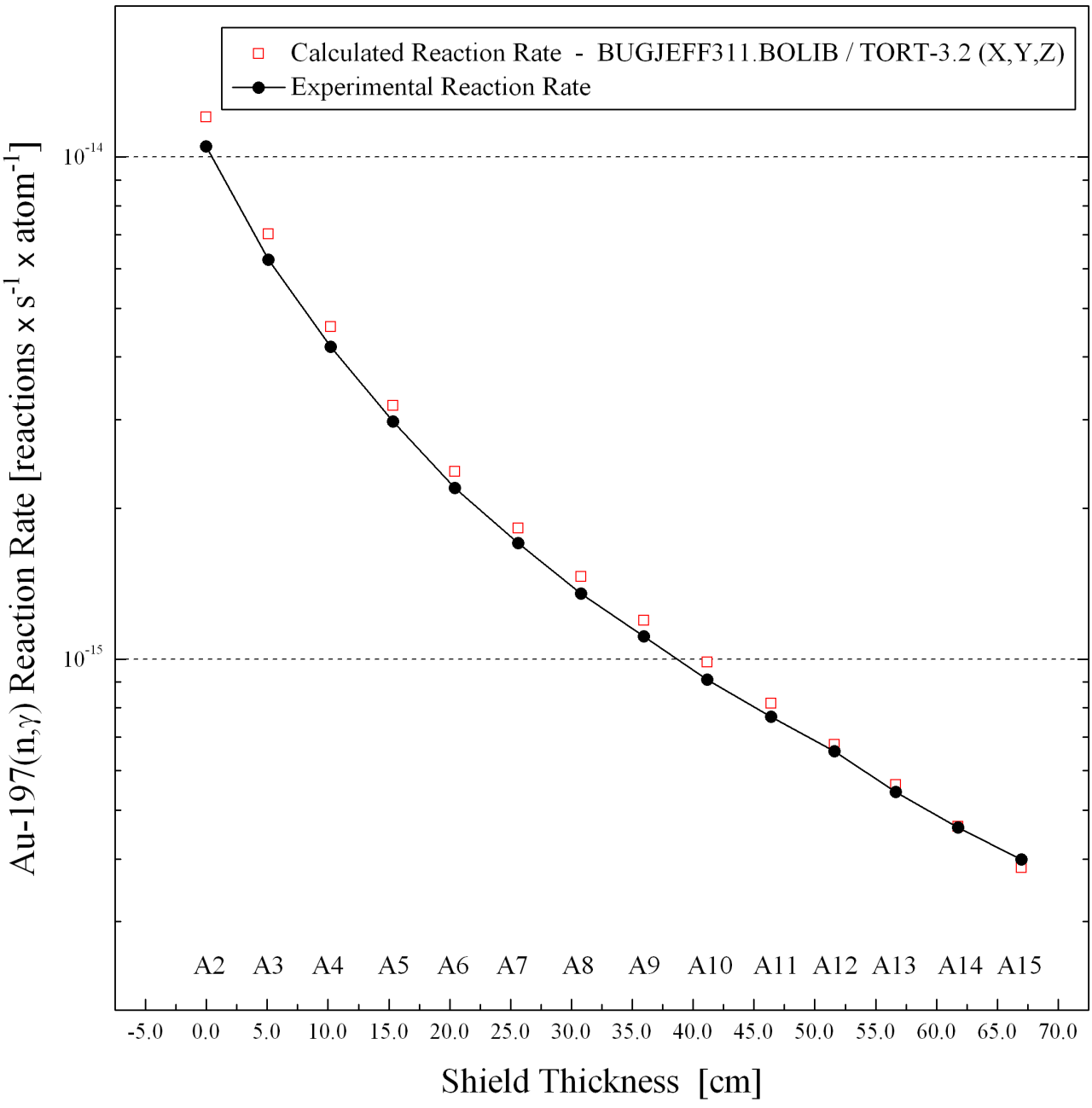

FIG. 5.32

Iron-88 - Rh-103(n,n')Rh-103m Reaction Rates
at the NESTOR Reactor Maximum Power (30 kW)
on the Z Horizontal Axis.
[reactions × s^{-1} × $atom^{-1}$]

Comparison of Experimental and Calculated Reaction Rates.

P_3-S_8 Calculation Using the BUGJEFF311.BOLIB Library
and 1/4 T PV Weighting Dosimeter Cross Sections.

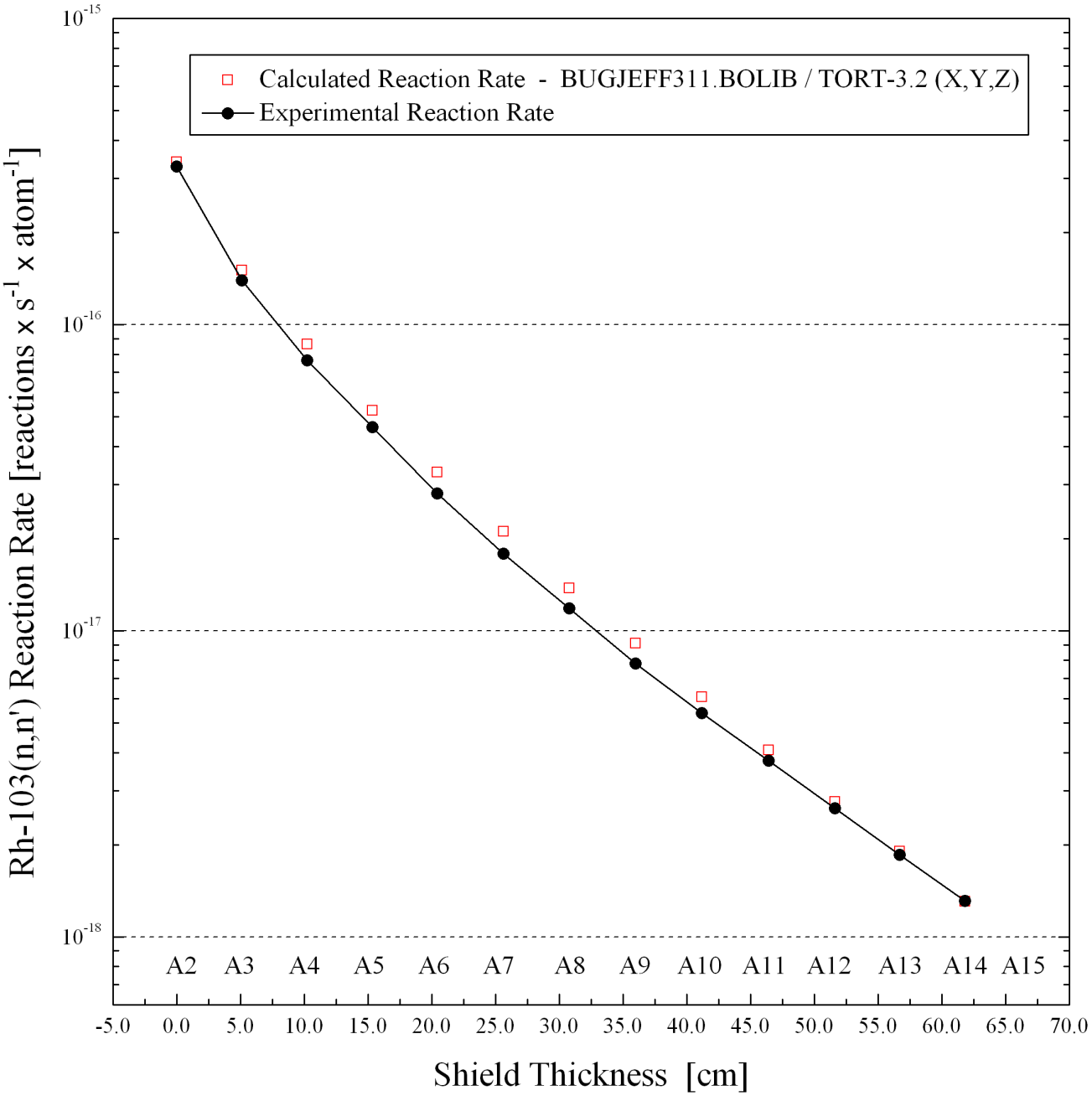

FIG. 5.33

Iron-88 - In-115(n,n')In-115m Reaction Rates
at the NESTOR Reactor Maximum Power (30 kW)
on the Z Horizontal Axis.
[reactions × s^{-1} × $atom^{-1}$]

Comparison of Experimental and Calculated Reaction Rates.

P_3-S_8 Calculation Using the BUGJEFF311.BOLIB Library
and 1/4 T PV Weighting Dosimeter Cross Sections.

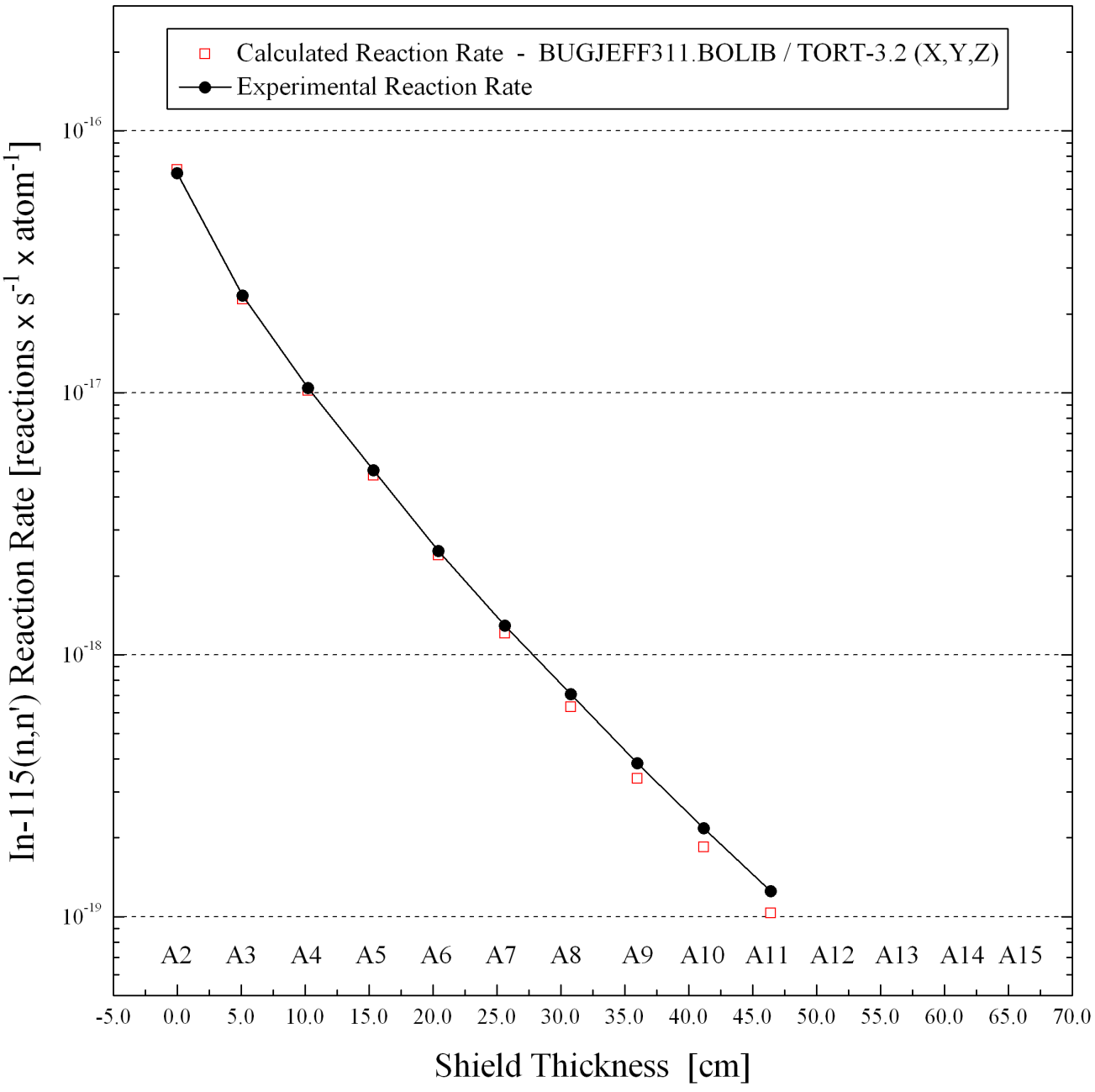

FIG. 5.34

Iron-88 - S-32(n,p)P-32 Reaction Rates
at the NESTOR Reactor Maximum Power (30 kW)
on the Z Horizontal Axis.
[reactions × s^{-1} × $atom^{-1}$]

Comparison of Experimental and Calculated Reaction Rates.

P_3-S_8 Calculation Using the BUGJEFF311.BOLIB Library
and 1/4 T PV Weighting Dosimeter Cross Sections.

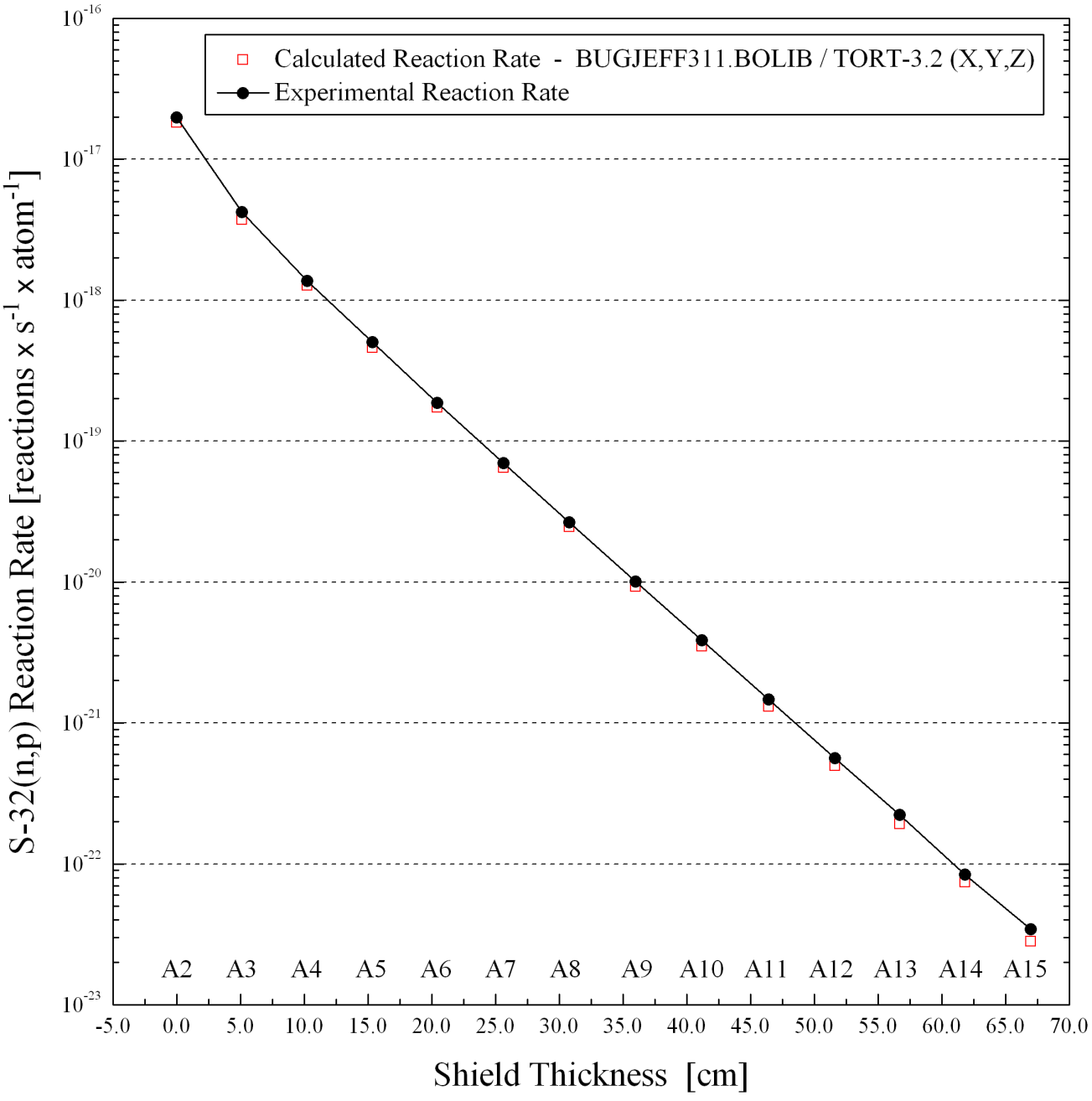

FIG. 5.35

Iron-88 - Al-27(n,α)Na-24 Reaction Rates
at the NESTOR Reactor Maximum Power (30 kW)
on the Z Horizontal Axis.
[reactions × s^{-1} × $atom^{-1}$]

Comparison of Experimental and Calculated Reaction Rates.

P_3-S_8 Calculation Using the BUGJEFF311.BOLIB Library
and 1/4 T PV Weighting Dosimeter Cross Sections.

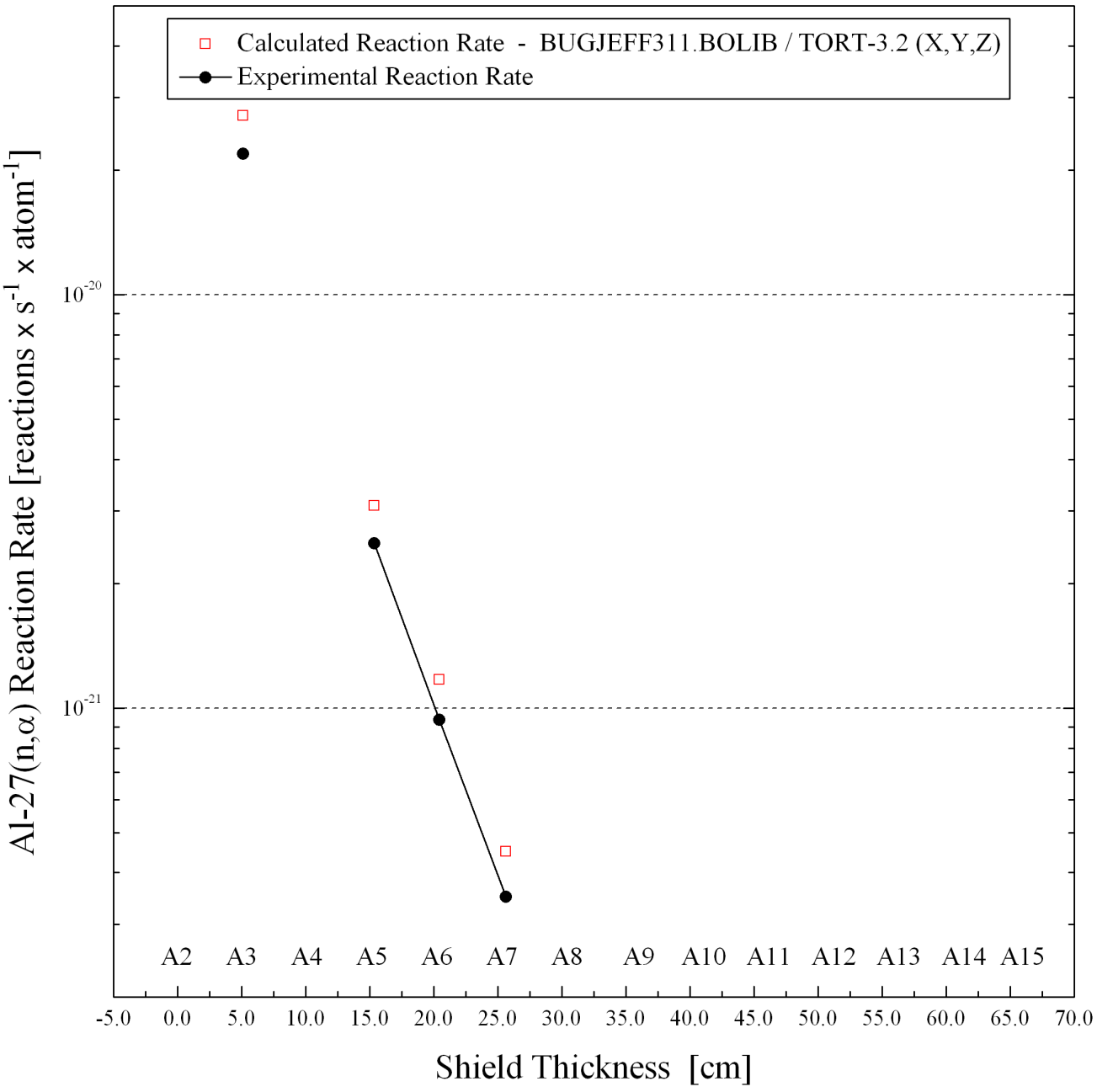

FIG. 5.36

Iron-88 - Spatial Distribution of the Neutron Fluxes at the NESTOR Reactor Maximum Power (30 kW) for Neutron Energy > 0.414 eV.
[neutrons × barn^{-1} × s^{-1}]

Horizontal Section at Y = 0.0 cm.
Dosimeter Locations "×", 73X×79Y×278Z Spatial Meshes.

P_3-S_8 Calculation Using the BUGJEFF311.BOLIB Library.

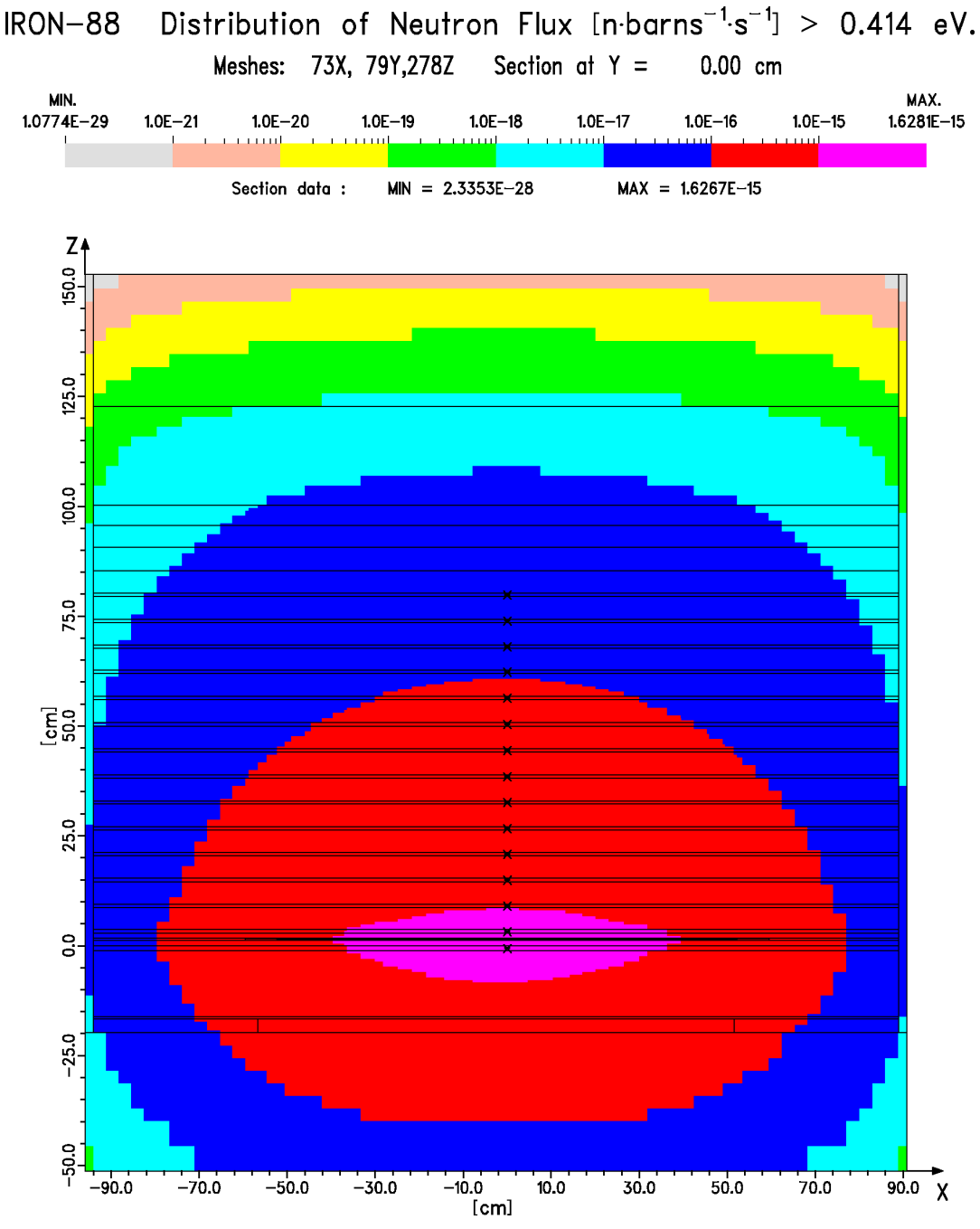

FIG. 5.37

Iron-88 - Spatial Distribution of the Neutron Fluxes at the NESTOR Reactor Maximum Power (30 kW) for Neutron Energy > 0.1 MeV.
[neutrons × barn^{-1} × s^{-1}]

Horizontal Section at Y = 0.0 cm.
Dosimeter Locations "×", 73X×79Y×278Z Spatial Meshes.

P_3-S_8 Calculation Using the BUGJEFF311.BOLIB Library.

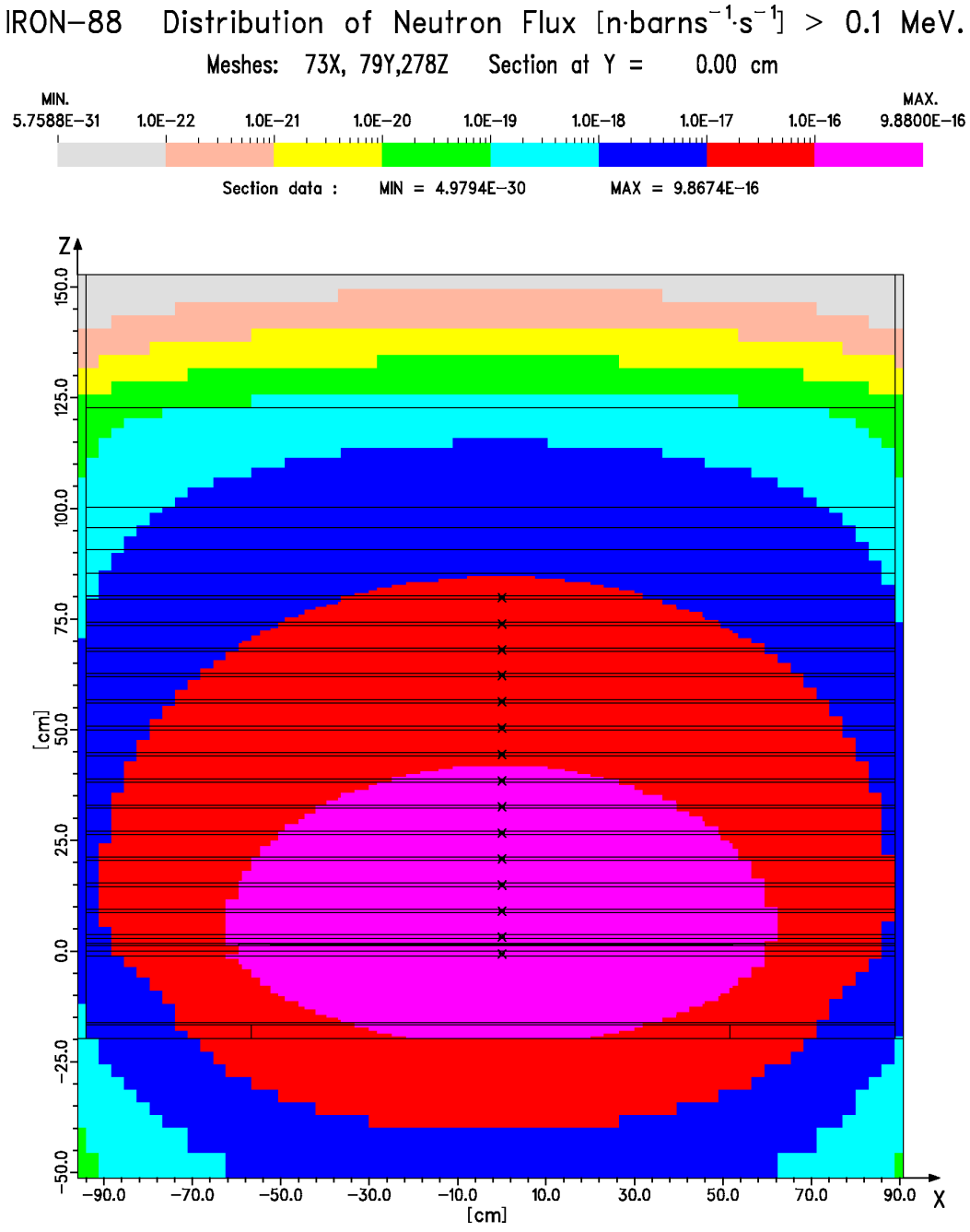

FIG. 5.38

Iron-88 - Spatial Distribution of the Neutron Fluxes at the NESTOR Reactor Maximum Power (30 kW) for Neutron Energy > 1.0 MeV.
[neutrons × barn^{-1} × s^{-1}]

Horizontal Section at Y = 0.0 cm.
Dosimeter Locations "×", 73X×79Y×278Z Spatial Meshes.

P_3-S_8 Calculation Using the BUGJEFF311.BOLIB Library.

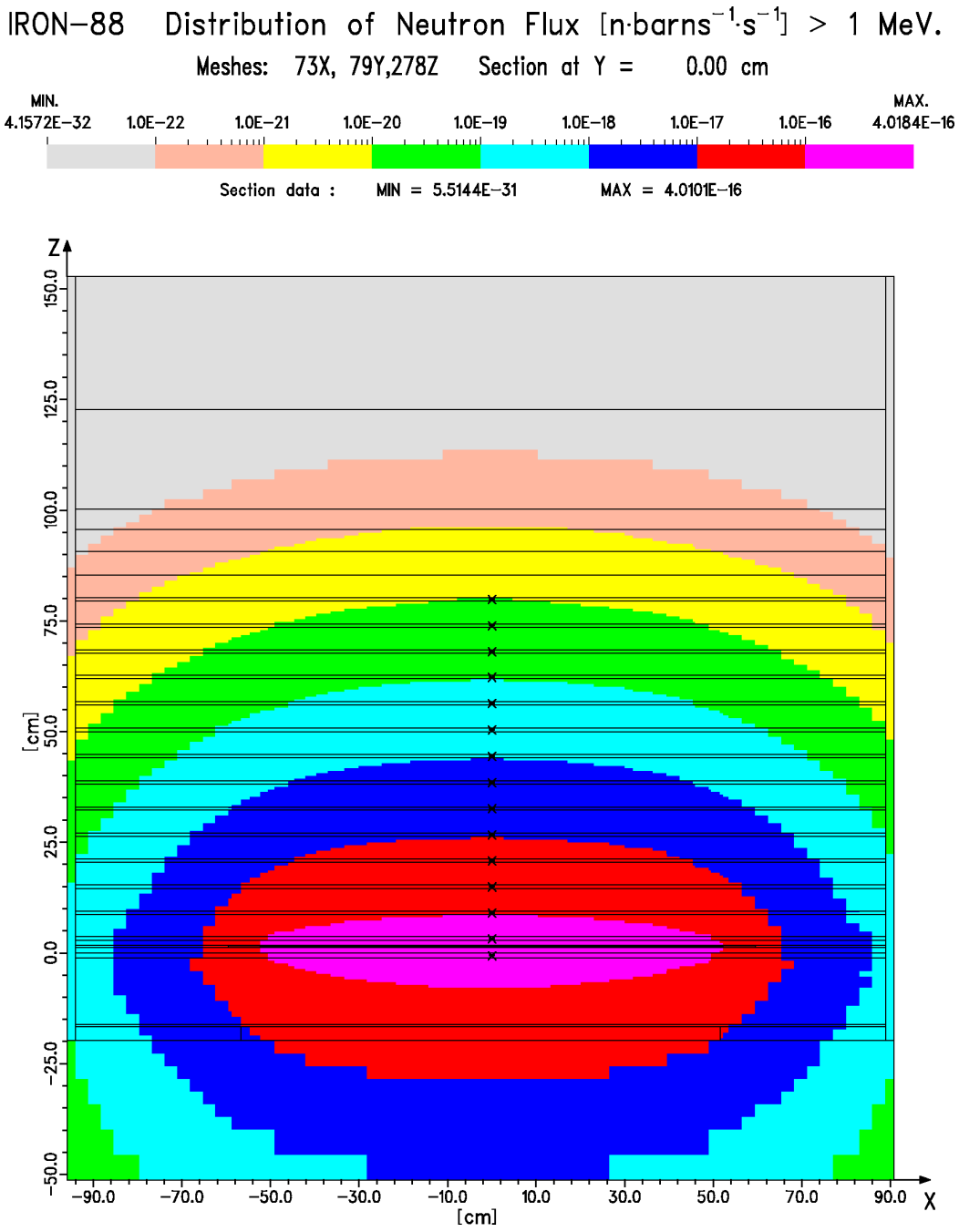

FIG. 5.39

Iron-88 - Spatial Distribution of the Neutron Fluxes at the NESTOR Reactor Maximum Power (30 kW) for Neutron Energy > 3.0 MeV.
[neutrons × barn^{-1} × s^{-1}]

Horizontal Section at Y = 0.0 cm.
Dosimeter Locations "×", 73X×79Y×278Z Spatial Meshes.

P_3-S_8 Calculation Using the BUGJEFF311.BOLIB Library.

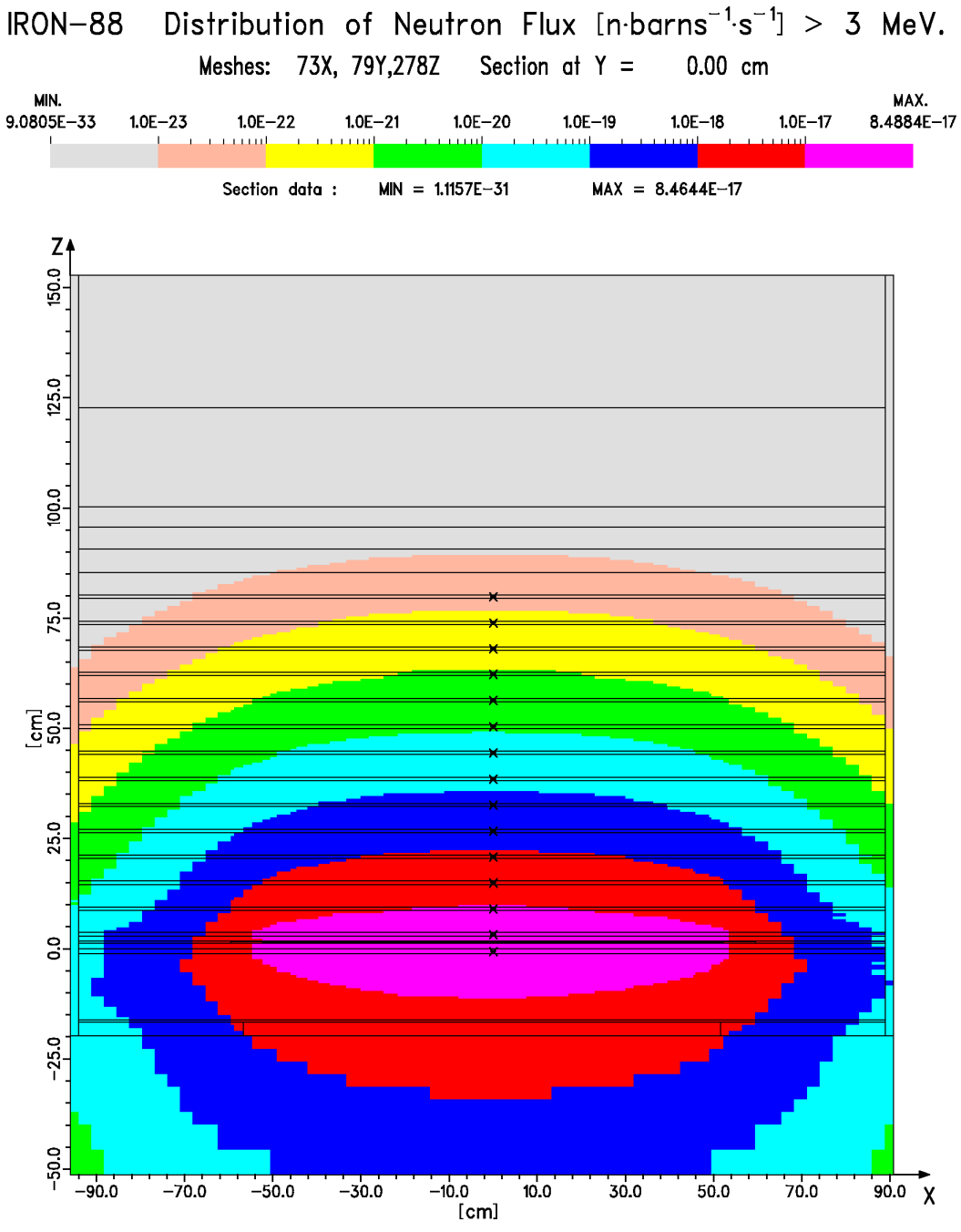

FIG. 5.40

Iron-88 - Spatial Distribution of the Neutron Fluxes at the NESTOR Reactor Maximum Power (30 kW) for Neutron Energy > 8.0 MeV.
[neutrons × barn^{-1} × s^{-1}]

Horizontal Section at Y = 0.0 cm.
Dosimeter Locations "×", 73X×79Y×278Z Spatial Meshes.

P_3-S_8 Calculation Using the BUGJEFF311.BOLIB Library.

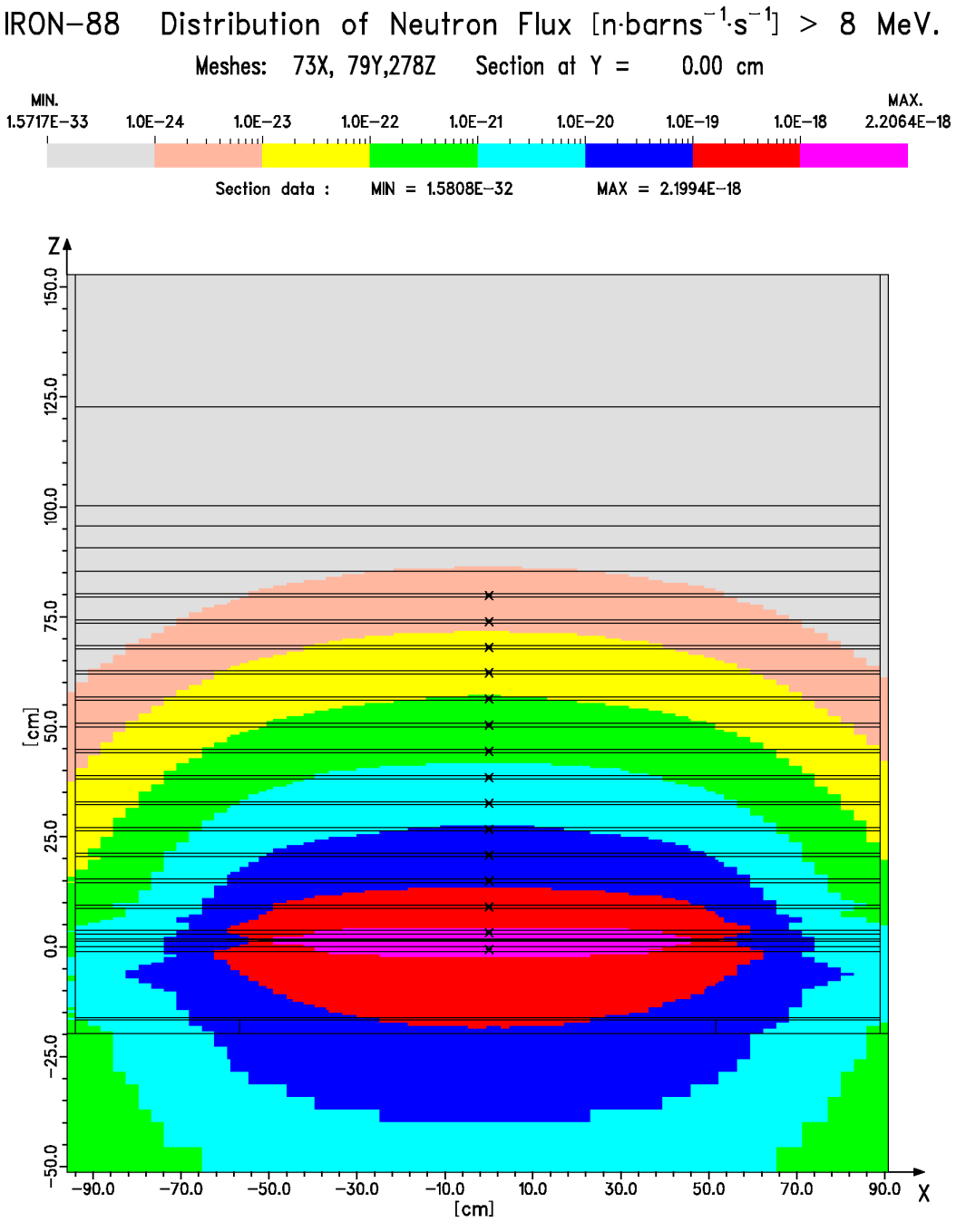

FIG. 5.41

Iron-88 - Spatial Distribution of the Au-197(n,γ)Au-198 epi-Cadmium Reaction Rates
at the NESTOR Reactor Maximum Power (30 kW).
[reactions × s^{-1} × $atom^{-1}$]

Horizontal Section at Y = 0.0 cm.
Dosimeter Locations "×", 73X×79Y×278Z Spatial Meshes.

P_3-S_8 Calculation Using the BUGJEFF311.BOLIB Library
and 1/4 T PV Weighting Dosimeter Cross Sections.

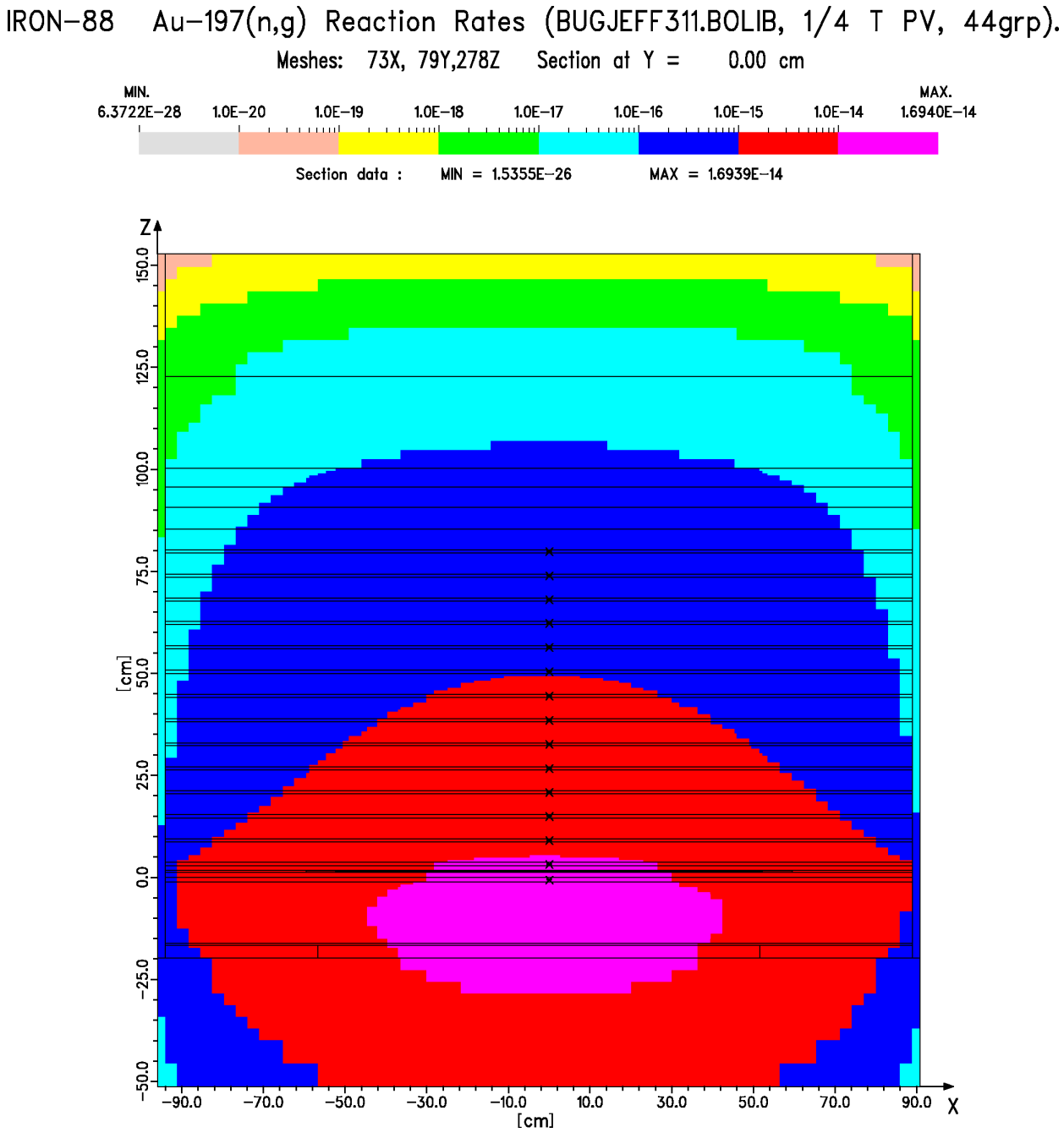

FIG. 5.42

Iron-88 - Spatial Distribution of the Rh-103(n,n')Rh-103m Reaction Rates
at the NESTOR Reactor Maximum Power (30 kW).
[reactions × s^{-1} × $atom^{-1}$]

Horizontal Section at Y = 0.0 cm.
Dosimeter Locations "×", 73X×79Y×278Z Spatial Meshes.

P_3-S_8 Calculation Using the BUGJEFF311.BOLIB Library
and 1/4 T PV Weighting Dosimeter Cross Sections.

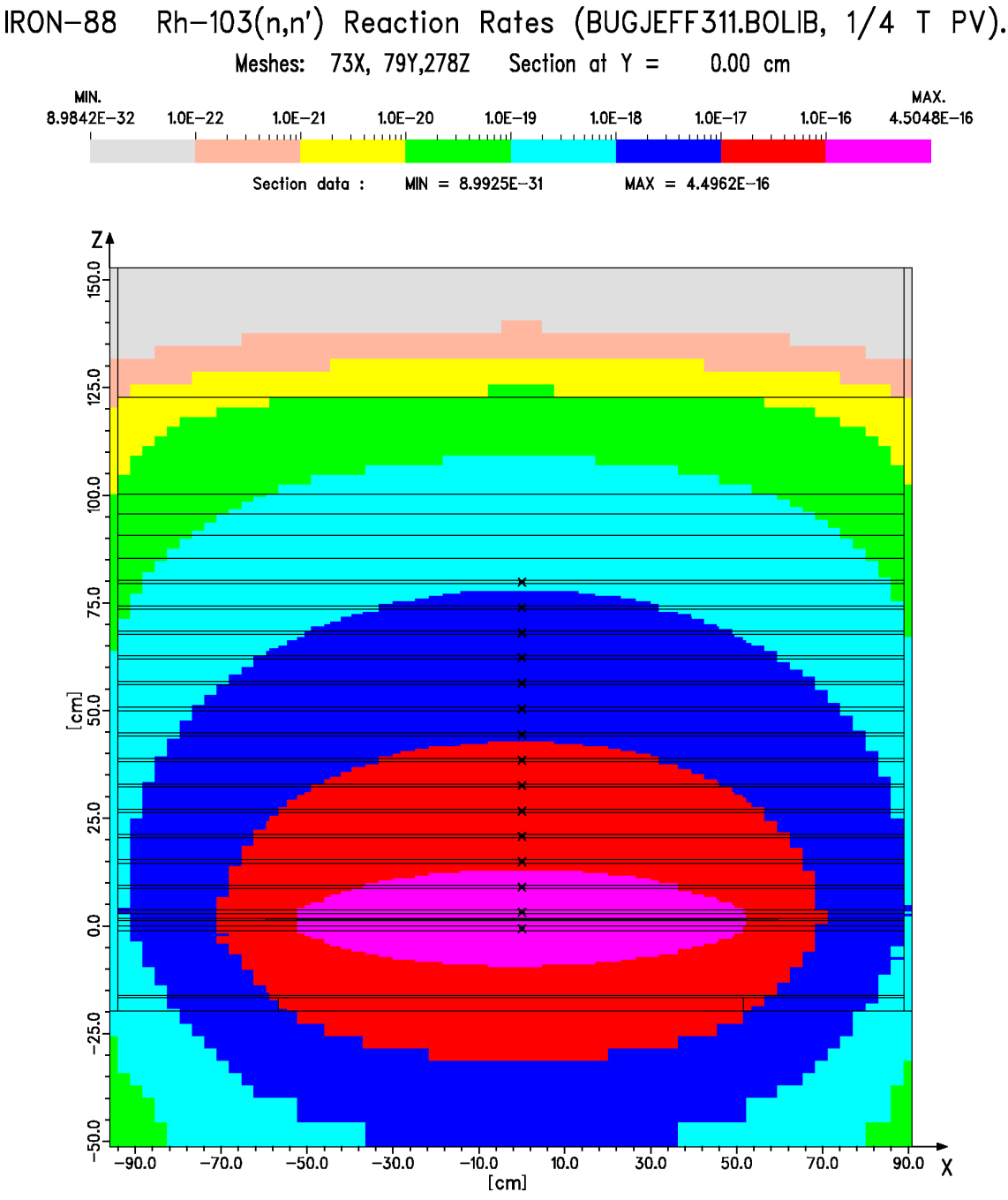

FIG. 5.43

Iron-88 - Spatial Distribution of the In-115(n,n')In-115m Reaction Rates
at the NESTOR Reactor Maximum Power (30 kW).
[reactions × s^{-1} × $atom^{-1}$]

Horizontal Section at Y = 0.0 cm.
Dosimeter Locations "×", 73X×79Y×278Z Spatial Meshes.

P_3-S_8 Calculation Using the BUGJEFF311.BOLIB Library
and 1/4 T PV Weighting Dosimeter Cross Sections.

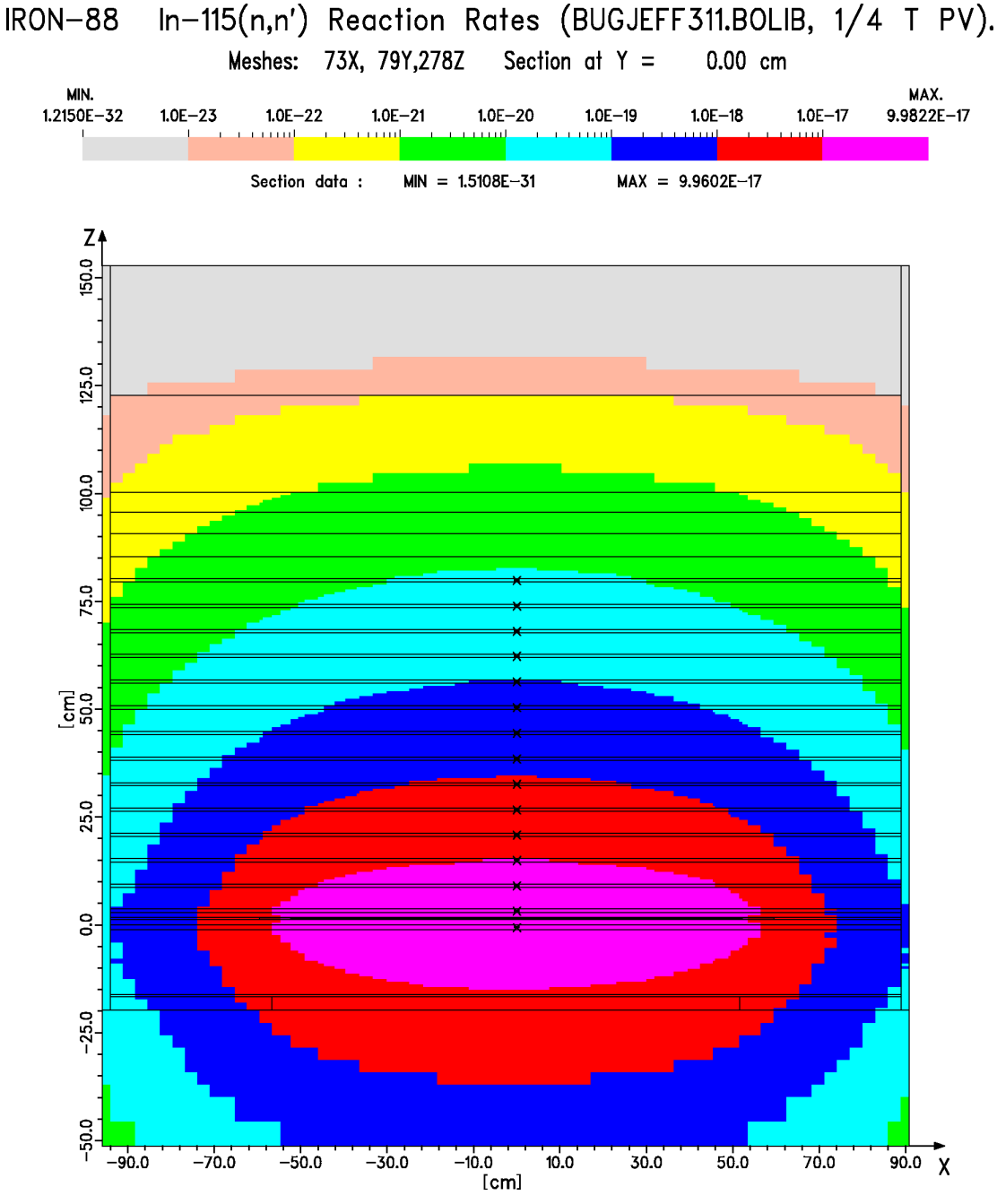

FIG. 5.44

Iron-88 - Spatial Distribution of the S-32(n,p)P-32 Reaction Rates
at the NESTOR Reactor Maximum Power (30 kW).
[reactions × s^{-1} × $atom^{-1}$]

Horizontal Section at Y = 0.0 cm.
Dosimeter Locations "×", 73X×79Y×278Z Spatial Meshes.

P_3-S_8 Calculation Using the BUGJEFF311.BOLIB Library
and 1/4 T PV Weighting Dosimeter Cross Sections.

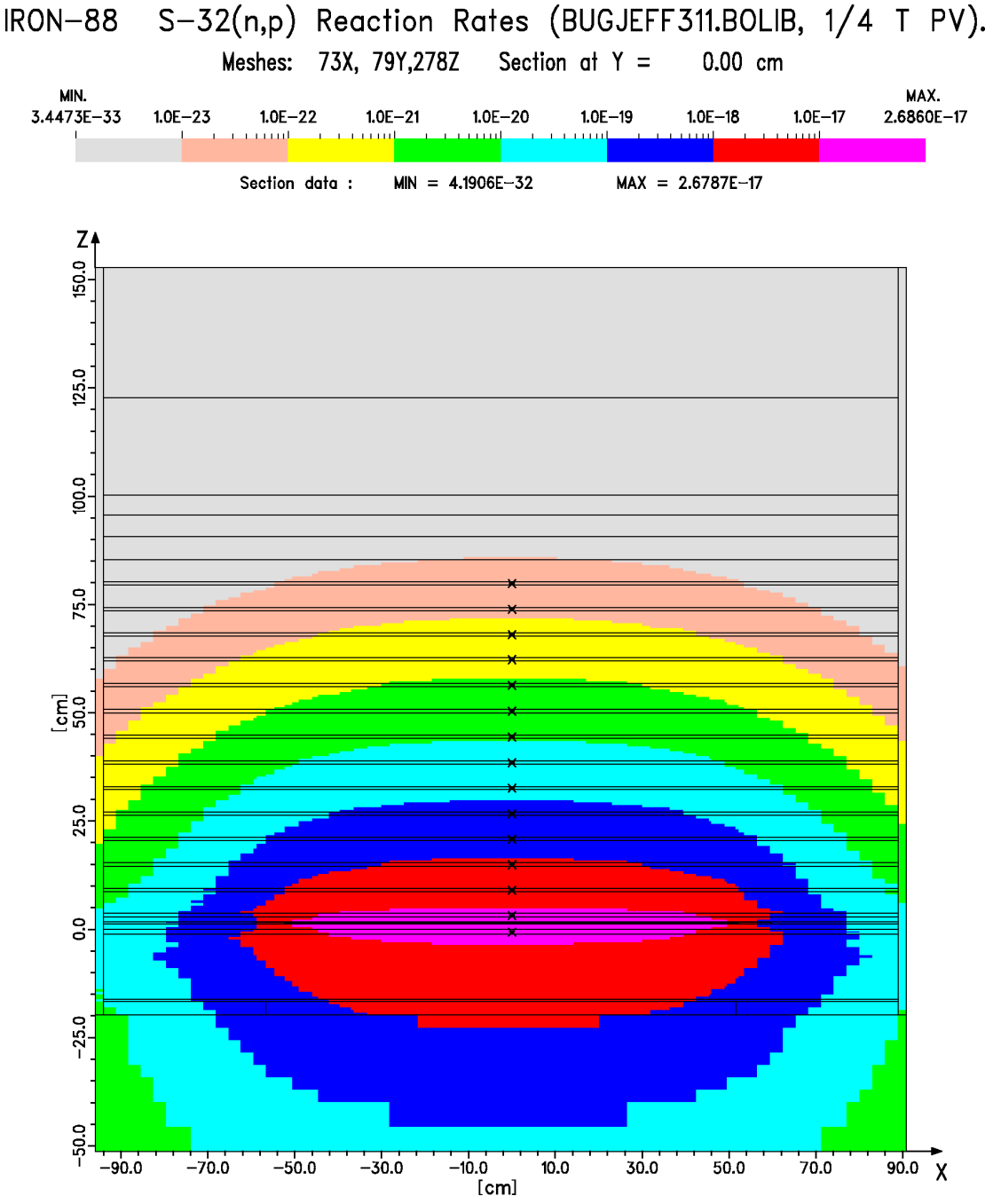

FIG. 5.45

Iron-88 - Spatial Distribution of the Al-27(n,α)Na-24 Reaction Rates
at the NESTOR Reactor Maximum Power (30 kW).
[reactions × s^{-1} × $atom^{-1}$]

Horizontal Section at Y = 0.0 cm.
Dosimeter Locations "×", 73X×79Y×278Z Spatial Meshes.

P_3-S_8 Calculation Using the BUGJEFF311.BOLIB Library
and 1/4 T PV Weighting Dosimeter Cross Sections.

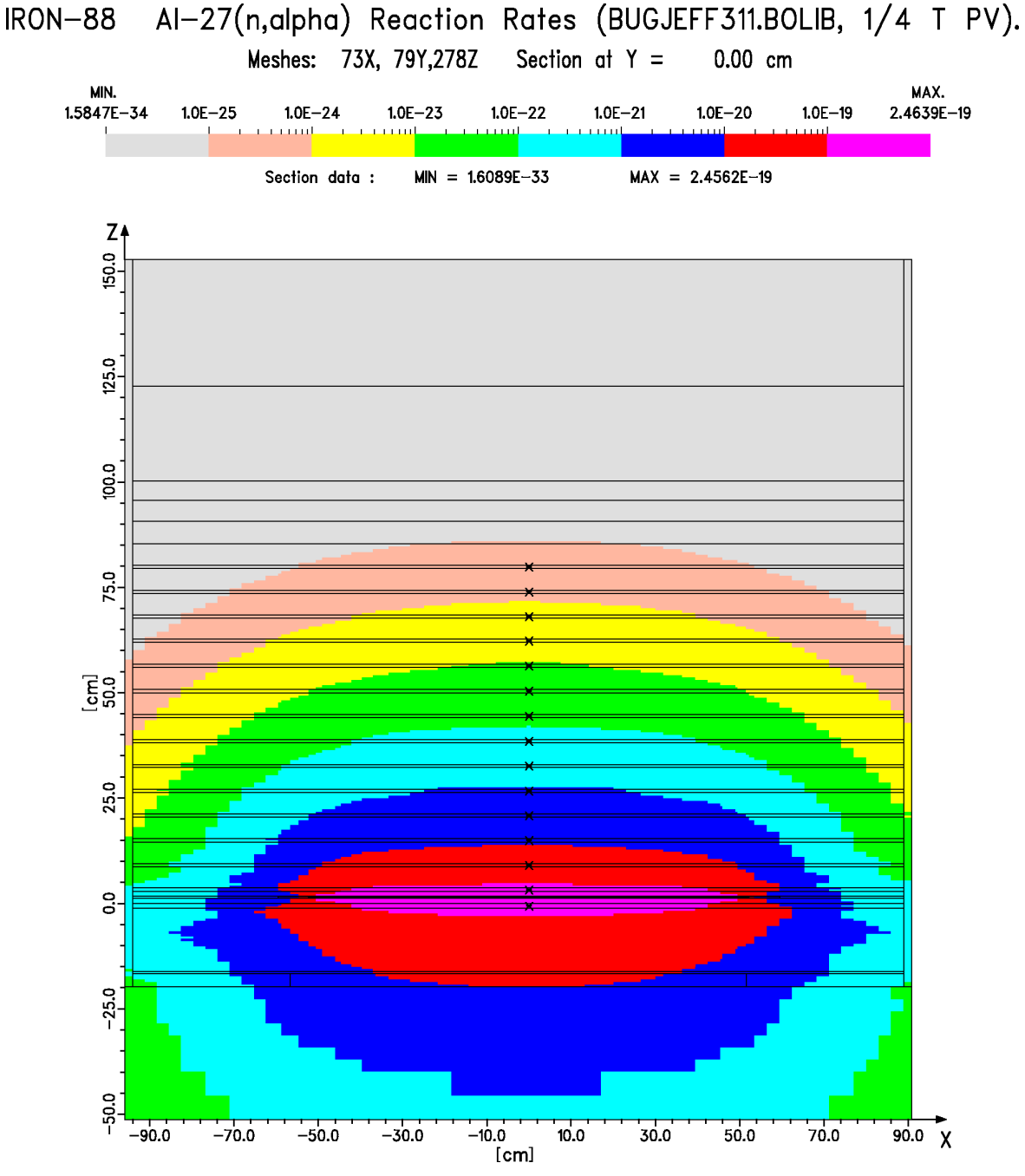

FIG. 5.46

Iron-88 - Calculated Neutron Spectra in Mild Steel at the A2, A4, A8, A12 and A15 Measurement Positions for Neutron Energy > 0.414 eV.

P_3-S_8 Calculation Using the BUGJEFF311.BOLIB Library.

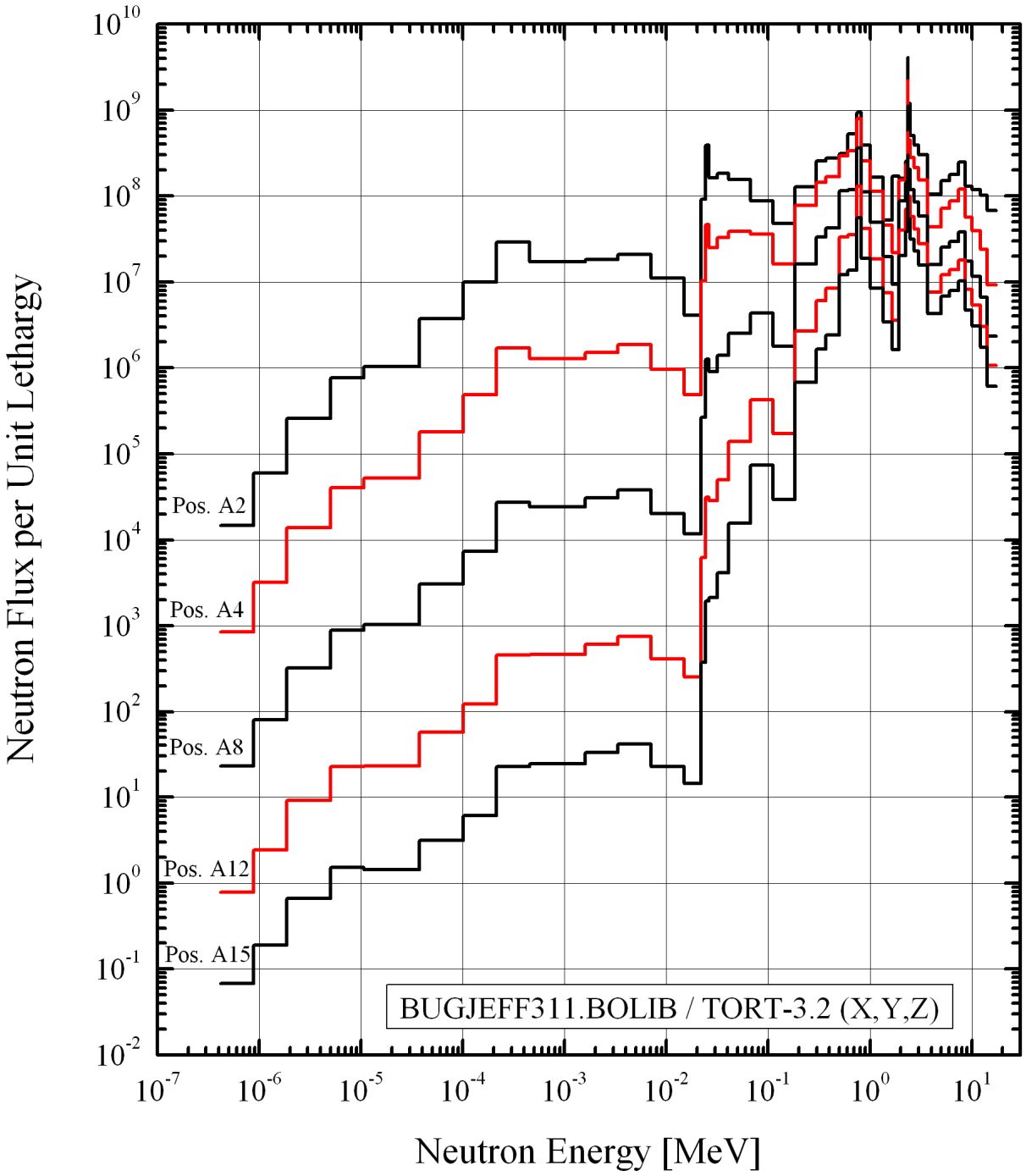

FIG. 5.47

Iron-88 - Calculated Neutron Spectra in Mild Steel at the A2, A4, A8, A12 and A15 Measurement Positions for Neutron Energy > 0.1 MeV.

P_3-S_8 Calculation Using the BUGJEFF311.BOLIB Library.

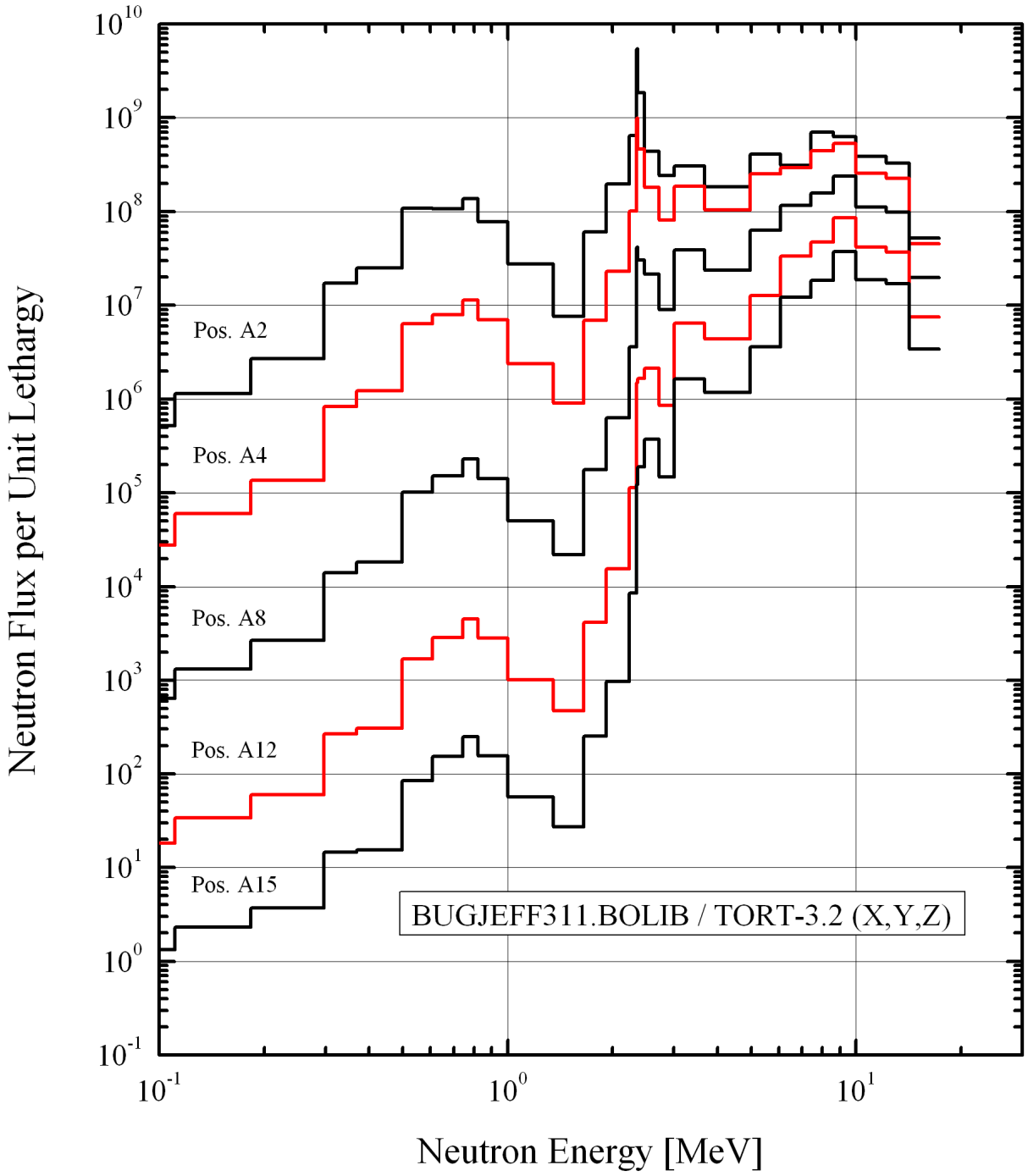

6 - CONCLUSION

Four freely-released broad-group coupled (47 n + 20 γ) working cross section libraries in FIDO-ANISN format, specifically conceived for LWR shielding and pressure vessel dosimetry applications, were validated on the Iron-88 single-material (iron) neutron shielding benchmark experiment, included in the SINBAD REACTOR international database. Two ENEA-Bologna (BUGJEFF311.BOLIB and BUGENDF70.BOLIB) libraries and two ORNL (BUGLE-B7 and BUGLE-96) libraries, freely-released at OECD-NEADB and ORNL-RSICC, were tested on the Iron-88 experiment through three-dimensional fixed source transport calculations in Cartesian (X,Y,Z) geometry, using the ORNL TORT-3.2 discrete ordinates (S_N) code. The ENEA BOT3P-5.3 pre/post-processor ancillary system of multi-dimensional deterministic codes was used for the automatic spatial mesh generation and the graphical verification of the compositional and geometrical model.

The calculated reaction rates for the five activation dosimeters Au-197(n,γ)Au-198/Cd, Rh-103(n,n')Rh-103m, In-115(n,n')In-115m, S-32(n,p)P-32 and Al-27(n,α)Na-24) used in the Iron-88 experiment were obtained through the corresponding dosimeter cross section sets, derived from the IAEA IRDF-2002 dosimetry file, and were compared with the corresponding experimental results. Two types of dosimeter cross section weighting were employed using the following spectra: constant flat neutron spectra and 1/4 T PV neutron spectra calculated at one quarter depth (1/4 T) in the steel of a PWR pressure vessel (PV).

The 1/4 T PV weighting dosimeter cross section files permit to obtain reaction rate results with the four libraries in general more adherent to the corresponding experimental results than those obtained through the use of the flat weighting dosimeter cross section files. In particular the impact of the 1/4 T PV weighting dosimeter cross section files is meaningful for the Au-197(n,γ)Au-198/Cd and Al-27(n,α)Na-24) calculated reaction rate results, obtained through the four BUGLE-type libraries.

Taking into account the total experimental uncertainties at the confidence level of one standard deviation (1σ) of the Au-197(n,γ)Au-198/Cd, Rh-103(n,n')Rh-103m, In-115(n,n')In-115m and S-32(n,p)P-32 dosimeters, the corresponding calculated reaction rate results presented in this work exhibit good statistical consistency with the corresponding measurements. In particular all the calculated reaction rate results obtained using 1/4 T PV weighting dosimeter cross sections are contained within a confidence level of the total experimental uncertainty of ±3σ (99.7% of probability that the measurement result is between ±3 standard deviations), corresponding to deviations of ±15%-20% from the corresponding experimental results. On the contrary, the reaction rate results of the Al-27(n,α)Na-24 dosimeters with the highest effective threshold energy (7.30 MeV) and a minor part of the corresponding results of the Rh-103(n,n')Rh-103m and In-115(n,n')In-115m dosimeters with the lowest effective threshold energies (0.69 MeV and 1.30 MeV respectively) are not included in the same previously cited uncertainty confidence level. In particular the calculated results with all the BUGLE-type libraries give reaction rate results for the Al-27(n,α)Na-24 dosimeters systematically and excessively overestimated (from 20% up to about 30%) with respect to the corresponding experimental results.

The two libraries BUGENDF70.BOLIB and BUGLE-B7, based on ENDF/B-VII.0 evaluated nuclear data, give meaningful discrepancies, in some calculated reaction rate results, above

about 20.0 cm of neutron penetration depth in the Iron-88 steel slab. This fact is evident for the Au-197(n,γ)Au-198/Cd dosimeters and, in particular, for the Rh-103(n,n')Rh-103m and In-115(n,n')In-115m threshold dosimeters with the lowest effective threshold energies (0.69 MeV and 1.30 MeV respectively). In particular, the results obtained using BUGENDF70.BOLIB overestimate those obtained from BUGLE-B7, increasing the neutron penetration depth in the Iron-88 steel slab. Taking into account the 90% response energy ranges, typical of the previously cited threshold activation dosimeters, the mentioned result discrepancies approximately occur in the neutron energy range 1.0 MeV - 6.0 MeV.

Further effort on the sensitivity and uncertainty analysis should be performed.

REFERENCES

/1/ W.W. Engle, Jr., A Users Manual for ANISN, A One Dimensional Discrete Ordinates Transport Code with Anisotropic Scattering, ORNL K-1693, Updated June 6, 1973. Available from OECD-NEA Data Bank as CCC-254 ANISN-ORNL.

/2/ M. Pescarini, V. Sinitsa, R. Orsi, M. Frisoni, BUGJEFF311.BOLIB - A JEFF-3.1.1 Broad-Group Coupled (47 n + 20 γ) Cross Section Library in FIDO-ANISN Format for LWR Shielding and Pressure Vessel Dosimetry Applications, ENEA-Bologna Technical Report UTFISSM-P9H6-002, May 12, 2011. ENEA-Bologna Technical Report UTFISSM-P9H6-002 Revision 1 published on March 14, 2013. Available from OECD-NEA Data Bank as NEA-1866/02 ZZ BUGJEFF311.BOLIB and from ORNL-RSICC as DLC-254 BUGJEFF311.BOLIB.

/3/ M. Pescarini, V. Sinitsa, R. Orsi, M. Frisoni, BUGENDF70.BOLIB - An ENDF/B-VII.0 Broad-Group Coupled (47 n + 20 γ) Cross Section Library in FIDO-ANISN Format for LWR Shielding and Pressure Vessel Dosimetry Applications, ENEA-Bologna Technical Report UTFISSM-P9H6-008, January 1, 2013. Available from OECD-NEA Data Bank as NEA-1872/01 ZZ BUGENDF70.BOLIB and from ORNL-RSICC, as DLC-262 BUGENDF70.BOLIB.

/4/ The JEFF-3.1.1 Nuclear Data Library, JEFF Report 22, OECD-NEA Data Bank, 2009.

/5/ The JEFF-3.1 Nuclear Data Library, JEFF Report 21, OECD-NEA Data Bank, 2006.

/6/ M.B. Chadwick et al., ENDF/B-VII.0: Next Generation Evaluated Nuclear Data Library for Nuclear Science and Technology, Nuclear Data Sheets, Volume 107, Number 12, pp. 2931-3060, December 2006.

/7/ J.M. Risner, D. Wiarda, M.E. Dunn, T.M. Miller, D.E. Peplow, B.W. Patton, Production and Testing of the VITAMIN-B7 Fine-Group and BUGLE-B7 Broad-Group Coupled Neutron/Gamma Cross-Section Libraries Derived from ENDF/B-VII.0 Nuclear Data, Oak Ridge, ORNL Report ORNL/TM-2011/12, NUREG/CR-7045, September 2011. VITAMIN-B7 and BUGLE-B7 libraries available from OECD-NEA Data Bank as DLC-0245 ZZ-VITAMINB7/BUGLEB7.

/8/ J.E. White, D.T. Ingersoll, R.Q. Wright, H.T. Hunter, C.O. Slater, N.M. Greene, R.E. MacFarlane, R.W. Roussin, Production and Testing of the Revised VITAMIN-B6 Fine-Group and the BUGLE-96 Broad-Group Neutron/Photon Cross-Section Libraries Derived from ENDF/B-VI.3 Nuclear Data, Oak Ridge, ORNL Report ORNL-6795/R1, NUREG/CR-6214, Revision 1, January 1995. VITAMIN-B6 library available from OECD-NEA Data Bank as DLC-0184 ZZ VITAMIN-B6. BUGLE-96 library available from OECD-NEA Data Bank as DLC-0185 ZZ BUGLE-96.

/9/ P.F. Rose, ENDF/B-VI Summary Documentation, Brookhaven National Laboratory, BNL-NCS-17541 (ENDF-201) 4th Edition, October 1991.

/10/ G.A. Wright, M.J. Grimstone, Benchmark Testing of JEF-2.2 Data for Shielding Applications: Analysis of the Winfrith Iron-88 Benchmark Experiment, AEA Report AEA-RS-1231, March 1993.

/11/ Radiation Shielding Integral Benchmark Archive Database (SINBAD), OECD-NEA Data Bank/ ORNL-RSICC, SINBAD REACTOR, NEA-1517, 2009 Edition.

/12/ I. Kodeli, E. Sartori, B. Kirk, SINBAD Shielding Benchmark Experiments Status and Planned Activities, The American Society's 14th Biennial Topical Meeting of the Radiation Protection and Shielding Division, Carlsbad, New Mexico, USA, April 3-6, 2006.

/13/ W.A. Rhoades, D.B. Simpson, The TORT Three-Dimensional Discrete Ordinates Neutron/Photon Transport Code (TORT Version 3), Oak Ridge, ORNL Report ORNL/TM-13221, October 1997.

/14/ DOORS3.1: One-, Two- and Three-Dimensional Discrete Ordinates Neutron/Photon Transport Code System, ORNL, RSIC Computer Code Collection CCC-650, August 1996. Available from OECD/NEA Data Bank as CCC-0650/04 DOORS-3.2A.

/15/ R. Orsi, ADEFTA Version 4.1: A Program to Calculate the Atomic Densities of a Compositional Model for Transport Analysis, ENEA-Bologna Technical Report FPN-P9H6-010, May 20, 2008. Available from OECD-NEA Data Bank as NEA-1708/06 ADEFTA 4.1.

/16/ R. Orsi, BOT3P Version 5.3: A Pre/Post-Processor System for Transport Analysis, ENEA-Bologna Technical Report FPN-P9H6-011, October 22, 2008. Available from OECD-NEA Data Bank as NEA-1678/09 BOT3P-5.3.

/17/ R. Orsi, The ENEA-Bologna pre-post-Processor Package BOT3P for the DORT and TORT Transport Codes (Version 1.0 - December 1999), JEF/DOC-828, JEFF Working Group Meeting on Benchmark Testing, Data Processing and Evaluations, OECD-NEA Data Bank, Issy-les-Moulineaux, France, May 22-24, 2000.

/18/ R. Orsi, BOT3P: Bologna Transport Analysis Pre-Post-Processors Version 1.0, Nuclear Science and Engineering, Technical Note, Volume 142, pp. 349-354, 2002.

/19/ R. Orsi, BOT3P: Bologna Transport Analysis Pre-Post-Processors Version 3.0, Nuclear Science and Engineering, Technical Note, Volume 146, pp. 248-255, 2004.

/20/ R. Orsi, M. Pescarini, V. Sinitsa, Dosimetry Cross Section Processing from IRDF-2002 in the BUGLE-96 (47 n) Neutron Group Structure Using Flat and Updated Problem Dependent Neutron Spectra, ENEA-Bologna Technical Report UTFISSM-P9H6-006, May 9, 2012.

/21/ O.Bersillon, L.R. Greenwood, P.J. Griffin, W. Mannhart, H.J. Nolthenius, R. Paviotti-Corcuera, K.I. Zolotarev, E.M. Zsolnay, International Reactor Dosimetry File 2002 (IRDF-2002), IAEA, Vienna, Austria, Technical Reports Series No. 452, 2006.

/22/ American National Standard, American Nuclear Society, Neutron and Gamma-Ray Cross Sections for Nuclear Radiation Protection Calculations for Nuclear Power Plants, ANSI/ANS-6.1.2-1999 (R2009).

/23/ M. Pescarini, R. Orsi, Preliminary Results of the BUGJEFF311.BOLIB Library Validation on the Iron-88 (Fe) Neutron Shielding Benchmark Experiment, ENEA-Bologna Technical Report ADPFISS-LP1-064, June 28, 2016.

/24/ M. Pescarini, R. Orsi, Final Results of the BUGJEFF311.BOLIB Library Validation on the Iron-88 (Fe) Neutron Shielding Benchmark Experiment, ENEA-Bologna Technical Report ADPFISS-LP1-087, November 8, 2017.

/25/ I.J Curl, CRISP - A Computer Code to Define Fission Plate Source Profiles, RPD/IJC/934.

/26/ M.J. Armishaw, J. Butler, M.D. Carter, I.J Curl, A.K. McCracken, A transportable Neutron Spectrometer (TNS) for radiological applications, AEEW-M2365, 1986.

/27/ J.H. Baard, W.L. Zijp, H.J. Nolthenius, Nuclear Data Guide for Reactor Neutron Metrology, Kluwer Academic Publishers, 1989.

/28/ G. Hehn, A. Sohn, M. Mattes, G. Pfister, IKE Calculations of the OECD/NEA Benchmarks VENUS-1 and VENUS-3 for Computing Radiation Dose to Reactor Pressure Vessel and Internals, Universität Stuttgart, Institut für Kernenergetik und Energiesysteme, IKE 6 NEA 2, December 1997.

/29/ M. Pescarini, V. Sinitsa, R. Orsi, VITJEFF311.BOLIB - A JEFF-3.1.1 Multi-Group Coupled (199 n + 42 γ) Cross Section Library in AMPX Format for Nuclear Fission Applications, ENEA-Bologna Technical Report UTFISSM-P9H6-003, November 10, 2011. ENEA-Bologna Technical Report UTFISSM-P9H6-003 Revision 1 published on March 14, 2013. Available from OECD-NEA Data Bank as NEA-1869/01 ZZ VITJEFF311.BOLIB.

/30/ I.I. Bondarenko, M.N. Nikolaev, L.P. Abagyan, N.O. Bazaziants, Group Constants for Nuclear Reactors Calculations, Consultants Bureau, New York, 1964.

/31/ V. Sinitsa, M. Pescarini, ENEA-Bologna 2007 Revision of the SCAMPI (ORNL) Nuclear Data Processing System, ENEA-Bologna Technical Report FPN-P9H6-006, September 13, 2007.

/32/ SCAMPI Collection of Codes for Manipulating Multigroup Cross Section Libraries in AMPX Format, ORNL, RSIC Peripheral Shielding Routine Collection PSR-352, September 1995. Available from OECD-NEA Data Bank as PSR-0352/05 SCAMPI, version of the ORNL SCAMPI system corresponding to the last ENEA-Bologna 2007 Revision (see /31/).

/33/ M. Pescarini, V. Sinitsa, R. Orsi, M. Frisoni, VITENDF70.BOLIB - An ENDF/B-VII.0 Multi-Group Coupled (199 n + 42 γ) Cross Section Library in AMPX Format for Nuclear Fission Applications, ENEA-Bologna Technical Report UTFISSM-P9H6-005, May 25, 2012. Available from OECD-NEA Data Bank as NEA-1870/01 ZZ VITENDF70.BOLIB.

/34/ D. Wiarda, M.E. Dunn, N.M. Green, M.L. Williams, C. Celik, AMPX-6: A Modular Code System for Processing ENDF/B Evaluations, Oak Ridge, ORNL Report ORNL/TM-2016/43, April 2016.

/35/ D.E. Cullen, PREPRO 2007: 2007 ENDF/B Pre-processing Codes (ENDF/B-VII Tested), LLNL, owned, maintained and distributed by IAEA-NDS, Vienna, Austria, IAEA Report IAEA-NDS-39, Rev. 13, March 17, 2007. Available from OECD-NEA Data Bank as IAEA-1379 PREPRO-2007.

/36/ R.E. MacFarlane, NJOY-99, "README0", ORNL, RSIC Peripheral Shielding Routine Collection PSR-0480/02, December 31, 1999.

/37/ N.M. Greene, J.L.Lucius, L.M. Petrie, W.E. Ford III, J.E. White and R.Q. Wright, AMPX: A Modular Code System for Generating Coupled Multigroup Neutron-Gamma Libraries from ENDF/B, Oak Ridge, ORNL Report ORNL/TM-3706, March 1976, informally revised to level of AMPX-II in December 1978. See in particular Chapter 9.12: BONAMI - AMPX Module to Perform Bondarenko Resonance Self-Shielding.

/38/ K.H. Beckurts and K. Wirtz, Neutron Physics, Springer Verlag, 1964.

/39/ MCBEND User Guide to Version 7, ANSWERS/MCBEND(91)7.

/40/ J.K. Tuli, Nuclear Wallet Cards (6^{th} Edition), National Nuclear Data Centre, Brookhaven National Laboratory, Upton, New York 11973-5000, USA, January 2000.

Titolo

Production of the ANITA-NC system able to treat material activation due to neutral or charged particles

Descrittori

Tipologia del documento: Rapporto tecnico

Collocazione contrattuale: Accordo di programma ENEA-MSE su sicurezza nucleare e reattori di IV generazione

Argomenti trattati: Fisica nucleare, dati nucleari, attivazione dei materiali.

Sommario

ANITA-NC (Analysis of Neutron Induced Transmutation and Activation – Neutral and Charged) is an inventory system developed in ENEA-Bologna, capable of modelling the material activation induced by several neutral and charged projectiles (neutron, proton, alpha, deuteron and gamma).
It is suitable to be applied to the study of the irradiation effects on materials in facilities like the International Fusion Materials Irradiation Facility (IFMIF) and, more recently, the DEMO Oriented Neutron Source (DONES), in which a considerable amount of neutrons with energies above 20 MeV is produced. In fact, in these facilities the deuterons will themselves cause activation, particularly in the accelerator structure and in the lithium target.
ANITA-NC includes and extends the capabilities of the ANITA-IEAF code, able to assess the activation of materials exposed to neutrons with energies up to 55 MeV. ANITA-IEAF was released by ENEA to OECD-NEADB where is in free distribution (NEA-1638). In this report the main characteristics of ANITA-NC are given. An example of calculation for both deuteron and proton activation performed by ANITA-NC are also shown. The results are compared with the FISPACT-II predictions.

Note

Author: Manuela Frisoni

Copia n. **In carico a:**

REV.	DESCRIZIONE	DATA		REDAZIONE	CONVALIDA	APPROVAZIONE
2			NOME			
			FIRMA			
1			NOME			
			FIRMA			
0	EMISSIONE	14/11/18	NOME	M. Frisoni	F. Padoani	F. Rocchi
			FIRMA	Manuela Frisoni	F. Padoani	Federico Rocchi

CONTENTS

FIGURE LIST

TABLE LIST

Production of the ANITA-NC system able to treat material activation due to neutral or charged particles

Manuela Frisoni

November 2018

1 INTRODUCTION

ANITA-NC is a package (code and libraries), developed in ENEA-Bologna, able to assess the activation of materials exposed both to neutrons and charged particles. It is an updating/extension of previous ANITA versions as ANITA-2000, able to handle neutrons with energies up to 20 MeV, widely used and validated in the past by ENEA [1][2][3][4][5][6] and ANITA-IEAF, able to treat neutrons with energies up to 55 MeV, actually in free distribution at OECD-NEADB with the identification NEA-1638 [7][8].

The ANITA-NC package is needed in order to perform neutron activation calculations for some facilities as the International Fusion Materials Irradiation Facility (IFMIF) and, more recently, the DEMO Oriented Neutron Source (DONES), that have been proposed as neutron sources to test samples of candidate materials to be used in future fusion power plants. In both these facilities the neutron source is produced through the reaction of 40 MeV deuterons impinging on a liquid lithium target and a considerable amount of neutrons with energies above 20 MeV is produced.

In these devices the deuterons can themselves cause activation, particularly in the accelerator structure and in the lithium target. So, in these facilities the capability to perform deuteron activation calculations is also required.

The main component of the ANITA-NC system is the activation code ANITA-NC able to compute the radioactive inventory of a material exposed to n, p, d, α and γ irradiation, continuous or stepwise. It traces back to the ANITA code (Analysis of Neutron Induced Transmutation and Activation) [9][10].

The ANITA-NC code provides activity, atomic density, decay heat, biological hazard, clearance index and decay gamma-ray sources versus cooling time. Results are given as for each nuclide as for the material.

The ANITA-NC code package requires the following files/libraries in order to perform the activation calculations:

1) Multi-group activation cross sections data library (file “libanita”).
2) Decay, Hazard and Clearance data library (file “fl1”), containing the quantities describing the decay properties of unstable nuclides.

3) Gamma library (file “fl2”), containing the gamma ray spectra emitted by the radioactive nuclei.

ANITA-NC reads multi-group activation cross section libraries in the LIBOUT format of the FOUR ACES code (ENEA Bologna). The only available libraries in this format are the EAF libraries produced for the EASY activation systems. In particular, ANITA-NC uses the EAF-2010 activation cross libraries contained in the original EASY-2010 code package [11], actually included in the FISPACT-II Release 4.0 system [12] in free distribution at NEA Data Bank (NEA- 1890). These libraries contain cross sections for neutrons, deuterons and protons only. ANITA-NC uses a neutron activation cross section data library based on the EAF-2010 group-wise library “eaf_n_gxs_211_flt_20010” in the VITAMIN-J+ (211 energy group structure) up to 55 MeV. For deuterons and protons it uses libraries based on the corresponding EAF-2010 libraries, “eaf_d_gxs_211_flt_20010” and “eaf_p_gxs_211_flt_20010” in the same VITAMIN-J+ (211 energy group structure) up to 55 MeV.

So, although ANITA-MC is structured in order to perform also the activation of materials induced by alpha particles and photons, actually, for these projectiles, activation libraries in the format required by ANITA-NC are not available.

The data contained in the fl1 and fl2 files are based on the JEFF-3.1.1 Radioactive Decay Data Library [13].

In this report a brief description of the characteristics of the code and the libraries contained in the package is given.

Two sample problems, related to deuteron and proton activation, are also presented. The ANITA-NC results are compared with the FISPACT-II corresponding ones.

2 DATA LIBRARIES

The ANITA-NC activation code requires the following data libraries:

- Decay, Hazard and Clearance data library (file "fl1")
- Gamma library (file "fl2")
- Neutron, deuteron and proton activation cross section data library (file "libanita")

The schematic block diagram of the data/libraries required by the ANITA-NC code is shown in Figure 1.

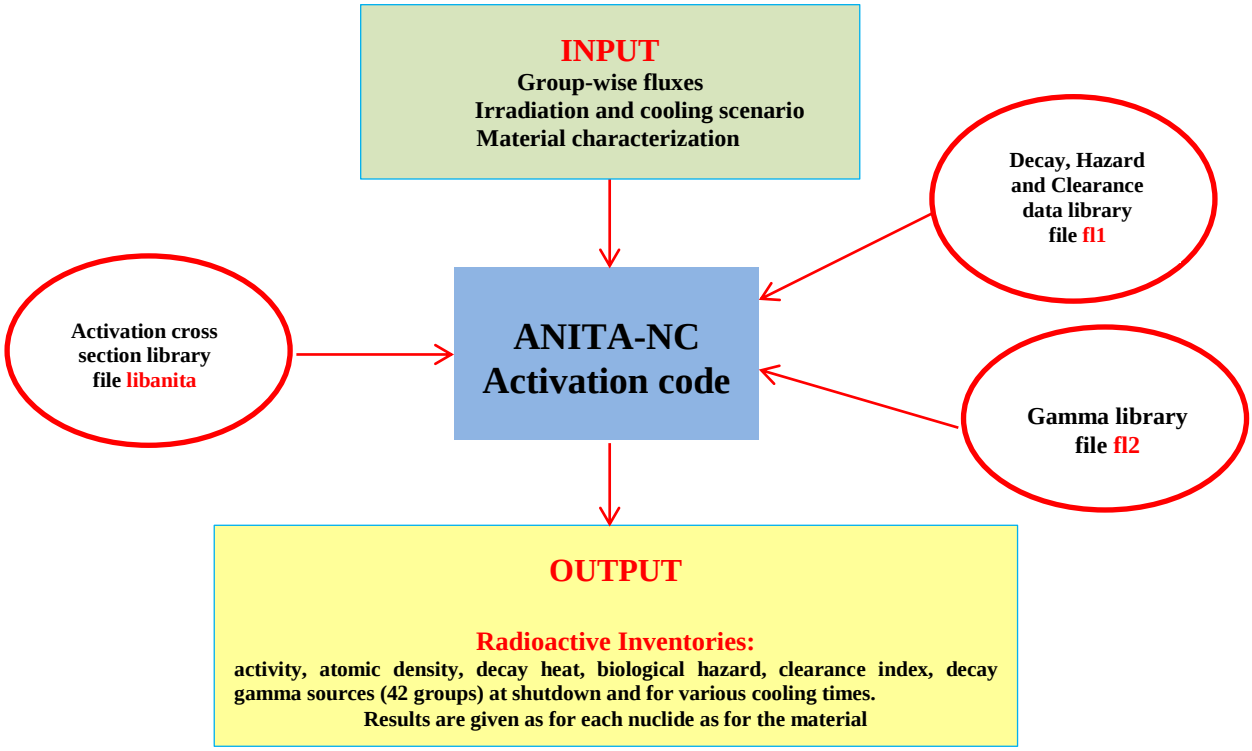

Figure 1 – ANITA-NC activation code block diagram

2.1 Decay, Hazard and Clearance Data library (file "fl1")

This library contains the information describing the decay properties of unstable nuclides useful for the calculations performed by ANITA-NC.

For each nuclide, the decay data, as the decay mode, the decay constant (s^{-1}), the total energy (MeV) released in the decay and the energy (MeV) released in the form of gamma or X-rays are provided. Different competitive decay modes are taken into account when contemporary.

The file contains also the hazard data (ALI) for each radionuclide describing its potential biological impact on human beings. The ALI quantities are defined as the Annual Limit of Intake (Bq) by ingestion or inhalation for the public or workers.

The library contains also the clearance level for each radionuclide.

The fl1 file contains data for 3433 nuclides.

2.2 Gamma Library (file "fl2")

This data base contains the gamma ray spectra emitted by the radioactive nuclei in the Vitamin-J 42-γ energy group structure given in Table 1.

Energy Group N.	Upper Boundary [eV]
1	5.00E+07
2	3.00E+07
3	2.00E+07
4	1.40E+07
5	1.20E+07
6	1.00E+07
7	8.00E+06
8	7.50E+06
9	7.00E+06
10	6.50E+06
11	6.00E+06
12	5.50E+06
13	5.00E+06
14	4.50E+06
15	4.00E+06
16	3.50E+06
17	3.00E+06
18	2.50E+06
19	2.00E+06
20	1.66E+06
21	1.50E+06
22	1.34E+06
23	1.33E+06
24	1.00E+06
25	8.00E+05
26	7.00E+05
27	6.00E+05
28	5.12E+05
29	5.10E+05
30	4.50E+05
31	4.00E+05

32	3.00E+05
33	2.00E+05
34	1.50E+05
35	1.00E+05
36	7.50E+04
37	7.00E+04
38	6.00E+04
39	4.50E+04
40	3.00E+04
41	2.00E+04
42	1.00E+04

Table 1 – Upper boundaries of the Vitamin-J 42-γ energy group structure

The data contained in the library are based on the JEFF-3.1.1 evaluated decay data file (gamma radiation spectra). The data given in the gamma library are used in ANITA-NC to compute the intensity and the energy distribution of the gamma-rays emitted by the irradiated material. This gamma-ray source (photons×cm^{-3}×s^{-1}) in the VITAMIN-J 42-γ energy group structure may be given as input to a radiation transport code in order to compute the space and energy distribution of the decay gamma-rays and the relative dose equivalent rate.

2.3 Activation cross section data library (file “libanita”)

The ANITA-NC code requires a multi-group activation cross section data library in order to perform the activation calculations. A different library is needed for each incident projectile.

The format of these multi-group libraries is the LIBOUT format of the FOUR ACES code (ENEA Bologna) with two additional comment lines for each reaction. Actually, the ANITA-NC code uses activation cross section libraries based on the EAF-2010 group-wise libraries “eaf_n_gxs_211_flt_20010”, “eaf_d_gxs_211_flt_20010” and “eaf_p_gxs_211_flt_20010”, for neutrons, deuterons and protons respectively, in the VITAMIN-J+ (211 energy group structure) up to 55 MeV.

The VITAMIN-J+ (211 energy group structure) is listed in Table 2.

In the ANITA-NC code new MT numbers have been introduced, from 151 to 200, the same as in FISPACT code, that allow describing reactions with up to 8 emitted particles corresponding to a set of unallocated numbers in the standard ENDF-6 format.

In Table 3, Table 4 and Table 5 the 85 MT values used in the ANITA-NC code for n, p and d are shown, respectively. In the Tables, in column 3, for each MT, the corresponding reaction label that describes the reaction is given. Each reaction corresponds to a well-defined ZA (ZA=Z*1000+A) change with respect to the target nuclide and this Δ(ZA) is used in the activation code to create and follow the decay chains.

In the activation cross sections libraries, for the reaction numbers the ENDF-reaction number MT multiplied by 10 has been adopted, with the convention that for the excitation of each isomeric state the reaction number is increased by one. The material numbers, MAT, consist of Z, A and an identifier, LIS, to indicate ground or isomeric target (MAT=Z*10000+A*10+LIS). The order of the cross sections of the libraries is in accordance with increasing Z,A,LIS and MT. The cross section values of each reaction MT are in accordance with decreasing energy of the VITAMIN-J+ group structure.

The neutron, deuteron and proton libraries are provided in card-image format. The MODBIN module must be used for the conversion of the card image file to libanita (see Figure 1) in binary format as required by the ANITA-NC code.

Table 2 – Energy group boundaries of the Vitamin-J +(211- energy group structure)

Energy Group N.	Upper Boundary [eV]
1	5.5000E+07
2	5.4000E+07
3	5.3000E+07
4	5.2000E+07
5	5.1000E+07
6	5.0000E+07
7	4.9000E+07
8	4.8000E+07
9	4.7000E+07
10	4.6000E+07
11	4.5000E+07
12	4.4000E+07
13	4.3000E+07
14	4.2000E+07
15	4.1000E+07
16	4.0000E+07
17	3.9000E+07
18	3.8000E+07
19	3.7000E+07
20	3.6000E+07
21	3.5000E+07
22	3.4000E+07
23	3.3000E+07
24	3.2000E+07
25	3.1000E+07
26	3.0000E+07
27	2.9000E+07
28	2.8000E+07
29	2.7000E+07
30	2.6000E+07
31	2.5000E+07
32	2.4000E+07
33	2.3000E+07
34	2.2000E+07
35	2.1000E+07
36	2.0000E+07
37	1.9640E+07
38	1.7333E+07
39	1.6905E+07
40	1.6487E+07
41	1.5683E+07
42	1.4918E+07
43	1.4550E+07
44	1.4191E+07
45	1.3840E+07
46	1.3499E+07
47	1.2840E+07
48	1.2523E+07
49	1.2214E+07
50	1.1618E+07
51	1.1052E+07
52	1.0513E+07
53	1.0000E+07
54	9.5123E+06

Energy Group N.	Upper Boundary [eV]
55	9.0484E+06
56	8.6071E+06
57	8.1873E+06
58	7.7880E+06
59	7.4082E+06
60	7.0469E+06
61	6.7032E+06
62	6.5924E+06
63	6.3763E+06
64	6.0653E+06
65	5.7695E+06
66	5.4881E+06
67	5.2205E+06
68	4.9659E+06
69	4.7237E+06
70	4.4933E+06
71	4.0657E+06
72	3.6788E+06
73	3.3287E+06
74	3.1664E+06
75	3.0119E+06
76	2.8651E+06
77	2.7253E+06
78	2.5924E+06
79	2.4660E+06
80	2.3852E+06
81	2.3653E+06
82	2.3457E+06
83	2.3069E+06
84	2.2313E+06
85	2.1225E+06
86	2.0190E+06
87	1.9205E+06
88	1.8268E+06
89	1.7377E+06
90	1.6530E+06
91	1.5724E+06
92	1.4957E+06
93	1.4227E+06
94	1.3534E+06
95	1.2874E+06
96	1.2246E+06
97	1.1648E+06
98	1.1080E+06
99	1.0026E+06
100	9.6164E+05
101	9.0718E+05
102	8.6294E+05
103	8.2085E+05
104	7.8082E+05
105	7.4274E+05
106	7.0651E+05
107	6.7206E+05
108	6.3928E+05

Energy Group N.	Upper Boundary [eV]
109	6.0810E+05
110	5.7844E+05
111	5.5023E+05
112	5.2340E+05
113	4.9787E+05
114	4.5049E+05
115	4.0762E+05
116	3.8774E+05
117	3.6883E+05
118	3.3373E+05
119	3.0197E+05
120	2.9849E+05
121	2.9721E+05
122	2.9452E+05
123	2.8725E+05
124	2.7324E+05
125	2.4724E+05
126	2.3518E+05
127	2.2371E+05
128	2.1280E+05
129	2.0242E+05
130	1.9255E+05
131	1.8316E+05
132	1.7422E+05
133	1.6573E+05
134	1.5764E+05
135	1.4996E+05
136	1.4264E+05
137	1.3569E+05
138	1.2907E+05
139	1.2277E+05
140	1.1679E+05
141	1.1109E+05
142	9.8037E+04
143	8.6517E+04
144	8.2503E+04
145	7.9499E+04
146	7.1998E+04
147	6.7379E+04
148	5.6562E+04
149	5.2475E+04
150	4.6309E+04
151	4.0868E+04
152	3.4307E+04
153	3.1828E+04
154	2.8501E+04
155	2.7000E+04
156	2.6058E+04
157	2.4788E+04
158	2.4176E+04
159	2.3579E+04
160	2.1875E+04
161	1.9305E+04
162	1.5034E+04
163	1.1709E+04
164	1.0595E+04
165	9.1188E+03

Energy Group N.	Upper Boundary [eV]
166	7.1017E+03
167	5.5308E+03
168	4.3074E+03
169	3.7074E+03
170	3.3546E+03
171	3.0354E+03
172	2.7465E+03
173	2.6126E+03
174	2.4852E+03
175	2.2487E+03
176	2.0347E+03
177	1.5846E+03
178	1.2341E+03
179	9.6112E+02
180	7.4852E+02
181	5.8295E+02
182	4.5400E+02
183	3.5358E+02
184	2.7536E+02
185	2.1445E+02
186	1.6702E+02
187	1.3007E+02
188	1.0130E+02
189	7.8893E+01
190	6.1442E+01
191	4.7851E+01
192	3.7267E+01
193	2.9023E+01
194	2.2603E+01
195	1.7604E+01
196	1.3710E+01
197	1.0677E+01
198	8.3153E+00
199	6.4760E+00
200	5.0435E+00
201	3.9279E+00
202	3.0590E+00
203	2.3824E+00
204	1.8554E+00
205	1.4450E+00
206	1.1254E+00
207	8.7643E-01
208	6.8256E-01
209	5.3158E-01
210	4.1399E-01
211	1.0000E-01
212	1.0000E-05

Table 3 – List of MT numbers (neutron induced reactions) used in ANITA-NC package

Ordering Number	MT	Reaction label	Change in ZA of the target
1	4	(n, n')	0
2	16	(n, 2n)	-1
3	17	(n, 3n)	-2
4	22	(n, nα)	-2004
5	11	(n, 2nd)	-1003
6	23	(n, n3α)	-6012
7	24	(n, 2nα)	-2005
8	25	(n, 3nα)	-2006
9	28	(n, np)	-1001
10	29	(n, n2α)	-4008
11	30	(n, 2n2α)	-4009
12	32	(n, nd)	-1002
13	33	(n, nt)	-1003
14	34	(n, n^3He)	-2003
15	35	(n, nd2α)	-5010
16	36	(n, nt2α)	-5011
17	37	(n, 4n)	-3
18	41	(n, 2np)	-1002
19	42	(n, 3np)	-1003
20	44	(n, n2p)	-2002
21	45	(n, npα)	-3005
22	102	(n, γ)	+1
23	103	(n, p)	-1000
24	104	(n, d)	-1001
25	105	(n, t)	-1002
26	106	(n, ^{3}He)	-2002
27	107	(n, α)	-2003
28	108	(n, 2α)	-4007
29	109	(n, 3α)	-6011
30	111	(n, 2p)	-2001
31	112	(n, pα)	-3004
32	113	(n, t2α)	-5010
33	114	(n, d2α)	-5009
34	115	(n, pd)	-2002
35	116	(n, pt)	-2003
36	117	(n, dα)	-3005
37	152	(n, 5n)	-4
38	153	(n, 6n)	-5
39	154	(n, 2nt)	-1004
40	155	(n, tα)	-3006
41	156	(n, 4np)	-1004
42	157	(n, 3nd)	-1004
43	158	(n, ndα)	-3006
44	159	(n, 2npα)	-3006
45	160	(n, 7n)	-6
46	161	(n, 8n)	-7

Ordering Number	MT	Reaction label	Change in ZA of the target
47	162	(n, 5np)	-1005
48	163	(n, 6np)	-1006
49	164	(n, 7np)	-1007
50	165	(n, 4nα)	-2007
51	166	(n, 5nα)	-2008
52	167	(n, 6nα)	-2009
53	168	(n, 7nα)	-2010
54	169	(n, 4nd)	-1005
55	170	(n, 5nd)	-1006
56	171	(n, 6nd)	-1007
57	172	(n, 3nt)	-1005
58	173	(n, 4nt)	-1006
59	174	(n, 5nt)	-1007
60	175	(n, 6nt)	-1008
61	176	(n, 2n^{3}He)	-2004
62	177	(n, 3nHe^3)	-2005
63	178	(n, 4nHe^3)	-2006
64	179	(n, 3n2p)	-2004
65	180	(n, 3n2α)	-4010
66	181	(n, 3npα)	-3007
67	182	(n, dt)	-2004
68	183	(n, npd)	-2003
69	184	(n, npt)	-2004
70	185	(n, ndt)	-2005
71	186	(n, npHe^3)	-3004
72	187	(n, ndHe^3)	-3005
73	188	(n, ntHe^3)	-3006
74	189	(n, ntα)	-3007
75	190	(n, 2n2p)	-2003
76	191	(n, pHe^3)	-3003
77	192	(n, dHe^3)	-3004
78	193	(n, He^{3}α)	-4006
79	194	(n, 4n2p)	-2005
80	195	(n, 4n2α)	-4011
81	196	(n, 4npα)	-3008
82	197	(n, 3p)	-3002
83	198	(n, n3p)	-3003
84	199	(n, 3n2pα)	-4008
85	200	(n, 5n2p)	-2006

Table 4 – List of MT numbers (proton induced reactions) used in ANITA-NC package

Ordering Number	MT	Reaction label	Change in ZA of the target
1	4	(p, n)	1000
2	16	(p, 2n)	999
3	17	(p, 3n)	998
4	22	(p, nα)	-1004
5	11	(p, 2nd)	-3
6	23	(p, n3α)	-5012
7	24	(p, 2nα)	-1005
8	25	(p, 3nα)	-1006
9	28	(p, np)	-1
10	29	(p, n2α)	-3008
11	30	(p, 2n2α)	-3009
12	32	(p, nd)	-2
13	33	(p, nt)	-3
14	34	(p, nHe^3)	-1003
15	35	(p, nd2α)	-4010
16	36	(p, nt2α)	-4011
17	37	(p, 4n)	997
18	41	(p, 2np)	-2
19	42	(p, 3np)	-3
20	44	(p, n2p)	-1002
21	45	(p, npα)	-2005
22	102	(p, γ)	1001
23	103	(p, p)	0
24	104	(p, d)	-1
25	105	(p, t)	-2
26	106	(p, He^3)	-1002
27	107	(p, α)	-1003
28	108	(p, 2α)	-3007
29	109	(p, 3α)	-5011
30	111	(p, 2p)	-1001
31	112	(p, pα)	-2004
32	113	(p, t2α)	-4010
33	114	(p, d2α)	-4009
34	115	(p, pd)	-1002
35	116	(p, pt)	-1003
36	117	(p, dα)	-2005
37	152	(p, 5n)	996
38	153	(p, 6n)	995
39	154	(p, 2nt)	-4
40	155	(p, tα)	-2006
41	156	(p, 4np)	-4
42	157	(p, 3nd)	-4
43	158	(p, ndα)	-2006
44	159	(p, 2npα)	-2006
45	160	(p, 7n)	994
46	161	(p, 8n)	993

Ordering Number	MT	Reaction label	Change in ZA of the target
47	162	(p, 5np)	-5
48	163	(p, 6np)	-6
49	164	(p, 7np)	-7
50	165	(p, 4nα)	-1007
51	166	(p, 5nα)	-1008
52	167	(p, 6nα)	-1009
53	168	(p, 7nα)	-1010
54	169	(p, 4nd)	-5
55	170	(p, 5nd)	-6
56	171	(p, 6nd)	-7
57	172	(p, 3nt)	-5
58	173	(p, 4nt)	-6
59	174	(p, 5nt)	-7
60	175	(p, 6nt)	-8
61	176	(p, 2nHe^3)	-1004
62	177	(p, 3nHe^3)	-1005
63	178	(p, 4nHe^3)	-1006
64	179	(p, 3n2p)	-1004
65	180	(p, 3n2α)	-3010
66	181	(p, 3npα)	-2007
67	182	(p, dt)	-1004
68	183	(p, npd)	-1003
69	184	(p, npt)	-1004
70	185	(p, ndt)	-1005
71	186	(p, npHe^3)	-2004
72	187	(p, ndHe^3)	-2005
73	188	(p, ntHe^3)	-2006
74	189	(p, ntα)	-2007
75	190	(p, 2n2p)	-1003
76	191	(p, pHe^3)	-2003
77	192	(p, dHe^3)	-2004
78	193	(p, He^3α)	-3006
79	194	(p, 4n2p)	-1005
80	195	(p, 4n2α)	-3011
81	196	(p, 4npα)	-2008
82	197	(p, 3p)	-2002
83	198	(p, n3p)	-2003
84	199	(p, 3n2pα)	-3008
85	200	(p, 5n2p)	-1006

Table 5 – List of MT numbers (deuteron induced reactions) used in ANITA-NC package

Ordering Number	MT	Reaction label	Change in ZA of the target
1	4	(d, n)	1001
2	16	(d, 2n)	1000
3	17	(d, 3n)	99
4	22	(d, nα)	-1003
5	11	(d, 2nd)	-2
6	23	(d, n3α)	-5011
7	24	(d, 2nα)	-1004
8	25	(d, 3nα)	-1005
9	28	(d, np)	0
10	29	(d, n2α)	-3007
11	30	(d, 2n2α)	-3008
12	32	(d, nd)	-1
13	33	(d, nt)	-2
14	34	(d, nHe^3)	-1002
15	35	(d, nd2α)	-4009
16	36	(d, nt2α)	-4010
17	37	(d, 4n)	998
18	41	(d, 2np)	-1
19	42	(d, 3np)	-2
20	44	(d, n2p)	-1001
21	45	(d, npα)	-2004
22	102	(d, γ)	1002
23	103	(d, p)	1
24	104	(d, d)	0
25	105	(d, t)	-1
26	106	(d, He^3)	-1001
27	107	(d, α)	-1002
28	108	(d, 2α)	-3006
29	109	(d, 3α)	-5010
30	111	(d, 2p)	-1000
31	112	(d, pα)	-2003
32	113	(d, t2α)	-4009
33	114	(d, d2α)	-4008
34	115	(d, pd)	-1001
35	116	(d, pt)	-1002
36	117	(d, dα)	-2004
37	152	(d, 5n)	997
38	153	(d, 6n)	996
39	154	(d, 2nt)	-3
40	155	(d, tα)	-2005
41	156	(d, 4np)	-3
42	157	(d, 3nd)	-3
43	158	(d, ndα)	-2005
44	159	(d, 2npα)	-2005
45	160	(d, 7n)	995
46	161	(d, 8n)	994

Ordering Number	MT	Reaction label	Change in ZA of the target
47	162	(d, 5np)	-4
48	163	(d, 6np)	-5
49	164	(d, 7np)	-6
50	165	(d, 4nα)	-1006
51	166	(d, 5nα)	-1007
52	167	(d, 6nα)	-1008
53	168	(d, 7nα)	-1009
54	169	(d, 4nd)	-4
55	170	(d, 5nd)	-5
56	171	(d, 6nd)	-6
57	172	(d, 3nt)	-4
58	173	(d, 4nt)	-5
59	174	(d, 5nt)	-6
60	175	(d, 6nt)	-7
61	176	(d, 2nHe^3)	-1003
62	177	(d, 3nHe^3)	-1004
63	178	(d, 4nHe^3)	-1005
64	179	(d, 3n2p)	-1003
65	180	(d, 3n2α)	-3009
66	181	(d, 3npα)	-2006
67	182	(d, dt)	-1003
68	183	(d, npd)	-1002
69	184	(d, npt)	-1003
70	185	(d, ndt)	-1004
71	186	(d, npHe^3)	-2003
72	187	(d, ndHe^3)	-2004
73	188	(d, ntHe^3)	-2005
74	189	(d, ntα)	-2006
75	190	(d, 2n2p)	-1002
76	191	(d, pHe^3)	-2002
77	192	(d, dHe^3)	-2003
78	193	(d, He^3α)	-3005
79	194	(d, 4n2p)	-1004
80	195	(d, 4n2α)	-3010
81	196	(d, 4npα)	-2007
82	197	(d, 3p)	-2001
83	198	(d, n3p)	-2002
84	199	(d, 3n2pα)	-3007
85	200	(d, 5n2p)	-1005

3 Sample problems

Two examples of application of the ANITA-NC code, related to deuteron and proton activation, are shown in the following sections.

3.1 Deuteron activation

As test case for the deuteron activation calculation, the test181 case of the FISPACT-II package was chosen. This case is referred to deuteron induced activation on Titanium.

In the present calculations more cooling times were considered than in the original FISPACT input. The deuteron spectrum provided in the FISPACT-II package was used.

The FISPACT-II input and the corresponding ANITA-NC one are reported in Table 6 and Table 7. In FISPACT-II the deuteron projectile is identified by the keyword PROJ=2. In ANITA-NC the deuteron projectile is identified by the parameter nproj=3.

Table 6 – FISPACT-II input file

```
<< -----get nuclear data----- >>
CLOBBER
MONITOR 1
PROJ 2
LIBV 0
NOERROR
GETXS 0
GETDECAY 0
FISPACT
* IRRADIATION OF TI IFMIF
<< -----set initial conditions----- >>
MASS 1.0 1
Ti 100.0
MIND 1.E5
GRAPH 5 0 1 1 2 3 4 5
FLUX 1.0E+13
ATOMS
HAZARDS
HALF
<< -----irradiation phase----- >>
TIME 1.0 YEARS
ATOMS
<< -----cooling phase----- >>
FLUX 0.
ZERO
TIME 1         ATOMS
TIME 59         ATOMS
TIME 29 MINS       ATOMS
TIME 30 MINS       ATOMS
TIME 5   HOURS       ATOMS
TIME 4   HOURS       ATOMS
TIME 10  HOURS       ATOMS
TIME 4  HOURS       ATOMS
TIME  6 DAYS ATOMS
TIME 358 DAYS ATOMS
TIME 2 YEARS ATOMS
TIME 2 YEARS ATOMS
TIME 5 YEARS ATOMS
TIME 10 YEARS ATOMS
```

```
TIME 10 YEARS ATOMS
TIME 10 YEARS ATOMS
TIME 10 YEARS ATOMS
TIME 10 YEARS ATOMS
TIME 10 YEARS ATOMS
TIME 10 YEARS ATOMS
TIME 10 YEARS ATOMS
TIME 10 YEARS ATOMS
TIME 400 YEARS ATOMS
TIME 9500 YEARS ATOMS
TIME 90000 YEARS ATOMS
TIME 900000 YEARS ATOMS
END
* END
```

Table 7 – ANITA-NC input file

```
3
test181_inv
test181_clr
test181_sg
    1   40nYTitanium
Case Test181
 4.51      1.0000-12  1.0      Titanium
TI  100.
         1        26
3.15570+070.0
1.00000+006.00000+011.80000+033.60000+032.16000+043.60000+047.20000+04
8.64000+046.04800+053.15570+079.46710+071.57780+083.15570+086.31140+08
9.46710+081.26228+091.57785+091.89342+092.20899+092.52456+092.84013+09
3.15570+091.57785+103.15570+113.15570+123.15570+13
   1
0.00112
        -1
```

In Figure 2 and Figure 3 the results of specific activity (Bq/kg) and decay heat (kW/kg) are given. The ANITA-NC predictions are compared with those obtained by FISPACT-II by using the same deuteron activation cross section library (EAF-2010).

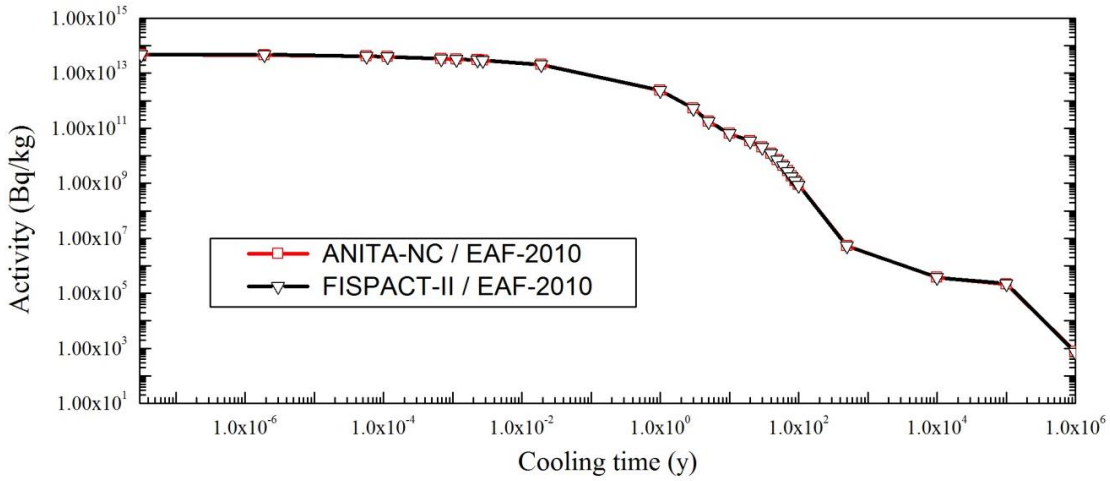

Figure 2 – Deuteron induced activity on Titanium vs. cooling time.

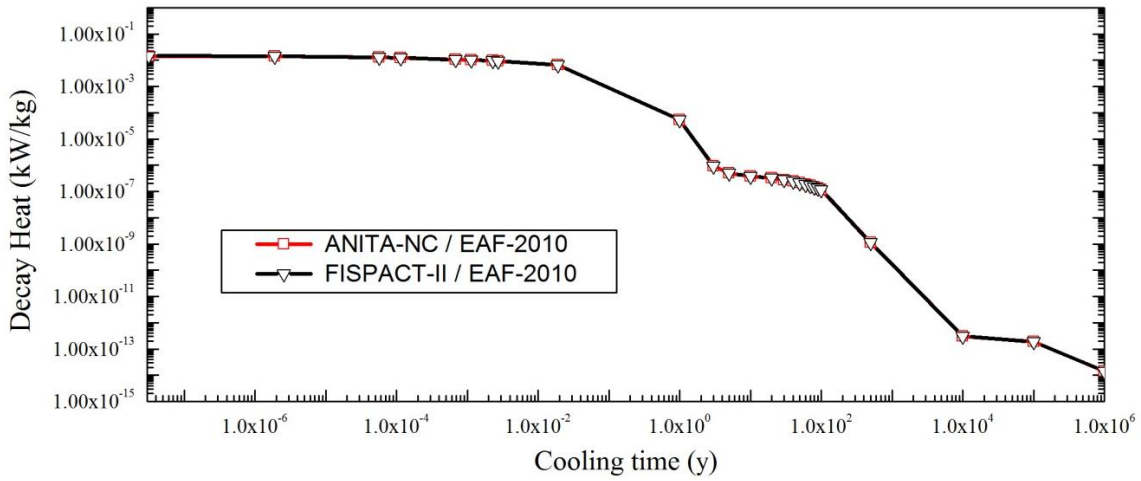

Figure 3 – Deuteron induced decay heat on Titanium vs. cooling time

3.2 Proton activation

A proton induced activation calculation was performed by using the same irradiation scenario and spectrum of test181 case for deuteron activation. Copper was chosen in this case as target material. In FISPACT-II the proton projectile is identified by the keyword PROJ=3. In ANITA-NC the proton projectile is identified by the parameter nproj=2. In Figure 4 and Figure 5 the results the specific activity (Bq/kg) and decay heat (kW/kg) obtained by ANITA-NC are shown and compared with the corresponding FISPACT-II predictions.

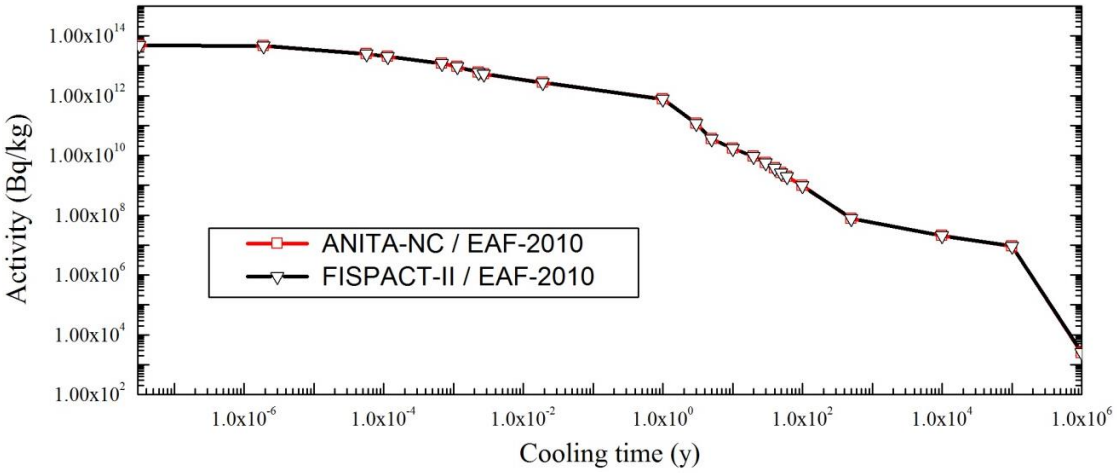

Figure 4 – Proton induced activity on Copper vs. cooling time.

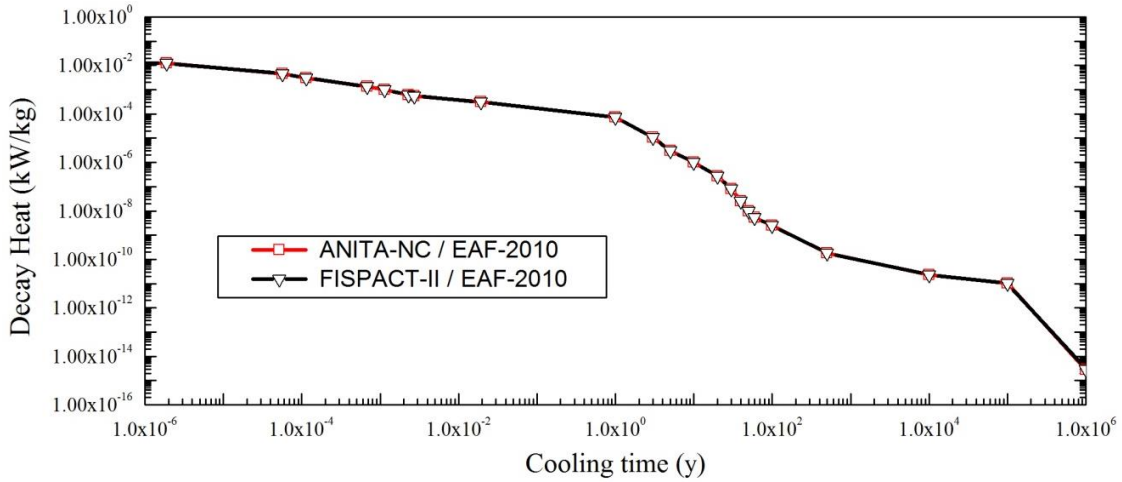

Figure 5 – Proton induced decay heat on Copper vs. cooling time.

4 Conclusion

The ANITA-NC (Analysis of Neutron Induced Transmutation and Activation – Neutral and Charged) inventory system has been developed in order to treat the material activation induced by neutrons, protons, alphas, deuterons and gammas.

It extends the capabilities of ANITA-IEAF which is able to treat only neutrons up to 55 MeV.

The ANITA-NC uses the EAF-2010 neutron, deuteron and proton activation cross sections. Actually there are not available activation cross section files in EAF format for α and γ.

Two examples of application for deuteron and proton activation are given in this report. The ANITA-NC results are compared with those obtained by FISPACT-II . A good agreement between ANITA-NC and FISPACT-II predictions is found.

REFERENCES

[1] D.G. Cepraga, G. Cambi, M. Frisoni, ANITA-2000 Activation Code Package. Part I - Manual, ENEA ERG-FUS/TN-SIC TR 16/2000, November 2000.

[2] D.G. Cepraga, G. Cambi, M. Frisoni, ANITA-2000 Activation Code Package. Part II : Code validation, ENEA FUS-TN-SA-SE-R-020, June 2001.

[3] D.G. Cepraga, E. Menapace, A. Musumeci, G. Cambi, M. Frisoni, Validation of activation and decay data libraries with respect to integral decay heat experiments, EFF-DOC-654, JEFF/EFF/EAF Meeting, NEA Head Quarter, Paris, September 14-15, 1998.

[4] D.G. Cepraga, G. Cambi, M. Frisoni, ANITA-2000 photon and electron decay heat validation based on FNG-Frascati experimental data and comparison with EASY-99 results, EFDA Task No. TW1-TSS-SEA5, Milestone 3, Final Report, ENEA FUS-TN-SA-SE-R-65, December 2002.

[5] G. Cambi, D.G. Cepraga, M. Frisoni, L. Manzana, F. Carloni, M.L. Fiandri, Anita-2000 activation code package: clearance assessment of ITER activated materials, Proc. of the 19th Symposium on Fusion Engineering SOFE, Atlantic City, NJ, USA, January 22-25, 2002, pp. 44-47, IEEE Catalog No. 02CH37231C, ISBN 0-7803-7075-9 - U.S.A. 2002.

[6] D.G. Cepraga, G. Cambi, M. Frisoni, D. Ene, ANITA-2000 activation code package development and validation. Part 2: a) Gamma source calculation with Anita-2000-D, b) Sn discrete ordinate method and MCNP dose rate calculation, c) Experimental-calculated results comparison, EFDA Task No. TW1-TSS-SEA5 Milestone D2, Final Report, ENEA FUS-TN-SA-SE-R-64, December 2002.

[7] M. Frisoni, ANITA-IEAF activation code package – updating of the decay and cross section data libraries and validation on the experimental data from the Karlsruhe Isochronous Cyclotron. EPJ Web of Conferences 153, 07002 (2017) DOI: 10.1051/epjconf/20171530, *ICRS-13 & RPSD-2016*.

[8] M. Frisoni, ANITA-IEAF:an intermediate energy neutron activation system, ENEA report, ADPFISS-LP1-089 (2017).

[9] C. Ponti and S. Stramaccia, ANITA: Analysis of Neutron Induced Transmutation and Activation, EUR 12622 EN report, 1989.

[10] C. Ponti, Calculation of radioactive decay chains produced by neutron irradiation, EUR 9389, 1984.

[11] EASY-2010 OECD NEA Data Bank NEA-1564/13, 16 December 2011.

[12] The FISPACT-II User Manual, Editors: Michael Fleming, Thomas Stainer, Mark Gilbert, UKAEA-R(18)001, January 2018 .

[13] M.A. Kellet, The JEFF-3.1.1 Decay Data Library, JEFDOC-1188, June 2007.